NOTICE

AVIS

The quality of this microform is heavily dependent upon the quality of the original thesis submitted for microfilming. Every effort has been made to ensure the highest quality of reproduction possible.

La qualité de cette microforme dépend grandement de la qualité de la thèse soumise au microfilmage. Nous avons tout fait pour assurer une qualité supérieure de reproduction.

If pages are missing, contact the university which granted the degree.

S'il manque des pages, veuillez communiquer avec l'université qui a conféré le grade.

Some pages may have indistinct print especially if the original pages were typed with a poor typewriter ribbon or if the university sent us an inferior photocopy.

La qualité d'impression de certaines pages peut laisser à désirer, surtout si les pages originales ont été dactylographiées à l'aide d'un ruban usé ou si l'université nous a fait parvenir une photocopie de qualité inférieure.

Canada

University of Alberta

Mathematical Modelling of Non-Isothermal Gravity Drainage of
Heavy Oil and Bitumen in Porous Media

by

Mehran Pooladi-Darvish   Ⓒ

A thesis submitted to the Faculty of Graduate Studies and Research in partial fulfillment
of the requirements for the degree of Doctor of Philosophy
in
Petroleum Engineering
Department of Mining, Metallurgical and
Petroleum Engineering

Edmonton, Alberta
Spring 1996

ISBN   0-612-10626-8

Canada

University of Alberta

Library Release Form

Name of Author: Mehran Pooladi-Darvish

Title of Thesis: Mathematical Modelling of Non-Isothermal Gravity
                          Drainage of Heavy Oil and Bitumen in Porous Media

Degree for which this Thesis was Presented: Doctor of Philosophy in
                                                     Petroleum Engineering

Year this Degree Granted   1996

M. Pooladi- Darvish.

606 Chemical and Mineral Bldg.
University of Alberta
Edmonton, Alberta
Canada T6G 2G6
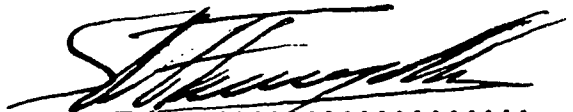
Dated. Oct. 31, 1995

"May we be among those who make life fresh.
You, lords of wisdom,
and you who bring happiness through truth and precision,
be single-minded in the realm of inner intellect."

Zoroaster 18th century BC.
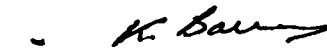
University of Alberta

Faculty of Graduate Studies and Research

The undersigned certify that they have read, and recommend to the Faculty of Graduate Studies and Research for acceptance, a thesis entitled Mathematical Modelling of Non-Isothermal Gravity Drainage of Heavy Oil and Bitumen in Porous Media submitted by Mehran Pooladi-Darvish in partial fulfillment of the requirements for the degree of Doctor of Philosophy in Petroleum Engineering.
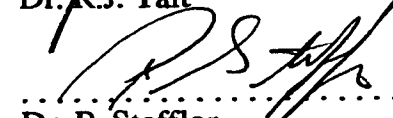
Co-Supervisor Dr. S.M. Farouq Ali

Co-Supervisor Dr. W.S. Tortike

Dr. R.G. Bentsen

Dr. K. Barron

Dr. R.J. Tait

Dr. P. Steffler

Dr. R.M. Butler

Dated ...Oct. 27, 95..........

To my parents

ABSTRACT

Reservoirs producing under gravity drainage are known to achieve high recoveries. In this work mathematical models are developed for thermal gravity drainage of heavy oil and bitumen. Naturally fractured reservoirs are considered first, and by means of a time scale analysis it is shown that the two processes of heat and fluid flow can be decoupled for a typical single block. The time scale analysis is used later to develop a scaling criterion for physical modelling of thermal gravity drainage. The Heat Integral Method (HIM) is then used which permits an analytical solution for thermal gravity drainage in a single block. The solution indicates that the production rate is linearly proportional to oil mobility at steam temperature. It is also found that the average block temperature can be used as a representative temperature for oil rate calculations with minimal error. Using this assumption, very simple equations are obtained which are then used to examine the importance of thermal gravity drainage in fractured reservoirs. Three analytical and semi-analytical models are developed to show the application of HIM in thermal recovery processes. The models are then used to study the relevant processes. Thermal gravity drainage is a moving boundary process in high permeability systems. A new interface equation is derived to model accurately the interface behaviour. This is then combined with the conservation laws for energy, mass and momentum to develop a numerical model for a Steam-Assisted Gravity Drainage (SAGD) process. A transformation is used to make the interface stationary, which allows fine-gridding where high accuracy is required. The model is validated against a newly developed analytical model for a moving boundary process in porous media and other available analytical solutions. By performing a case study, it is found that the application of the numerical model is limited to cases where the interface does not completely separate from the vertical axis. Using the 2-D temperature and potential profiles from the numerical model it was found that the potential distribution can be assumed to be steady-state; however, heat flow should be modeled as an unsteady-state process.

ACKNOWLEDGMENTS

TABLE OF CONTENTS

LIST OF TABLES

LIST OF FIGURES

NOMENCLATURE[1]

Latin Letters:

a Coefficients of discretized equations

$a(\tau)$ Coefficient of temperature distribution

A Pattern area

A_1 Constant [see Table 5.2]

A_2 Constant [see Table 5.2]

b_1 Constant in Equation B.2

b_2 Constant in Equation B.3

$b(\tau)$ Coefficient of temperature distribution

B_2 Dimensionless group related to Rayleigh No.

B_3 Dimensionless group related to Rayleigh No.

B_4 Dimensionless group related to Rayleigh No.

c Fluid compressibility

c Specific heat capacity

c Geometric factor related to pattern shape

$c(\tau)$ Coefficient of temperature distribution

C Net to gross thickness ratio

d Differentiation operator

d Distance between two producing well

$d(\tau)$ Coefficient of temperature distribution

D Total derivative

D_1 Constant [see Equation (6.1.2.6)]

D_2 Constant [see Equation (6.1.2.10)]

e Tangential flux

$e(\tau)$ Coefficient of temperature distribution

---

[1]   The equations in this work are written in a consistent set of units, unless otherwise stated. Hence, the units of variables and parameters are not specified here.

$f(\tau)$	Coefficient of temperature distribution
F	Function [see Equation (7.6.13)]
g	Acceleration due to gravity
$g(\tau)$	Coefficient of temperature distribution
h	Oil column height
h	Geometric relation of transformation
H	Block height
H	Formation height
J	Jacobian of transformation
J_0	Bessel function of zeroth order
J_1	Bessel function of first order
k	Permeability
k_t	Thermal conductivity
L	Half of block width
L_1	Thickness of porous medium
m	Heavy Oil characteristic [see (Equation B.1)]
m_1	Constant [see table 5.2]
m_2	Constant [see table 5.2]
n	Degree of polynomial
N_{Pe}	Peclet number
N_{Ra}	Rayleigh number
P	Pressure
P	Peclet cell number
q	Volumetric flow rate per unit cross-sectional area
$\dot{q}$	Volumetric flow rate
Q	Heat flux
Q_1	Heat flux to the rear

Q_2 Heat flux to the front

r Space coordinate in cylindrical system

R Radius of cylinder

$s(t)$ Interface location

S Saturation

t Time

T Temperature

u Darcy velocity

U Interface velocity

v Variable of integration

x Space coordinate in Cartesian system

X Dimensionless space coordinate in Cartesian system

z Space coordinate in Cartesian system

Z Dimensionless space coordinate in Cartesian system

Greek Letters:

α Thermal conductivity

α Geometric relation of transformation

β_n Roots of $J_0(\beta) = 0$

β Ratio of thermal to hydraulic diffusivity

β Geometric relation of transformation

∂ Partial differentiation

δ Dimensionless heat penetration depth

δ Distance between two computational nodes

Δ Denoting difference

Δ Distance between two faces of control volume

∇ Gradient

ε	Ratio of thermal conductivity of surrounding rock to that of formation
ϕ	Porosity
φ	Potential
Φ	Dimensionless potential
γ	Ratio of volume change of a unit volume fluid due to compression to oil saturation change
Γ	Diffusion coefficient
μ	Dynamic viscosity
υ	Kinematic viscosity
λ	Geometric relation of transformation
λ	Constant [see Equation (8.2.4.1.25)]
Π	Dimensionless pressure
ρ	Density
θ	Dimensionless temperature
Θ	Interface inclination angle
τ	Dimensionless time
τ	Characteristic time
ζ	Space coordinate in Cartesian system ahead of the interface
ξ	Dimensionless space coordinate in computational domain
ξ	Dimensionless space coordinate in Cartesian system ahead of the interface
Ψ	Stream function
η	Dimensionless space coordinate in computational domain
η	Dimensionless space coordinate in Cartesian system
χ	Dimensionless space coordinate in cylindrical system ahead of the interface

Subscripts:

av.	Average
d	Drainage

D	Dimensionless
e	Eastern control volume face
E	Eastern control volume
F	Front
hc	Heat conduction
n	Northern control volume face
ne	North-eastern corner of control volume
nw	North-western corner of control volume
N	Northern control volume
NE	North-eastern control volume
NW	North-western control volume
o	Oil
P	Central control volume
R	Initial reservoir condition
s	Steam temperature
s	Southern face of control volume
se	South-eastern corner of control volume
sw	South-western corner of control volume
S	Southern control volume
SE	South-eastern control volume
SW	South-western control volume
w	Western face of control volume
W	Western control volume
W	Wellbore
x	Along horizontal direction
z	Along vertical direction

Superscripts

−	Function at average temperature
^	Interface location
0	Previous time step

Symbols

$\vert\ \vert$	Absolute value
$\Vert\ \Vert$	Maximum value

1. INTRODUCTION

Heavy oil occurring in carbonate reservoirs, mostly fractured, is an important resource which accounts for one-third of the total heavy oil world-wide. Many fractured reservoirs in the Middle East, the former Soviet Union and Canada are candidates for thermal recovery. Processes such as steam injection were not applied to the fractured reservoirs until the last decade or so. It was believed that the injected steam would bypass the oil through the fractures, leaving most of the oil unrecovered. Later, publication of the field results of steam injection in fractured reservoirs showed very promising results. Initial mathematical studies indicated that the very large surface area of the matrix blocks exposed to the fractures provided a means for effective heat transmission, alleviating the problem of steam breakthrough. The same behaviour had been observed previously in geothermal reservoirs. In the latter case, projects could be designed such that the cold water injected through the fractures of a geothermal reservoir turned to steam before it reached the production well.

A review of the literature indicated that satisfactory models for predicting the performance of steam injection in fractured reservoirs are not available, and there is no consensus on the major mechanisms responsible for heat and fluid flow in such operations. This work was initially aimed to take a first step by modelling the matrix-fracture heat transfer accompanied with thermal gravity drainage of the oil. Gravity drainage was considered, because this mechanism achieves high displacement and high sweep efficiency if implemented under stable conditions. Field results indicate recovery factors as high as 70% for gravity drainage under favourable conditions. Gravity drainage is known to be the major recovery mechanism for many light oil fractured reservoirs. Improvement of the gravity drainage of heavy oil from a single block was previously studied experimentally by the author.

Thermal gravity drainage of heavy oil from a single block of a fractured reservoir is a combined heat and fluid flow process. Heat is transferred to the oil, and the oil drains simultaneously due to the gravity force. If the drainage rate is slow enough compared with the heat flow rate, the two processes can be decoupled. The low permeability of fractured reservoirs permits the decoupling assumption. In high permeability formations, however, heat transfer and fluid flow compose a combined process. Large resources of heavy oil and bitumen occur in such high permeability reservoirs, and recovery processes based on thermal gravity drainage have been shown to be attractive in such formations.

1

Butler, McNab and Lo introduced the Steam-Assisted Gravity Drainage (SAGD) process for thermal recovery from high permeability formations. The SAGD process takes advantage of the gravity drainage of the heated oil ahead of an expanding steam zone. Numerous experimental and theoretical studies and field results indicate that the SAGD process is an attractive recovery method for the bituminous reservoirs of Alberta. Simplistic mathematical models of the SAGD process have been used for the purpose of some mechanistic studies, and computationally expensive thermal simulators have been used for field studies. It seems that the capability of incorporating complex input data, and a lack of confidence in the assumptions involved in the simpler analytical and semi-analytical models have persuaded industry to use the complex thermal simulators. A review of the literature indicated that there is no thermal simulator that is specifically designed for the SAGD process. Availability of such a model is needed, because in commercially available thermal simulators, accurate modelling of the heat and fluid flow processes in the vicinity of the steam interface, where most of the oil flow occurs, is only possible if fine-gridding is implemented for the global domain. This, in turn, results in impractical computational time.

In the SAGD process, a steam-oil interface is formed which passes through the reservoir. The petroleum literature indicates few attempts at numerical modelling of moving boundary phenomena. In other engineering fields, however, various transformation and dynamic gridding techniques have been developed which permit accurate modelling of the process of interest. A requirement for accurate modelling of a moving boundary problem is availability of an interface equation which reveals the interface location. An objective of this work is to develop a numerical model for the thermal gravity drainage of heavy oil in high permeability porous media, which permits mechanistic studies as well. A new interface equation is to be derived and state of the art modelling of moving boundary processes is to be implemented. An attempt will be made to combine the advantages of previous analytical and numerical models. In order to validate the model, an analytical solution is to be developed which is analogous to the SAGD process in one dimension and without temperature effects. Similar to other mathematical models, especially the first attempts, it will be found that the developed model has its own limitations. These limitations and suggestion as how to alleviate them are discussed in parts of this study.

In the process of developing the analytical model for thermal gravity drainage in fractured reservoirs, an integral method is used to simplify the solution of heat flow

2

problem. Such integral methods have been used rarely in the petroleum literature. This is despite their broad application for modelling diffusion dominated processes such as those explaining heat conduction and single phase fluid flow in porous media. To show the application of the Heat Integral Method (HIM) in modelling thermal recovery processes, three relevant analytical and semi-analytical models are developed as another part of this work. Figure 1.1 illustrates the scheme of this work.
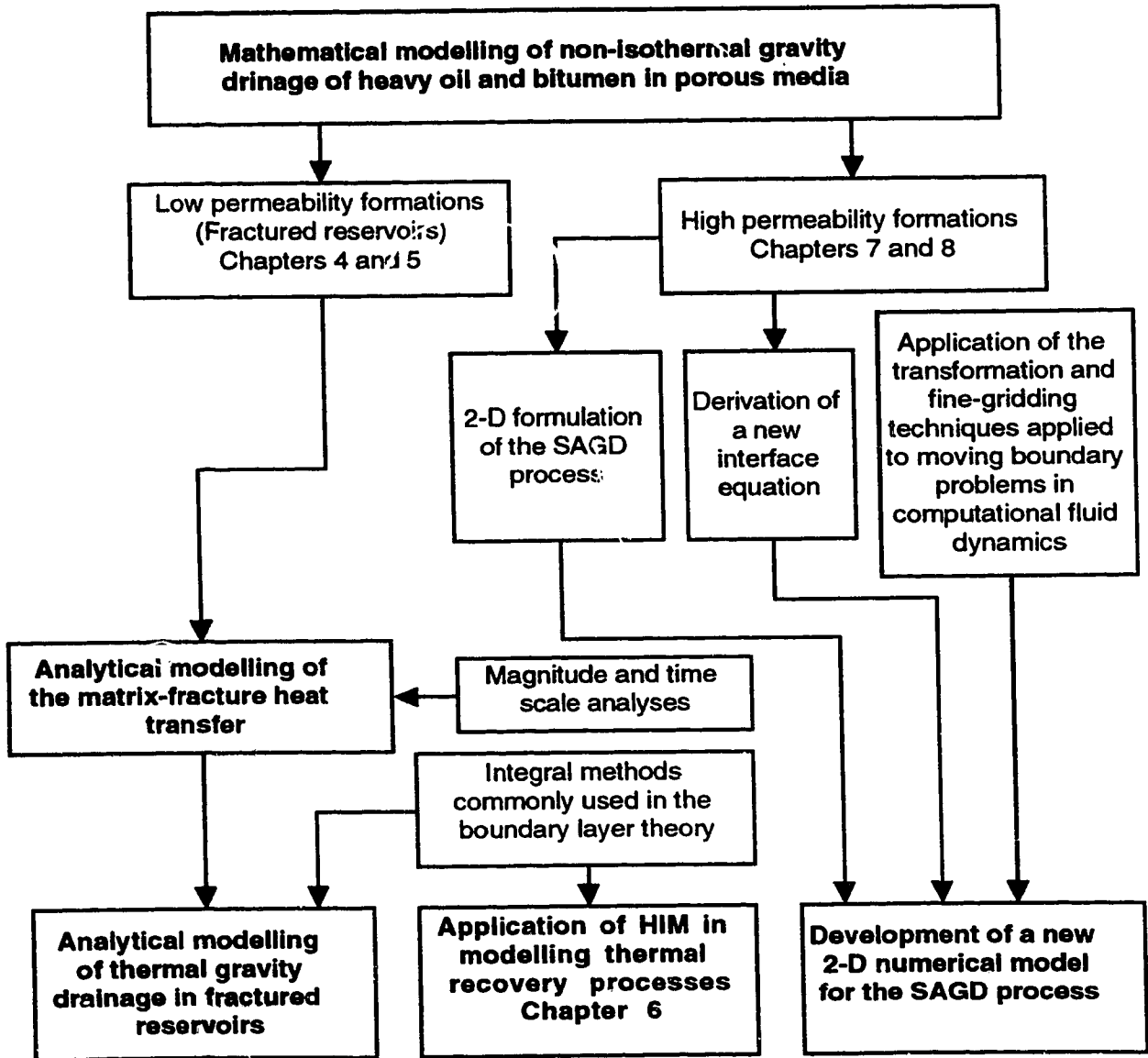
Figure 1.1 Schematic presentation of different parts of the current work and their inter-relation. (The major contributions of this work are high-lighted)

2. REVIEW OF LITERATURE

The oil sand and bituminous resources of Canadian reservoirs are estimated to be as large as those of conventional crude oil, world-wide [Farouq Ali 1994]. In Alberta, bituminous reservoirs are of two types: high permeability porous media (and/or tar sands), and low matrix permeability naturally fractured reservoirs[1]. Athabasca, Cold Lake and Peace River reservoirs are examples of the former, and the fissured vugular Grosmont formation with more than one trillion barrels of bitumen in place [Cordell 1982] is an example of the latter.

It is essential to heat the immobile bitumen systematically so that a high sweep efficiency is attained, and to avoid cooling of the bitumen before it reaches the production site. Pilot tests in the Grosmont formation [Cordell 1982], and field results in the former U.S.S.R. [Antoniadi, Budnikov and Garushev 1988] have indicated that the fracture network permitted fast distribution of the injected steam in the formation. Subsequently, the oil in the matrix blocks was heated and drained to the fracture network. In high permeability porous media, Steam-Assisted Gravity Drainage (SAGD) has shown promising results. In both cases of low and high permeability systems, gravity drainage has been found to be an important recovery mechanism.

Reservoirs producing under gravity drainage are known to achieve high recoveries [Saidi 1987, Hagoort 1980, Dykstra 1978, Cardwell and Parsons 1948]. This is because stable gravity drainage leads to both high displacement efficiency and high sweep efficiency. King, Stiles, and Waggone [1970] reported a displacement efficiency of 87% due to gravity drainage from the Hawkins filed in Texas. Saidi [1991] presented an example of 70% recovery from the Lakeview pool of the Midway Sunset field under natural depletion and gravity drainage mechanisms. A recovery factor of 40% was reported by Murty, Al-Saleh, and Dakessian [1987] due to gravity drainage in the 0.050 μm^2 Mauddud reservoir. As early as 1953, Higgins [1953] reported an experimental study on the gravity drainage of light and heavy oil. He suggested that "recoveries by gravity drainage may be higher than those expected by waterflooding." Based on his experimental studies and field performances, he suggested that "a combination of sand permeability, gravity of the oil (hence, its viscosity) and formation thickness may be such

---

1   In this work the term "high permeability porous media" is used to refer to usual, non-fractured reservoirs in contrast to "naturally fractured reservoirs" or simply "fractured reservoirs".

4

that gravity drainage is a more efficient recovery mechanism than encroaching edge-water."

In steam drive projects, pressure forces are the main driving force for oil production before breakthrough; however, the production rate might be low due to the low mobility of heavy oil [Vogel 1992]. After breakthrough, the pressure drop in the steam zone drops to a small value which exerts minimal driving force on the oil bank, and gravity drainage of the heated oil below the expanding steam zone dominates the process. Vogel [1992] believed that the main recovery mechanism in such reservoirs was gravity drainage of a thin layer of heated oil adjacent to the steam interface.

In such cases where the hot fluids drain along the steam interface and do not penetrate ahead of the interface, heat transfer is dominated by conduction ahead of a moving boundary. Experimental and theoretical studies as well as field results have indicated that gravity drainage of the heated oil in high permeability porous media is a moving boundary phenomenon [Butler et al. 1981, Edmunds, Kovalsky, Gittins, and Pennacchioli 1994]. Heat flows ahead of a steam-oil interface that travels through the formation due to drainage of oil ahead of the interface. In naturally fractured reservoirs, however, the effect of the moving boundary can be negligible, if the permeability of the formation is low enough. Under the latter conditions the two processes of heat and fluid flow can be decoupled as will be shown in this study. Due to the difference in behaviour, the two problems of thermal gravity drainage in naturally fractured reservoirs and in high permeability porous media have been discussed separately in the literature. The previous studies concerning thermal processes in naturally fractured reservoirs are reviewed first with an emphasis on gravity drainage, and later the literature on non-isothermal gravity drainage in high permeability porous media will be reviewed.

2.1. Non-Isothermal Gravity Drainage in Naturally Fractured Reservoirs

Heavy oil occurring in carbonate reservoirs, mostly fractured, is an important resource which accounts for one-third of the total heavy oil world-wide [Briggs, Barron, Fulleylove, and Wright 1988]. Many fractured reservoirs in the Middle East [Macaulay, Krafft, Hartemink, and Escovedo 1995], the former Soviet Union [Antoniadi et al. 1988, Baibakov and Garushev 1989] and Canada [Cordell 1982] are candidates for thermal heavy oil recovery. Processes like steam injection, or other thermal recovery methods, which have extensively been used to recover heavy oil from non-fractured reservoirs,

5

were not applied to fractured reservoirs until the last decade or so. This was primarily because of the belief that the injected steam would bypass the oil through the fractures, leaving most of the oil unrecovered. The results of the experimental, theoretical and pilot tests published since the early 1980's show the feasibility of heavy oil recovery from fractured reservoirs using steam injection. However, satisfactory models are not available to predict the performance of this process, and there is no consensus on the major mechanism responsible for heat and fluid flow in these reservoirs, as reviewed below.

2.1.1. Experimental Studies

Nolan, Ehrlich, and Crookston [1980] performed experimental studies to show the applicability of steam injection in fractured reservoirs. They placed live-oil saturated cores in a steam environment, and observed that the bubble point pressure of the oil within the core was exceeded because of the temperature increase, and that the solution gas drive mechanism caused oil expulsion. Sahuquet and Ferrier [1982] reported hot water and steamflooding of fractured cores at high pressure and temperature. They found that natural imbibition was responsible for 13% recovery, another 9.5% was produced when hot water was used, and steamflooding caused an additional 44.5% recovery of the original oil-in-place (OOIP). Dreher, Kenyon, and Iwere [1986] performed experiments on fractured cores and found that imbibition at high temperature and CO_2 generation were among the active recovery mechanisms. Baibakov and Garushev [1989] tested the effect of temperature on imbibition and found that more oil was recovered at higher temperatures. It is worth noting that the imbibition process can be explained by a nonlinear diffusion equation [Dutra and Aziz 1992]. It is well known that the time scale of diffusion processes is inversely proportional to the second power of the characteristic length of the domain. Performing experiments under laboratory conditions with very small length scales compared to field conditions is believed to have exaggerated the role of capillary forces and the imbibition mechanism in many of the previous studies.

In order to investigate the recovery mechanisms during pressure cycling of fractured reservoirs under steam injection, Briggs, Beck, Black, and Bissell [1992] conducted several experiments. They found that flashing of the steam condensate and CO_2 generation were two of the important mechanisms in oil production. Reis [1992-a] reported low and high temperature imbibition experiments on various rock samples. He found that the average oil recovery at high temperatures was 50% more than that at low temperatures. He also conducted some experiments on samples with high carbon content,

6

that is kerogen, and found an increase of 13% in the porosity and 20-30% in the OOIP. The increase in OOIP was due to chemical alteration of the kerogen to liquid hydrocarbon. Jensen and Sharma [1991] conducted steam and hot waterflooding experiments through fractured and non-fractured cores. They found that imbibition was not an important recovery mechanism in oil-wet carbonate rocks. Instead, thermal expansion was found to be the dominant mechanism.

2.1.2. Field Studies

Few field tests of steam injection in fractured heavy oil reservoirs have been reported; however, positive results were obtained. Sahuquet and Ferrier [1982] reported a pilot test on the highly fractured carbonate reservoir of Lacq Supérieur in France. In spite of a high initial water saturation, and a low matrix permeability, the results of the pilot test have been promising. They observed an increase in the production rate shortly after steam injection, and reported no heat breakthrough during the operation. Cordell [1982] reported on the encouraging results obtained from a single well cyclic steam stimulation pilot test performed on the fractured vugular formation of Grosmont. The OOIP of the reservoir was estimated to be above one trillion barrels of bitumen [Cordell, 1982]. Antoniadi et al. [1988] reported on cyclic steam injection in the heavy oil fractured reservoir of Zybza in the former U.S.S.R. Initial cycles increased the production rate 10 to 20 times. The cumulative steam-oil ratio (SOR) was 3-3.5. Continuous steam injection in the fractured Usinskoye reservoir was reported also by Antoniadi et al. [1988]. Due to early steam breakthrough the operation was later changed to water alternating steam injection. This improved the thermal efficiency of the operation and the SOR averaged 2. A pilot steam drive operation on the heterogeneous fractured formation of Emeraude was reported by Couderc, Monfrir Quettier, and Sahuquet [1989]. After 14 years of primary production only 3% of the OOIP was recovered. A pilot steam drive was initiated to decrease the viscosity of the 100 mPa s crude and to introduce an additional drive mechanism into the reservoir. After two years of operation, the production rate had increased significantly in some of the producing wells. Although the expansion of the steam zone was not uniform and a temperature increase in some of the producing wells was observed, no steam breakthrough had been reported after two years of operation. The cumulative SOR was about 3.6 during this period.

2.1.3. Mathematical Studies

Different numerical and a few analytical predictive models have been developed to study steam injection in heavy oil fractured reservoirs. Based on the assumption that heat conduction from steam carrying fractures to the matrix blocks can smooth out the propagation of the heat front, Nolan *et al.* [1980] used a conventional thermal simulator with average matrix-fracture properties. Later, double-porosity models were used. Briggs [1989] developed a simulator for predicting the performance of cyclic steam injection in naturally fractured reservoirs and investigated the process. No attempt was made to use grid refinement. However, single block studies using sub-domain techniques have shown that erroneous results are obtained if the matrix block is modelled as a single grid point. Dividing individual matrix blocks into several computational grids for refined modelling of transient phenomena such as gravity drainage and gas diffusion was suggested by Saidi [1975]. He used a double-porosity model incorporating the fine-gridding approach to match the history of a naturally fractured reservoir in Iran [Saidi, 1975] . While Saidi [1983] qualitatively explained the sources of error that would occur when matrix blocks are simulated by a single grid, recent studies [Palatnik, Shandrygin, and Segin 1992] quantified some of these errors. The first double-porosity thermal simulator which incorporated fine-gridding was developed by Pruess and Narasimhan [1985]. They used their model to study the behaviour of geothermal reservoirs. Later, Chen, Wasserman, and Fitzmorris [1987] allowed sub-gridding in their thermal simulator and studied steam injection in a five-spot in a naturally fractured reservoir. They found that gravity drainage could be one of the important recovery mechanisms. The authors concluded that heat was transferred by both conduction and convection mechanisms. Dreher *et al.* [1986] studied heat and fluid flow in fractured reservoirs numerically, and found that conduction only, was the dominant mechanism for heat transfer. Lee and Tan [1987] incorporated a triple porosity idea [Abdassah and Ershaghi 1986] in their thermal model. They also accounted for fluid flow between matrix blocks; that is, their model applied to multiple permeability systems as well. Through their isothermal single phase examples, Lee and Tan [1987] showed that fine-gridding was necessary for modelling the transient behaviour within the matrix blocks. Jensen and Sharma [1991] used fine-gridding in a conventional thermal simulator to model their experimental results of water and steamflooding through fractured cores. Oballa, Coombe, and Buchanan [1993] performed a sensitivity analysis to study different fine-gridding techniques in various double-porosity and double-permeability thermal models. Recently Sumnu, Aziz, Brigham, and Castanier [1994] used

8

a commercial thermal model to perform sensitivity studies on certain flow properties, e.g., capillary pressure, and also to design their experimental study.

Several investigators using mesh refinement have concluded that modelling transient phenomena within individual blocks is crucial in accurate modelling of the response of fractured reservoirs [Saidi 1983, Gilman 1986, Chen *et al.* 1987, Hoire, Firoozabadi, and Ishimoto 1990]. Although such models were able to predict the detailed behaviour of individual blocks with significant accuracy, these models incorporated large systems of equations and required increased computational time and memory. In an attempt to overcome this problem Pruess and Wu [1993] developed a semi-analytical double-porosity model, which used simple trial functions representing the transient temperature distribution due to heat conduction from fractures into the matrix blocks. The functions were obtained at each time step by satisfying an integrated form of the heat equation for the corresponding block. As this assumed no convective heat transfer, the authors used their model for a fracture network within an impermeable medium where no fluid flow could occur between the fracture and the matrix blocks. They extended their model to single phase non-isothermal flow between a fracture system and permeable matrix blocks, where gravity and capillary forces were not important, such as geothermal reservoirs containing hot and cold water. In such a system, fluid flow could be explained by a single phase diffusivity equation, which is analogous to the heat conduction equation. Satman [1988] used an analytical approach to study heat flow in a fractured geothermal reservoir. He ignored the effect of fluid flow within the blocks and solved the heat equation analytically for the fracture and the matrix.

As noted, different studies have revealed different mechanisms to be the dominant one in heavy oil recovery from fractured reservoirs. This is due to the fact that thermal recovery of heavy oil from fractured reservoirs is a complicated process. Heat transfer mechanisms – conduction and convection – are coupled with fluid flow in two different media, through the temperature dependence of viscosity in Darcy's law. Multiphase fluid flow occurs under the interaction of gravity, capillary and viscous forces, with different degrees of importance of the forces in the fracture network and in the primary porosity. Considering capillary forces, for example, recovery is enhanced from a water-wet matrix block when these forces are stronger and water imbibition is active, and the reverse is true when gas-oil gravity drainage is active. In the fracture medium the role of capillary forces is traditionally neglected. However, many studies show a large effect of fracture capillarity on the behaviour of double-porosity systems [Saidi, Tehrani, and Wit 1979,

9

Firoozabadi and Hauge 1990, Labastie 1990, Oballa *et al.* 1993]. Although the interest in understanding the behaviour of naturally fractured reservoirs has grown considerably, recent studies [McDonald, Beckner, Chan, Jones, and Wooten 1991, Palatnik *et al.* 1992] show that there are even more areas that should be investigated thoroughly, before one can model even the isothermal processes effectively.

2.1.4. Gravity Drainage

In the process of oil recovery from fractured reservoirs different recovery mechanisms are involved. However, imbibition and gravity drainage are believed to play the largest role [Saidi, 1987]. There is ongoing debate on the superiority of gravity drainage over imbibition [Saidi 1987, Chen *et al.* 1987, Briggs *et al.* 1992]; however, different studies have indicated that in fractured reservoirs that exhibit oil-wet behaviour the displacement efficiency by gas-oil gravity drainage is higher than that by water [Saidi 1987, van Wunnik and Wit 1992, Macaulay *et al.* 1995]. Unfortunately, few pieces of information on thermal gravity drainage of heavy oil in fractured reservoirs have been published. Pooladi-Darvish [1992] and Kharrat, Jamialahmadi, Pooladi-Darvish, and Vossoughi [1993] reported on experimental results of thermal gravity drainage of heavy oil from a single block. Their experiments were not scaled and they chose a high permeability for a 2-D sand pack model to be able to perform their experiments in a reasonable time. They concluded that the process was dominated by heating of oil in a thin layer ahead of the steam-oil interface, reducing the oil viscosity to a small value, and then the drainage of the oil due to the density difference with steam. In their experiments gravity drainage of heating oil occurred ahead of an advancing steam-oil interface which swept the porous medium from top and lateral fractures toward the bottom of the sand pack. van Wunnik and Wit [1992] assumed gravity drainage of heated oil from blocks of fractured reservoirs. They proposed the improved gas-oil gravity drainage of the heavy oil of the Qarn Alam reservoir in Oman by steam injection. They considered small matrix blocks and assumed thermal equilibrium between the fracture and matrix media. In other words no temperature gradient was allowed in the blocks hence, the gravity drainage occurred always as a 1-D top down process. The numerical studies of Chen *et al.* [1987] indicated that gravity drainage became an important recovery mechanism during the later stages of steam injection in a double-porosity system. However, this was not confirmed by other studies. Using a thermal simulator, Dreher *et al.* [1986] found that gravity drainage was not an important recovery mechanism in thermal recovery from fractured reservoirs.

10

2.2 Non-Isothermal Gravity Drainage in High Permeability Porous Media

Thermal oil recovery by steam injection is by far the most important enhanced oil recovery (EOR) method. In 1988 and 1994, respectively, more than 70% and 60% of the oil recovered by various EOR methods in the U.S. was produced by the application of steam [Blevins 1990, Moritis 1994]. Traditionally, two methods of steam injection have been implemented: steamflooding and cyclic steam stimulation (CSS). However, advances in technology and ease in drilling of horizontal wells on one hand, and special fluid and rock properties of different reservoirs on the other, have resulted in innovative methods of heavy oil recovery by steam injection. In reservoirs which contain a heavy oil with very high viscosity and low initial steam injectivity, formation parting has been used to introduce the required heat into the reservoir. Formation fracturing has been implemented in CSS techniques at Cold Lake [Denbina, Boberg, and Rotter 1991], and in steamflooding techniques in the bituminous reservoirs of Texas [Soni and Harman 1986]. Numerous studies have shown that gravity drainage of heated oil is an active recovery mechanism in all of the above techniques. This is especially true for thick reservoirs with high vertical permeability.

The large contact area of the horizontal wells with the formation provides the condition to take advantage of the slow process of gravity drainage and satisfy economic requirements of a project through the Steam-Assisted Gravity Drainage (SAGD) process [Edmunds *et al.* 1994].

In the following the above techniques are briefly reviewed, and the role of gravity drainage is explained as an important recovery mechanism.

2.2.1 Cyclic Steam Stimulation (CSS)

Farouq Ali [1994] recently reviewed the success of the CSS process in Canada, and pointed out the modifications that the process has experienced to achieve high performance in the bituminous reservoirs of Alberta. While CSS might vary from field to field [Farouq Ali 1994], the basic process uses a single well as an injector and producer. Steam is injected into the reservoir for two to four weeks, and the formation is allowed to absorb the heat for a few days after injection ceases. The injection well is then put on production, and the heated oil around the well is produced. The cycles may be repeated as

11

long as the process is economical. CSS is mostly known as a stimulation technique, and its success relies on the drive mechanisms in the reservoir which were less active prior to steam injection due to the high oil viscosity. In the CSS process the heated mobile oil is produced without any necessity to drive it through the cold reservoir, as required in the steamflooding technique. Hence, CSS is an attractive recovery method when high in-situ viscosity of the oil does not permit a continuous steam drive. The disadvantages of the process are the low ultimate recovery achieved by the process, and the high density of the wells required.

As previously mentioned the success of the process mostly relies on the recovery mechanisms present in the reservoir. During the initial cycles the primary drive mechanism is often reservoir compaction and solution gas drive [de Haan and van Lookeren 1969, Denbina et al. 1991]. Later, however, these mechanisms lose their importance and gravity drainage of the heated oil plays a stronger role. A comprehensive simulation study of CSS operations in Cold Lake [Denbina et al. 1991] indicated that gravity drainage became a significant recovery mechanism in later cycles. Unfortunately, modelling of CSS is complicated by severe multiphase flow in the heated region and repeating saturation and desaturation of the porous medium. Solutions of the highly nonlinear equations of such a process are obtained by numerical methods using thermal simulators [Tortike and Farouq Ali 1993] and is beyond the scope of this study. Under major simplifications, however, an analytical model was developed. Towson and Boberg [1967] developed the earliest model for predicting gravity driven oil flow by cyclic steam injection. They considered a heated zone saturated with heavy oil at a constant viscosity where most of the oil flow occurred. In their model the authors accounted for gravity and pressure driven flow. The study showed that gravity drainage of the heated oil was an important recovery mechanism, especially in thick formations with high permeability.

2.2.2. Steamflooding

In steam drive projects pressure forces are the main driving force for oil production before breakthrough; however, the production rate might be low due to the low mobility of heavy the oil [Vogel 1992]. After breakthrough the pressure gradient in the steam zone drops to a small value which exerts a minimal driving force on the oil bank, and gravity drainage of the heated oil below the expanding steam zone dominates the process [Vogel 1992]. A steamflood project is called mature if the overlying steam breaks through to the production well. Edmunds [1984] studied the effect of pressure

12

drop due to steam flow on oil production after breakthrough. He concluded that steam was not an efficient fluid for creating a pressure drop because its kinematic viscosity is too small as compared to its heat content.

Several analytical and semi-analytical models have been reported in the literature to predict the behaviour of thermal recovery processes under strong overlay conditions. Miller and Leung [1985] considered a horizontal stationary oil-steam interface and used the analytical solution for heat conduction in a semi-infinite reservoir to describe the temperature distribution. Numerical integration was used to obtain the oil flow. Kumar, Patel, and Denbina [1986] accounted for the downward movement of the horizontal interface and obtained the temperature solution. Again, numerical integration was necessary to incorporate the effect of varying viscosity on the flow rate, and also to proceed in time. Closmann [1995] considered mature steam drive projects under strong override conditions. He used the exponential form of the temperature distribution ahead of a horizontal interface which corresponded to steady-state conditions, obtaining analytical solutions for the oil rate under gravity drainage where oil was allowed to flow horizontally only. Recently, Kimber, Deemer, Luce, and Sharpe [1995] developed a model to calculate the oil flow rate by gravity drainage and pressure forces in mature steamfloods. They used a normalized equation to approximate the unsteady-state temperature distribution ahead of an advancing steam front. The authors assumed a heated region with a constant viscosity around the production well. They found that implementing an extra pressure drop by producing steam beyond the heat requirement of the process marginally increases the net oil production rate when the steam zone is small. It was shown that it is detrimental to the process to produce extra steam for an additional pressure drop when the steam zone gets large in the later periods of the process.

Most of the predictive models either neglected the effect of a moving interface or assumed steady-state for the heating process. These two cases refer to two extremes considering the movement of the interface. The effect of the moving boundary can be neglected when the interface is moving very slowly, and the steady-state assumption may be justified when the interface is moving fast. However, none of these assumptions may be valid when many of the heavy oil reservoirs are considered. This is because the interface movement is fast enough to affect the heating process considerably, but is not fast enough for steady-state conditions to be assumed.

13

As noted, most of the available models assumed an *a priori* known shape of the oil-steam interface; that is, horizontal in the case of override problems. A major contribution in modelling the shape of an oil-steam interface was due to van Lookeren [1983]. He analytically obtained an equation for the steam zone thickness. His solution incorporated a pseudo-mobility ratio M^*, which was a function of oil viscosity at an unknown temperature. In practice the oil viscosity at steam temperature has been used [van Lookeren 1983, Palmgren, Bruining, and de Haan 1989]. The parameter M^* included the local steam and oil velocities, which were unknown unless the flow equations were completely solved. Nevertheless, the equation derived by van Lookeren satisfactorily predicted the oil-steam interface in several cases [van Lookeren 1983, Palmgren *et al.* 1989].

Palmgren *et al.* [1989, 1991] developed a numerical model for steam drive processes which was fundamentally different from other thermal simulators. They assumed a sharp interface between the steam and oil zones, and used an interface equation in analogy with fresh-salt water interface movement in porous media. This interface equation was coupled with a steady-state heat balance on the interface, and fluid flow equations written in the stream function formulation. Their formulation applied to incompressible fluids. The steady-state heat and fluid flow assumptions permitted de-coupling of the processes and offered major simplifications in the model [Bruining, Duijn, and Palmgren 1990]. They considered two possibilities for the steam condensate to penetrate ahead of the interface. The two fluids were considered to make a single phase with average properties, or the water was permitted to form an under-running water tongue under steady-state conditions. The mathematical model was then solved using finite element techniques. They included heat loss effects and concluded that heat loss to the cap rock postponed steam breakthrough. The authors performed experimental studies to validate their model and reported qualitative agreements. Palmgren and Bruining [1992] presented a similar model applying to steady-state heat and fluid flow ahead of the interface. They invoked the Dupuit assumption and obtained a first order nonlinear hyperbolic equation for the location of the interface. The latter was subsequently solved using the method of characteristics. The authors compared their solutions with those of van Lookeren [1983], and Marx and Langenheim [1959].

The Dupuit assumption or segregated flow theory, as used by many of the previous investigators, neglects any flow in the vertical direction; that is, normal to the bedding in tilted formations. The fluids are considered to flow horizontally due to

potential gradients caused by gravity forces. It has been shown by Dietz [1953] and Yortsos [1991] that segregated flow theory can be a good approximation for 2-D flow in homogeneous systems; however, its application to thermal recovery processes, where a large viscosity variation is present over short distances, is not yet justified.

2.2.3. Fracture-Assisted Steamflood Technology (FAST)

Steam injectivity in bituminous reservoirs is usually very low. This is due to the high viscosity and immobility of the in-situ oil. Fracturing is used to attain the necessary injectivity. The Fracture-Assisted Steamflood Technology (FAST) was developed and implemented in the bituminous reservoirs of Texas [Britton, Martin, Leibrecht, and Harman 1983]. In the FAST process, each producing well is hydraulically fractured to create horizontal fractures and then stimulated to heat the formation around the wellbore. Subsequently, the injection well is fractured to create communication between the injector and producers. This is followed by high rate steam injection to keep the horizontal fracture open. Subsequent to communication between the injector and producers, the injection rate is lowered to permit distribution of steam over a larger portion of the pay zone. Water injection through the horizontal fractures is used as the last stage in the process to recover additional oil.

Application of the FAST process in two pilot tests has been reported in the literature. Britton *et al.* [1983] presented the results of bitumen recovery from the Street Ranch pilot containing ~2 °API crude. They achieved a steam-oil ratio (SOR) of 10.9. In a second pilot the SOR was improved to 8.02 [Stang and Soni 1987]. Soni and Harman [1986] performed simulation studies to investigate the important recovery mechanisms in the FAST process. The authors concluded that gravity displacement of the tar from the rock matrix to the horizontal fracture was the primary recovery mechanism in the FAST process. The tar in the fracture was then pushed towards the production well as an oil-water emulsion.

Counter-current flow of oil and steam above steam-heated fractures was observed previously by Closmann and Smith [1983]. The authors found that a steam-oil interface was formed and traveled upwards through the reservoir, while the oil above the interface was heated and drains downwards to the fracture. Edmunds [1984] referred to this process as ceiling drainage. Of course, not much of the oil below the fracture is produced

15

due to gravity forces, as the lighter steam is already located in a stable situation above the heavy oil.

The gravity drainage of oil from the rock matrix as observed in the FAST process, and its subsequent transfer to the production well is very similar to the underlying recovery mechanism in steamflooding of naturally fractured reservoirs as practiced in the Usinskoye field [Antoniadi *et al.* 1988]. In the latter case, of course, fracturing of the injection and production wells is not required.

2.2.4. Steam-Assisted Gravity Drainage (SAGD)

Conventional steamflooding has been used for many years in heavy oil reservoirs where the in-situ oil is mobile at the reservoir temperature. However, application of the same process for bituminous reservoirs is limited due to the high viscosity of the bitumen flowing towards the production well through the cold reservoir. The Steam-Assisted Gravity Drainage (SAGD) process was proposed as a thermal recovery method which permits bitumen production while it is hot [Butler, McNab, and Lo 1981]. In the SAGD process, for the most part, the gravity forces are responsible for the stable displacement of the oil. The stability of the process ensures a high displacement efficiency at the pore level. Gravity forces, however, create a limited potential gradient in a reservoir, resulting in a low flow rate. For example in a heavy oil reservoir the maximum potential gradient created by gravity forces is about 10 kPa/m.

The oil recovery methods based on gravity drainage are successful only if a large portion of the reservoir is contributing to flow. A high production rate from the light oil naturally fractured reservoirs of Iran with a matrix permeability in the range of 1 md, for example, is possible only because a large number of matrix blocks located in the secondary gas cap of these reservoirs contribute to flow. The high permeability of the fracture network ensures a minimal required pressure gradient in the fractures for oil flow. Hence, the producing wells can be located far from each other [Saidi 1987]. A well-spacing of 1000 m is not rare in these cases. The gravity drainage process in this case is analogous to rain. Although the rainfall per unit area might not be high, high flow rates in the collecting streams might be attained if the water is collected from a large area. In the SAGD process the large surface area required for flow is provided by the application of horizontal wells. The application of horizontal heaters to improve gravity drainage of heavy oil was investigated as early as 1953 by Higgins. His experimental studies showed

16

increased ultimate recovery from 40.4% to slightly above 52% when the viscosity of the oil was lowered from 6000 mPa s to about 50 mPa s. Realizing the importance of uniform heating, he used a horizontal heater and concluded that "the application of heat to stimulate gravity drainage from field reservoirs containing viscous oil will be practical if and when means are devised to heat the formation uniformly and at low cost." It seems that the SAGD process offers one means of achieving this goal. .

In the original version of the SAGD process [reviewed by Butler 1991] two horizontal wells are drilled at the base of the oil-bearing formation, one above the other. During the initial stage, steam is circulated through both of the wells to heat the bitumen located between the two wells and hence to establish communication between them. Subsequently, the upper well is used as the injection well, while the condensate and the heated oil is produced from the lower well as it is mobilized by the process. It is essential to avoid excessive differential pressure between the injector and producer to eliminate the chance of high steam production. During the early stages of the process, steam flows upwards in the reservoir while the bitumen located above the steam drains downwards in an unstable manner. Once, the steam reaches the top of the formation the process enters a new stage. The tendency of steam to override the bitumen ensures that the oil would be located below the steam. A steam-oil interface is formed that travels sideways through the reservoir as the oil adjacent to the interface is heated and flows downwards due to gravity forces. As the steam zone expands the inclination angle of the interface with the horizon decreases and the potential gradients due to gravity forces along the interface decrease. The systematic expansion of the steam zone ensures a high volumetric efficiency for the process.

Modifications of the SAGD process were proposed later to improve upon its performance. Application of vertical wells as injectors and producers was suggested by Griffin and Trofimenkoff [1985] and Joshi and Threlkeld [1985].

In order to avoid the cost of drilling two horizontal wells, a vertical injector together with a horizontal producer was used in Cold Lake. In such cases it is difficult to achieve uniform steam throughout the length of the horizontal well. This would decrease the active length of the well and would reduce the superiority of the horizontal wells over the vertical ones.

Hamm and Ong [1995] discussed the application of Enhanced Steam-Assisted Gravity Drainage (ESAGD). In the ESAGD process a pressure differential between two adjacent steam zones is created, once bitumen mobility far from the interface is obtained. This would accelerate the expansion of the steam zone, and is reported to improve the ultimate oil recovery [Hamm and Ong 1995].

The SAGD process is similar to the cyclic steam stimulation (CSS) in the sense that the hot oil is produced without any requirement to drive it through the reservoir. Many theoretical and experimental studies, as well as pilot tests have been performed to study the feasibility of the process and to determine if the low potential gradients created by the gravity forces are adequate for economical oil production.

2.2.4.1. Experimental Studies

Butler *et al.* [1981] reported limited experimental data using a 2-D model representing the application of horizontal wells in the SAGD process, and a 3-D model representing the expansion of the steam zone around a vertical well. The authors explained that the physical models were scaled to the Cold Lake reservoirs using two dimensionless groups. One of them ensured similarity of heat conduction between the field and model, and the other one was related to the movement of the interface. The authors presented an analytical model for the SAGD process that slightly overpredicted the experimental data. Griffin and Trofimenkoff [1985] presented experimental data, using 2-D and 3-D models. They investigated the expansion of a steam zone created around a vertical injector located above a horizontal producer. The authors modified the original SAGD theory [Butler *et al.* 1981] to obtain closer agreement with their experimental data. They concluded that the surface area of the steam zone exposed to the overburden for heat loss was not as predicted by the original theory, and that the process was feasible. Joshi and Threlkeld [1985] performed experiments to study the effect of various well configurations on the SAGD process. They examined three well configurations: a horizontal wellpair, a vertical injector located above a horizontal producer, and a single vertical well with dual completion used as injector and producer. As mentioned earlier, it is possible to perform the SAGD process with short distances between the injector and producer sites, because the pressure drop between them can be kept minimal. The authors varied the withdrawal rate from the producer and found that the increased production rate resulted in steam breakthrough, reducing the efficiency of the process. Among the three well configurations, the authors concluded that the

18

horizontal wellpair performed the best. Joshi and Threlkeld [1985] studied the effect of fractures on the process and found that vertical fractures improved gravity drainage of the heated oil, hence improving the performance of the process.

Chung and Butler [1988-a, 1988-b] reported the results of several 2-D experiments representing the application of horizontal wells. Their experiments were scaled based on a criterion given by Butler [1985-b] for Cold Lake and Athabasca reservoirs. The authors reported general agreement between the experimental data and the theoretical predictions of a semi-analytical model presented by Butler [1985-b], and indicated that closer spacing between horizontal wells improved the performance of the SAGD process; however, it did not affect the ultimate recovery. Chung and Butler [1988-b] also studied the effect of location of the injection well. When the injection site was located farther up in the reservoir the heat communication between the two wells was established by circulating steam in a vertical injector. Of course, this would not be easily possible if a horizontal injector were located up in the reservoir. Introducing steam from the upper part of the reservoir enhanced the performance of the process by reducing the amount of water-oil emulsion that was produced, particularly when the steam zone rose in the reservoir. Of course, the relative importance of the location of the injector would depend on the duration of the upward movement of the steam zone compared with the period of sideways spreading of it under field conditions.

Further experiments on the application of the vertical wells as injectors were reported by Liebe and Butler [1991]. The authors used a scaled cylindrical model where the scaling was performed based on dimensionless groups found previously for the linear case and application of horizontal wells [Butler 1985-b]. A combination of a vertical injector with three types of producer were studied. Vertical, horizontal and planar production wells were used. The producing wells could be thought of as a point, a line, and a plane sink at the bottom of the steam zone, for the three well types named above, respectively. Although the experiments were scaled for gravity forces as the driving mechanism, pressure forces were implemented, too. Steam production was avoided, however. The results indicated that the planar well achieved the highest production rate followed by the horizontal and the vertical well. A ratio of 2 to 3 was the difference in production rate when different production wells were implemented. The authors reported experimental results for two different pressures and two different reservoir crudes.

Recently, Zhou, Zhang, Shen, and Pu [1995] reported the results of several scaled experimental studies where they investigated various well configurations for heavy oil recovery from a reservoir containing an 11,000 mPa s crude at the initial reservoir temperature. The experiments were scaled for gravity and pressure forces using the criteria developed by Pujol and Boberg [1972]. Their reported experimental data showed that the scaling criterion given by Butler [1985-b] was nearly satisfied in their experiments. The results indicated that application of horizontal wells in a line drive configuration gave much better results compared to the other configurations experimented with, including the wellpair configuration in the SAGD process. The authors explained that a process based on gravitational forces, SAGD, was much slower than a line drive process where gravitational and pressure forces were both implemented. In a slow thermal process there is much time for heat loss, resulting in a poor thermal efficiency. Regarding the above conclusions two important points should be considered. Realizing the fact that heat loss would be more severe in a slow process with the same degree of override behaviour, it is not clear if the experiments performed by Zhou et al. [1995] were scaled with respect to heat loss effects. If not, their results would not show the performance of a thermal project under field conditions with respect to heat efficiency. Secondly, pressure forces can be used in a reservoir where the oil at initial reservoir temperature has some mobility. For the bituminous reservoirs of Alberta with initial viscosities in the range of 10^5 to 10^6 mPa s, pressure forces cannot play a major role unless significant heating has occurred. In the case of the bituminous reservoir the advantage of the horizontal injectors is to improve sweep efficiency. This is because high injectivities can be obtained by the application of horizontal injectors while keeping the local steam velocity low, establishing a more stable process compared with vertical wells. The large contact area of the horizontal injector with the formation provides the opportunity to create a large steam zone in a stable manner and in a relatively short period of time, minimizing the heat loss.

The study reported by Zhou et al. [1995], however, suggests that in a SAGD process after appreciable heating of oil between adjacent steam zones has occurred, pressure forces may be used to accelerate the process and to improve efficiency. The ESAGD process, as explained previously, aims to take advantage of the pressure forces by creating a differential pressure between adjacent steam zones and creating some drive mechanism, while the oil drained by gravity forces is produced as well. It can be speculated that changing the process from SAGD to a line drive might be more efficient at a certain time in the project.

The benefits that horizontal wells offer in performing thermal oil recovery with improved efficiency is an area of active research and interest. Escovedo [1995] proposed different conceptual steamflood designs using horizontal wells for three different fields with the aim of maximizing project profitability. In his conceptual designs he tried to maximize the sweep efficiency before breakthrough and to minimize the negative effects of steam on producing wells, should breakthrough occur.

2.2.4.2 Field Studies

Adegbesan, Leaute, and Courtnage [1991] described the first pilot test of the SAGD process. In this pilot a single vertical injector was placed above a horizontal producer in the oil sands of Cold Lake. After the initial stimulation of the production well, steam was injected above formation parting pressure and the horizontal well was put on production. A combination of log analysis, temperature measurements, seismic data and mathematical modelling was used to investigate the process and estimate the contribution of the different drive mechanisms. It was found that the main drive was due to pressure forces at the initial stages of the process, whereas gravity drainage of the heated oil played an important role during the later years of the operation. The authors concluded that the horizontal well produced about 20 to 30 percent of the oil in the heated area in 8 years of operation with a cumulative SOR of 2.85. It was believed that about 40% of the length of the horizontal well actively contributed to the production, and the other 60% was located beyond the steam zone, and did not contribute to the production.

The first pilot test of the SAGD process using horizontal wellpairs was performed by AOSTRA and industry at the Underground Test Facility (UTF) at Fort McMurray, Northern Alberta. Numerous articles have discussed different stages of Phase A of this operation, which was performed by using three wellpairs of 60 m length, located about 25 m apart from each other [Edmunds 1987, Edmunds et al. 1988, 1994]. Design considerations, preliminary numerical simulation studies and discussion of the sources of uncertainty in the operation were presented by Edmunds [1987]. The effect of vertical permeability and accumulation of non-condensable gases were thought to be the most critical parameters affecting the performance of the process. Lower vertical permeability than expected would have caused a lower drainage rate. On the other hand, non-condensable gases would have accumulated at the oil-steam interface and resulted in a lower steam temperature. This was believed to lower the drainage rate, but not to increase

the SOR due to the insulation effects of the gases at the cap rock. A single horizontal well cyclic steaming process was examined using a thermal simulator and was suggested as an alternative to the wellpair process. As pointed out previously, one of the benefits that horizontal wells offer over vertical wells is the extended area exposed to the reservoir. In the SAGD process this factor can be considered to be beneficial to the process if the total length of the well is exposed to the hot oil draining from beyond the steam zone. In a cyclic steam stimulation process it is difficult to achieve uniform steam injection over the length of the horizontal injector [Farouq Ali 1994]. The experience of the UTF project indicated that this can be more easily achieved in a continuous steam injection and oil production process.

In a later paper, Edmunds, Haston, and Best [1988] investigated in more detail the different stages of a SAGD process and examined the effect of different variables on the performance of each stage of the process. During the initial stage of upward movement of the steam zone, the process was believed to be governed by a counter-current flow of oil and steam. The authors explained that a CSS process was not used because in such a process counter-current flow would take much longer. Of course, due to relative permeability effects, counter-current flow of oil and steam is much slower than single phase flow of steam behind and that of oil ahead of the interface. The second stage, called slope drainage, occurred after the steam zone reached the cap rock and expanded sideways. During the latter stage the heated oil ahead of the interface drained downwards due to gravity forces.

Recently, Edmunds et al. [1994] reviewed the experience of Phase A of the SAGD process at the UTF site. Three years of operation were explained in detail. The SAGD process as implemented at the UTF site was followed by a blowdown period during which a large portion of the heat accumulated in the steam zone was recovered by evaporation of the irreducible water while pressure dropped. After three years of operation, 50% of the original bitumen in place within the pattern area was recovered at a cumulative SOR of 2.5. No major problems, common to in-situ operations were reported. The authors briefly described Phase B of the operation involving three horizontal wellpairs of 500 m length.

After the successful experience of the SAGD process at the UTF site in Fort McMurray much interest has been shown in using the SAGD process for thermal recovery of heavy oil and bitumen in Canada. This is because large resources of bitumen

22

in Alberta seem to be amenable to economical production using this process [Donnelly and Chmilar 1995]. Variations of the process are being considered should they improve the economy and performance of the project. Flue gas injection was suggested by Edmunds and Suggett [1995] as a means of heat recovery after substantial heat is stored in the steam zone. The injector and producer were designed to be far from each other, although above one another, to partially take advantage of pressure forces before steam communication between the two wells is established. Of course, initial mobility of reservoir crude is necessary for such a design.

Hamm and Ong [1995] discussed the application of an Enhanced Steam-Assisted Gravity Drainage (ESAGD) process to the bituminous reservoirs of Peace River, Alberta. In the ESAGD process a differential pressure is created between adjacent steam zones, once the oil far from the interface is adequately heated. Simulation studies of Hamm and Ong [1995] indicated that a relatively small differential pressure, of the order of 500 kPa, was required to achieve the desired enhancements. After sufficient time, 10 years for the cases studied, up to 50% increase in oil recovery was observed. This did not adversely affect the thermal efficiency of the process and an SOR of about 3 was obtained. The authors studied the effect of different factors, including the magnitude of the pressure differential, pattern spacing and accumulation on non-condensable gases. They found that the accumulation of the non-condensable gases was negligible if limited steam production from the production wells was allowed, and negligibly affected the steam zone temperature. The ESAGD process is believed to improve the economy of thermal recovery methods presently employed in Peace River, and is currently in the production phase.

2.2.4.3. Mathematical Studies

But McNab and Lo [1981] introduced the concept of the SAGD process, and presented the first analytical model for predicting the performance of this thermal recovery method. The analytical model was developed for the sideways expanding phase of the steam zone, and offered closed form solutions for the shape of the curved interface, and the oil production rate. It should be noted that the SAGD process is a combined heat and fluid flow problem ahead of a moving boundary. The shape and location of the boundary is unknown *a priori*, and is found as a part of the solution. Such moving boundary problems are nonlinear, and analytical solutions can be obtained only under simplified conditions. Butler *et al.* [1981] neglected the time dependence of both the

23

processes of heat and fluid flow. The gravity driven fluid flow process approaches steady-state quickly, because oil reservoirs typically have a very large hydraulic diffusivity. This is especially true in the heated zone, where most of the flow is occurring. A steady-state assumption for the heat flow problem, however, might not be realistic. Butler [1985-b] presented an improved semi-analytical model by relaxing the steady-state assumption in the heat flow problem. In addition to the steady-state assumption, both the heat and fluid flow processes were considered to be one dimensional. Hence, the temperature distribution ahead of the moving interface was approximated by an analytical solution of 1-D heat conduction ahead of an interface moving with constant velocity. The velocity was allowed to vary in the vertical direction, but was assumed to be independent of time. Fluid flow, that is, gravity drainage of heavy oil, was considered to occur parallel to the interface at any location. Many other authors (for example, see Towson and Boberg [1967], van Lookeren [1983]) neglected the potential gradients in the vertical direction and assumed horizontal oil flow. It has been shown by Dietz [1953] and later by Yortsos [1991] that this assumption, that is, a segregated flow, can be a good approximation for 2-D flow in homogeneous systems, but its application for thermal recovery processes, where a large viscosity variation is present over short distances, has not been investigated yet. More discussion of this assumption is presented in Section 4.3 and in Chapter 8.

An additional implicit assumption in the development of the analytical SAGD model concerns the production of the drained oil from the bottom of the steam zone. It was assumed that all the heated oil ahead of the interface was produced once it reached the bottom of the steam zone. In other words no horizontal potential gradient was considered necessary for production of the oil ahead of the interface at the bottom of the steam zone. In practice, the required potential gradient may be provided by the established differential pressure between the injector and the producer. In the SAGD process, the production pressure is adjusted such that excessive steam production is avoided.

The analytical model predicted a curved steam-oil interface that traveled through the reservoir. A singularity was found for the location of the top of the interface just below the cap rock. This behaviour was also observed in a later 1-D model reported by Butler [1985-b]. The analytical model presented by Butler et al. [1981] successfully matched the production rate as obtained from a 2-D experimental model. Butler and Stephens [1981] presented a modification of the original SAGD model, that resulted in a more realistic shape for the interface. The bottom of the interface, as predicted by the

24

original model, moved horizontally away from the production site. In reality, the bottom of the interface must be at the production site to avoid steam production. The authors suggested that tangents drawn from the production site to the curves predicted by the original theory would represent the actual steam-oil interface more realistically. The authors showed that the modification decreased the predicted production rate to about 87% of that predicted by the original model. The modification improved the match between the model and the experimental data. In a second part of their paper, Butler and Stephens [1981] developed a semi-analytical model that incorporated the effect of a no-flow boundary. In practice, a series of horizontal wellpairs are drilled parallel to one another. After sufficient time, the steam zones expand and coalesce. This would result in a reduced gravity head and decreased flow rate. The production rate as predicted by the original model for a steady-state moving interface in a semi-infinite medium was invariant with time. Incorporation of the no-flow boundary, that is, the coalescence of the adjacent steam zones, resulted in a production rate that decreased with time.

A further improvement on the original SAGD model was given by Butler [1985-b], when the 1-D heat flow was considered to be unsteady-state. A hot zone at steam temperature was considered ahead of the interface, and the extent of the hot zone was called the heat penetration depth. By performing a heat balance on the interface, the author derived an ordinary differential equation explaining the variation of the heat penetration depth with time. This method for finding an approximate temperature distribution for conduction dominated processes is very similar to the Heat Integral Method (HIM) as detailed in Section 4.3.

Using the above modification, Butler [1985-b] developed a semi-analytical model to predict the advance of a vertical element of interface with time. Hence, the shape of the interface and the production rate were found. An important measure of success of a thermal recovery method, i.e., thermal efficiency, unresolved by the previous models was discussed in more detail using this model. As mentioned previously, the singularity of the location at the top of the interface provided an infinite surface area of the overburden exposed to heat loss. Unfortunately, the same behaviour was observed in the semi-analytical model [Butler 1985-b] if small vertical elements were chosen. The author explained that there were other mechanisms controlling the velocity of the tip of the interface which were not considered in the model. The existence of a capillary region that restricts the steam flow behind the interface, and the effect of non-condensable gases that by reducing the steam temperature reduce the interface velocity, were mentioned among

others. Nevertheless, Butler [1985-b] presented his results using 20 vertical elements. The same number of elements was later used by Chung and Butler [1988-b]. The results indicated an oil rate of the same order as that obtained from the earlier models. Using this model, the authors studied the effect of variables such as well-spacing and steam temperature [Chung and Butler 1988-b].

Butler [1985-b] introduced a dimensionless group, B_3 in the development of the theory. The dimensionless group was a measure of convective fluid flow to the conductive heat transfer, as is the Rayleigh Number. More details on the effect of the Rayleigh No. in the SAGD process are given later. The semi-analytical model developed by Butler [1985-b] was later used in the study of the SAGD process [1988-a, 1988-b].

Reis [1992-b] presented a simple analytical model to predict the behaviour of the SAGD process. In addition to the major assumptions used by Butler *et al.* [1981], other simplifying assumptions were made to simplify the model. The shape of the steam zone was approximated by an inverted triangle. In other words, the author neglected any curvature in the shape of the interface. The bottom of the interface remained at the production site, and the top of the interface slid away along the cap rock. Reis [1992-b] assumed a temperature distribution in an exponential form, similar to the steady-state solution to 1-D heat conduction ahead of a moving boundary. He also incorporated an empirically found constant, so that the proposed model matched the previous experimental data. Due to the simplicity of the model, Reis [1992-b] was able to obtain closed-form solutions for the energy balance and the steam-oil ratio. The author compared the predictions of his model with the previous experimental data. Recently, Donnelley and Chmilar [1995] used Reis's approach to screen the bituminous reservoirs of Alberta for the SAGD process, and to select those that would meet certain economical limits. The authors indicated that Reis's model matched the results of the numerical simulation models for the UTF Phase B project more closely, when the shape of the steam zone was approximated by a half-ellipse rather than an inverted triangle. The authors assumed this would hold for all the cases studied.

Reis [1993] used an approach similar to that used in his linear model, to model the SAGD process in cylindrical coordinates for a vertical injector. He approximated the shape of the steam zone by an inverted cone. Again, an exponential expression was used to approximate the temperature distribution ahead of the interface. Analogous equations

for flow rate and heat requirement were found. His example showed an ever-increasing oil production rate with a constant slope.

Apart from the analytical and semi-analytical models reviewed above, commercial thermal simulators have been used to study the SAGD process [for example see Edmunds *et al.* 1988, 1994]. The numerical approach is totally different from that used in the analytical models. The thermal simulators evenly treat the whole domain under consideration, whereas the analytical models focus on the phenomena occurring ahead of the interface only. Additionally, more rigorous equations are solved in the commercial thermal simulators. Heat flow is modelled by solving a 2-D[2] conduction-convection equation and the potential distribution is found by solving a 2-D diffusive equation accounting for physical property variations with spatial coordinates. Both processes are considered to be unsteady-state. Other major differences concern the modelling of steam flow in gaseous and condensate forms and incorporation of capillary phenomena in thermal simulators. Despite the rigour of thermal simulators, they have their own drawbacks. In steam injection processes the potential gradients created in the steam zone are negligible compared to those in the oil zone. This results in a steam zone with an approximately constant steam temperature. A thermal simulator, however, does not distinguish between the steam zone and the oil zone, and performs all the calculations for both regions. Additionally, a process such as SAGD is believed to be minimally under multiphase flow. Numerical studies of the SAGD process have shown little dependence on the shape of the relative permeability curves assumed [for example see Kisman and Yeung 1995]. Capillary effects were also found to have minimal effect at the oil-steam interface in thermal processes [Palmgren *et al.* 1989]. In a thermal simulator, however, the highly nonlinear equations of multiphase flow are solved at each grid block without any optimization to use them if and where they are needed. The combination of the above effects makes it expensive to run a thermal simulator using fine grids. Additionally, in the SAGD process the maximum heat and fluid flow occurs in the vicinity of the moving steam-oil interface. The majority of thermal simulators, however, are based on fixed global coordinates, and are not designed for adaptive gridding with time.

In conclusion, thermal simulators might not be able to calculate accurately the temperature and potential distribution where these variables are most needed, that is at the interface. Nevertheless, the application of thermal simulators for field case studies is

---

2   3-D numerical modeling of the SAGD process has rarely been reported due to high computational expense of running thermal simulators for 3-D geometry.

practical due to the complexity of the input data. For mechanistic studies, however, simpler models are desirable. Development of a numerical model that is properly designed for the SAGD process, and accurately calculates the temperature and pressure potential fields where they are most important, that is, in the vicinity of the interface, and perform more approximate solutions in other regions is most needed. A first attempt to develop such a numerical model is discussed in Chapters 7 and 8.

2.3 Mathematical Modelling of Moving Boundary Problems

In many areas of engineering, formulation of a physical phenomenon considers a domain with moving boundaries. In these systems, equations can be written that specify the conditions on the moving interfaces; however, the shape and location of the boundaries are not known prior to the solution of the problem. Such problems occur in a wide range of engineering applications. Fluid flow through porous media, diffusion and heat transfer accompanied with change of phase or chemical reactions, formation of shock waves in gas dynamics and propagation of cracks in solids are among the examples named by Crank [1988]. The wide occurrence of moving boundary phenomena, and the challenge of modelling such processes have motivated researchers to develop mathematical models which have been published as numerous articles and books. In order to clarify the choice of the numerical model developed in Chapter 7, the different mathematical strategies are pointed out and their properties and behaviour are discussed briefly. The following review is restricted to numerical methods only.

2.3.1 Moving and Stationary Grids

Solution of partial differential equations of conservation laws for mass, momentum and energy in moving boundary processes which are formulated in the form of convection-diffusion equations are generally performed using two methods with respect to the computational grids. In the traditional fixed grid method a stationary computational domain is superimposed on the whole physical domain, and the conservation equations are solved for all the computational nodes. In such methods the moving interfaces travel through the computational domain. Voller, Swaminathan, and Thomas [1990] reviewed such methods with reference to the solution of one family of moving boundary problems, i.e., problems involving change of phase.

28

Alternatively, the moving physical domain may be transformed onto a general curvilinear and often non-orthogonal computational domain, where the moving boundaries are immobilized. In such methods, additional equations are required to follow the location of the interface. The solution of the interface equation is used to generate a new computational domain at each time step. The advantage of the latter method is that the governing equations can be solved on a fixed rectangular and often uniformly spaced grid system, with no loss of accuracy of computation near the curved boundaries. A comprehensive review of such adaptive gridding techniques is given by Hawken [1987].

A few articles have been presented that compare different aspects of both methods. Lacroix and Voller [1990] studied the problem of melting of a pure metal using the above methods. They considered conduction heat transfer in the solid region, and allowed for natural convection in the melt region. The authors concluded that for processes which involve a sharp moving interface, introducing a transformed computational domain was the obvious choice. If there was a considerable transition zone, of the order of the block sizes used, the fixed boundary methods appeared more attractive. This is because fixed grid systems smear the interface behaviour over one or more grids. The authors also pointed out that obtaining a higher accuracy in the vicinity of the moving interface where the flow variables changed more rapidly could be easily achieved in the transformed techniques. Hawken [1987] showed that, by locating more computational nodes in the regions of high gradient, higher accuracy and/or a saving in computational time was obtained. The authors discussed various methods that are used to properly distribute the computational grids over the region of interest. Viswanath and Jaluria [1993] studied a problem similar to that of Lacroix and Voller [1990], and compared the behaviour of models developed using the fixed and the moving grid techniques. The authors found that among the two computational strategies the transformed-grid method showed higher accuracy in predicting the interface location. Their transformed grid method typically required half of the computational time as compared to that required by the fixed grid method [Viswanath and Jaluria 1993].

A review of the literature indicates that in some studies involving flow through porous media, a sharp interface assumption has been used successfully to model a given process [Bear 1972, Crank 1988]. This assumption would of course, facilitate using the transformed grid approach. In many other studies, however, the transition capillary region was not neglected. Beckmann and Viskanata [1988] and Weaver and Viskanta [1986] studied problems involving change of phase in porous media. In these studies a fixed grid

29

approach was used and the conservation equations were solved over the whole domain. This approach is similar to what is used in the commercially available thermal simulators. To the best of the author's knowledge, apart from the simplistic analytical and semi-analytical solutions that were previously reviewed, there has been no numerical simulator developed for thermal recovery processes satisfying the transient conservation laws over an explicitly defined interface. In Chapter 7 a numerical model is developed which is based on conservation of mass, momentum and energy for the oil phase ahead of a moving boundary. An additional equation is derived to model the behaviour and location of the interface. In Chapter 8 the model is validated, and its applications and limitations are discussed. In the following section the transformed grid techniques, as used in the present numerical model, are discussed.

2.3.2. Discretization Approaches

Differential equations are generally solved using finite difference or finite element techniques. The traditional finite difference formulation is mostly replaced by a geometrically conservative form of this technique, called a finite volume formulation. In the latter technique, conservation is guaranteed regardless of the size of the grid blocks used in the modelling [Patankar 1980].

Hawken [1987] pointed out that the finite difference techniques require a higher degree of orthogonality and grid smoothness, compared with finite element methods, when used for the solution of moving boundary problems. Both of the methods have, however, their own advantages, and either of them may be chosen depending on the problem of interest and personal preference. Ramanathan and Ranganathan [1988] studied the problem of transient heat conduction in complex geometries, using both methods of finite volume and finite element techniques. They used a transformation through the solution of a set of elliptic equations in order to transfer the physical domain onto a simpler computational domain for their finite volume formulation. The technique guaranteed a high degree of orthogonality as will be reviewed next. For the cases studied they found that the transformed grid technique resulted in more accurate solutions while requiring less storage and computational time. Kececiouglu [1993] showed that adaptive gridding can be successfully used through a finite element formulation to accurately model convection-diffusion equations encountered in some porous media problems.

30

2.3.3. Transformed Gridding – Numerical versus Algebraic Techniques

There are generally two techniques available to map a physical domain with arbitrary and/or moving boundaries onto a fixed regularly shaped computational domain. To generate the computational coordinate system, algebraic transformations or solution of partial differential equations may be used. Thompson and Warsi [1982] and Thompson, Warsi, and Mastin [1985] presented a comprehensive discussion of the application of these techniques. In the algebraic method simple techniques such as normalization of boundary curves, and interpolation from boundary surfaces are implemented. The numerical technique, however, involves solution of a set of elliptic or hyperbolic differential equations. In many studies involving stationary but arbitrarily shaped domains, the numerical technique is preferred because it provides a higher degree of orthogonality and grid smoothness. This not only simplifies the development of the mathematical model, but also reduces the errors encountered when highly skewed grids are used. In the case of moving boundary problems, however, solution of the differential equations to generate the appropriate coordinate system at each time step might be computationally more expensive than solution of the actual conservation equations [Lacroix 1989]. In such cases an algebraic transformation is normally chosen.

A transformation named after Landau [1950] and its variants have been the most popular ones in the algebraic transformation of moving boundary problems incorporating change of phase. Landau [1950] introduced a normalization transformation to immobilize the moving interface between liquid and solid regions in a 1-D melting problem, and obtained an analytical solution. Other investigators used the above transformation in the numerical solution of multidimensional problems [Duda, Malone, and Notter 1975, Hsu, Sparrow, and Patankar 1981, Kim and Kaviany 1990, Lacroix and Garon 1992].

2.3.4. Complexities of Solution on General Curvilinear Coordinates

Thompson and Warsi [1982], among others, presented the general form of the partial differential equations on a non-orthogonal curvilinear coordinate system. The general transformation used created additional terms absent in the original equations. Physical interpretation and accurate modelling of such terms have been the subject of many articles. In the following the physical interpretation of these additional terms, when conservation equations are transformed onto a general non-orthogonal system, is reviewed, and their incorporation in the mathematical model is discussed.

31

2.3.4.1 Convective Term

When a transformation is used to immobilize a moving boundary, the coordinate lines of the new system pass through the physical transport domain, as if a convective flow existed in the final coordinate system. Hawken [1987] pointed out three methods that are commonly used to incorporate the additional convective term. In two of the approaches the convective term is initially ignored. In such cases the field variables obtained at the end of one, or a few, time steps are shifted to the new location of the coordinate system. An interpolation scheme is generally used for this purpose. If the movement of the coordinates is accounted for after every time step the method is called alternating node movement. The method is called a periodic node movement, if the adjustment is performed after a few time steps. The third approach is called simultaneous node movement and implies a technique where the convective terms are modelled as a part of the final differential equation. Earlier works on modelling moving boundary systems implemented the periodic and alternating approaches [Sparrow, Patankar, and Ramadhyani 1977]; however, the recent works consider the more accurate simultaneous node movement. Hawken [1987] pointed out that in processes that involve different time scales, stiff systems, instabilities may occur if the simultaneous node movement is not implemented.

In cases where the coordinate lines move in space, a geometric constraint, called the Geometric Conservation Law, has to be satisfied along with the original conservation laws. This is discussed later.

2.3.4.2. Cross-Diffusion Terms

Implementing a conservation law on diffusive flow involves flux terms that are perpendicular to the boundaries of a particular control volume. On a non-orthogonal coordinate system, the fluxes can only be computed along the coordinate lines which are generally not perpendicular to the boundaries of an element. For a 2-D problem then, fluxes along both coordinate lines should be incorporated to represent accurately a perpendicular flux. One of these terms, called the cross-diffusion term [Hsu et al. 1981], takes the form of a cross derivative term in the differential form of a conservation equation on non-orthogonal grids. Hsu et al. [1981] called these terms cross-diffusion terms in analogy with diffusion fluxes in anisotoropic systems, where a potential gradient

32

along one coordinate line creates fluxes along the other. The cross-diffusion terms have been neglected in earlier works [Sparrow *et al.* 1977], however, this is not recommended. Neglecting the cross-diffusion terms might lead to large errors depending on the degree of non-orthogonality of the coordinate system, and the importance of diffusive fluxes compared to convective ones. A review of the literature indicates that many articles were published in recent years to present a better physical interpretation of the cross-diffusion terms and to offer more accurate and trouble-free strategies to model them [Peric 1987, Halal and Lilley 1988, Karki and Patankar 1988, Schreiber 1990].

For a 2-D problem, incorporation of cross-diffusion terms in a finite volume formulation involves all 8 neighbouring nodes around a central node. This might result in a non-diagonally dominant matrix of coefficients which can lead to divergence in iterative solution techniques. It is for this reason that in the numerical solution of transport equations on non-orthogonal grids most of the researchers have treated the cross-diffusion terms as explicit, so that they appear at the constant side of the system of equations. For processes which involve different time scales, explicit incorporation of such terms can lead to unstability, unless very small time steps are selected.

2.3.4.3. Geometric Conservation Law

Thomas and Lombard [1979] explained that, when a transformation is applied to a differential form of a conservation equation, extra terms are introduced into the equation, and the Jacobian of the transformation appears as a multiplier inside the unsteady-state term. In cases where the Jacobian of the transformation is time-dependent, a geometric equation must be satisfied. The authors showed that the geometric constraint was in the form of the original conservation equations. Hence, the geometric constraint was named a Geometric Conservation Law (GCL). Thomas and Lombard [1979] solved the GCL simultaneously with the other conservation equations in the transformed domain. Demirdzic and Peric [1988] pointed out that the volume of a space element may change with time, if the problem is modelled on a general curvilinear coordinate with moving coordinate lines. They showed that the volume change of the space element should be accounted for, in order to avoid introduction of artificial mass sources. The Jacobian of a transformation is a representation of the volume of a space element in the transformed domain, and that the latter explanation of the Geometric Conservation Law was in accordance with that of Thomas and Lombard [1979]. Demirdzic and Peric [1988] showed that GCL is naturally satisfied if the coordinate system is moving in one direction

only. The authors introduced a procedure to satisfy the geometric conservation law in the solution of the conservation equations in the transformed domain, without any requirement to solve the GCL separately.

Hindman [1982] compared four different ways that a transformation may be performed on an unsteady-state transport equation in a differential form. The four methods were named non-conservation law form and strong, weak, and chain rule conservation law forms. He discussed the errors introduced if inconsistent methods are used for solving the equations in the transformed domain. His examples indicated that the chain rule conservation law form did not require any special condition, while it captured the shock behaviour of a nonlinear equation more accurately than the other methods. The computational time for solving the equations in the chain rule conservation law form was shown to be the minimum. The author concluded that: "More work is needed on the idea of geometrically induced errors," when conservation equations are solved on a general curvilinear coordinate system.

3. STATEMENT OF THE PROBLEM

Existing analytical models of gravity drainage do not consider thermal effects. The first objective of this work is to find analytical solutions for the fracture-matrix heat transfer and the gravity drainage problem under non-isothermal conditions. This model is to be used to study thermal gravity drainage in fractured reservoirs and the major factors affecting it. A scaling criterion for designing physical models for the study of non-isothermal gravity drainage in fractured reservoirs is to be derived.

The second objective of this work is to devise a new formulation and numerical model for non-isothermal gravity drainage in a porous medium. A new interface equation is to be developed, which could be used to locate the moving boundary to achieve the above goal. The numerical model is to be used to study the Steam-Assisted Gravity Drainage (SAGD) process, and the major parameters affecting it.

A third objective of the current work is to introduce the Heat Integral Method (HIM) for modelling diffusion dominated processes in porous media.

4. DEVELOPMENT OF THE ANALYTICAL MODEL

It was previously mentioned that gravity drainage is one of the most important recovery mechanisms in naturally fractured reservoirs [Saidi 1987]. However, an analytical model for non-isothermal gravity drainage of heavy oil in naturally fractured reservoirs, allowing for the unsteady-state temperature distribution in a single block, has not yet been reported. A previous analytical model [van Wunnik and Wit 1992] neglected the temperature gradients and assumed thermal equilibrium between the matrix and the fracture. Accurate modelling of gravity drainage requires an accurate model for heat flow. This is especially true for heavy oil and bitumen, since the viscosity of these liquid hydrocarbons is strongly dependent on temperature. There has been no consensus on the dominant heating mechanism in fractured reservoirs. Dreher *et al.* [1986] concluded that the rate of conducted heat into matrix blocks was the controlling factor; however, Chen *et al.* [1987] found that conduction and convection were both important. Experimental studies on high permeability matrix blocks reported by Kharrat *et al.* [1993] indicated that convective flow of steam into the porous medium was coupled with heat conduction into the cold oil. In their experiments a moving boundary was formed which was separated from top and vertical fractures and formed a concave downward interface between the steam and the oil [Pooladi-Darvish 1992, Kharrat *et al.* 1993]. Hence, these authors concluded that heat is transferred via conduction ahead of a moving boundary.

The first objective of this chapter is to examine if heat conduction is the only important heat transfer mechanism when a matrix block saturated with heavy oil is surrounded by fractures filled with steam. After this is confirmed the gravity driven oil flow will be modelled analytically.

4.1 General Features and Assumptions of the Model

Figure 4.1 shows schematically a cross section of a fractured reservoir where steam injection has driven the oil in the fracture network, and a steam zone is created surrounding low permeability matrix blocks saturated with heavy oil. Double-porosity theory [Warren and Root 1963] assumes that fractures are the only path for flow and matrix blocks act as individual sinks or sources in the fracture system. Based on the hypothetical behaviour explained above, it was decided to study a single block of a fractured reservoir under steam injection. By using the assumption involved in the theory of double-porosity models any interaction between individual matrix blocks was ignored.

Consider a single block in the shape of slab or cylinder with a large ratio of height to width. This assumption is made so 1-D heat flow may be considered. In reality, a matrix block has a 3-D configuration, and steam will be in contact with a single block from all six surfaces. It is believed that the steam-oil interfaces at the top and the bottom of the block are not as active as the lateral ones. This is because the downward movement of the heated oil at the top is hindered by the cold viscous oil located beneath it, and the movement of the interface from the bottom is restricted by counter-current flow of oil and steam. Limited single block experimental observations performed by Pooladi-Darvish [1992] confirms these ideas. On the other hand, the other four vertical sides of the block are effectively identical. A vertical slab of thickness $2L$ or a vertical cylinder of radius R will be analyzed.

Figure 4.1. Cross section of an ideal fractured reservoir after steam injection.

The other assumption is to neglect the capillary transition zone. As will be discussed later, conclusions of this study are not violated if this assumption is relaxed. Also, it is assumed that the only flowing phase behind the oil-steam interface is steam, and that ahead of the interface is oil, that is, a sharp interface separating the two zones is assumed. This assumption states that the steam condensate and the heated oil do not flow across the interface, but flow downwards along the interface, that is, any convective heat

37

flow is caused by advance of the steam-oil interface only. This approximation has been previously used in thermally enhanced gravity driven processes, where the oil-steam interface advances upon removal of the heated oil [Butler 1991]. Many other models of oil recovery by steam injection used the above assumption [Miller and Leung 1985, Kumar *et al.* 1986].

There are a large number of recovery mechanisms that become active in a steam injection process in a fractured reservoirs. The interaction of these mechanisms such as imbibition, induced gas drive, CO_2 generation and thermal expansion on gravity drainage are not considered so as to be able to obtain an analytical solution. Pooladi-Darvish [1992] reviewed and presented discussions of the following mechanisms being active in a steam injection process in a fractured reservoir. (1) Chemical reactions, such as rock dissolution, and chemical alteration of kerogen to liquid hydrocarbon at steam temperature. (2) Recovery mechanisms, other than gravity drainage, such as thermal expansion, water imbibition, induced gas drive, and oil distillation. (3) Change in flow behaviour due to changes in interfacial tension, relative permeability, and absolute permeability.

In the following, a brief description of some of the neglected effects are presented. For a detailed discussion, Pooladi-Darvish [1992] can be referred to.

1) Thermal Expansion: Heating of a matrix block, due to the surrounding steam in the fractures, expands the fluids within, and causes expulsion of the fluids from the block. Nolan *et al.* [1980] and Reis [1992-a] reported that thermal expansion is one of the major recovery mechanisms in fractured reservoirs. Fractured reservoirs with smaller blocks benefit more from this mechanism, since the heating period of the individual blocks is shorter. Butler [1986] pointed out that the thermal expansion of heavy hydrocarbons is about 50% more than that of water. A 200 °C increase in temperature creates 10% to 15% additional fluid volume [Pruess and Narasimhan 1985]. The additional pressure caused by thermal expansion drives the fluids out. Similar to any other flow problem in porous media, it is the mobility of the fluids that determines the ratio of the fluids produced. Should there be gas or water present at a mobile saturation in the block, their low viscosity would favour their production.

Butler [1986] found that, the extra pressure generated within the pore space, caused by thermal expansion, can exceed the formation parting pressure. He considered

rocks with a range of permeability of 0.0645 to 4 darcy. Lower permeability of carbonate rocks reduces the chance of the expanded fluids to flow, before the pressure exceeds the fracturing pressure. This, if occurs, can improve the matrix permeability.

2) Imbibition: During a steam injection process, steam condenses around a block, and the condensate is imbibed into the block. It was reviewed in Chapter 2 that many experimental studies indicated that counter-current imbibition is one of the important recovery mechanisms in fractured reservoirs. It is worth noting that, an increase in water saturation in the outer part of a block reduces the effective permeability to the oil, and traps the oil inside the block. Dreher *et al.* [1986] pointed out that the initial saturation distribution was a major factor affecting the effectiveness of imbibition. Another major factor in the performance of the imbibition process is the wetability of the matrix. Jensen and Sharma [1991] found that imbibition was not a major recovery mechanism in their experimental studies of steam injection through fractured oil-wet rocks.

3) Induced Gas Drive: There are three ways that gaseous phase may be generated in a matrix block of a fractured reservoirs.

a) The reduced solubility of the hydrocarbon gases in liquids at high temperatures can initiate a solution gas drive process. Nolan *et al.* [1980] studied this process experimentally, and Dreher *et al.* [1986] performed theoretical studies to investigate the importance of solution gas drive.

b) Carbonate rocks, most common in fractured reservoirs, decompose at high temperatures. The generated CO_2 creates an extra drive mechanisms. CO_2 generation was reported and studied by many investigators, including Sahuquet *et al.* [1982], Briggs *et al.* [1992], and Reis [1992-a]. Rock dissolution not only creates additional drive, but also increases the matrix permeability by enlarging the pores.

c) Reis [1992-a] pointed out that "pressure may drop more quickly than the temperature of matrix can decline by thermal conduction. Thus flashing of hot condensate might occur during the blow down phase." Flashing of the hot condensate during the blow down period was studied by Baibakov and Garushev [1989] and Briggs *et al.* [1992]. This is a complex process, where thermodynamics

and kinetics of nuclei generation and bubble growth interact with flow mechanisms in porous media.

4) Capillary Effects: Capillarity plays many roles in the process of heavy oil recovery from fractured reservoirs. The role of capillary forces in the imbibition process was briefly described. In a gas-oil, i.e., steam-oil gravity drainage, the final saturation in a block is determined by the capillary-gravity equilibrium [Saidi 1987]. Considering a single low permeability block, as will be considered in this study, more than 50% of the oil may be held in the block when the equilibrium is reached. (see Saidi [1987] for the exact figures and more discussion). Recent studies [Saidi 1987, Dindoruk and Firoozabadi 1994], however, indicated that, depending on the fracture characteristics, there may be large effects of capillary continuity between blocks. That is, the matrix blocks located vertically above each other can behave close to a continuous column. The subject of capillary continuity in fractured reservoirs is an ongoing area of research.

It should be noted that none of the above mechanisms are incorporated in the present study. These are ignored so that an analytical solution for thermal gravity drainage of the heating oil from a single block can be obtained. What will be considered, consists of heating of a single block heated by the steam surrounding it, and non-isothermal gravity drainage of the heating oil, accounting for the transient temperature distribution within the block.

4.2. Heat Flow Problem

Consider a single block of a natu..ally fractured reservoir saturated with heavy oil and surrounded by steam in fractures as in Figure 4.1. Heat conduction occurs from steam to oil, and oil drains simultaneously due to the gravity force. If the drainage rate is slow enough, compared with the conduction rate, the process can be represented by two different periods. In the first period the block is heated by conduction with minor oil production, while in the second period drainage of heated oil from the matrix occurs which is now approximately at constant temperature.

Production during the latter period can simply be modelled in one dimension, i.e., vertical flow of oil with a constant viscosity as explained by Saidi [1987]. However, if the drainage rate is fast compared to conduction [Kharrat et al. 1993], a thin layer of oil is heated and flows downwards, allowing further contact of steam with the unheated oil.

40

Figure 4.2 shows the schematic shape of the moving interface detected by temperature measurements and visual observations from a single block study [Pooladi-Darvish 1992].
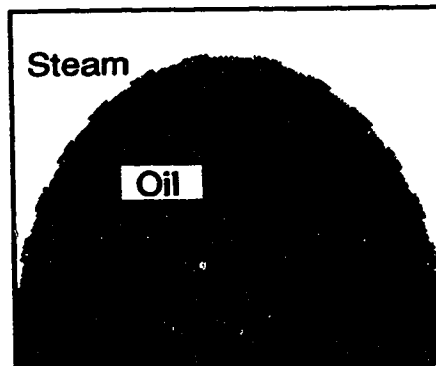
Figure 4.2
Schematic behaviour of non-isothermal gravity drainage in
a high permeability single block [Pooladi-Darvish 1992].

The moving interface introduces a nonlinearity into the problem, because the location of the boundary is not known *a priori*. Bear [1972] discussed the difficulties of modelling isothermal free and moving boundary problems in porous media. Crank [1988] reviewed many approximate methods to solve moving boundary problems mostly using numerical models. In the context of heavy oil recovery, Palmgren and Bruining [1992] solved approximately a moving boundary problem using the method of characteristics to predict the shape of the interface in a steam drive affected by steam override. Butler and his co-workers (reviewed by Butler [1991]) modelled the moving boundary process of Steam-Assisted Gravity Drainage (SAGD). They originally used the steady-state assumption for temperature distribution ahead of the moving interface [Butler *et al.* 1981]. The SAGD model was successfully used for the experimental results of drainage of oil from a single block surrounded by steam [Kharrat *et al.* 1993]. However, scaling considerations shown later indicate that the high permeability of the sand pack in the experiments had altered the response of the system, so that the SAGD theory [Butler *et al.* 1981] would not be valid for modelling the response of a typical matrix block.

One-dimensional[3] heating of the matrix block in the shape of a slab of thickness $2L$ can be expressed by the heat conduction equation ahead of a moving boundary as

$$\frac{\partial^2 T}{\partial x^2} = \frac{1}{\alpha}\frac{\partial T}{\partial t} \qquad s(t) \le x \le L \qquad t > 0 \qquad \dots\dots\dots\dots\dots\dots(4.2.1)$$

where α is the thermal diffusivity of the medium, and $s(t)$ is the interface location. The initial and boundary conditions of the problem can be expressed as

$$T = T_R \qquad s(t) \le x \le L \qquad t = 0 \qquad \dots\dots\dots\dots\dots\dots(4.2.2)$$

$$T = T_S \qquad x = s(t) \qquad t > 0 \qquad \dots\dots\dots\dots\dots\dots(4.2.3)$$

$$\frac{\partial T}{\partial x} = 0 \qquad x = L \qquad t > 0 \qquad \dots\dots\dots\dots\dots\dots(4.2.4)$$

The location of the moving boundary is not known until the complete heat and fluid flow problem is solved. The unknown location of the boundary condition is avoided by introducing a coordinate system, ζ, that travels with the interface. The location of the moving interface in one dimension can be expressed as $s(t)$, and so;

$$\zeta(x,t) = x - s(t) \qquad \dots\dots\dots\dots\dots\dots(4.2.5)$$

where,

$$s(t) = \int_0^t U dv \qquad \dots\dots\dots\dots\dots\dots(4.2.6)$$

where U is the velocity of the interface, and v is the variable of integration. The transformation fixes the moving boundary at $\zeta = 0$ for all time. Using the chain rule [Crank 1988] one obtains

$$\frac{\partial^2 T}{\partial x^2} = \frac{\partial^2 T}{\partial \zeta^2} \qquad \dots\dots\dots\dots\dots\dots(4.2.7)$$

---

3   It will be discussed later that the conclusions of this analysis would be equally valid for two-dimensional heat conduction.

$$\frac{\partial T}{\partial t} = \frac{\partial T}{\partial \zeta}\frac{\partial \zeta}{\partial t} + \frac{\partial T}{\partial t} = -U\frac{\partial T}{\partial \zeta} + \frac{\partial T}{\partial t} \qquad \ldots \ldots \ldots \ldots \ldots \ldots \ldots \ldots \ldots \ldots .(4.2.8)$$

and substituting from Equations (4.2.7) and (4.2.8) into (4.2.1) and rearranging,

$$\frac{\partial^2 T}{\partial \zeta^2} + \frac{U}{\alpha}\frac{\partial T}{\partial \zeta} = \frac{1}{\alpha}\frac{\partial T}{\partial t} \qquad \ldots \ldots \ldots \ldots \ldots \ldots \ldots \ldots .(4.2.9)$$

Equation (4.2.9) is a convection-diffusion PDE, where the convective term, $\frac{U}{\alpha}\frac{\partial T}{\partial \zeta}$,

enters into the equation because of the movement of the coordinate system. This term acts as a convective flow of heat in a direction opposite to ζ and causes steepness in temperature gradients that are created by the diffusive term.

Although Equation (4.2.9) expresses different terms, i.e., the diffusive, the convective, and the unsteady-state term, the equation does not reveal the relative importance of the different terms with respect to each other. In the next section the normalization technique is used on Equation (4.2.9) that enables one to comment on the relative importance of the different terms.

4.2.1 Magnitude Analysis

Analyzing the governing differential equations of a physical process in dimensionless and normalized form enables one to evaluate the importance of different terms with respect to others. Magnitude analysis, a form of scale analysis [Farouq Ali and Redford 1977, Farouq Ali, Redford, and Islam 1987] is used in this section to evaluate the effect of the moving boundary. In this technique, the value of each variable is divided by its maximum value, to normalize the variable between zero and one. The magnitude of the coefficients for each term in the final dimensionless equation is an estimate of the importance of the corresponding term [Lock 1986]. The dimensionless variables are defined such that they are scaled between zero and unity:

$$\theta = \frac{T - T_R}{T_s - T_R} \qquad \ldots \ldots \ldots \ldots \ldots \ldots \ldots (4.2.1.1)$$

$$\xi = \frac{\zeta}{L} \qquad \ldots \ldots \ldots \ldots \ldots \ldots \ldots .(4.2.1.2)$$

43

$$\tau = \frac{\alpha t}{L^2} \qquad\qquad\qquad \ldots\ldots\ldots\ldots\ldots\ldots\ldots(4.2.1.3)$$

Although time cannot be scaled between zero and one, Equation (4.2.1.3) ensures that the unsteady-state term is normalized with respect to the diffusive term, as $\theta_{av.} \approx 1$ @ $\tau = 1$ in a conductive problem [Carslaw and Jaeger 1959]. On substituting the dimensionless variables in Equation (4.2.9), one obtains

$$\frac{\partial^2\theta}{\partial\xi^2} + \frac{UL}{\alpha}\frac{\partial\theta}{\partial\xi} = \frac{\partial\theta}{\partial\tau} \qquad\qquad \ldots\ldots\ldots\ldots\ldots\ldots\ldots (4.2.1.4)$$

In Equation (4.2.1.4) the convective and the diffusive terms are properly normalized and the unsteady-state term is normalized with respect to the diffusive term. Thus, the value of the coefficient $\frac{UL}{\alpha}$, also called the Peclet Number, N_{Pe}, signifies the importance of the convective term. In the study of forced convection, N_{Pe} represents the thickness of the thermal boundary layer. A small thermal layer, that is, a highly convective system, corresponds to a large N_{Pe} [Gebhart 1971].

4.2.2. Evaluating the Importance of the Convective Term, that is, the Peclet Number

To evaluate N_{Pe}, a set of rock and fluid properties should be considered. Some of the parameters of fractured reservoirs, such as matrix permeability and block size vary by orders of magnitude from a reservoir to another. For example, matrix permeability can vary from essentially zero to 10^2 md, and the block size can vary from a fraction of a meter to tens of meters. Table 4.1 shows a range, which is most common in naturally fractured reservoirs containing heavy oil, and a selected value which represents the naturally fractured reservoirs of Iran [Saidi 1987, Moshtaghian, Malekzadeh, and Azarpanah 1988], together with the heavy oil properties of the Grosmont formation in Alberta [Cordell 1982]. In most of the calculations in this work the representative value, referred to as "typical" value, is used.

The values of L and α can be directly substituted from Table 4.1. The velocity of the interface is generally unknown and variable with time and position. However, for the simple case where the temperature distribution ahead of the front is approximated by the steady-state equation, an analytical solution for the advance rate of the interface was

44

obtained [Butler *et al.* 1981], and will be used to give an upper limit for U as explained later.

$$U = \sqrt{\frac{kg\alpha}{2m\upsilon_{os}z\phi\Delta S_o}} \qquad \qquad \ldots\ldots\ldots\ldots\ldots\ldots\ldots(4.2.2.1)$$

Table 4.1
Typical physical properties of heavy oil naturally fractured reservoirs

Permeability k	(0.1-10 md) 1 md [10^{-15} m^2]
Oil viscosity at steam temperature μ_{os}	(2-10 cp) 10 cp [10^{-2} Pa s]
Oil density ρ	1 g/cm^3 [1000 kg/m^3]
Porosity $\times$ Saturation change $\phi\Delta S_o$	(5%-15%) 10%
Block height (size) H(2L or 2R)	(3-10 m) 4 m
Thermal diffusivity α	(0.7-1.5 mm^2/s) 1 mm^2/s [10^{-6} m^2/s]
See Equation (4.3.2) m	(3-4) 4

Equation (4.2.2.1) indicates that, under steady-state conditions, the velocity of interface is independent of time, and is a function of the height of any point at the interface, z. Equation (4.2.2.1) gives an unrealistic velocity of infinity at $z=0$ (top of formation) and decreases as the bottom of the formation is approached [Butler 1991]. Evaluating the velocity half way from the top of the block, $z=2$ m, an approximate value for the velocity of the interface can be calculated using the typical values of Table 4.1.

$$U = O(10^{-8}) \text{ ms}^{-1} \qquad \qquad \ldots\ldots\ldots\ldots\ldots\ldots(4.2.2.2)$$

Using these values N_{Pe} can be evaluated.

$$\frac{UL}{\alpha} = O(10^{-2}) \qquad \qquad \ldots\ldots\ldots\ldots\ldots\ldots\ldots(4.2.2.3)$$

Using the most extreme data of Table 4.1, a maximum value of $N_{Pe}=0.4$ is obtained. However, it should be noted that, in the above analysis the steady-state velocity of the interface was considered which is its maximum value. A steady-state situation is achieved when the rate of heat transferred ahead of the interface is equal to the rate of

heat left behind the interface. Under unsteady-state conditions the rate of heat transferred ahead of the interface is more than that left behind. The latter situation occurs when the interface moves with a velocity less than the steady-state value. Of course, the unsteady-state moving boundary process with a slower interface velocity approaches the steady-state conditions at large times; however, at a constant time the interface velocity for the steady-state process is larger than the corresponding unsteady-state one. For example, the process of heat conduction in a semi-infinity medium does not reach steady-state for the limiting case of zero interface velocity.

Furthermore, capillary forces were ignored previously. In a steam-oil drainage system, steam is the non-wetting phase. Thus, capillary forces are in favour of uniformly distributing fluids in the block, holding back oil from drainage. Hence, Equation (4.2.2.3) shows the upper limit, and indicates that for the typical properties of Table 4.1 the coefficient of the convective term is two orders of magnitude smaller than the coefficient of the diffusive term, which is equal to one in Equation (4.2.1.4). In other words, the effect of the moving boundary is negligible.

Although the above calculation gives an upper limit for N_{P_e}, however; the range of data in Table 4.1 indicates the effect of the moving interface may not be negligible in some reservoirs. In such cases, errors in heat flow calculations would occur if the moving boundary effect is neglected. This is discussed in Sections 4.2.5 and 5.4 again.

In analyzing the heat flow process ahead of the moving steam-oil interface a 1-D conduction model was considered. In general, the shape of the interface is unknown and the heat flows in two dimensions. However, the above analysis suggests that the effect of the moving boundary on the heat flow process is negligible. In other words, the average temperature of the block approaches that of steam, before much of the oil is produced, and the shape of the interface is affected. This justifies the assumption of 1-D heat conduction ahead of the steam-oil interface.

The above analysis was performed for the typical properties of Table 4.1; however, the theory of normalization suggests [Lock 1986] that for other cases the importance of the convective term varies proportionally with N_{P_e}.

46

4.2.3. Time Scale Analysis

In order to compare the importance of the convective term with respect to the diffusive term a magnitude analysis was performed in Section 4.2.2 based on the differential equation describing the process. Here, a similar analysis is performed to compare the time scales of the two different, but interacting processes, that is, heat flow and fluid flow. Of course the latter is responsible for the movement of the interface, as indicated by the convective term in Equation (4.2.9). It is intended to compare the characteristic time required for each of the two transfer mechanisms. If one assumes that heat transfer is governed by conduction, the characteristic time can be estimated using Equation (4.2.3.1) [Carslaw and Jaeger 1959],

$$\tau_{hc} = \frac{L^2}{\alpha} \qquad \dots\dots\dots\dots\dots\dots(4.2.3.1)$$

where τ_{hc} is the characteristic time for heat conduction. A characteristic time for drainage can be obtained by dividing the block height by the frontal velocity due to drainage,

$$\tau_d = \frac{H}{U} \qquad \dots\dots\dots\dots\dots\dots(4.2.3.2)$$

where τ_d is the characteristic time for drainage, H is the block height, and U is the frontal velocity due to drainage. Ignoring capillary forces and steam viscosity, an upper limit for U can be obtained by writing the frontal velocity due to Darcy flow,

$$U = \frac{k}{\mu_{os}} \frac{\Delta \rho g}{\phi \Delta S_o} \qquad \dots\dots\dots\dots\dots\dots(4.2.3.3)$$

where isothermal drainage at steam temperature is considered as an upper limit for U. Using the typical values of Table 4.1 and Equations (4.2.3.1) to (4.2.3.3) one obtains

$$\tau_d \gg \tau_{hc} \qquad \dots\dots\dots\dots\dots\dots(4.2.3.4)$$

The inequality (4.2.3.4) demonstrates that the heat conduction process acts much faster than does the drainage process. Hence, production of oil during the heating period minimally affects the heat transfer process.

47

4.2.4. Evaluating the Unsteady-State Term

It was pointed out previously that, in Equation (4.2.1.4) the diffusive and the unsteady-state terms are of similar importance. The same conclusion can be obtained considering a heat balance on the moving interface. In the problem of interest, heat is transferred ahead of the interface by conduction, and heat is left behind the interface as it moves forwards in the matrix. The difference between these two corresponds to the accumulated heat and signifies the importance of the unsteady-state term. Heat flux to the rear, defined as the rate of heat left behind the moving interface per unit area of the interface, can be written as Equation (4.2.4.1)

$$Q_1 = U\rho c(T_S - T_R) \qquad \dots\dots\dots\dots\dots\dots\dots\dots\dots(4.2.4.1)$$

Note that the coordinates are moving with the interface, and account should be taken for oil as well as rock left behind the interface, as in Equation (4.2.4.1). Heat flux ahead of the interface is found from Fourier's law,

$$Q_2 = -k_t \frac{\partial T}{\partial \zeta}\Big|_{\zeta=0} \qquad \dots\dots\dots\dots\dots\dots\dots\dots(4.2.4.2)$$

The dimensionless heat flux is defined as

$$Q_D = \frac{QL}{k_t(T_S - T_R)} \qquad \dots\dots\dots\dots\dots\dots\dots\dots(4.2.4.3)$$

Thus, the dimensionless heat flux to the rear and that ahead of the interface can be written as Equations (4.2.4.4) and (4.2.4.5), respectively,

$$Q_{D_1} = \frac{UL}{\alpha} \qquad \dots\dots\dots\dots\dots\dots\dots\dots\dots(4.2.4.4)$$

and,

$$Q_{D_2} = -\frac{\partial \theta}{\partial \xi}\Big|_{\xi=0} \qquad \dots\dots\dots\dots\dots\dots\dots\dots(4.2.4.5)$$

The dimensionless heat flux to the rear is the Peclet Number, N_{Pe}, written as Equation (4.2.4.4), which was found to be of the order of 10^{-2} for a typical case. Based on the theory of magnitude analysis $Q_L = O(1)$, since the variables on the right hand side of Equation (4.2.4.5) are normalized [Lock 1986]. It can be concluded that there is a large accumulation of heat in the system.

Under certain approximations, Equation (4.2.4.5) can be evaluated. First, the effect of the moving interface can be neglected, since it was shown to have little effect. Using the exact solution for pure conduction in a slab with initial zero temperature and a boundary condition of unit step-function, the dimensionless heat flux can be found as [Carslaw and Jaeger 1959]

$$-\frac{\partial\theta}{\partial\xi}\bigg|_{\xi=0} = 2\sum_{n=1}^{\infty}\exp\left[-\left(\frac{2n-1}{2}\right)^2\pi^2\tau\right] \quad\quad\quad\quad\quad\quad\quad (4.2.4.6)$$

As another model the unsteady-state heat transfer ahead of a constant velocity moving boundary into a semi-infinite medium can be considered. For such a system [Carslaw and Jaeger 1959], Equation (4.2.4.5) can be evaluated as

$$-\frac{\partial\theta}{\partial\xi}\bigg|_{\xi=0} = \frac{\exp\left[-\left(\frac{N_{Pe}}{2}\right)^2\tau\right]}{\sqrt{\pi\tau}} + \frac{N_{Pe}}{2}\text{erfc}\left(-\frac{N_{Pe}}{2}\sqrt{\tau}\right) \quad\quad\quad\quad (4.2.4.7)$$

It should be noted that for $N_{Pe}=0$, Equation (4.2.4.7) simplifies to $-\frac{\partial\theta}{\partial\xi}\bigg|_{\xi=0} = \frac{1}{\sqrt{\pi\tau}}$, which corresponds to the heat flux from the surface of a semi-infinite medium in a 1-D conduction problem [Carslaw and Jaeger 1959].

Equations (4.2.4.6) and (4.2.4.7) are plotted along with Equation (4.2.4.4) in Figure 4.3. As shown in Figure 4.3, the heat flux to the rear is $\frac{UL}{\alpha}$, and is of the order of 10^{-2}. This value is much less than the heat flux ahead of the interface, as shown in Figure 4.3, where the dimensionless time is between zero and one. Carslaw and Jaeger [1959] showed that the average temperature in the slab at $\tau=1$ is $T_{av.} \approx T_s$. This is why the heat flux for the slab case approaches the value of 0.01. In fact for much larger times it will be almost zero because heat transfer ceases when the block is at steam temperature.

49

However, dimensionless times greater than one are not of interest, since gravity drainage is occurring approximately at constant temperature.
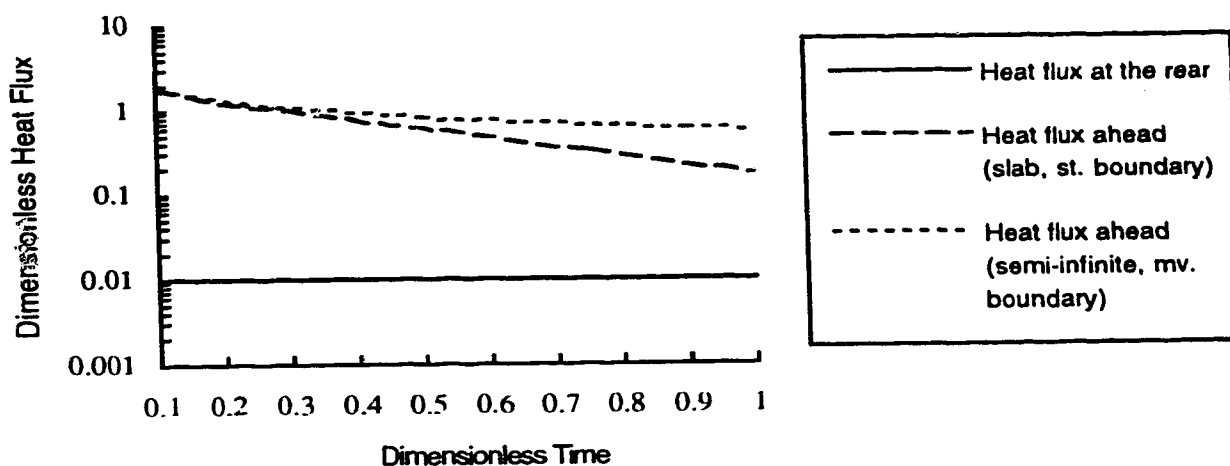
Figure 4.3. Heat flux ahead and at the rear
of the moving interface

Before proceeding to the next step, note that magnitude analysis, in the heat flow part of this study, has limitations [Lock 1986]. As an example, it was found previously that the dimensionless heat flux ahead of the interface was a normalized quantity; hence, it should be of the order of unity. Figure 4.3 indicates that this prediction is valid for the semi-infinite case but, the behaviour of the finite thickness slab is over-predicted by the normalization theory.

4.2.5 The Alternate Linear Heat Flow Problem

Using magnitude analysis it was found that, for the typical properties of Table 4.1, the moving boundary term has a negligible effect in the heating process and that the diffusive and unsteady-state terms are dominant. Based on these findings, it is proposed that steam heating of a typical single block under gravity drainage can be modelled by the linear problem of unsteady-state conduction from stationary boundaries. This idea is examined by considering a semi-infinite problem, since exact solutions are available for the latter case. The semi-infinite assumption is valid while the no-flow boundary of the actual block does not affect the interface behaviour. Discussion of this assumption is

given later. A solution to the moving boundary problem with con—'.ent frontal velocity is given by Carslaw and Jaeger [1959], as Equation (4.2.5.1),

$$\theta = \frac{1}{2}\left[\operatorname{erfc}\left(\frac{\xi + N_{Pe}\tau}{2\sqrt{\tau}}\right) + e^{-N_{Pe}\xi} \times \operatorname{erfc}\left(\frac{\xi - N_{Pe}\tau}{2\sqrt{\tau}}\right)\right] \qquad \ldots\ldots(4.2.5.1)$$

Here, it is suggested to use the well-known solution to unsteady-state heat conduction ahead of a stationary boundary,

$$\theta = \operatorname{erfc}\left(\frac{\xi}{2\sqrt{\tau}}\right) \qquad \ldots\ldots\ldots\ldots\ldots\ldots\ldots\ldots\ldots\ldots\ldots (4.2.5.2)$$

The temperature distributions predicted by Equations (4.2.5.1) and (4.2.5.2) are compared in Figure 4.4 for two different dimensionless times before the temperature rises much at the no-flow boundary. The two solutions are identical to the third decimal place. The temperature distribution corresponding to the steady-state solution of Equation (4.2.1.3) as used in the SAGD theory [Butler *et al.* 1981] is very close to one, for the entire range of the dimensionless distance between zero and one as shown in Figure 4.4. This confirms that behaviour of a matrix block is far from steady-state for the typical properties of Table 4.1.

For the purpose of plotting Figure 4.4, a value of $N_{Pe} = 0.01$ was used in Equation (4.2.5.1), as was found before. Figure 4.4 indicates that the dimensionless time corresponding to the approach of the heat front to the no-flow boundary is less than 0.1. In Equation (4.2.5.1) dimensionless distance varies between zero and one. Hence, the value of $N_{Pe}\tau$ is in the order of 10^{-3}, and for the most part much less than ξ. In this case, Equation (4.2.5.1) can be simplified to Equation (4.2.5.2), which further justifies using the stationary instead of the moving boundary model.

The above numerical and analytical treatments indicate that using Equation (4.2.5.2) instead of Equation (4.2.5.1) is permissible before the effect of the no-flow boundary is felt. In theory, the temperature at the no-flow boundary of a finite thickness system is affected instantaneously as a result of any change at the surface [Zauderer 1989]. However, this effect dies out to almost zero far from the surface. For the case studied in Figure 4.4, it can be assumed that there is no disturbance at $\xi = 1$ for $\tau < 0.05$, for example. Based on this argument the above conclusion can be extended to finite size

51

problems, and the unsteady-state solution of heat conduction from stationary boundaries can be used to model heat flow in a single matrix block in the shape of slab and cylinder. However, the proper boundary condition at the no-flow boundary will be accounted for.
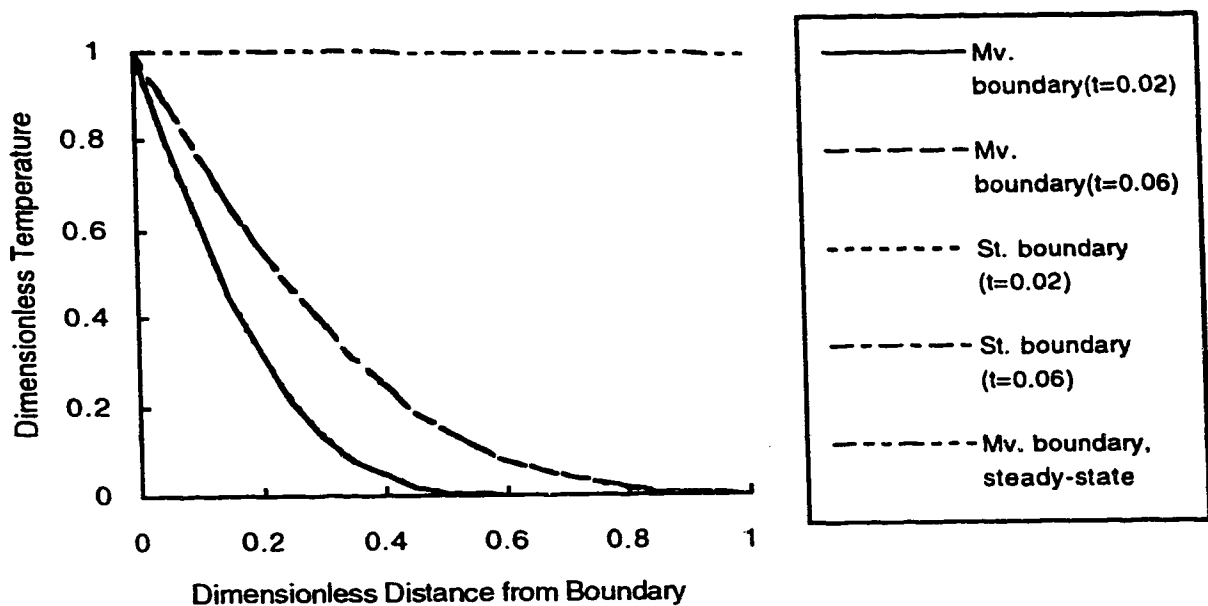
Dimensionless Distance from Boundary
Figure 4.4. Comparison between prediction response by different models

It should be noted that, if the flow properties of a fractured reservoir are such that there is a considerable effect of the moving interface, larger errors in heat flow calculations would occur if its effect is neglected. In the next section the effect of the moving interface is neglected, as found for the typical properties of table 4.1. Solution methods for the cases where the effect of the moving interface should be incorporated are discussed in Chapters 6 and 7.

Next, a detailed solution for non-isothermal gravity drainage for cylindrical blocks is presented and the corresponding solution for matrix blocks in the shape of a slab is given in Appendix A.

Many numerical and experimental studies have indicated that cylindrical blocks can duplicate the behaviour of cubic blocks [Saidi 1975, Chen et al. 1987, Saidi 1987].

Obviously 2-D modelling of cylindrical blocks is a major advantage over the 3-D modelling required for cubic blocks. For a cylindrical block of infinite height with the same initial and boundary conditions as the slab block, the solution of the pure conduction problem is given as Equation (4.2.5.3) [Carslaw and Jaeger 1959]

$$\theta = 1 - 2\sum_{n=1}^{\infty} \frac{J_0(\beta_n \chi)}{\beta_n J_1(\beta_n)} \exp(-\beta_n^2 \tau) \qquad \dots\dots\dots\dots (4.2.5.3)$$

where χ is the dimensionless radius of the cylinder and β_n, $n = 1,2,\dots$, are roots of $J_0(\beta) = 0$. Using Equation (4.2.5.3) the heat consumption by a single cylindrical block can be found as a function of time. Gravity flow calculations can also be performed for a circular element of constant distance from the surface. However, as it is shown below, a simpler form of temperature distribution is required for analytical integration of flow.

4.3 Fluid Flow Problem

To obtain the gravity driven oil flow rate from a single block, three equations should be coupled. One is Darcy's law, which is written for a circular element of thickness dr of constant temperature as:

$$d\dot{q} = \frac{k}{\mu_o(T)} \Delta\rho g (2\pi r dr) \qquad \dots\dots\dots\dots\dots\dots (4.3.1)$$

where piston-like displacement over the element is assumed and capillary pressure is neglected.

In Equation (4.3.1), viscosity is a function of temperature. Hence, an equation is needed defining the dependence of viscosity on temperature, which will be called an equation of state (EOS). In this work, the equation suggested by Butler et al. [1981] is used, which was introduced in the development of the Steam-Assisted Gravity Drainage (SAGD) theory.

$$\frac{\upsilon_{os}}{\upsilon_o} = \left(\frac{T - T_R}{T_s - T_R}\right)^m \qquad \dots\dots\dots\dots\dots\dots (4.3.2)$$

After being used successfully in the SAGD theory (reviewed by Butler [1991]). Closmann [1995] and Reis [1992-b] used Equation (4.3.2) in the analytical solution of the flow of heavy oil in steam injection processes. It is noted that by using Equation (4.3.2) it is implicitly assumed that oil flow at initial reservoir temperature is zero. In the cases where oil flow at reservoir temperature is significant, the additional flow can be estimated separately and added to the oil flow resulting from thermal processes, as suggested by Butler [1985-a]. Butler [1985-a] offered a new interpretation for the exponent m, so that m could be evaluated by using the viscosity-temperature relationship of the particular heavy oil. However, the assumption of zero oil flow at initial reservoir temperature was not relaxed. Recently, Butler [1994] gave another calculation procedure for finding m. The latter method was derived for the steady-state SAGD process. An example of calculating m for the bitumen of Grosmont is given in Appendix B.

The last required equation is the temperature distribution within the block, Equation (4.2.5.3). The analytical coupling of Equations (4.2.5.3) to (4.3.2) is not possible. For this purpose, the Heat Integral Method (HIM) is used to find a simple form of temperature distribution. Analytical incorporation of such a solution into the oil flow equation is possible in some cases, and is shown here. The ease of application of HIM relies on the fact that simple polynomial equations are found to approximate the temperature distribution within the formation. As HIM is essential in this study and is little used in the petroleum literature, it is reviewed in the following section before it is applied to the problem of interest.

4.3.1. Temperature Distribution Using the Heat Integral Method (HIM)

Integral methods have been used to approximate the solution of diffusion dominated nonlinear problems. In the field of fluid mechanics they were first introduced to solve boundary layer problems [Pohlhausen 1921]. Schlichting [1955] presented a detailed discussion on the use of integral methods in boundary layers. In the study of unsteady-state heat conduction the method was first used by Goodman [1958] for solving problems involving a phase change. As reviewed by Crank [1988], one advantage of using integral methods in linear heat transfer problems is that: "only the value of the unknowns on the boundaries of the domain enter into the formulation."

HIM will be used only to find a good approximation to the exact solution in polynomial form which is appropriate for later integration. In HIM, a particular form of

54

temperature distribution, for example, a polynomial, is considered which pertains to an unknown heat penetration depth corresponding to the boundary layer thickness in hydrodynamics. The coefficients of the polynomial are found using the actual as well as the auxiliary boundary conditions. The latter are defined using the definition of heat penetration depth, so that there is no effect of heat transfer beyond the penetration depth. Having obtained the equation for temperature distribution, the heat transfer equation is integrated over the appropriate interval, and the two equations are combined to obtain an ordinary differential equation for the unknown penetration depth. Upon solving this differential equation, the heat penetration depth is obtained which can then be used to find other parameters, in particular the temperature distribution.

In the petroleum literature a few cases are available where integral methods were used in heat flow problems; however, no reference was given to the Heat Integral Method. Vinsome and Westerveld [1980] used an integral method to approximate 1-D heat loss to the cap and base rocks in thermal recovery processes. They used the product of a polynomial with an exponential function to represent a trial function approximating the temperature distribution. The coefficients of the trial functions were numerically obtained for the case of a time-dependent boundary temperature. Their examples showed the high accuracy of the integral method. Later, Pruess and Wu [1993] used Vinsome and Westerveld's method in a semi-analytical model to obtain the temperature distribution in matrix blocks of geothermal reservoirs. They modelled cooling of non-permeable blocks by conduction. In a semi-analytical model for predicting the behaviour of the SAGD process, Butler [1985-b] used a step function to approximate the heat penetration depth by using an integral method.

It should be noted that the Heat Integral Method provides only an approximation for the solution, since the assumed function describing the temperature distribution is forced to satisfy only the integrated form of the original equation. The accuracy of the solution can be increased by defining different profiles at different regions of the heated interval [Bell 1978]. In the following, HIM is used to obtain the proper temperature distribution in a cylindrical matrix block. After the temperature rises at the center of the block, two profiles are required corresponding to two intervals, each one half of the domain, as it leads to higher accuracy compared to a single profile.

A temperature distribution in a polynomial form[4] will be considered, similar to the expansion of Bessel function of zeroth order $J_0(\chi)$, which is the basis of the exact solution, Equation (4.2.5.3)

$$\theta = a(\tau) - b(\tau)\chi^2 + c(\tau)\chi^4 \qquad \dots\dots\dots\dots (4.3.1.1)$$

Using the actual boundary condition (4.3.1.2) and the auxiliary boundary conditions (4.3.1.3) and (4.3.1.4) one can obtain the coefficients of the polynomial (4.3.1.1), and θ can be written in the form of Equation (4.3.1.5)

$$\theta = 1 \qquad @ \quad \chi = 1 \qquad\qquad\qquad \dots\dots\dots\dots (4.3.1.2)$$

$$\theta = 0 \qquad @ \quad \chi = 1 - \delta \qquad\qquad \dots\dots\dots\dots (4.3.1.3)$$

$$\frac{\partial\theta}{\partial\chi} = 0 \qquad @ \quad \chi = 1 - \delta \qquad\qquad \dots\dots\dots\dots (4.3.1.4)$$

$$\theta = \frac{\left[\chi^2 - (1-\delta)^2\right]^2}{\left[1 - (1-\delta)^2\right]^2} \qquad\qquad \dots\dots\dots\dots (4.3.1.5)$$

Note that the auxiliary boundary conditions (4.3.1.3) and (4.3.1.4) indicate that there is no effect of heat flow ahead of the penetration depth δ. Next, the dimensionless form of the heat equation in radial coordinates is integrated over the heat penetration depth, obtaining

$$\left.\chi\frac{\partial\theta}{\partial\chi}\right|_{1-\delta} - \left.\chi\frac{\partial\theta}{\partial\chi}\right|_1 = \frac{d}{d\tau}\int_1^{1-\delta}\chi\theta\, d\chi \qquad \dots\dots\dots\dots (4.3.1.6)$$

Upon substitution of the temperature profile (4.3.1.5) in Equation (4.3.1.6) and by using the auxiliary boundary condition (4.3.1.4), an ordinary differential equation (ODE) is obtained for the heat penetration depth

---

4   It is shown by Lardner and Polhe [1961] that an equation in the form of a product of a logarithmic term and a polynomial offers more accuracy for approximating the temperature distribution in cylindrical coordinates. However, the logarithmic term will be excluded; otherwise, it will not be possible to obtain analytically the drainage rate by combining the three equations (4.2.5.3) to (4.3.2).

$$\frac{d\left[1-(1-\delta)^2\right]}{d\tau} = \frac{24}{\left[1-(1-\delta)^2\right]} \qquad \dots\dots\dots\dots\dots\dots (4.3.1.7)$$

Equation (4.3.1.7) along with the initial condition (4.3.1.8) can be solved to obtain the heat penetration depth as Equation (4.3.1.9)

$$\delta = 0 \qquad\qquad \tau = 0 \qquad\qquad \dots\dots\dots\dots\dots\dots (4.3.1.8)$$

$$1-\delta = \sqrt{1-\sqrt{48\tau}} \qquad \tau \le \frac{1}{48} \qquad \dots\dots\dots\dots\dots\dots (4.3.1.9)$$

By combining Equations (4.3.1.5) and (4.3.1.9), the unsteady-state temperature distribution can be written as a function of τ and χ

$$\theta = \frac{\left(\chi^2 - 1 + \sqrt{48\tau}\right)^2}{48\tau} \qquad \tau \le \frac{1}{48} \qquad \dots\dots\dots\dots\dots\dots (4.3.1.10)$$

Equation (4.3.1.10) is valid so long as $\delta \le 1$, since Equations (4.3.1.3) and (4.3.1.4) are not valid afterwards. In fact there is no meaning for the heat penetration depth after the temperature at the no-flow boundary of the cylinder is raised above the initial value. Any attempt to represent the temperature distribution using a single polynomial after this time would result in poor accuracy. Hence, two different polynomials are considered each pertaining to half of the cylinder radius. The coefficients of the polynomials are obtained using the actual boundary conditions of the problem, and the statements of continuity of temperature and heat flux where different polynomials meet. This method is used below to obtain better accuracy for the temperature distribution compared to that obtained using a single polynomial.

$$\theta_1 = a(\tau) + b(\tau)\chi + c(\tau)\chi^2 \qquad \frac{1}{2} \le \chi \le 1 \qquad \dots\dots (4.3.1.11)$$

$$\theta_2 = e(\tau) + f(\tau)\chi + g(\tau)\chi^2 \qquad 0 \le \chi \le \frac{1}{2} \qquad \dots\dots (4.3.1.12)$$

Four of the coefficients can be found using the appropriate boundary conditions (4.3.1.13) to (4.3.1.16)

57

$$\theta_1 = 1 \qquad\qquad \chi = 1 \qquad\qquad\qquad \dots\dots\dots(4.3.1.13)$$

$$\frac{\partial \theta_2}{\partial \chi} = 0 \qquad\qquad \chi = 0 \qquad\qquad\qquad \dots\dots\dots(4.3.1.14)$$

$$\theta_1 = \theta_2 \qquad\qquad \chi = \frac{1}{2} \qquad\qquad\qquad \dots\dots\dots(4.3.1.15)$$

$$\frac{\partial \theta_1}{\partial \chi} = \frac{\partial \theta_2}{\partial \chi} \qquad\qquad \chi = \frac{1}{2} \qquad\qquad\qquad \dots\dots\dots(4.3.1.16)$$

The temperature distribution equations can be simplified using the above equations to:

$$\theta_1 = 1 + b(\tau)(\chi - 1) + c(\tau)(\chi^2 - 1) \qquad \frac{1}{2} \le \chi \le 1 \qquad \dots\dots\dots(4.3.1.17)$$

$$\theta_2 = 1 + b(\tau)(\chi^2 - \frac{3}{4}) + c(\tau)(\chi^2 - 1) \qquad 0 \le \chi \le \frac{1}{2} \qquad \dots\dots\dots(4.3.1.18)$$

Now, Equations (4.3.1.17) and (4.3.1.18) are forced to satisfy the integrated form of heat equation over their corresponding half radii. Hence,

$$\chi \frac{\partial \theta_1}{\partial \chi}\Big|_{\frac{1}{2}}^{1} = \frac{d}{d\tau} \int_{\frac{1}{2}}^{1} \chi \theta_1 d\chi \qquad \dots\dots\dots(4.3.1.19)$$

$$\chi \frac{\partial \theta_2}{\partial \chi}\Big|_{0}^{\frac{1}{2}} = \frac{d}{d\tau} \int_{0}^{\frac{1}{2}} \chi \theta_2 d\chi \qquad \dots\dots\dots(4.3.1.20)$$

After doing the required algebra one obtains two ODEs for $b(\tau)$ and $c(\tau)$ as:

$$b(\tau) + c(\tau) = -\frac{5}{32}\frac{db(\tau)}{d\tau} - \frac{7}{32}\frac{dc(\tau)}{d\tau} \qquad \dots\dots\dots(4.3.1.21)$$

$$b(\tau) + 3c(\tau) = -\frac{1}{6}\frac{db(\tau)}{d\tau} - \frac{9}{32}\frac{dc(\tau)}{d\tau} \qquad \dots\dots\dots(4.3.1.22)$$

Simultaneous solution of Equation (4.3.1.21) and (4.3.1.22) with the corresponding initial conditions yields $b(\tau)$ and $c(\tau)$ as functions of τ

$$b(\tau) = 24.47112A_1 \exp(m_1\tau) - 1.47112A_2 \exp(m_2\tau) \qquad \dots (4.3.1.23)$$

$$c(\tau) = A_1 \exp(m_1\tau) + A_2 \exp(m_2\tau) \qquad \dots (4.3.1.24)$$

where $m_1 = -6.30105$
       $m_2 = -42.3946$

Coefficients A_1 and A_2 are obtained by satisfying the equality of temperature and heat flux, when the second set of temperature profiles (4.3.1.17), (4.3.1.18) are used instead of the first Equation (4.3.1.10)

$$\theta_2 = 0 \qquad\qquad \chi = 0 \qquad\qquad \dots (4.3.1.25)$$

$$\frac{\partial \theta_1}{\partial \chi} = \frac{\partial \theta}{\partial \chi} = 4 \qquad\qquad \chi = 1 \qquad\qquad \dots (4.3.1.26)$$

Using Equations (4.3.1.25) and (4.3.1.26) which are valid at $\tau = \frac{1}{48}$, and A_2 are obtained:

$$A_1 = 0.08283$$
$$A_2 = 9.49929$$

Figures 4.5 and 4.6 compare the exact solutions with the approximate ones. These figures indicate that a reasonable approximation is obtained by using HIM. Note that the approximate solutions follow the exact solution both in space and time.
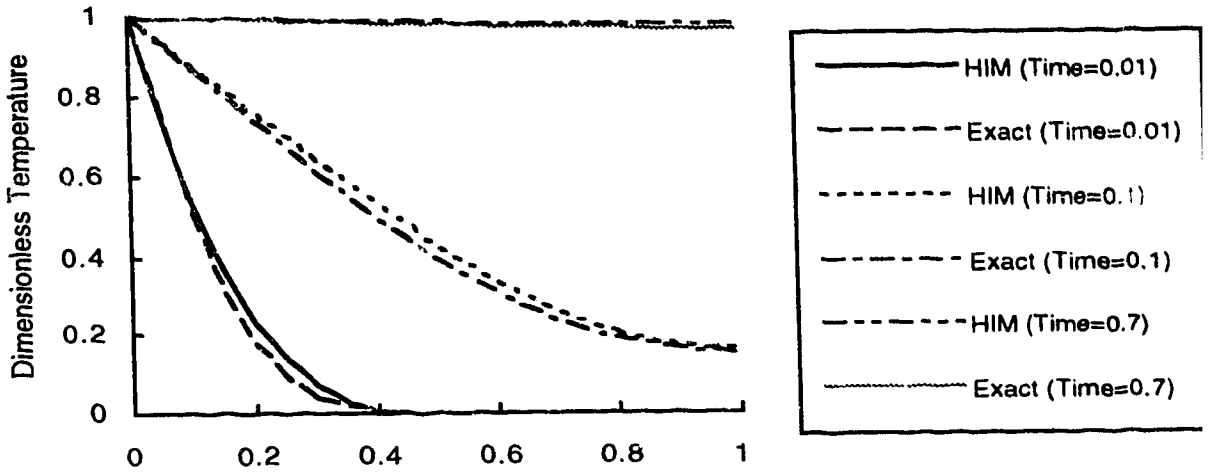
Figure 4.5. Temperature distribution by
HIM and exact solution (Cylinder)

Legend:
- HIM (Time=0.01)
- Exact (Time=0.01)
- HIM (Time=0.1)
- Exact (Time=0.1)
- HIM (Time=0.7)
- Exact (Time=0.7)
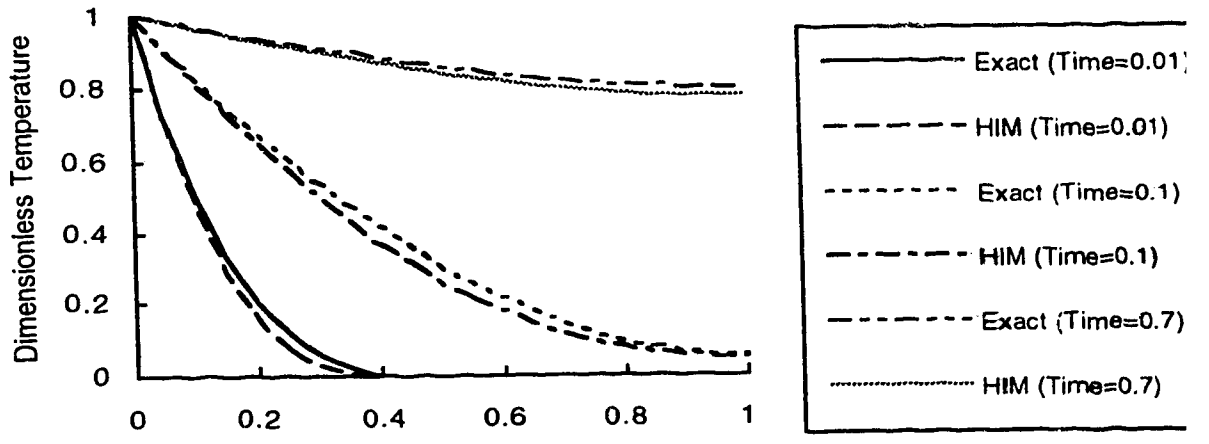
Figure 4.6. Temperature distribution by
HIM and exact solution (Slab)

Legend:
- Exact (Time=0.01)
- HIM (Time=0.01)
- Exact (Time=0.1)
- HIM (Time=0.1)
- Exact (Time=0.7)
- HIM (Time=0.7)

60

4.3.2 Thermal Gravity Drainage from a Single Block

To obtain non-isothermal gravity drainage Darcy's law, Equation (4.3.1) is combined with the EOS (4.3.2) to obtain:

$$q = \frac{kg}{R^2 v_{os}} \int_0^R \theta^m 2r dr \qquad\qquad \ldots\ldots (4.3.2.1)$$

where it has been assumed that $\Delta\rho = \rho_o$. The parameter q is the production rate per unit surface area of the block.

To be able to perform analytically the above integration and to obtain a closed-form solution for non-isothermal gravity drainage, the approximate temperature distributions in polynomial form that were found in Section 4.3.1. are used. Hence,

$$q_D(\tau) = \frac{\left(48\tau + \sqrt{48\tau} - 1\right)^{2m+1} - \left(\sqrt{48\tau} - 1\right)^{2m+1}}{(2m+1)(48\tau)^m} \qquad \tau \le \frac{1}{48} \qquad \ldots\ldots (4.3.2.2)$$

In Equation (4.3.2.2) q_D is normalized with respect to the maximum drainage rate at steam temperature:

$$q_D(\tau) = \frac{q(\tau)}{q_s} \qquad\qquad \ldots\ldots\ldots\ldots\ldots\ldots\ldots (4.3.2.3)$$

where,

$$q_s = \frac{kg}{v_{os}} \qquad\qquad \ldots\ldots\ldots\ldots\ldots\ldots\ldots (4.3.2.4)$$

Thus, $q_D(\tau) = 1$ corresponds to isothermal gravity drainage at steam temperature. Equations (4.3.2.3) and (4.3.2.4) indicate that non-isothermal gravity drainage from a single block, similar to the corresponding isothermal one, is inversely proportional to the oil viscosity at steam temperature and linearly proportional to matrix permeability.

Equation (4.3.2.2) is valid for $\tau \le \frac{1}{48}$; however, for $\tau \ge \frac{1}{48}$ Equations (4.3.1.17) and (4.3.1.18) are used and the analytical integration is performed for a value of $m=4$, as obtained in Appendix B for the Grosmont bitumen of Alberta. The solution is plotted in

61

Figure 4.7, which shows that the drainage rate approaches that at steam temperature after $\tau = 1$. For comparison the thermal gravity drainage is plotted when the exact temperature distribution, Equation (4.2.5.3), is considered. Obviously, the latter is obtained using numerical estimation of the infinite series and numerical integration of the final flow integral. Also, the solution from a free equation of state, that is, Equation is.3, from Appendix B, is shown. The close similarity of the solutions indica how the approximations involved in using the temperature distribution from HIM and also in evaluating the exponent m in Appendix B are all justified.
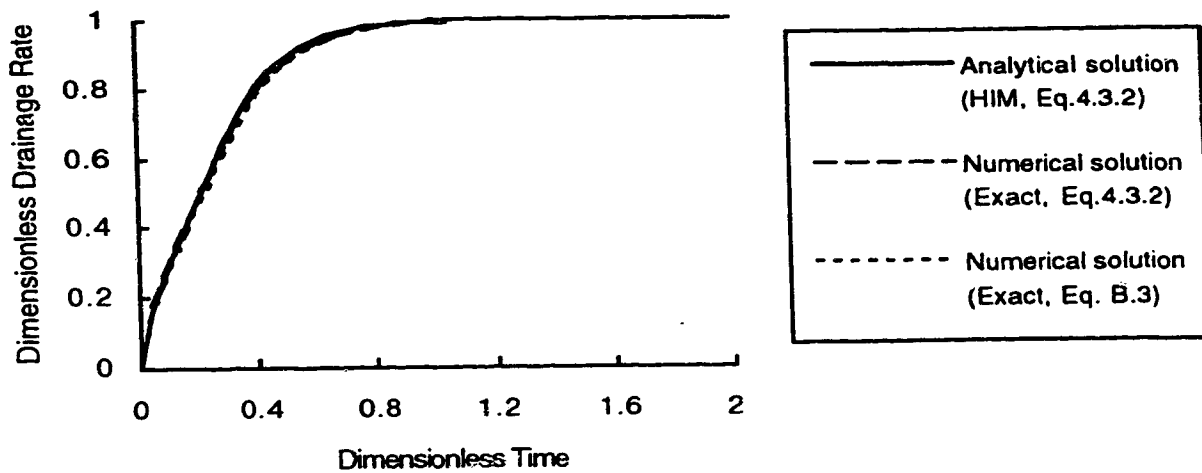
Figure 4.7. Thermal drainage from a single block (cylinder)—Analytical and numerical solutions

The corresponding solution for a slab is shown in Figure 4.8. A comparison is shown between the analytical solution with the numerical solutions using the exact temperature distribution (see Appendix A) and two different EOS. Again, the close similarity indicates that the analytical solution proposed here is successful in predicting the thermal gravity drainage from a single block.
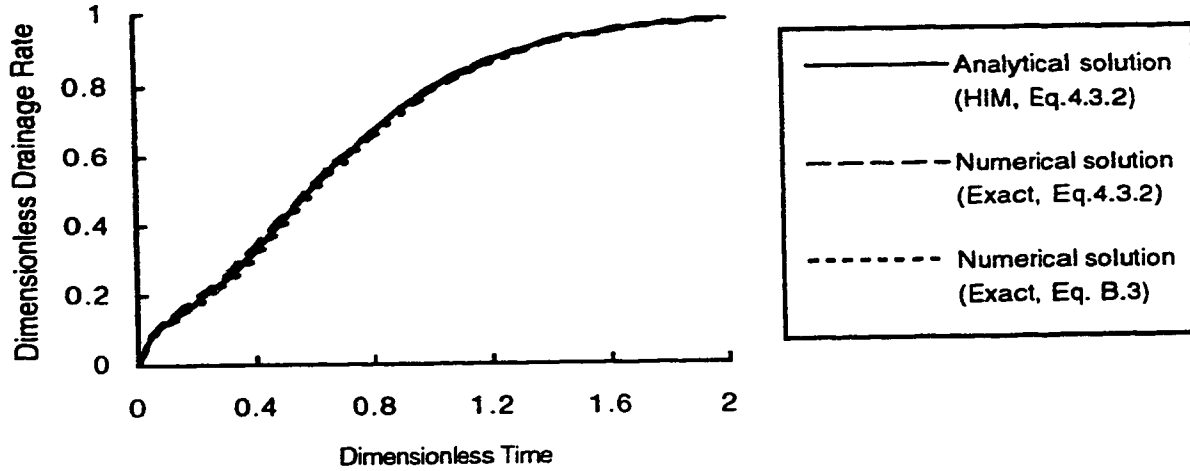
Figure 4.8. Thermal drainage from a single
block (slab)—Analytical and numerical
solutions

4.3.3. Average Temperature Assumption

In the previous section the temperature distribution was analytically incorporated into the integral of the flow rate from a single block. If at any time, the average temperature is accurate enough to approximate the flow rate at that time, then an analytical solution of flow equation using the exact temperature solution with any EOS is possible. Under the average temperature assumption thermal gravity drainage from a single block can be evaluated using

$$\bar{q} = \frac{kg}{\upsilon(\bar{T}_{av.})} = q_s \frac{\upsilon_{os}}{\upsilon_o(\bar{T}_{av.}(\tau))} \qquad \dots\dots\dots\dots\dots\dots\dots\dots\dots (4.3.3.1)$$

or,

$$\bar{q}_D(\tau) = \frac{\upsilon_{os}}{\upsilon_o(\theta_{av.}(\tau))} \qquad \dots\dots\dots\dots\dots\dots\dots\dots\dots (4.3.3.2)$$

where the bar sign indicates a production rate at the average temperature.

63

Equation (4.3.3.2) is valid for both the cylinder and the slab cases. If the Equation of State of (4.3.2) is used, Equation (4.3.3.2) can be written as

$$\bar{q}_D(\tau) = \left[\bar{\theta}_{av}(\tau)\right]^m \quad\quad\quad\quad \dots\dots\dots\dots\dots\dots\dots (4.3.3.3)$$

By using temperature distributions from HIM (see Table 5.2), one obtains

$$\bar{q}_D(\tau) = \left(\frac{16}{3}\tau\right)^{\frac{m}{2}} \quad\quad\quad\quad \tau \le \frac{1}{48} \quad\quad \dots\dots\dots\dots\dots (4.3.3.4)$$

$$\bar{q}_D(\tau) = \left[1 - \frac{31}{96}b(\tau) - \frac{1}{2}c(\tau)\right]^m \quad\quad \tau \ge \frac{1}{48} \quad\quad \dots\dots\dots\dots\dots (4.3.3.5)$$

for cylinders, and

$$\bar{q}_D(\tau) = (1.5\tau)^{\frac{m}{2}} \quad\quad\quad\quad \tau \le \frac{1}{24} \quad\quad \dots\dots\dots\dots\dots (4.3.3.6)$$

$$\bar{q}_D(\tau) = \left[1 + \frac{11}{24}b(\tau) + \frac{1}{4}c(\tau)\right]^m \quad\quad \tau \ge \frac{1}{24} \quad\quad \dots\dots\dots\dots\dots (4.3.3.7)$$

for slabs, where $b(\tau)$ and $c(\tau)$ are listed in Table 5.2 for both cases of the cylinder and the slab.

The drainage rate at the average temperature, Equations (4.3.3.6) and (4.3.3.7), is compared in Figure 4.9 with the drainage rate using the exact temperature distribution, Equation (4.2.5.3) and EOS (B.3). Figure 4.9 indicates that the drainage rate is underpredicted at early times using the average temperature, and the reverse is true at later times in the heating period. The solutions for the slab case, based on the Equations presented in Appendix A, are shown in Figure 4.10.

It was found that the area under the average temperature curve is only 2% less than that for the exact curve, for the time in Figure 4.9. This suggests that using average temperature due to conduction in a block under thermal gravity drainage is a very good approximation for the exact drainage rate, and that Equation (4.3.3.2) is accurate. This is a general conclusion and does not require implementation of HIM. However, by using

64

HIM very simple equations, such as Equations (4.3.3.4) to (4.3.3.7), are obtained for drainage rate calculations. Figure 4.10 present similar results for the slab case.
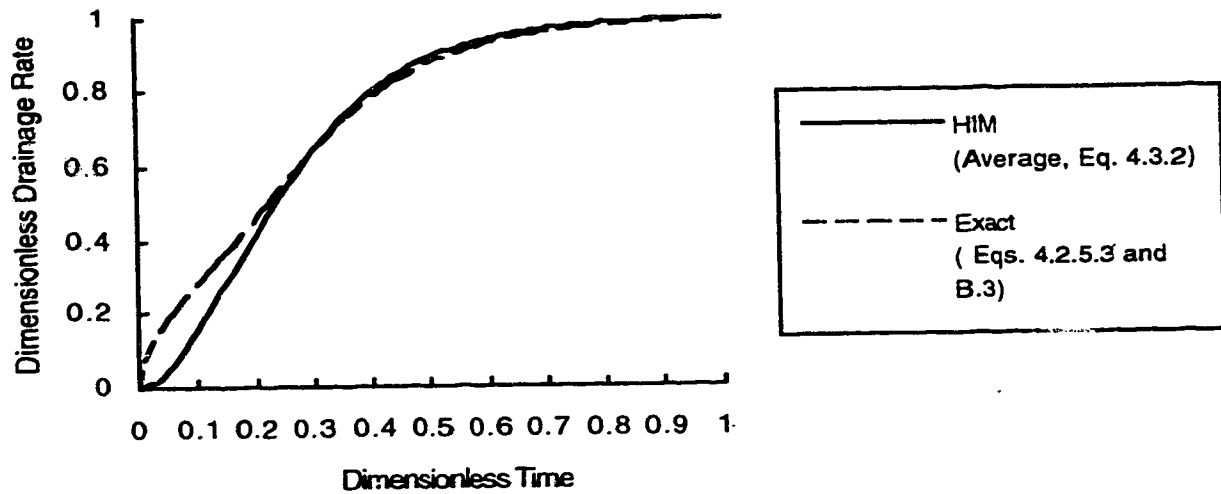
Figure 4.9. Thermal gravity drainage
from a cylinder (Evaluating the average
temperature assumption)
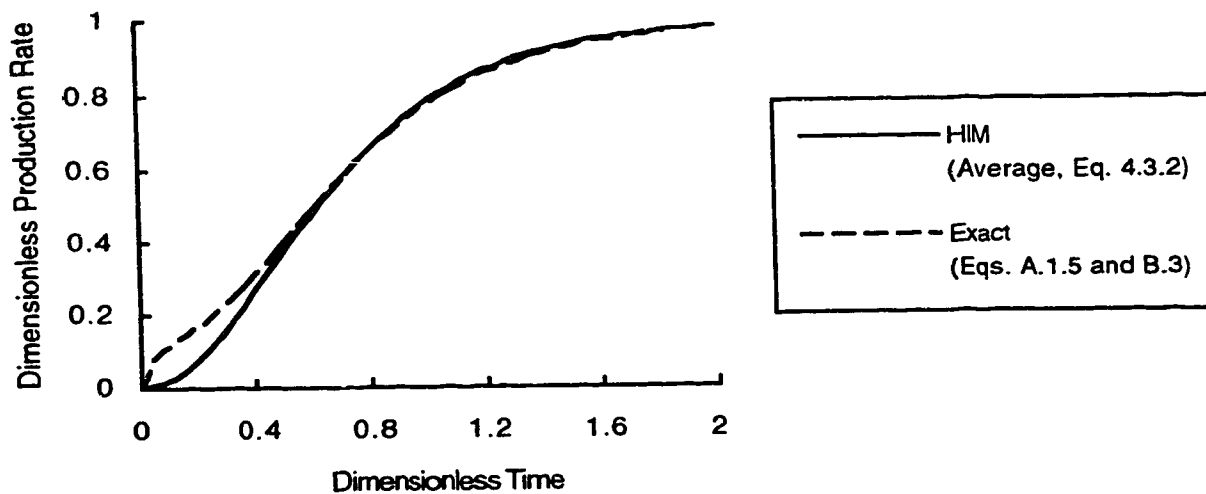
Figure 4.10 Thermal drainage from a
slab (Evaluating the average
temperature assumption)

5. RESULTS AND DISCUSSION – ANALYTICAL MODEL

5.1 Dual Behaviour of Thermal Gravity Drainage – Time Scale and Magnitude Analysis

In the analysis of heating of a matrix block a magnitude analysis was implemented and it was concluded that for typical properties of naturally fractured reservoirs, the effect of the moving interface, i.e., the Peclet No. is small. Previous experimental studies of non-isothermal gravity drainage from single blocks, however, indicated a significant effect of the moving boundary [Pooladi-Darvish 1992, Kharrat et al. 1993]. Table 5.1 gives the physical properties used in the thermal gravity drainage experiments performed by Pooladi-Darvish [1992].

Table 5.1
Physical properties of two experimental models [Pooladi-Darvish 1992]

	Model (1)	Model (2)
Height H	36 cm [0.36 m]	30 cm [0.3 m]
Width 2 L	34 cm [0.34 m]	30 cm [0.3 m]
Thickness L_1	2.5 cm [0.025 m]	5.5 cm [0.055 m]
Permeability k	650 D [6.5 $\times 10^{-10}$ m^2]	650 D [6.5 $\times 10^{-10}$ m^2]
Porosity ϕ	%35	%35
Thermal diffusivity α (estimated)	0.75 mm^2/s [7.5 $\times 10^{-7}$ m^2/s]	0.75 mm^2/s [7.5 $\times 10^{-7}$ m^2/s]
Saturation change ΔS_o	0.8	0.8
Initial temperature T_R	31 C	35 C
Steam temperature T_s	100 C	100 C
m	2.76	2.57
Density difference $\Delta \rho$	0.928	0.928
Kinematic viscosity at steam temperature v_{os}	58.7 cS [5.87 $\times 10^{-5}$ m^2/s]	58.7 cS [5.87 $\times 10^{-5}$ m^2/s]

66

If N_{Pe} is calculated using the data of Table 5.1 and if a frontal velocity of 5-10 cm/hr (about 2×10^{-5} m/s), as observed during the experiments of Pooladi-Darvish [1992] is used, a Peclet No. of the order of one is obtained, which explains the strong moving boundary behaviour of the experiments.

A time scale analysis can be performed to compare the velocity of the two simultaneous processes of heat flow and gravity drainage. Using Equations (4.2.3.1) to (4.2.3.3) it is found that $\tau_d \ll \tau_{hc}$. This suggests that the heated oil could easily flow and allow further movement of the steam-oil interface.

The above comparisons explain why using a high permeability sand pack had altered the behaviour of the process, and that for typical properties of naturally fractured reservoirs the heating process acts much faster than the fluid flow process, and hence, the effect of fluid flow on heat transfer can be ignored.
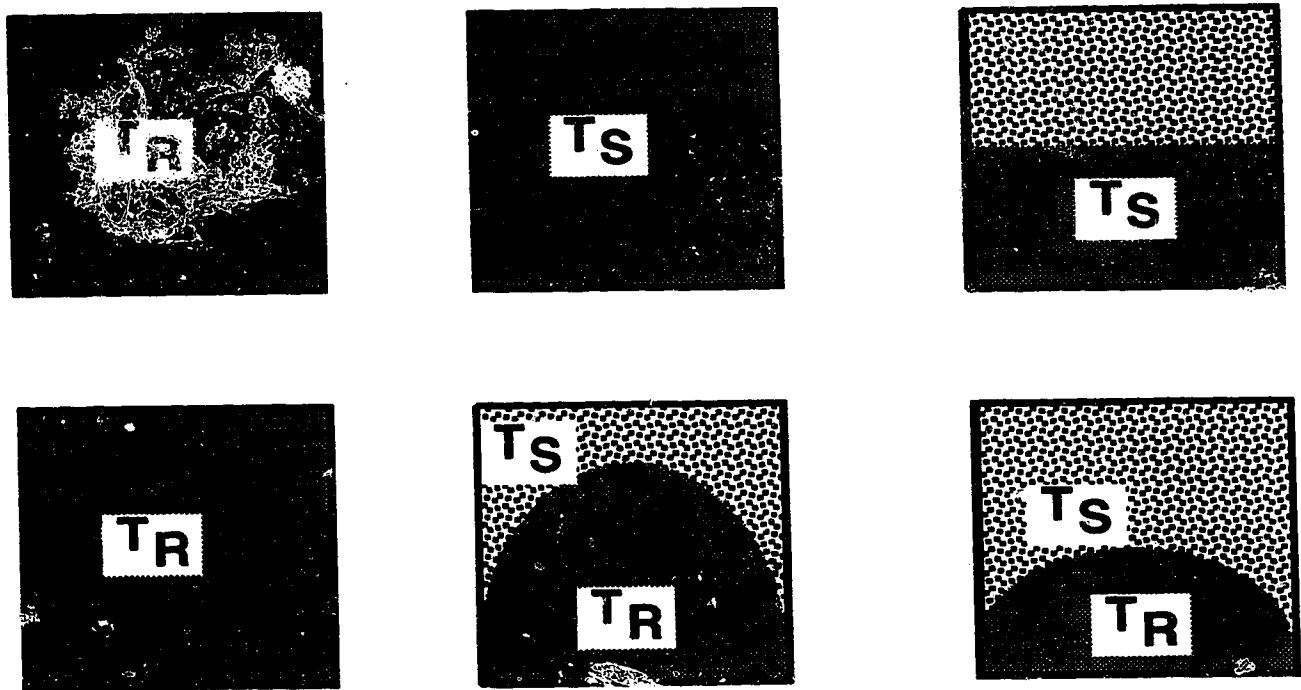
Figure 5.1   Different stages of heating and drainage of heavy oil from a single block. Above: reservoir conditions, Below: experimental conditions of Pooladi Darvish [1992]

Figure 5.1 shows schematically the gravity drainage of heavy oil from a single block under typical field conditions and under experimental conditions of Pooladi-Darvish [1992].

5.2. Scaling Considerations for Physical Modelling of Non-Isothermal Gravity Drainage from Fractured Reservoirs

Pooladi-Darvish [1992] used a high permeability matrix block so that he could perform his experiments in a reasonable time. It was discussed above, that his experiments did not represent the behaviour of gravity drainage under field conditions. Thus a question may be raised, as to whether it is possible to perform experimental studies of thermal gravity drainage from single blocks that represent field conditions. To answer this question the above time scale analysis is used to design experiments that represent a constant ratio between the time scales of heat flow and gravity drainage, between the field and the model.

$$\left(\frac{\tau_{hc}}{\tau_d}\right)_{field} = \left(\frac{\tau_{hc}}{\tau_d}\right)_{model} \qquad \dots\dots\dots\dots(5.2.1)$$

Using Equations (4.2.3.1) to (4.2.3.3) it is concluded that Equation (5.2.1) will be satisfied if other than the geometric similarity, Equation (5.2.2) is followed.

$$(N_{Ra})_{field} = (N_{Ra})_{model} \qquad \dots\dots\dots\dots(5.2.2)$$

where the Rayleigh No., N_{Ra}, signifies the importance of convective flow to conductive heat transfer. In this problem, the convective flow is due to gravity drainage of oil from the block.

$$N_{Ra} = \frac{kgL\Delta\rho}{\phi\Delta S_G\mu_{os}} \times \frac{1}{\alpha} \qquad \dots\dots\dots\dots(5.2.3)$$

In subsequent chapters it will be shown that the Rayleigh No., as defined by Equation (5.2.3), is an important dimensionless group in non-isothermal gravity drainage of oil in high permeability systems, too.

It is interesting to note that the above criterion satisfies the equality of the Peclet No. in the model and prototype, as was found to be important in Chapter 4. Once the scaling criterion is obtained it should be checked if materials can be found to satisfy the criterion, and also to allow performing the experiments in reasonable time and space. Suppose one would like to scale an actual case with the typical properties of Table 4.1 with materials representing a mobility of 1 darcy/cp. This would allow performing the experiments in a reasonable period of time. To satisfy Equation (5.2.2) one has to choose an experimental model such that $\frac{L\Delta\rho}{\alpha\phi\Delta S_o}$ is smaller than that in the field by a factor of 10^4.

By having dimensions in the range of 10 to 100 times smaller than the actual case and by having a thermal diffusivity 10^2 times larger than field, for example, by using metal beads, it is possible to satisfy Equation (5.2.2).

Care should be taken such that, while non-isothermal gravity drainage is scaled, other recovery mechanisms are not enhanced or suppressed. For example, using metal beads might increase the effect of oil recovery due to thermal expansion. As another example, it was pointed out in Chapter 2 that capillary forces affect the recovery more, when the size of the model is reduced. On the other hand, increasing the permeability reduces the capillary forces. Here, it is not intended to present a complete set of scaling criteria for thermal recovery from fractured reservoirs, but it is desired to consider non-isothermal gravity drainage and present guidelines for experimental study of the process.

5.3. The Error Introduced by the Assumption of Thermal Equilibrium

The detailed discussions in Chapter 4 indicated that, for typical properties of naturally fractured reservoirs, one can approximate the nonlinear problem of heating of a matrix block by a linear conduction problem. In a later part of the same chapter, the Heat Integral Method was used to obtain conductive temperature distributions in polynomial form. A summary of the temperature profiles for the slab and cylindrical cases obtained from HIM along with the exact solutions [Carslaw and Jaeger 1959] are given in Table 5.2. The approximate profiles were compared with the exact ones in Figures 4.5 and 4.6. and it was shown that HIM provided good approximations for the linear conductive problems.

Figures 4.5 and 4.6 indicated that the average temperature of a matrix block approached that of steam after a dimensionless time of $\tau = 1$. This corresponds tr

approximately 2 months for the typical properties of Table 4.1. By assuming thermal equilibrium between the fracture and the matrix a two months period during which oil drainage is significantly lower than that at steam temperature is ignored. This may or may not be significant in the design and evaluation of a thermal project. van Wunnik and Wit [1992] assumed thermal equilibrium between the fracture and the matrix, and studied gravity drainage of oil from matrix blocks. They never estimated the error that the thermal equilibrium assumption might have introduced.

Table 5.2 Summary of exact and approximate temperature profiles

---

• Single block-slab

Exact: $\displaystyle 1 - \frac{4}{\pi} \sum_{n=1}^{\infty} \frac{\sin\left(\frac{(2n-1)\pi}{2}\xi\right)}{2n-1} \exp\left[-\left(\frac{2n-1}{2}\right)^2 \pi^2 \tau\right]$

Approximate: $\displaystyle \left(1 - \frac{\xi}{\sqrt{24\tau}}\right)^3$ $\tau \leq \frac{1}{2J}$

$1 + b(\tau)\xi + c(\tau)\xi^2$ $0 \leq \xi \leq \frac{1}{2}$ $\tau \geq \frac{1}{24}$

$1 + b(\tau)(-\frac{1}{4} + 2\xi - \xi^2) + c(\tau)(-\frac{1}{2} + 2\xi - \xi^2)$ $\frac{1}{2} \leq \xi \leq 1$ $\tau \geq \frac{1}{24}$

where

$b(\tau) = -0.58579 A_1 \exp(m_1\tau) - 3.41421 A_2 \exp(m_2\tau)$

$c(\tau) = A_1 \exp(m_1\tau) + A_2 \exp(m_2\tau)$

$m_1 = -31.689$

$m_2 = -2.5967$

$A_1 = 7.32903$

$A_2 = 0.60492$

• Single block-cylinder

Exact: $\displaystyle 1 - 2\sum_{n=1}^{\infty} \frac{J_0(\beta_n\chi)}{\beta_n J_1(\beta_n)} \exp\left(-\beta_n^2 \tau\right)$

where β_n, $n = 1, 2, \ldots$, are roots of $J_0(\beta) = 0$.

Approximate:
$$\theta = \frac{\left(\chi^2 - 1 + \sqrt{48\tau}\right)^2}{48\tau} \qquad \tau \leq \frac{1}{48}$$

$$\theta = 1 + b(\tau)(\chi - 1) + c(\tau)(\chi^2 - 1) \qquad \frac{1}{2} \leq \chi \leq 1 \qquad \tau \geq \frac{1}{48}$$

$$\theta = 1 + b(\tau)(\chi^2 - \frac{3}{4}) + c(\tau)(\chi^2 - 1) \qquad 0 \leq \chi \leq \frac{1}{2} \qquad \tau \geq \frac{1}{48}$$

where

$$b(\tau) = 24.47112 A_1 \exp(m_1\tau) - 1.47112 A_2 \exp(m_2\tau)$$

$$c(\tau) = A_1 \exp(m_1\tau) + A_2 \exp(m_2\tau)$$

$$m_1 = -6.30105$$

$$m_2 = -42.3946$$

$$A_1 = 0.08283$$

$$A_2 = 9.49929$$

5.4. Importance of Thermal Gravity Drainage in Fractured Reservoirs

In Section 4.3 the temperature distribution obtained from HIM was combined with a viscosity-temperature relationship and Darcy's law. This permitted a closed-form solution for thermal gravity drainage for some values of m. The average temperature assumption was then examined, and it was concluded that the viscosity of the oil at an average block temperature at any time was representative of the average viscosity of the block. By using the average temperature assumption very simple equations were obtained that described thermal gravity drainage from single blocks. The relations are expressed in dimensional form as Equations (5.4.1) and (5.4.2) for cylinders and slabs, respectively.

$$\bar{q} = \frac{k\Delta\rho g}{\mu_{os}}\left(\frac{16}{3}\frac{\alpha t}{R^2}\right)^{\frac{m}{2}} \qquad t \leq \frac{R^2}{48\alpha} \qquad \ldots\ldots (5.4.1.a)$$

$$\bar{q} = \frac{k\Delta\rho g}{\mu_{os}}\left[1 - 0.696\exp\left(m_1\frac{\alpha t}{R^2}\right) - 0.237\exp\left(m_2\frac{\alpha t}{R^2}\right)\right]^{m} \qquad t \geq \frac{R^2}{48\alpha} \qquad \ldots\ldots (5.4.1.b)$$

71

where,

$$m_1 = -6.30105$$
$$m_2 = -42.3946$$

and,

$$\bar{q} = \frac{k\Delta\rho g}{\mu_{os}}\left(\frac{3}{2}\frac{\alpha t}{L^2}\right)^{\frac{m}{2}} \qquad t \leq \frac{L^2}{24\alpha} \qquad \ldots\ldots (5.4.2.a)$$

$$\bar{q} = \frac{k\Delta\rho g}{\mu_{os}}\left[1 - 0.135\exp\left(m_1\frac{\alpha t}{L^2}\right) - 0.795\exp\left(m_2\frac{\alpha t}{L^2}\right)\right]^{m} \qquad t \geq \frac{L^2}{24\alpha} \qquad \ldots\ldots (5.4.2.b)$$

where,

$$m_1 = -31.689$$
$$m_2 = -2.5967$$

In Equations (5.4.1) and (5.4.2), m is a characteristic of heavy oil and is found using the viscosity-temperature relation of the heavy oil and Equation (B.1) in Appendix B. To develop Equations (5.4.1) and (5.4.2) capillary forces were neglected. Their effect can be incorporated when the block height is much larger than the threshold height of the block, by multiplying the right hand side of the above equations by $1 - \frac{H_c}{H}$, where H_c is the threshold height of the block [Saidi 1987].

▸ Equations (5.4.1) and (5.4.2) are very easy to use and that they relate the productic to the physical properties of the rock and fluids and the time of consideration.

The non-isothermal gravity drainage from a cylindrical and a slab block with typical properties of Table 4.1 is shown in Figures 5.2 and 5.3, respectively. It can be observed that the drainage rate increases at the beginning, because of the reduction of the viscosity of the heavy oil during the heating period, and it levels off when the temperature of the whole block has approached that of steam. At this time the drainage

72

rate corresponds to the isothermal drainage rate at steam temperature. Note that at large times, the term in the square bracket in Equations (5.4.1) and (5.4.2) approaches one.
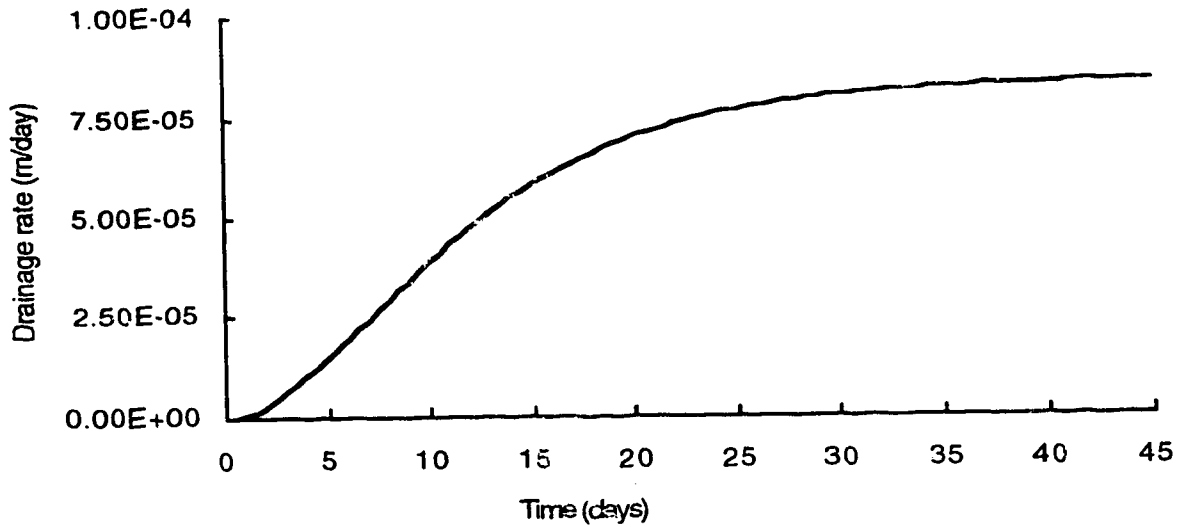
Figure 5.2. Non-isothermal drainage rate from a single block (average temperature for a cylinder)
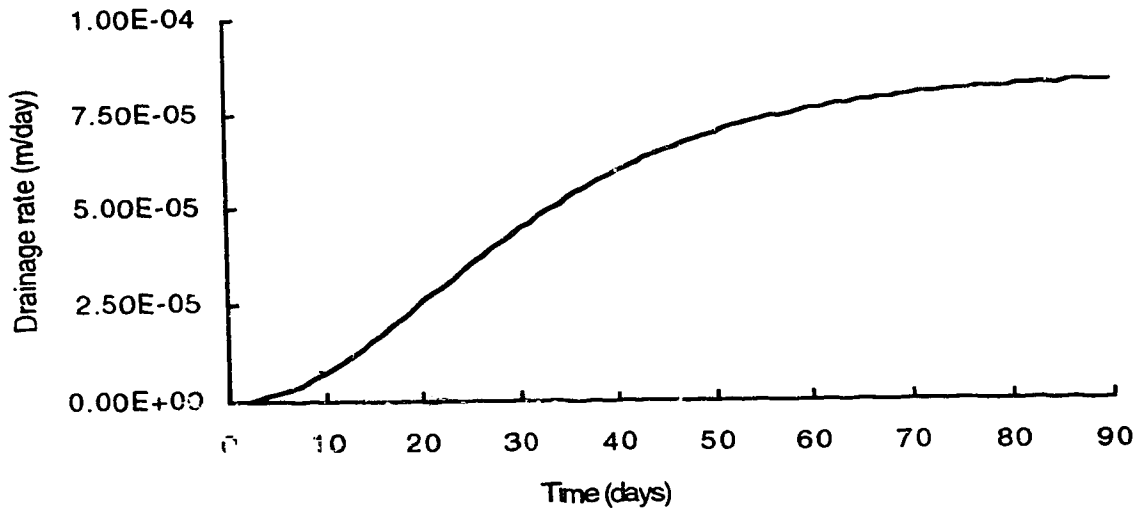
Figure 5.3. Non-isothermal drainage rate from a single block (average temperature for a slab)

Figures 5.2 and 5.3 indicate that the heating period is very short compared to the drainage time for typical fractured reservoirs (see also Equation 4.2.3.4). After the heating period, oil production corresponds to gravity drainage of the heated oil at steam temperature; hence, it can be concluded that the effectiveness of thermal gravity drainage depends on the ability to spread steam in the fracture network so that a large number of blocks start to be heated early in the operational life of the reservoir. Naturally fractured reservoirs allow high injection rates because of the high transmissibility of the fractures.

Figures 5.2 and 5.3 indicate that for the typical properties of Table 4.1 gravity drainage is a slow process for heavy oil recovery from fractured reservoirs. For example, if it is assumed that only one single block in the vertical direction contributes to drainage, for a production rate of 100 m³/day a drainage area of 10^6 m² would be required for each well.

It is worth noting that fractured reservoirs are characterized by high formation thickness. If we assume that fractured reservoirs behave as that predicted by the double-porosity theory [Warren and Root 1963], that is, if we assume that individual blocks act as individual source units and do not interact, a drainage area of 10^4 m² is required to achieve a production rate of 100 m³/day in a 40 m thick formation[5]. This thickness is not rare among fractured reservoirs [Saidi 1987].

For more favourable cases, however, gravity drainage may be an important mechanism. For example, Equations (5.4.1) and (5.4.2) suggest that the oil produced in a 10^4 m² pattern is about 100 m³/day, if the viscosity of the heavy oil is about 1 mPa s at steam temperature and the matrix permeability is about 10 md. It should be noted that, due to high transmissibility of the fracture network in fractured reservoirs, larger patterns are usually implemented. One notes that, Equations (5.4.1) and (5.4.2) give conservative results for such cases. This is because for higher mobilities at steam temperature, than typical values of Table 4.1, the effect of the moving boundary may not be negligible and a shorter time is required for the temperature in the matrix block to approach that of steam.

An example in Chapter 6 indicates that the error introduced by neglecting the effect of the moving boundary, even at a Peclet No. of 0.1, is not large (see Figure 6.5). In

---

5   A value of 4 m was assigned for block height as reported in Table 4.1.

such cases Equations (5.4.1) and (5.4.2) should give good approximations for thermal gravity drainage from single blocks.

5.5. Important Parameters Affecting Thermal Gravity Drainage

One of the important motivations in seeking analytical solutions is that the effect of different parameters can be studied easily once a closed-form solution is obtained. Equations 5.4.1 and 5.4.2 indicate that thermal gravity drainage of heavy oil in typical fractured reservoirs is proportional to the oil mobility at steam temperature. Although this may not sound surprising at first, a study of thermal gravity drainage in high permeability systems will indicate that this is not a general conclusion, and the thermal gravity drainage rate in such systems is proportional to the square root of the oil mobility at steam temperature [Butler et al. 1981]. The reason is that, in high permeability systems, not all of the oil is heated to steam temperature in a short time, as compared to the time scale of the process, whereas this occurs in low permeability systems[6].

Equations (5.4.1) and (5.4.2) indicate that average block size of a fractured reservoir is the other important parameter that affects thermal gravity drainage. A larger block size postpones the time corresponding to the maximum drainage rate. Other parameters, such as $\Delta \rho = \rho_o - \rho_s$ and α do not vary drastically among petroleum reservoirs.

5.6. Range of Application of HIM

The Heat Integral Method was used in Section 4.3 to obtain approximate solutions for a conduction problem. HIM simplifies the process of obtaining analytical solution by providing a means to find simple polynomial function to approximate conductive processes. The polynomial solutions are then combined with other equations and closed-form solutions may be obtained. HIM was used in Chapter 4 and it will be used again in Chapter 6 to obtain simple mathematical models for different thermal recovery processes.

---

6   In many places in this work the term "high permeability" systems in contrast with "low permeability" ones is used. The proper term is: systems with "high Rayleigh No." and the ones with "low Rayleigh No.".

To the best of the author's knowledge this is the first time that systematic application of HIM is introduced into the petroleum literature[7].

The application of HIM was explained in Section 4.3 and the derivation of the equations was shown in detail. Here, comments will be given on the range of its applications. (for a detailed discussion and further references, Crank [1988] and Ozisik [1980] may be referred to).

In HIM, a trial function is introduced and then is forced to satisfy an integrated form of the corresponding equation. The challenge is to propose an appropriate trial function which does not require complicated mathematical manipulation and offers a good approximation for the problem of interest. The use of high order polynomials does not necessarily increase the accuracy of the method. Applying HIM over subsequent sub-intervals, however, is known as a systematic way of improving the accuracy of the method. An example of such an exercise was given in Section 4.3, where the temperature distribution in a cylinder was approximated with two polynomials after the heat flow had affected the no-flow boundary.

An advantage of the Heat Integral Method is that it can be applied readily to nonlinear problems as well as linear ones. Solutions have been given for cases where the nonlinearity has been due to the differential equation itself and/or due to the boundary conditions. The solution of phase change problems is an example of the latter and that of heat conduction in a medium with temperature dependent properties is an example of the former. Although there have been successful attempts to use HIM for two- and three-dimensional problems, its use is most suited for 1-D problems. Finally, application of HIM has not been limited to the problems with uniform initial conditions, and solutions have been given for those with non-uniform initial conditions, too.

---

7   The fundamentals of HIM were previously used by Vinsome and Westerveld [1980] and Butler [1985-b], however, no reference to HIM was given. This is the first time that HIM is introduced as a general method for approximating diffusion dominated processes in the petroleum literature.

6. APPLICATION OF THE HEAT INTEGRAL METHOD (HIM) FOR MODELLING THERMAL RECOVERY METHODS UNDER CONDUCTION HEATING

It was shown in Chapter 4 that the oil flow rate from a single block under conduction heating could be modelled using analytical methods. A closed-form solution was possible, because the exact temperature distribution, typically expressed as infinite series or error function solutions, could be approximated by a polynomial function. The polynomial was forced to satisfy the original heat equation in an integrated form along with the appropriate initial and boundary conditions. Hence, the Heat Integral Method (HIM) provided an approximate solution for the problem. Comparisons showed, however, that the approximate solutions were in good agreement with the exact ones. Review of the literature indicates that HIM has been used successfully in approximating temperature distributions under conduction heating. In thermal recovery methods, heating is achieved by either or both of the heating mechanisms, namely conduction and convection. Field experience and modelling studies have indicated that conduction plays a major role in a variety of processes. It was shown in Section 4.2 that matrix heating under gravity drainage is governed by conduction. Conduction causes mobilization of heavy oil in the vicinity of artificial fractures created by steam injection above the formation parting pressure [Closmann and Smith 1983]. In mature steam drives with complete override, gravity drainage of oil heated by conduction was shown to be the major recovery mechanism [Closmann 1995]. Analytical and semi-analytical models of the SAGD process have considered conduction as the only heating mechanism, and numerous comparisons with experimental data suggest the validity of the assumption [see Butler 1991 and the references there].

In thermal recovery methods utilizing conduction heating, a steam-oil interface is considered and heating occurs ahead of the interface. The interface moves through the reservoir, while oil is produced. To simplify the modelling task, two assumptions have been used in the literature with respect to the behaviour of the moving interface. Some of the predictive models neglected the effect of the moving boundary, while others assumed a steady-state condition. It was shown in Section 4.2 that the movement of the interface can be neglected if the interface velocity is small. The criterion for estimating the importance of the interface velocity was given there. It can be shown, however, that steady-state conditions can be approached in a short period of time if the velocity of the

77

interface, i.e., the Peclet No., is large. If the velocity of the interface is somewhere in between, none of the above assumptions may be justified.

In this chapter simple predictive models are developed for such cases where the process is far from steady-state. Steady-state cases were previously discussed in the literature [Butler et al. 1981, Closmann 1995]. Both cases where the interface velocity is negligible and intermediate are considered. Through the application of HIM it will be possible to analytically perform a large portion, if not all, of the mathematical derivation and develop simpler and/or more accurate models.

As the first case, an analytical solution for a mature steamflood under steam-drag forces is developed, where the interface velocity can be neglected. Later, semi-analytical models are developed for the SAGD process in linear and cylindrical geometries. It will be shown that the effect of the moving interface cannot be neglected in the latter cases. In each case the model is first developed, and then some of the assumptions involved in the derivation are justified.

6.1. An Analytical Steam-Drag Model

Numerous researchers have developed simple mathematical models to calculate the oil production rate in mature steamflood projects under conduction heating. Miller and Leung [1985] considered a horizontal, stationary oil-steam interface and used the analytical solution of heat conduction in a semi-infinite reservoir to describe the temperature distribution. Numerical integration was used to obtain the oil flow. Kumar et al. [1986] accounted for the downward movement of the horizontal interface and obtained the temperature solution. Again, numerical integration was necessary to incorporate the effect of the varying viscosity on the oil flow rate, and also to proceed in time. Closmann [1995] used the exponential form of the temperature distribution ahead of a horizontal interface which corresponded to steady-state conditions. He obtained analytical solutions for gravity driven oil flow. Recently, Kimber et al. [1995] developed an analytical model to calculate the oil flow rate by gravity and pressure forces in mature steamfloods. They used a normalized equation to approximate the unsteady-state temperature distribution ahead of an advancing steam front. The authors assumed a heated region with a constant viscosity around the production well.

In this section, oil flow is found from a closed-form solution for those cases which are far from steady-state, and the temperature distribution corresponds to unsteady-state heat flow ahead of a stationary boundary. As was shown is Section 4.2 the stationary boundary assumption is valid provided that the velocity of the interface is small. The oil flow mechanism is considered to be drag flow caused by the pressure difference between the injector and producer. Different studies, reviewed earlier, have shown that the oil production rate due to pressure forces after steam breakthrough is minimal; however, a review of the literature indicates that there is interest in obtaining a simple solution for such a problem. This is achieved in this section by using the Heat Integral Method.
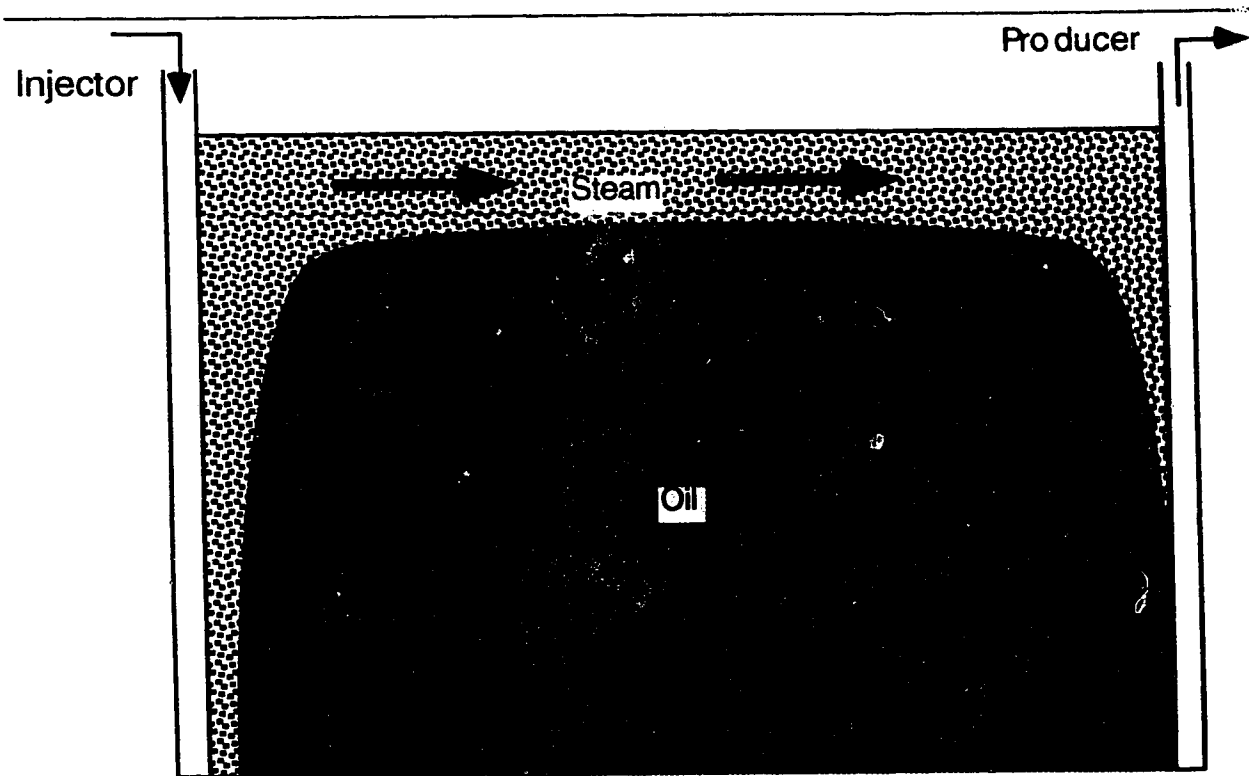
Figure 6.1. Schematic diagram of a mature steamflood project

Figure 6.1 shows a schematic diagram of a mature steamflood, where an overlying steam zone is considered above the oil column. Heat is transferred by conduction ahead of the steam-oil interface, assumed to be horizontal, and reduces the oil viscosity. The heated oil is driven towards the production well by the pressure difference between the injector and the producer. Single phase oil flow is assumed and capillary and

gravity forces are neglected. The steam zone temperature is assumed to correspond to the saturated steam temperature at the average steam zone pressure. The problem of interest is a combined heat and fluid flow problem. In the following an approximate solution for the heat flow problem is found. The latter is then used to obtain the oil production rate.

6.1.1. Heat Flow Problem

Heat conduction ahead of a horizontal oil-steam interface can be explained by Equations (6.1.1.1) to (6.1.1.4.), provided that the thermal diffusivity of the base rock is equal to that of the reservoir. This is assumed to be the case.

$$\frac{\partial^2 T}{\partial z^2} = \frac{1}{\alpha}\frac{\partial T}{\partial t} \qquad\qquad z \geq 0 \qquad\qquad t > 0 \qquad \ldots\ldots\ldots\ldots (6.1.1.1)$$

$$T = T_R \qquad\qquad z \geq 0 \qquad\qquad t = 0 \qquad \ldots\ldots\ldots\ldots (6.1.1.2)$$

$$T = T_S \qquad\qquad z = 0 \qquad\qquad t > 0 \qquad \ldots\ldots\ldots\ldots (6.1.1.3)$$

$$T = T_R \qquad\qquad z \to \infty \qquad\qquad t > 0 \qquad \ldots\ldots\ldots\ldots (6.1.1.4)$$

where $z = 0$ is the location of the stationary horizontal interface and z is considered positive downwards. Dimensionless variables are defined by Equations (6.1.1.5) to (6.1.1.7)

$$\theta = \frac{T - T_R}{T_S - T_R} \qquad\qquad\qquad \ldots\ldots\ldots\ldots (6.1.1.5)$$

$$\eta = \frac{z}{1} \qquad\qquad\qquad \ldots\ldots\ldots\ldots (6.1.1.6)$$

$$\tau = \frac{\alpha t}{1} \qquad\qquad\qquad \ldots\ldots\ldots\ldots (6.1.1.7)$$

The semi-infinite conduction problem of (6.1.1.1) to (6.1.1.4), in terms of dimensionless variables, can be expressed as:

$$\frac{\partial^2 \theta}{\partial \eta^2} = \frac{\partial \theta}{\partial \tau} \qquad\qquad \eta \geq 0 \qquad\qquad \tau > 0 \qquad \ldots\ldots\ldots\ldots (6.1.1.8)$$

80

$$\theta = 0 \qquad\qquad \eta \geq 0 \qquad \tau = 0 \qquad \dots\dots\dots\dots (6.1.1.9)$$

$$\theta = 1 \qquad\qquad \eta = 0 \qquad \tau > 0 \qquad \dots\dots\dots\dots (6.1.1.10)$$

$$\theta = 0 \qquad\qquad \eta \to \infty \qquad \tau > 0 \qquad \dots\dots\dots\dots (6.1.1.11)$$

The analytical solution of the Equations (6.1.1.8) to (6.1.1.11) can be written as Equation (6.1.1.12)

$$\theta = \text{erfc}\left(\frac{\eta}{2\sqrt{\tau}}\right) \qquad\qquad \dots\dots\dots\dots (6.1.1.12)$$

By using the Heat Integral Method and by performing steps very similar to those performed in Appendix A, one can find a third order polynomial to approximate Equation (6.1.1.12)

$$\theta = \left(1 - \frac{\eta}{\delta}\right)^3 \qquad 0 \leq \eta \leq \delta \qquad \tau > 0 \qquad \dots\dots\dots\dots (6.1.1.13)$$

where

$$\delta = \sqrt{24\tau} \qquad\qquad \dots\dots\dots\dots (6.1.1.14)$$

Equation (6.1.1.13) is the same as Equation (A.1.15) obtained in Appendix A, and is valid in the heated region, that is, $0 \leq \eta \leq \sqrt{24\tau}$. Based on the definition of the heat penetration depth, the temperature is equal to its initial value for $\eta \geq \sqrt{24\tau}$.

Figure 6.2 compares the exact solution with the solution found by the application of HIM. In Equations (6.1.1.6) and (6.1.1.7) the vertical direction is normalized by unit height. However, this does not affect the comparisons shown in Figure 6.2 since Equations (6.1.1.12) and (6.1.1.13) are independent of the value used for the normalization of z. Figure 6.2. indicates that the HIM solution is in good agreement with the exact solution.

In the next section Equation (6.1.1.13) is used as the temperature distribution in the heated zone to find an approximate solution for oil production rate.

81
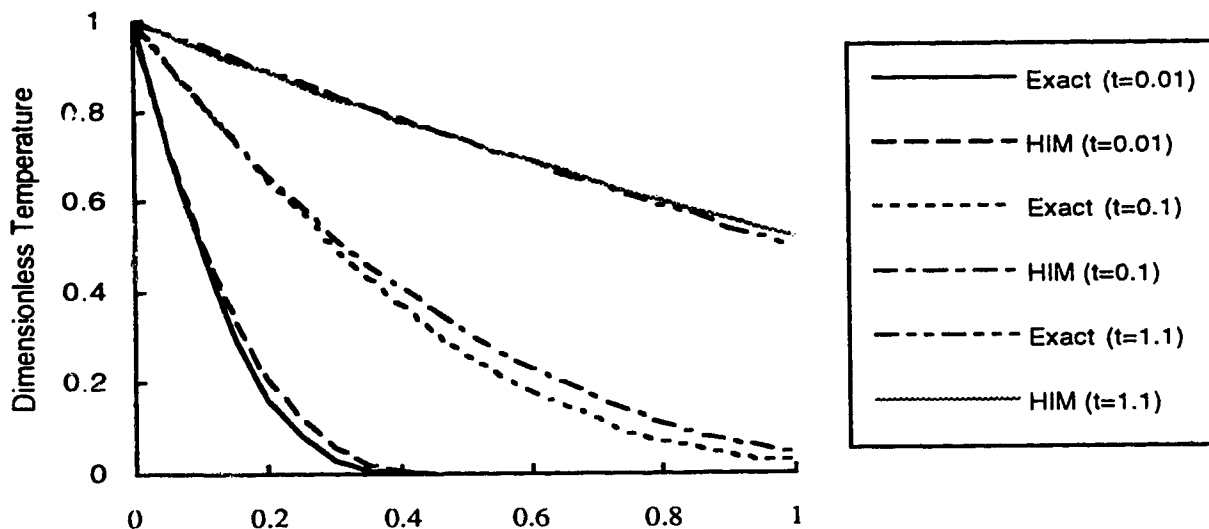
Figure 6.2. Temperature distribution by HIM
and exact solution (semi-infinite case)

6.1.2. Fluid Flow Problem

Because of the low mobility of cold oil far from the interface, oil flow is considered to be horizontal and induced by the pressure difference between the producer and the injector. In bituminous reservoirs where steam injection is carried out after creating horizontal fractures in the formation, the steam-drag model applies for oil flow below the fracture. Closmann and Smith [1983] showed that the temperature distribution below a steamed fracture could be duplicated precisely by using a heat conduction model from a stationary interface, that is, by Equation (6.1.1.12).

For an element of $d\eta$, located at a constant distance from the horizontal interface, and having a constant viscosity, similar to that proposed by Kumar *et al.* [1986] one can write

$$dq = \frac{k}{\mu_o(T)} c\Delta P C dz = \frac{k}{\mu_o(T)} c\Delta P C d\eta \times 1$$

. . . . (6.1.2.1)

where ΔP is the differential pressure between the injector and the producer. C is the net to gross ratio, and c is a geometric factor to account for the pattern shape. For a five-spot pattern, c is given by Equation (6.1.2.2) [Prats 1982]

$$c = \frac{\pi}{\ln\left(\frac{d}{r_W}\right) - 0.964} \qquad \qquad \dots \dots \dots \dots (6.1.2.2)$$

where d is the distance between the two production wells, and r_W is the wellbore radius. The total flow rate in the heated area can be obtained by integrating Equation (6.1.2.1)

$$\dot{q} = \int_0^\delta d\dot{q} = \frac{kc\Delta PC}{\rho} \int_0^\delta \frac{d\eta}{v_o(\theta)} \qquad \delta \le h \qquad \dots \dots \dots \dots (6.1.2.3)$$

The viscosity-temperature relationship of Equation (6.1.2.4)[8] is used again.

$$\frac{v_{os}}{v_*} = \left(\frac{T - T_R}{T_* - T_*}\right)^{-t} \qquad \qquad \dots \dots \dots \dots (6.1.2.4)$$

By combining Equation (6.1.2.2), (6.1.4.1), (6.1.2.3) and (6.1.2.4) a closed-form solution can be obtained for the production rate, Equation (6.1.2.5),

$$\dot{q}(t) = D_1 \sqrt{t} \qquad t \le \frac{h^2}{24\alpha} \qquad \dots \dots \dots \dots (6.1.2.5)$$

where,

$$D_1 = \frac{kc\Delta PC}{\mu_{os}(3m + 1)} \sqrt{24\alpha} \qquad \qquad \dots \dots \dots \dots (6.1.2.6)$$

Equation (6.1.2.5) is valid before the heat penetration depth δ equals the height of the oil column. The available oil column decreases with time as production continues. Hence, the value of h in Equation (6.1.2.5) is less than the initial height of the oil column. However, it was previously assumed that heat conduction occurs ahead of a stationary boundary. Now, it is stated that the steam-oil interface is advancing due to oil

---

8   For a discussion on Equation (6.1.2.4) please refer to Section 4.3.

production. It was previously shown that the stationary boundary assumption for the heat flow process is valid so long as the velocity of the steam-oil interface is small. In other words, the effect of the moving boundary in the heat flow process is neglected, but it is accounted for in the oil flow calculations. A quantitative estimation of the introduced error in the heat flow process will be discussed later. Using the assumption that the heat flow is not affected by the movement of the interface, one can say that the heat penetration depth reaches the base rock when

$$t = \frac{h^2}{24\alpha} \qquad \qquad \dots\dots\dots\dots (6.1.2.7)$$

where h is the remaining oil column. In order to find the value of h at any time the material balance Equation (6.1.2.8) is used.

$$-\frac{dh}{dt} = \frac{\dot{q}(t)}{A\phi\Delta S_o C} \qquad \qquad \dots\dots\dots\dots (6.1.2.8)$$

where A is the pattern area. Substituting from Equation (6.1.2.5) into Equation (6.1.2.8) and performing the integration one obtains

$$H - h = D_2 t^{\frac{3}{2}} \qquad \qquad \dots\dots\dots\dots (6.1.2.9)$$

where

$$D_2 = \frac{2D_1}{3A\phi\Delta S_o C} \qquad \qquad \dots\dots\dots\dots (6.1.2.10)$$

By substituting from Equation (6.1.2.7) into Equation (6.1.2.9) one obtains a cubic equation that can be solved for h.

$$h^3 + \frac{(24\alpha)^{\frac{3}{2}}}{D_2} h - \frac{(24\alpha)^{\frac{3}{2}}}{D_2} H = 0 \qquad \qquad \dots\dots\dots\dots (6.1.2.11)$$

After the heat penetration depth equals the available oil column as obtained by Equation (6.1.2.11), Equation (6.1.2.3) can not be used any more; instead

$$\dot{q} = \int_0^h d\dot{q} = \frac{kc\Delta P C}{\rho} \int_0^h \frac{d\eta}{v_o(\theta)} \qquad \qquad \dots\dots\dots\dots (6.1.2.12)$$

84

or upon integration

$$\dot{q}(t) = D_1 \left[1 - \left(1 - \frac{h}{\sqrt{24\alpha}} \right)^{3m+1} \right] \sqrt{t} \qquad \dots\dots\dots (6.1.2.13)$$

In Equation (6.1.2.13) h is a variable. Hence, Equation (6.1.2.13) should be simultaneously solved with the material balance (6.1.2.8). This can be done in the following sequence:

1)   Find the time when the heat penetration depth equals the available oil column from Equations (6.1.2.11) and (6.1.2.7).

2)   Prior to the above time, analytically calculate the production rate from Equation (6.1.2.5).

3)   Calculate the remaining h for a time step of Δt from Equation (6.1.2.8), using the final production rate.

4)   Find the flow rate using the value of h from step (3) and Equation (6.1.2.13).

5)   Go back to step (3).

The above semi-analytical scheme had to be devised, since the analytical solution of Equations (6.1.2.13) and (6.1.2.8) was not possible. However, if one assumes that Equation (6.1.2.5) is valid for $t \geq \frac{h^2}{24\alpha}$, Equations (6.1.2.5) and (6.1.2.8) can be combined and solved for h

$$h = H - D_2 t^{\frac{3}{2}} \qquad \dots\dots\dots (6.1.2.14)$$

Substituting from Equation (6.1.2.14) into Equation (6.1.2.13) one obtains a closed-form solution for the non-isothermal oil production rate, similar to Equation (6.1.2.5)

85

$$q(t) = D_1 \left[1 - \left(1 - \frac{H - D_2 t^{\frac{1}{2}}}{\sqrt{24\alpha t}} \right)^{3m+1} \right] \sqrt{t} \qquad\qquad t \geq \frac{h^2}{24\alpha} \quad\ldots\ldots\ldots\ldots (6.1.2.15)$$

where h is found from Equation (6.1.2.11).

6.1.3. Results and Discussion of the Steam-Drag Model

Kumar *et al.* [1986] presented a field example, and showed comparisons of their semi-analytical model as well as the semi-analytical model of Miller and Leung [1985] with actual field data. The same example will be used to examine the accuracy of the closed-form solutions (6.1.2.5) and (6.1.2.15). The important assumptions made in the development of the above model will be discussed, and finally some guidelines for their range of applicability will be given.

Rock and fluid properties of the steamflood project at Kern River Canfield reservoir are given in Table 6.1

Table 6.1
Rock and fluid properties of Kern River Canfield [Kumar *et al.* 1986, Closmann 1995]

Permeability k	300 md [296 $\times 10^{-15}$ m^2]
Oil viscosity at steam temperature μ_{os}	3.17 cp [3.17 $\times 10^{-3}$ Pa.s]
Pattern area A	1.09 $\times 10^4$ m^2
Porosity $\times$ Saturation change $\phi \Delta S_o$	0.31 $\times 0.27$
Formation thickness H	36.6 m
Thermal diffusivity α	1.18 $\times 10^{-6}$ m^2/s
See Equation (6.1.2.4) m	2.573
Wellbore radius r_w	0.076 m
Differential pressure ΔP	350 kPa
Ratio of the net to gross thickness C	0.667

Using the physical properties of Table 6.1 the height of the oil column is calculated at the time that the heat penetration depth reaches the base rock. Using

86

Equation (6.1.2.11) it is found that h=34.59, and the corresponding time is 1.34 years. In other words it takes about 1.34 years for heat to reach the base rock, and during this period the steam zone has expanded about 2 m.

To obtain the oil flow rate Equation (6.1.2.5) is used prior to above time, and Equation (6.1.2.15) thereafter. For comparison, the oil flow rate found using the calculation procedure described in Section 6.1.2. is performed also. The results are shown in Figure 6.3. along with the predictions of the semi-analytical models of Miller and Leung [1985] and Kumar et al. [1986].
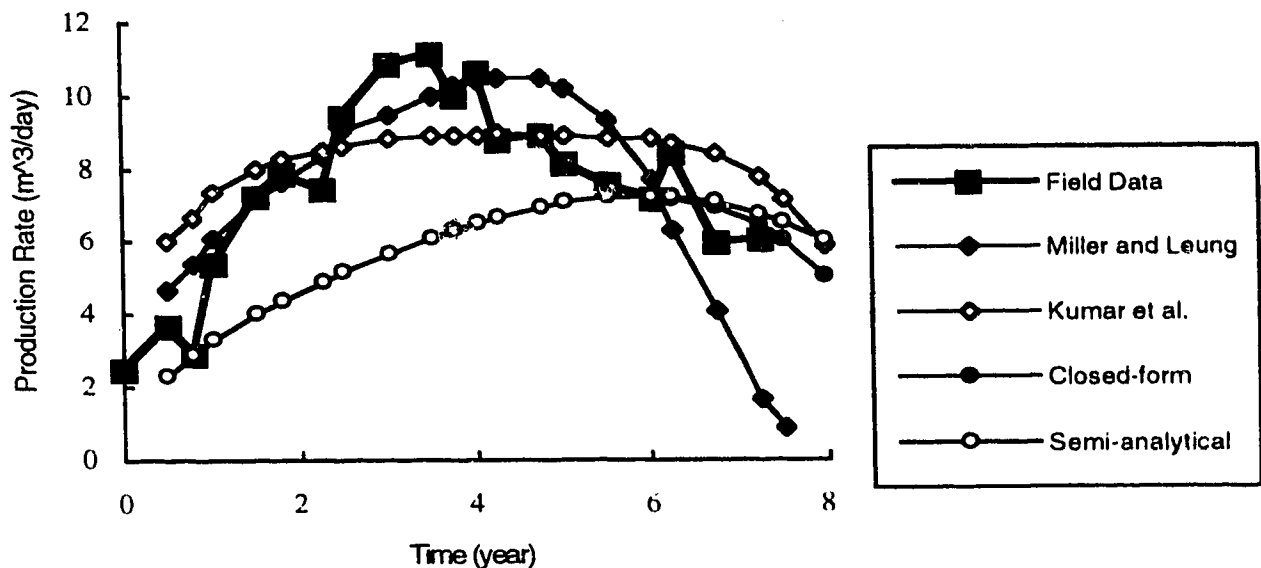
Figure 6.3. Oil production rate for Kern River Canfield

The results obtained from the closed-form solution, that is, Equations (6.1.2.5) and (6.1.2.15), are identical to those obtained from the semi-analytical scheme for the first six years, after which they differ slightly as shown in Figure 6.3. The closed-form solution, Equation (6.1.2.15), predicts a smaller production rate for the last two years, because Equation (6.1.2.5) accounts for oil flow in the total heated zone. A larger heated zone results in a larger production rate, especially at later times when the available oil column is small, and hence, a smaller available oil column for production. The remaining oil column as predicted by the two methods is shown in Figure 6.4.

87

Figure 6.4 indicates that the closed-form solution predicts a smaller oil column left in the reservoir compared to that predicted by the semi-analytical method. Substitution of the remaining oil column as predicted by the two methods, in Equation (6.1.2.13) results in slightly different production rates as shown in Figure 6.3.
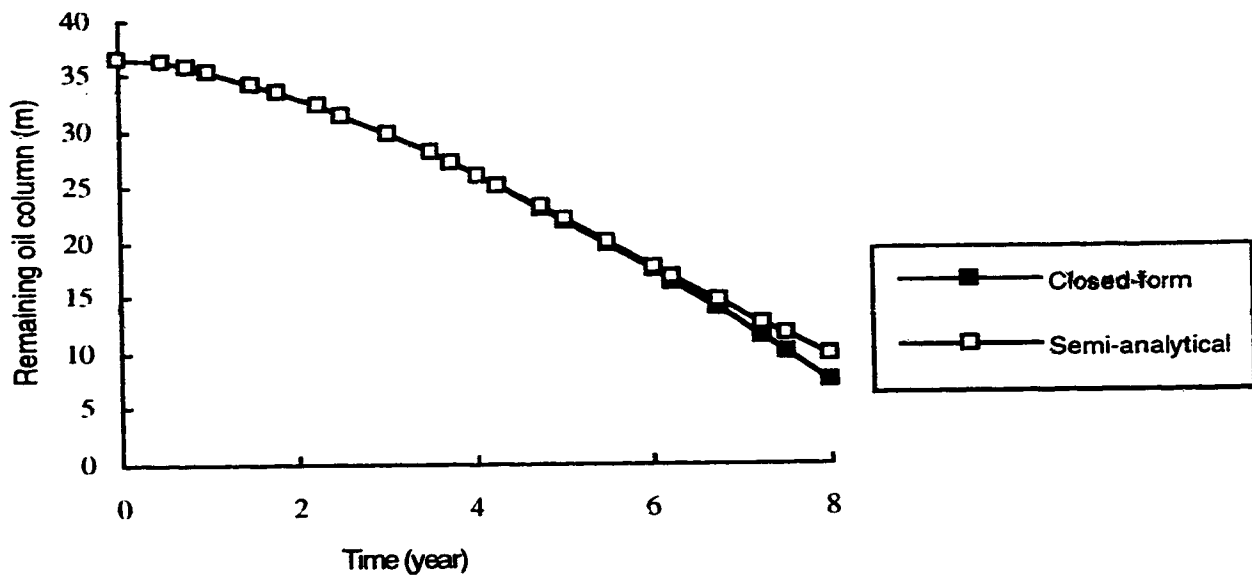
Figure 6.4. Oil column for Kern River Canfield

Kumar *et al.* [1986] used a permeability of 300 md, about one eighth of the formation permeability, to achieve a good match. The same data were used in this study as listed in Table 6.1. A combination of factors contribute to a lower permeability in the mathematical model than the absolute permeability of the formation. The effective permeability of the formation below an oil-steam interface is much less than the absolute permeability of the reservoir. The steam condensate penetrates ahead of the interface, and reduces the effective permeability to oil. Butler typically uses a reduction factor of 2.5 for the effective permeability of the formation ahead of a sloped oil-steam interface [see, for example, Butler 1994, P.178]. Additionally, the differential pressure between the injector and the producer was used as the effective pressure drop for driving the heated oil. The steam flow rate, however, decreases from the injector toward the producer due to steam condensation. Consequently, the effective pressure drop acting on the oil zone is less than

88

the differential pressure between the injector and producer. A quantitative evaluation of the effective pressure drop is not possible, unless more data regarding the steam injection and production rates, for example, are available. Due to the above factors, accuracy of the proposed model is best estimated if it is compared with similar models, i.e., those of Kumar et al. [1986] and Miller and Leung [1985].

In order to perform the oil flow rate calculations, Miller and Leung [1985] used the oil rate prior to steam injection enhanced by the reduced viscosity effects. The authors noted that, in order to keep the model simple, they did not consider any change in the driving mechanisms in the reservoir subsequent to steam injection, such as pressurization of the reservoir, etc. The authors incorporated an empirical factor to account for the size of the steam condensate region below the steam zone. Figure 6.3 indicates that their model follows the field data closely for the first six years, but declines much faster than the actual data thereafter.

Figure 6.3 shows that, the present model predicts smaller flow rates especially in the early stages of the project, compared to those obtained by Kumar et al. [1986]. This could be due to the fact that Equation (6.1.2.4) assumes a viscosity of infinity at reservoir temperature, while the actual viscosity is only 1700 mPa s. Hence, the present model predicts smaller flow rates when the reservoir is relatively cold, and as the reservoir temperature approaches that of steam the difference becomes smaller. This is because Equation (6.1.2.4) predicts a value equal to the actual oil viscosity at steam temperature. Similar behaviour was previously observed when Equation (6.1.2.4) was used [Griffin and Trofimenkoff 1985].

In the development of the steam-drag model, the effect of the moving interface in the heat flow solution was neglected. By using the data of Figure 6.4 one can estimate the velocity of the interface. The calculations indicate that the velocity of the interface in a dimensionless sense, the Peclet No., is very small initially and that it increases with time. Peclet No. reaches a value as high as 0.1 after about 3.5 years from the beginning of the project and stays fairly constant up to the end of project.

Figure 6.5 compares the exact temperature distribution ahead of a moving boundary with a constant N_{P_e} of 0.1, with that predicted by HIM, that is, Equations (6.1.1.13) and (6.1.1.14). Please note that the HIM solution is in good agreement with the

89

moving boundary solution where the oil flow rate is most important, that is in the hot region.

For such cases where the movement of the interface can not be neglected, an ordinary differential equation can be obtained that explains the behaviour of the heat penetration depth with time. This can be solved simultaneously with the fluid flow problem. In the next two sections the moving boundary problem of SAGD, in linear and cylindrical coordinates, is solved and account is taken for the movement of the interface. The same methodology can be used for similar 1-D conduction problems ahead of a moving boundary.

It is believed that the availability of simple closed-form solutions as obtained above, is useful for such cases where the interface velocity is negligible, or at least as an initial tool for evaluating the complexity of the problem, and choosing the appropriate mathematical model.
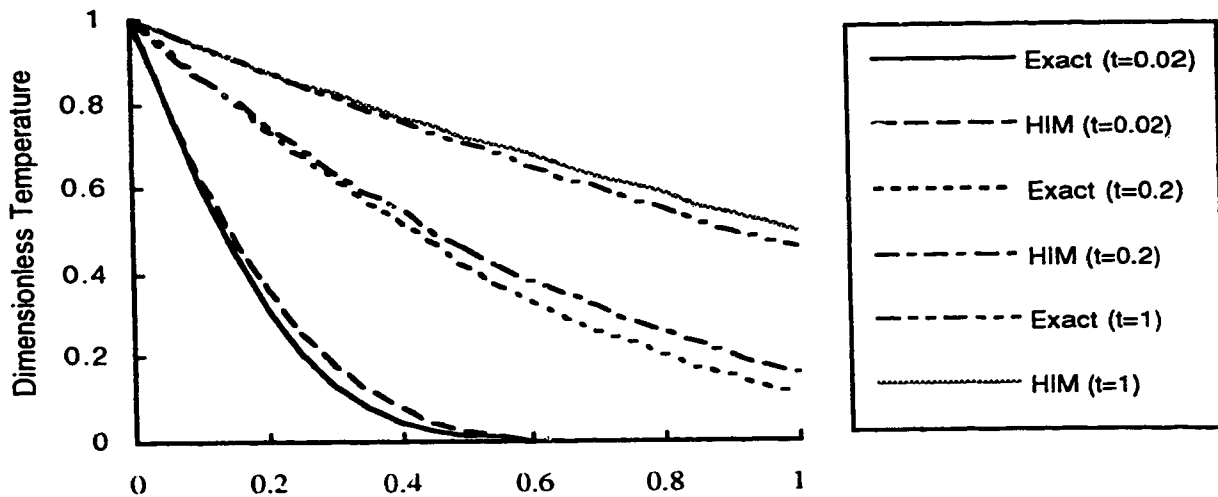
Dimensionless Distance from Boundary
Figure 6.5 Stationary boundary HIM vs exact
moving boundary solutions

6.2. A Semi-Analytical Model for the Linear SAGD Process

In this section a semi-analytical model is presented for predicting the behaviour of the SAGD process with the application of horizontal wells. It was noted previously that in the SAGD process steam is injected through a horizontal well. After the steam zone reaches the cap rock, the steam zone expands sideways while the heated oil ahead of the interface is drained in a stable manner. The sideways expanding stage of the process will be considered.

Reis [1992-b] assumed the curved interface could be represented by a straight line. Here, the shape and location of the interface are found as a part of the solution. Butler *et al.* [1981] presented an analytical model for the above process, assuming that the heat and fluid flow processes occurred one dimensionally and under steady-state conditions. Later, an improvement on the original SAGD model was given by Butler [1985-b], and the 1-D heat flow was considered to be unsteady-state. Since the present method is very similar to that presented by Butler [1985-b] the latter model is examined in more detail. Butler considered a hot zone at steam temperature ahead of the interface, and the extent of the hot zone was called the heat penetration depth. By performing a heat balance on the interface, Butler developed an ordinary differential equation describing the variation of the heat penetration depth with time. This method for finding an approximate temperature distribution for conduction dominated processes is very similar to the Heat Integral Method (HIM) as explained in detail in Section 4.3. However, no reference to the Heat Integral Method was given [Butler 1985-b].

In the Heat Integral Method, a polynomial is considered to approximate the temperature distribution. It was shown in Section 4.3. that the heat balance performed at the boundary relates the rate of heat flow from the boundary to the accumulation of heat in the medium. In order to approximate the accumulation term, Butler [1985-b] used a temperature distribution in the form of a step function. To improve upon this, the term explaining the flow rate of heat was approximated using a linear variation between two limiting cases, that is, the unsteady-state temperature distribution ahead of a stationary boundary (error function solution) and the steady-state temperature distribution ahead of a moving boundary interface. Finally the heat penetration obtained by the above procedure was used in the steady-sate, i.e., the exponential solution, to represent the temperature distribution ahead of the interface. Butler [1985-b] showed that the amount of accumulated heat ahead of the interface predicted by the approximate integral solution

91

was in good agreement with that obtained from an exact solution. No comparison, however, was given for the temperature distribution ahead of the interface as predicted by the two methods.

Here, HIM will be used to find an appropriate differential equation for the heat penetration depth. Later, the heat flow solution will be combined with other equations to find the flow rate and the shape and location of the interface with time.

6.2.1. Assumptions in the Linear SAGD Model

In developing the mathematical model, the following assumptions are made,

1) The fluids are incompressible.

2) Steam pressure is constant in the steam zone. This is a good approximation for modelling the SAGD process, because there is negligible pressure drop in the steam zone.

3) The only flowing phase behind the oil-steam interface is steam, and that ahead of the interface is oil, that is, a sharp interface is assumed separating the two zones. This assumption states that:

a) There is no capillary zone at the oil-steam interface. Palmgren *et al.* [1989] found that capillary forces are negligible at the steam-oil interface under field conditions.

b) The steam condensate does not penetrate ahead of the interface, but flows downwards along the interface, i.e., convective heat flow is neglected. This approximation has been previously used in thermally enhanced gravity driven processes, where the oil-steam interface advances upon removal of the heated oil [Butler *et al.* 1981, Reis 1992-b].

4) Temperature distribution in the oil zone, is found by solution of the 1-D heat equation along the horizontal direction.

In the above problem, the interface is an isotherm. Similar to that considered by Butler [1985-b], normal to the interface should be considered as the direction of heat

92

flow, since heat flows perpendicular to isotherms. In this model, however, the 1-D heat equation in the horizontal direction is used. This is chosen due to the following three reasons.

Firstly, in the SAGD process, the interface is curved-shaped. In the development of the semi-analytical models for the SAGD process, discrete straight segments are used to represent the interface (for example, see Butler [1985-b] or the following sections). In such cases, and depending on the curvature of the interface, either multiple values for temperature ahead of the interface is obtained, or some parts of the formation are left out, if the normal direction is chosen. This is because, normals to a curved interface intersect either ahead or behind the interface.

Secondly, in order to find the oil flow rate ahead of each element, the oil flow integration is performed in the total extent of the heated zone (see Equation (12) of Butler [1985-b] or Equation (6.2.3.2) in this work). It can be noted, however, that for the lowest part of the interface (see Figure 7 of Butler [1985-b] for example), the extent of the oil-bearing formation normal to the interface is limited. Hence, the flow integration in the heated region includes the base rock too. Accurate flow rate calculations for the lowest interface element is important, since the oil draining from this element is the one representing the produced oil from the SAGD process. The error due to the extra oil flow considered in the base-rock, however, may be small, since drainage rate declines sharply away from the interface. If the horizontal direction is considered as the primary direction of modelling, the above integration is totally performed in the oil-bearing zone.

Thirdly, development of a semi-analytical model based on the normal direction resulted in very elongated interface elements at the top of the interface. Improvements were obtained, when the horizontal direction was chosen for modelling purposes.

It was due to a combination of the above reasons that the horizontal direction was chosen as the primary direction of modelling.

5) The heated oil flows parallel to the interface.

Segregated flow theory, as used by many of previous investigators, neglects any flow in the vertical direction, i.e., normal to the bedding in tilted formations. The fluids are considered to flow horizontally due to potential gradients caused by gravity forces. Here, the segregated flow theory will not be used; however, it is assumed that the oil heated by conduction flows parallel to the interface.

In an incompressible system, an oil droplet on a tilted oil-steam interface (see Figure 6.6) does not move vertically, because the oil located vertically below the droplet is farther from the interface, and cannot flow at the same speed as the heated droplet. It will be assumed that the oil droplet moves along the least resistant path, that is, along the interface, and the droplets behind the interface move parallel to the interface.

The SAGD model, as developed in this work, neglects many mechanisms that occur in a field application of the process. A brief description of the neglected effects is presented in the following.

1) The SAGD model in this work considers the side-ways expansion of the steam zone. In the application of the SAGD process, as was reviewed in Chapter 2, steam flows initially upward from the horizontal injector, while the bitumen located above the steam is heated and drains downwards in an unstable manner. The duration of this initial stage is normally much shorter than the sideways expansion period [Butler 1991]. Butler [1987] developed a model to find the upward velocity of the rising steam fingers. The velocity was found to be proportional to reservoir permeability, and strongly dependent on oil viscosity at steam temperature.

2) The sharp interface assumption, as used in this study (see also Butler et al. [1981] and Butler [1985-b]), avoided the nonlinearities caused by multiphase flow. It is clear, however, that under actual conditions, multiphase flow occurs at least within a limited interval from the steam front. Steam flow through the multiphase region requires a driving force which is neglected in this work. The error due to this assumption may be small along a large portion of the interface, however; the ability of the formation to deliver the required steam at the top of the interface may be a controlling factor on the advancement of the interface there [Butler 1985-b]. This was reviewed in Chapter 2.

One of the fluid phases created at the steam front is a water-oil emulsion. The high viscosity of the in-situ generated emulsion can adversely affect the process [Chung and

Butler 1988-a]. The complexities involved in the generation, flow and coalescence of the emulsion hinders their inclusion in mathematical models. Chung and Butler [1988-a] studied the SAGD process experimentally, and found that if the injection well was located low in the reservoir, large amounts of emulsion was produced due to the counter-current flow of steam and oil.

3) It is well known that the displacement of oil by steam is not a piston-wise displacement process. Hence, appreciable amount of oil is left in the steam zone, while the steam front is advancing in the reservoir, contacting the virgin formation.

Although the oil in the steam zone is at steam temperature, hence has a uniform viscosity, its mobility is not constant. This is due to the variation of the oil saturation in the steam zone. Dykstra [1987] found an equation for the free fall gravity drainage of oil left behind the gas front. Butler [1991] suggested that the same equation can be used to find the additional oil produced in the steam zone. The above behaviour suggests that the oil saturation does not reduce abruptly to the residual oil saturation. This in turn, means that the velocity of the steam-oil interface is larger than that corresponding to an abrupt reduction in saturation to its final value.

In this study a sharp interface is assumed, which passes through the reservoir, leaving the residual oil behind. While performing mechanistic studies, however, a dimensionless group incorporating the value of the saturation change will be varied by orders of magnitude to study the behaviour of the process.

4) In steam injection processes, some amount of non-condensable gas, soluble in the steam generator water, may be injected together with the steam, and some may be generated in the reservoir. Such gases accumulate in the reservoir, especially at the interface, and reduce the steam temperature due to the reduced partial pressure of steam. Their effect was studied by Butler [1985-b, 1991] and Edmunds [1987], and was reviewed in Chapter 2.

5) In a thermal recovery process, fluids expand when heated. In a SAGD process, the oil ahead of the steam front expands. It was pointed out in Section 4.1 that the volume of the hydrocarbons can increase 10% to 15% when their temperature is increased about 200 °C. If the expanded oil partially saturates the porous media, such that it does not restrict the advancement of the steam interface, a thicker layer of oil will be draining at

95

the interface region. The effect of this increase in the draining oil is expected to affect the total production rate only minimally, as the oil production rate is measured at standard conditions.

It was mentioned previously, that the above mechanisms are neglected in the development of the SAGD model in this work. Incorporation of such mechanisms requires development of a comprehensive thermal simulator, which is beyond the scope of this work. The SAGD process, as modelled in this work, can be explained as follows.
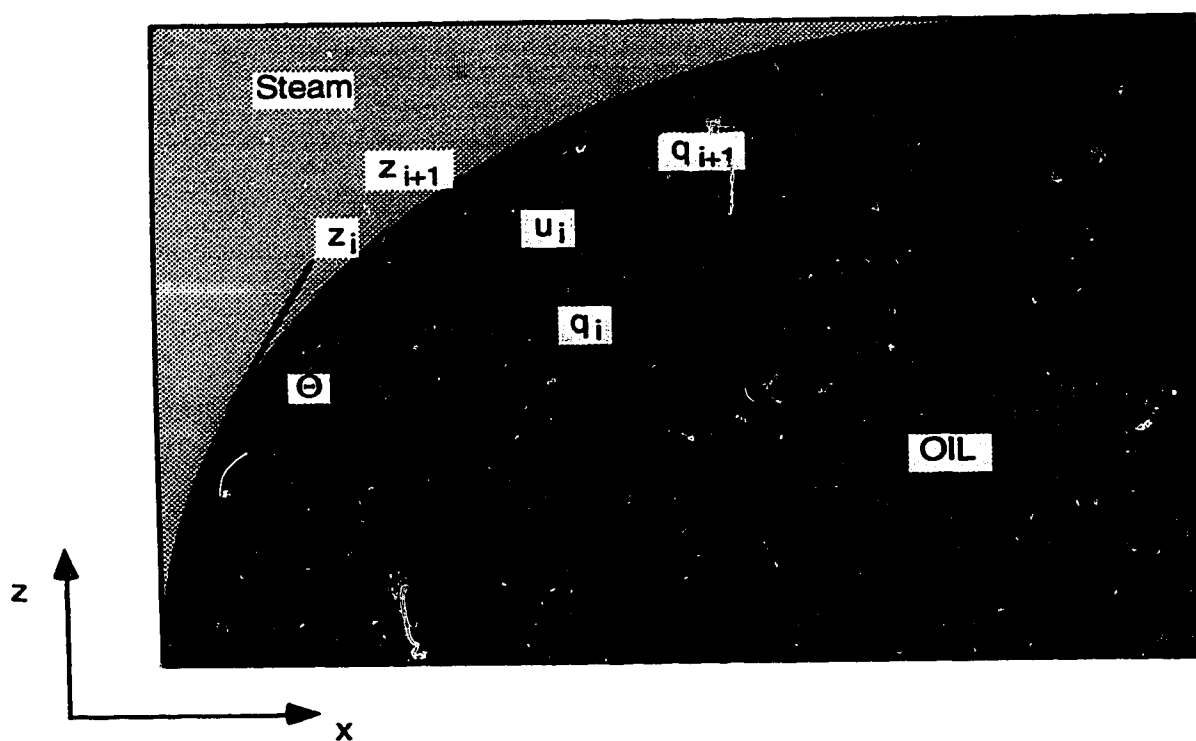
Figure 6.6. Schematic presentation of oil-steam interface under non-isothermal gravity drainage.

Figure 6.6 shows the oil-steam interface at an arbitrary time. The bottom of the interface is kept at the perforation site, to avoid any steam production. The top of the interface is either at the overburden or is connected to another interface creating a continuous steam zone above the oil column. The heat is conducted ahead of the interface and the heated oil drains towards the production site. Subsequently, the oil-steam interface advances in the reservoir. The velocity of the interface is generally a function of time and vertical position along the interface. Hence, a number of vertical elements are

96

considered parallel to each other, one of them shown in Figure 6.6. The temperature distribution in each element defines the velocity of the oil drained from the element. The difference between the amount of oil entered to each element, with that delivered to the next element dictates the velocity of the interface for that element. The latter, in turn, defines the available time for heat conduction ahead of the interface and hence the temperature distribution for that element. The physical problem as explained above is a combined heat and fluid flow problem. Each part is discussed separately.

6.2.2. Heat Flow Problem

Heat is transferred ahead of the interface by conduction. The 2-D problem is approximated by a 1-D heat equation,

$$\frac{\partial^2 T}{\partial x^2} = \frac{1}{\alpha} \frac{\partial T}{\partial t} \qquad\qquad \ldots\ldots\ldots\ldots\ldots\ldots\ldots (6.2.2.1)$$

It was explained in Section 6.2.1 that Equation (6.2.2.1) will be used along the horizontal direction to find the temperature distribution in the oil zone.

Performing very similar steps as those performed in Section 4.2 a dimensionless conduction-convection PDE similar to Equation (4.2.1.4) is obtained,

$$\frac{\partial^2 \theta}{\partial \xi^2} + N_{Pe} \frac{\partial \theta}{\partial \xi} = \frac{\partial \theta}{\partial \tau} \qquad\qquad \ldots\ldots\ldots\ldots\ldots\ldots\ldots (6.2.2.2)$$

where the dimensionless variables are normalized with respect to the reservoir thickness, H.

$$\theta = \frac{T - T_R}{T_S - T_R} \qquad\qquad \ldots\ldots\ldots\ldots\ldots\ldots\ldots (6.2.2.3)$$

$$\xi = \frac{\zeta}{H} \qquad\qquad \ldots\ldots\ldots\ldots\ldots\ldots\ldots (6.2.2.4)$$

$$\tau = \frac{\alpha t}{H^2} \qquad\qquad \ldots\ldots\ldots\ldots\ldots\ldots\ldots (6.2.2.5)$$

$$N_{Pe} = \frac{UH}{\alpha} \qquad\qquad \ldots\ldots\ldots\ldots\ldots\ldots\ldots (6.2.2.6)$$

97

where ζ is the horizontal distance from the interface. Equation (6.2.2.2) is a nonlinear convection-diffusion PDE. The convective term is related to the moving interface. Note that convection due to penetration of hot fluids ahead of the front is neglected. From now on, the definition of convection is due to the second term on the left hand side of PDE (6.2.2.2). The nonlinearity of the problem is due to the dependence of N_{Pe} on θ. A higher temperature results in a lower viscosity which in turn causes a higher interface velocity.

Now, the Heat Integral Method (HIM) is used to transform Equation (6.2.2.2) to a first order ODE, which can easily be solved using several numerical methods, e.g., Runge-Kutta methods. By performing steps very similar to those in Appendix A, or Section 6.1, one obtains a third order polynomial to describe the unsteady-state temperature distribution

$$\theta = \left(1 - \frac{\xi}{\delta(\tau)}\right)^3 \qquad \dots \dots \dots \dots \dots \dots \dots (6.2.2.7)$$

where $\delta(\tau)$ is the dimensionless heat penetration depth. Equation (6.2.2.2) is integrated over the heated region, $\delta(\tau)$, to find the heat penetration depth,

$$\left.\frac{\partial\theta}{\partial\xi}\right|_\delta - \left.\frac{\partial\theta}{\partial\xi}\right|_0 + N_{Pe}\left(\theta|_\delta - \theta|_0\right) = \frac{d}{d\tau}\int_0^\delta \theta d\xi \qquad \dots \dots \dots \dots \dots \dots (6.2.2.8)$$

Equation (6.2.2.8) can be simplified by substituting from the actual and auxiliary boundary conditions

$$-\left.\frac{\partial\theta}{\partial\xi}\right|_0 - N_{Pe} = \frac{d}{d\tau}\int_0^\delta \theta d\xi \qquad \dots \dots \dots \dots \dots \dots \dots (6.2.2.9)$$

Equation (6.2.2.9) is the same Equation obtained by Butler [1985-b]. As explained previously, the first term on the left hand side of Equation (6.2.2.9) was approximated by a linear variation of heat flux from a steady-state moving boundary solution and that from an unsteady-state stationary boundary solution. The right hand side was approximated by an accumulation term corresponding to a constant temperature in the heated zone [Butler 1985-b]. In this study HIM is used, and the appropriate expressions from the temperature

98

distribution (6.2.2.7) are substituted into Equation (6.2.2.9) to find an ordinary differential equation (ODE) for heat penetration depth, $\delta(\tau)$.

$$\frac{d(\delta^2)}{d\tau} = 8(3 - N_{Pe}\delta(\tau))$$

.... (6.2.2.10)

with the initial condition

$$\delta(\tau) = 0 \qquad\qquad \tau = 0$$

.... (6.2.2.11)

Solution of ODE (6.2.2.10), with Equation (6.2.2.7) defines the temperature distribution ahead of the interface. Note that N_{Pe} is known only when the fluid flow part of the problem is solved and the velocity of the interface is known.

It can be shown easily that for a polynomial of the order of n the corresponding ODE is in the form of

$$\frac{d(\delta^2)}{d\tau} = 2(n+1)(n - N_{Pe}\delta(\tau))$$

.... (6.2.2.12)

The ODE suggested by Butler [1985-b] can be written in the form of Equation (6.2.2.13) and the corresponding temperature distribution as Equation (6.2.2.14)

$$\frac{d(\delta^2)}{d\tau} = \frac{4}{\pi}(1 - N_{Pe}\delta(\tau))$$

.... (6.2.2.13)

$$\theta = \exp\left(-\frac{\xi}{\delta(\tau)}\right)$$

.... (6.2.2.14)

Figure 6.6 compares the temperature distribution as obtained from the Heat Integral Method, that suggested by Butler [1985-b] and the numerical solution of the exact differential equation (6.2.2.2) for a moving boundary problem with an interface velocity of $N_{Pe} = \exp(-\tau)$, after a dimensionless time of $\tau = 1$.

The function $N_{Pe} = \exp(-\tau)$ represents an interface velocity of $N_{Pe} = 1$ at early time. This corresponds to a conduction convection process in which both of the heating mechanisms are of the same order. The interface velocity was considered to decrease with

time, as happens in reality. Figure 6.7 indicates that both of the approximate methods are in good agreement with the numerical solution of the exact PDE, although the HIM solutions offer better accuracy. In the numerical solution a transformation was used so that a semi-finite domain could be modelled. Equal grid spacing in the computational domain has resulted in variable grid spacing in the physical domain in Figure 6.7. The grid sizes in the physical domain are smaller where the temperature gradients are highest, to increase the accuracy. The numerical model was validated against the analytical solution of Equation (6.2.2.2) (see Equation 4.2.5.1). A constant interface velocity of $N_{P_e} = 1$ was used for validation of the numerical model.
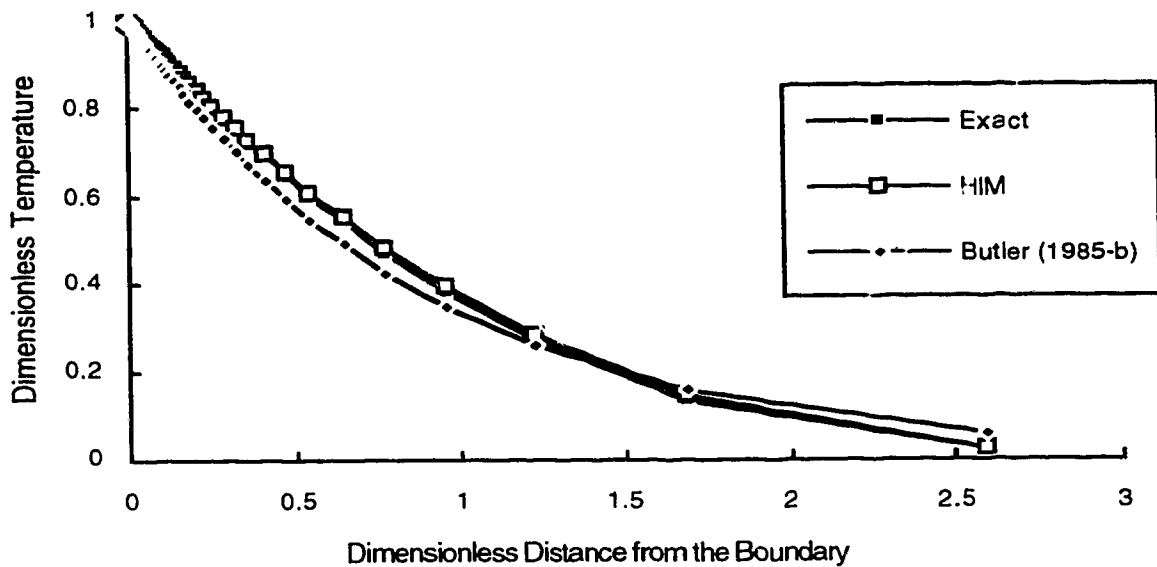
Figure 6.7 Temperature solution from different models (moving boundary semi-infinite case)

6.2.3. Fluid Flow Problem

The oil flow rate ahead of the interface can be expressed using Darcy's law (see Section 4.3.2, 6.1.2 or Butler *et al.* [1981]). For an element of constant viscosity and unit width in the direction parallel to the horizontal one can write

$$dq = \frac{\Delta \rho g H k}{\mu_o(T)} \sin(\Theta) d\xi \qquad \ldots\ldots\ldots\ldots\ldots\ldots\ldots (6.2.3.1)$$

where 1-D steady-state fluid flow parallel to the interface is assumed, and the viscosity of steam and the capillary forces are neglected The total flow rate in the heated zone can be obtained by integrating Equation (6.2.3.1)

$$\dot{q} = \int_0^\delta d\dot{q} = kgH \sin(\Theta) \int_0^\delta \frac{1}{v_o(T)} d\xi \qquad \dots\dots\dots\dots\dots\dots (6.2.3.2)$$

where it has been assumed that $\Delta\rho = \rho_o$, and the integration is performed in the heated region since the oil flow in the cold region is assumed to be negligible. Once again Equation (6.2.3.3) is used to define the viscosity-temperature relationship.

$$\frac{v_{os}}{v_o} = \left(\frac{T - T_R}{T_s - T_R}\right)^m \qquad \dots\dots\dots\dots\dots\dots (6.2.3.3)$$

Combining Equation (6.2.3.2) and (6.2.3.3) and substituting for dimensionless temperature from Equation (6.2.2.7) one obtains

$$\dot{q} = \frac{kgH \sin(\Theta)\delta}{v_{os}(3m + 1)} \qquad \dots\dots\dots\dots\dots\dots (6.2.3.4)$$

Equation (6.2.3.4) determines the production rate as a function of some dynamic variables as well as constant rock and fluid properties. The dynamic variables include the dimensionless heat penetration depth, δ, and the local angle of the interface with the horizon. The parameter δ is obtained from Equation (6.2.2.10).

To find the location of interface, the continuity equation (6.2.3.5) is written.

$$\frac{\partial \dot{q}}{\partial z} = -\phi \Delta S_o U \qquad \dots\dots\dots\dots\dots\dots (6.2.3.5)$$

where U, the location of the interface, is related to $\hat{\zeta}$, the interface location, by

$$U = \frac{\partial \hat{\zeta}}{\partial t} \qquad \dots\dots\dots\dots\dots\dots (6.2.3.6)$$

101

The slope of the interface can be obtained by knowing the interface velocity from Equation (6.2.3.6) and by using the geometric relation (6.2.3.7),

$$\tan \Theta = \left.\frac{\partial x}{\partial \zeta}\right|_{\zeta = \hat{\zeta}} \qquad \dots\dots\dots\dots\dots\dots (6.2.3.7)$$

By combining Equations (6.2.3.4) and (6.2.3.5), and writing the results in terms of dimensionless variables, one obtains

$$\frac{\partial \hat{\xi}}{\partial \tau} = -\frac{N_{Ra}}{3m+1}\frac{\partial(\sin(\Theta)\delta)}{\partial \eta} \qquad \dots\dots\dots\dots\dots\dots (6.2.3.8)$$

where $\hat{\xi}$ and η are the dimensionless location of the interface and the dimensionless height, respectively [with definitions similar to Equation (6.2.2.4)].

In Equation (6.2.3.8) the Rayleigh Number, N_{Ra}, is a dimensionless group signifying the importance of convective flow to the conductive heat transfer. In the above problem the convective term is caused by the movement of the interface, and N_{Ra} is defined by

$$N_{Ra} = \frac{kgH}{\phi \Delta S_o v_{os}} \times \frac{1}{\alpha} \qquad \dots\dots\dots\dots\dots\dots (6.2.3.9)$$

A similar definition of N_{Ra} was previously given by Saidi [1987, P. 312], where the conductive term was due to the diffusion of chemical species.

Butler et al. [1981] and Butler [1985-b, 1991] had previously introduced three similar dimensionless groups, B_2, B_3, and B_4, by examining the conduction process and the movement of the interface, whereas here, N_{Ra} was naturally found when the two flow processes were combined using dimensionless variables. The parameter N_{Ra} is related to the above three dimensionless groups by simple relations

$$N_{Ra} = \frac{B_2}{m} = m(B_3)^2 = (B_4)^2 \qquad \dots\dots\dots\dots\dots (6.2.3.10)$$

102

6.2.4. Initial and Boundary Conditions

Consider a cold reservoir subjected to steam injection. Accordingly the initial conditions of the problem are:

$T = T_R$, everywhere, which was previously expressed as Equation (6.2.2.11). At the beginning, the steam-oil interface is located on a vertical plane directly above the horizontal well, and

$$\sin \Theta = 1 \qquad\qquad 0 \le \eta \le 1 \qquad\qquad \tau = 0 \quad \ldots\ldots\ldots\ldots (6.2.4.1)$$

$$\hat{\xi} = 0 \qquad\qquad 0 \le \eta \le 1 \qquad\qquad \tau = 0 \quad \ldots\ldots\ldots\ldots (6.2.4.2)$$

Drainage starts when heat is introduced into the reservoir, which causes $\delta > 0$. This results in $\dot{q}(\tau) > 0$ from Equation (6.2.3.4). The interface becomes tilted because oil is produced from the bottom; however, it is not replaced from the top of the reservoir. In other words in Equation (6.2.3.5), $\frac{\partial \dot{q}}{\partial z} < 0$, since

$$\dot{q} = 0 \qquad\qquad \eta = 1 \qquad\qquad \tau > 0 \quad \ldots\ldots\ldots\ldots (6.2.4.3)$$

Equation (6.2.4.3) holds as the required boundary condition of Equation (6.2.3.5). Note that Equation (6.2.4.3) is similar to the proper boundary condition in two phase immiscible displacement, where the fractional flow of the displaced phase is set equal to zero at the inlet [Bentsen 1978, Shen and Ruth 1994].

When the interface reaches the drainage radius, or another interface, the horizontal movement of the interface is terminated and the available oil column decreases in height. Then, Equation (6.2.4.3) holds at the upper most point of the interface.

In the SAGD process, the production pressure is adjusted such that excessive steam production is avoided. For this to happen, the steam-oil interface should be at the production site. In the mathematical model, the condition (6.2.4.4) is introduced, which holds the interface at the perforation site.

$$\hat{\xi} = 0 \qquad\qquad \eta = 0 \qquad\qquad \tau > 0 \quad \ldots\ldots\ldots\ldots (6.2.4.4)$$

103

Having defined the differential equations and the initial and boundary condition, a numerical scheme is explained next to solve the equations.

6.2.5. Numerical Procedure

1) At the beginning of each time step δ is obtained from Equation (6.2.2.10). In this study a value of $n=3$ is used.

2) An oil rate corresponding to each node is calculated from Equation (6.2.3.4).

3) The interface velocity is found by using Equation (6.2.3.5) and (6.2.4.3), and then the interface location is found from Equations (6.2.3.6) and (6.2.4.2).

4) Finally, the interface inclination is obtained from Equation (6.2.3.7).

5) The drainage rate depleting the corresponding element is set to zero when the interface reaches the drainage radius; that is, a neighbouring steam-oil interface, as explained before. This leads to an interface velocity of zero from Equation (6.2.3.5), and the available oil column decreases in height.

The calculations can be repeated in an iterative form until convergence is obtained, before proceeding to the next time step. This is suggested due to the implicit nature of the Equations (6.2.2.10), (6.2.3.4), (6.2.3.5).

In practice, using a very large number of elements decreases the maximum time step before instabilities occur. Also, it unrealistically causes high interface velocities for the top element. The latter happens because, in Equation (6.2.3.5), the absolute value of $\left.\dfrac{\partial q}{\partial x}\right|_{z=H}$ grows rapidly, as $\Delta z \to 0$. Note that $q|_{z<H}$ has a finite positive value from Equation (6.2.3.4). Of course the interface velocity at the top of formation is limited. Butler [1985-b] suggested that the interface velocity is limited by the ability of the formation to provide the required amount of steam at the top of the interface. Steam condensation is at maximum there, because of the maximum effect of heat loss to the overburden, as well as the maximum amount of required steam to heat the formation ahead of the fast moving interface. The effect of steam flow behind the interface is ignored in this study.

104

It is interesting to note that there is no explicit representation of the available oil column in the equations. However, the combined behaviour of the equations realistically predicts a smaller oil rate, after the interface reaches the drainage radius, and the available oil column decreases in height. This can be explained by the fact that if the available oil column is small, the oil supplied to the upper most moving node is zero always, which leads to less production rate build-up as the horizontal producer is approached.

The above procedure was used and an implicit semi-analytical model was developed to study improved gravity drainage due to steam injection in heavy oil reservoirs.

6.2.6. Results and Discussion of the 1-D Linear SAGD Model

Experimental studies of the SAGD process were reviewed previously. Chung and Butler [1988-b] performed SAGD experiments using 2-D physical models that were scaled to the Cold Lake and Athabasca fields. The rock and fluid properties which were reported by the above authors and are listed in Table 6.2 were used. Comparisons will be shown with the experimental data reported by Chung and Butler [1988-b] and the semi-analytical model developed by Butler [1985-b].

Table 6.2
Rock and Fluid properties of 2-D SAGD experiments [Chung and Butler 1988-a, 1988-b]

Permeability k	9.44×10^{-10} m^2
Oil viscosity at steam temperature υ_{os}	104×10^{-6} m^2/s
Formation width L	0.175 m
Porosity $\times$ Saturation change $\phi\Delta S_o$	0.37
Height of the model H	0.21 m
Thermal diffusivity α	5.87×10^{-7} m^2/s
m	3.6
Oil density ρ_o	980 kg/m^3
Thickness of the model L_1	0.03 m

105

6.2.6.1. Semi-Infinite Case

If the SAGD process is performed using a single wellpair in a large reservoir, the extent of the formation ahead of the steam-oil interface may be assumed infinite. Figure 6.8 shows the oil production data for such a case. The physical properties of Table 6.2 were used for the calculations. A second semi-analytical model was written based on the model described by Butler [1985-b], and the results are shown in Figure 6.8 along with the predictions obtained from the present model.

Figure 6.9 shows the interface location of the same problem at equal intervals of an hour as predicted by the 1-D linear SAGD model.
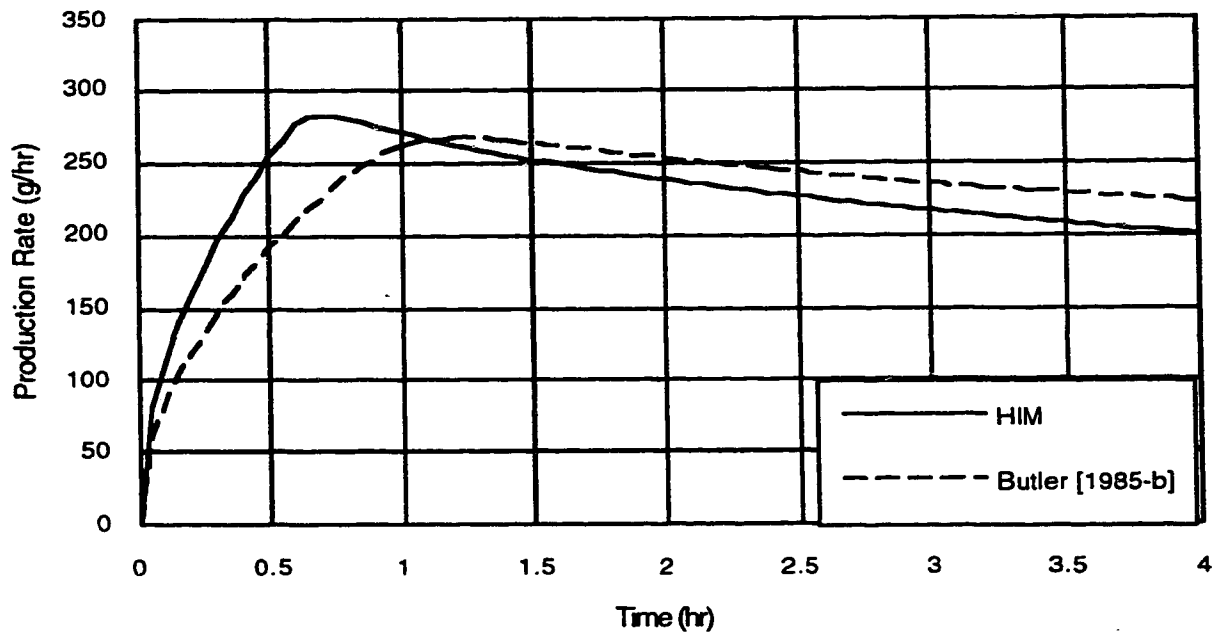
Figure 6.8. Production rate obtained from 1-D linear SAGD models

Figure 6.8 indicates that production rate increases from an initial value of zero to its maximum value in a relatively short period of time. The production rate drops slowly thereafter. A study of Figure 6.8 along with Equation (6.2.3.4) indicates that a relatively thin layer of oil ahead of the interface is heated during the early time, and the thickness of the heated zone stays relatively constant thereafter. In Equation (6.2.3.4), and for a

106

constant heat penetration depth, the production rate decreases with decreasing angle of the interface. Figure 6.9 indicates that the angle of the interface decreases as the steam zone expands side-ways.
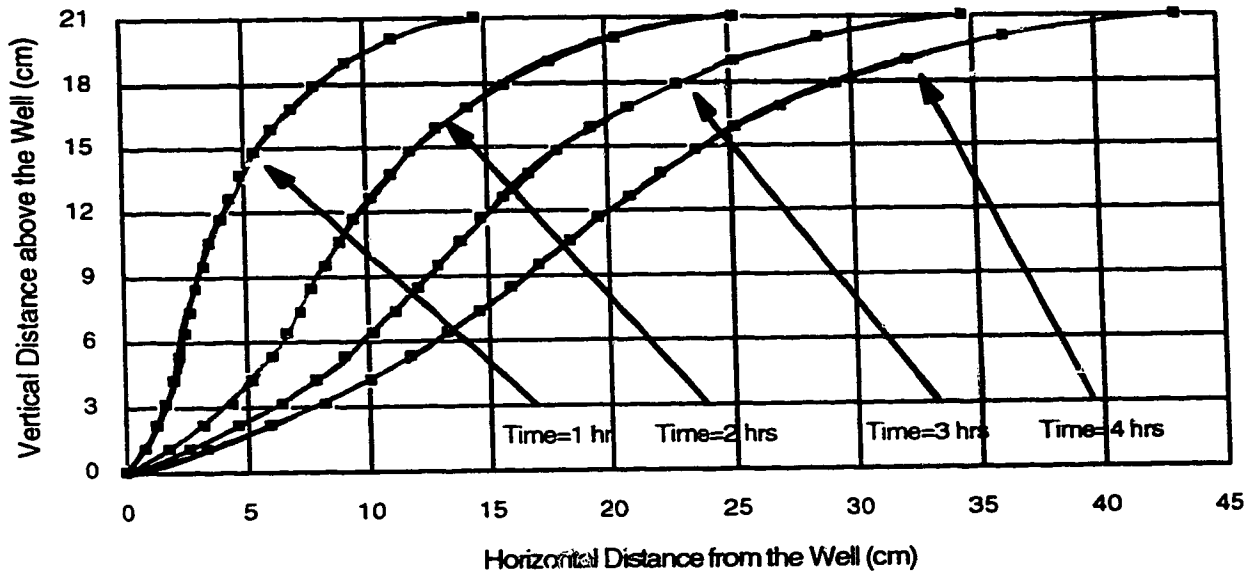
Figure 6.9. Interface location as predicted by the 1-D linear SAGD model

It is worth noting that the steady-state production rate, as predicted from the original SAGD theory [Butler et al. 1981], predicts a constant production rate of

$$q = 2L_1 \sqrt{\frac{2\phi \Delta S_o kg \alpha H}{m v_{os}}} = 318 \ \text{g/hr}$$

The corresponding production rate from the Tandrain theory [Butler and Stephens 1981] is $q = 277$ g/hr, which is in general agreement with the predictions of the above semi-analytical models.

6.2.6.2. Finite Case

Figures 6.8 and 6.9 indicate that in the SAGD process, the production rate decreases with time while the surface area exposed to the cap rock increases. The above behaviour reduces the thermal efficiency of the project and reduces its profitability. In

107

commercial projects, however, a series of wellpairs are drilled to deplete the reservoir before heat loss effects dominate the process. This was studied by Butler and Stephens [1981], and its application was reported by Edmunds *et al.* [1988, 1994]. In such cases a symmetry plane exists between the adjacent steam zones (symmetry line for a 2-D case). When the neighbouring steam-oil interfaces reach the symmetry plane, a single steam zone is created, and the available oil column decreases as oil is produced. To model the above process, the oil production rate for the element at the drainage radius was set equal to zero, and the usual calculations were performed for the other elements[9]. This method was used to predict the oil rate and interface location for the experiments of Chung and Butler [1988-b], and the results are shown in Figures 6.10 and 6.11.
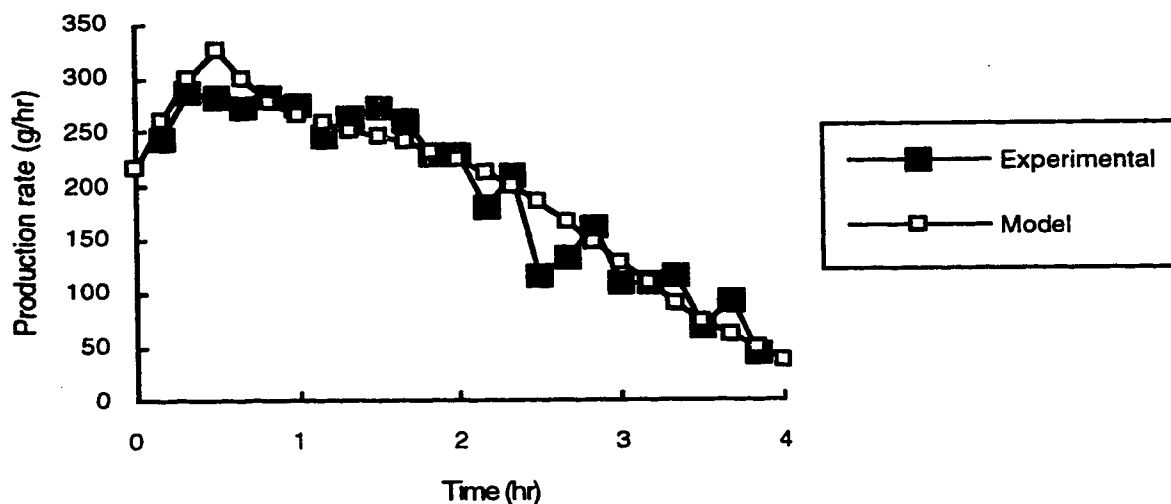
Figure 6.10. Production rate obtained from
1-D linear SAGD model

Butler [1985-b] suggested that the interface movement can be modelled along the vertical direction when coalescence of the steam zones occur. A model based on the above method was written. The predictions of the latter model indicated an artificial increase in production rate at the time of coalescence. The same anomaly was observed in

---

9   In reality, the symmetry plane is felt by the process when the heat penetration depth, and not the interface, reaches the no-flow boundary. It was noted before that the heat penetration depth is small for the above cases. This is especially the case for the moving element at the top of the interface, where the velocity of the interface is the largest. In the above model the effect of the no-flow boundary was considered when the steam-oil interface reached the symmetry plane.

the calculations performed by Butler [1985-b, Figure 12]. The reason for the increase in production seems to be related to a redistribution of heat, i.e., the mobile fluids, when the length and direction of the movement of the elements are changed.
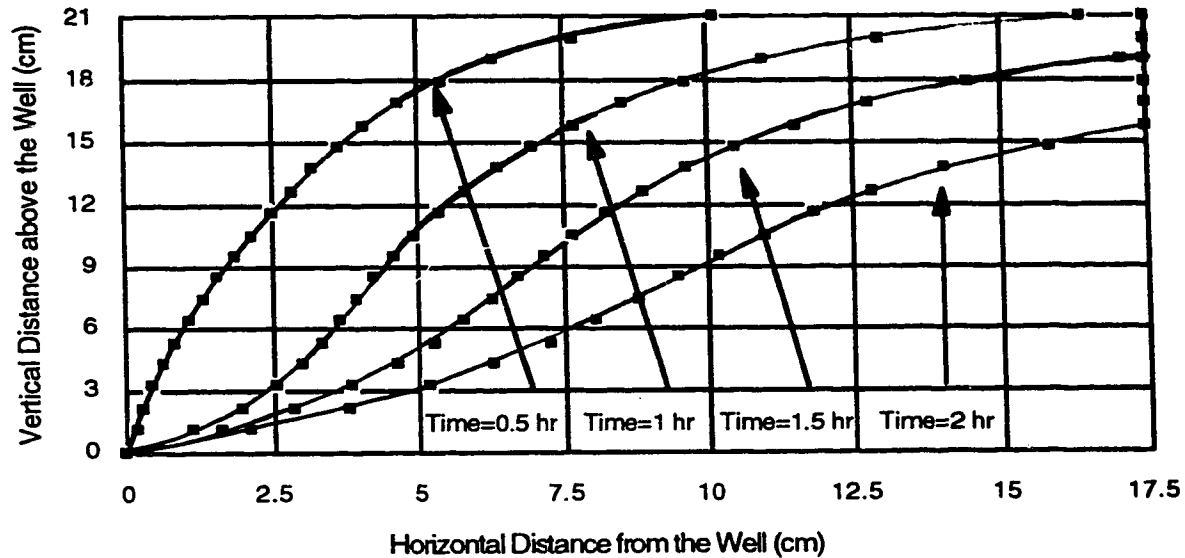
Figure 6.11. Interface location as predicted by the 1-D linear SAGD model
(finite case)

Figure 6.10 indicates that the fluids are mobile at the beginning of production. Chung and Butler [1988-b] noted that they initially heated the formation using a vertical well that was located directly above the producer. The authors reported that a temperature of 77 °C was measured at a distance of 0.02 m away from the vertical well. The initial reservoir temperature and the steam temperature were 25 °C and 107 °C, respectively. In the above calculations the initial dimensionless heat penetration depth was calculated from Equation (6.2.2.7) and was set equal to δ=0.644 for all the elements.

Figure 6.10 exhibits a maximum in production rate in about half an hour from the beginning of the experiment. This corresponds to the time when appreciable oil is heated ahead of the steam interface, while the inclination of the interface is not so large to counter-act the reduced viscosity effect. Production rate falls thereafter similar to that observed and explained in Figure 6.8. In Figure 6.10, however, the production rate declines fast after about an hour and half in the experiment. This corresponds to the time,

when the steam interface has reached the drainage radius and the thickness of the remaining oil column is decreasing. Such a behaviour was not observed in Figure 6.8 since the formation extended semi-infinitely there.

Figure 6.11 shows the location of the steam-oil interface for the above example at equal intervals of 30 minutes. Obviously, at later stages of the process, when the available oil column is small the accuracy of the above semi-analytical method is low due to very elongated elements. A redistribution of the initial number of elements over the descending interface can be performed after coalescence occurs. Again care should be taken to conserve the amount of heat stored ahead of the interface. Such a model was developed; however, the oil rate as predicted by such a model exhibited small oscillations and unrealistic behaviour (not shown here). This was possibly due to the fact that the model tried to conserve the amount of heat ahead of the interface. However, this does not necessarily ensure conservation of the mobile fluids.

The linear SAGD process is governed by 2-D heat and fluid flow mechanisms. A more accurate predictive model can be obtained if the transfer phenomena are considered to be 2-D. Chapter 7 of this work elaborates on 2-D modelling of the linear SAGD process.

6.2.6.3. A Study on the Effect of Different Parameters

It was noted previously that the steady-state analytical model [Butler *et al.* 1981] showed a singularity for the location of the interface at the top of the interface. Butler [1985-b] reported the same behaviour in his semi-analytical model, when he used small elements. In order to study this effect, calculations similar to those of Figure 6.9 were performed using 40 and 200 elements. Figure 6.12 shows a comparison of the two cases. Data corresponding to 20 elements were previously shown in Figure 6.9.

Figure 6.12 indicates the sensitivity of the location of the top of the interface with the grid size chosen. The reason might be the one explained in Section 6.2.5. Briefly, in Equation (6.2.3.5), the absolute value of $\left.\frac{\partial q}{\partial z}\right|_{z=H}$ grows rapidly, as $\Delta z \to 0$. This is because $q|_{z<H}$ has a finite positive value from Equation (6.2.3.4). Figure 6.12. suggests that the oil production rate is not very sensitive to the grid size chosen, as the area above the steam-oil interface of Figure 6.12 does not vary much with the grid size. The area exposed to

110

cap-rock, which is an important parameter in the calculation of the thermal efficiency of a thermal recovery method, however, is sensitive to the grid size chosen. Ignoring one or a combination of the mechanisms that control the movement of the interface under the cap rock is believed to create the singularity there. The ignored mechanisms include flow of steam behind the interface, capillary phenomena, and 2-D heat and fluid flow ahead of the interface.

It was shown previously that one of the dimensionless groups controlling the behaviour of the SAGD process is the Rayleigh No., N_{Ra}. The Rayleigh No. signifies the importance of convective flow to conductive heat transfer.

$$N_{Ra} = \frac{kgH}{\phi \Delta S_o \upsilon_{os}} \times \frac{1}{\alpha}$$ . . . .(6.2.6.3.1)
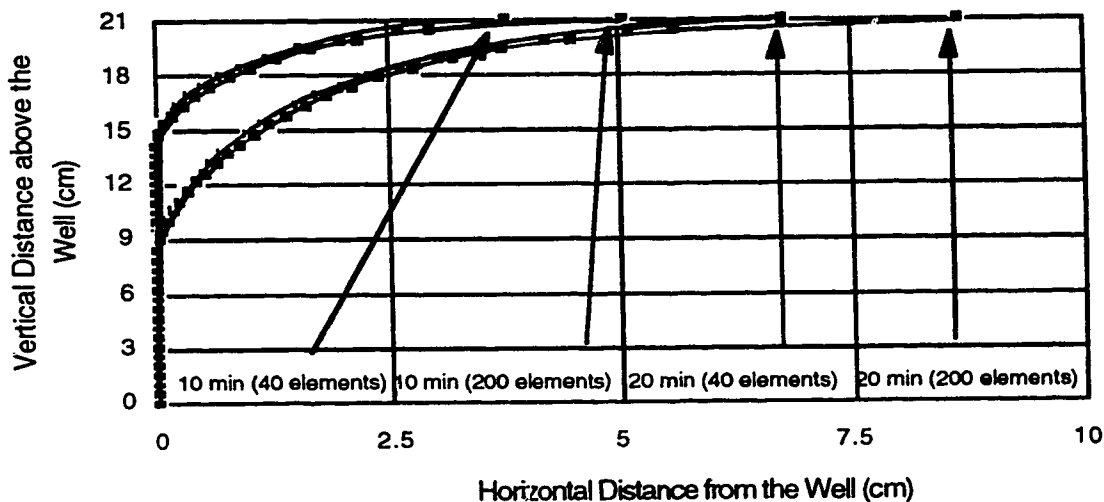
Figure 6.12. Interface location using different size of elements

In petroleum reservoirs, the oil mobility at steam temperature, $\frac{k}{\upsilon_{os}}$, might vary by orders of magnitude from one reservoir to another, or by injecting steam at different temperatures. It is noted that changing the steam temperature, hence υ_{os}, affects the movement of the interface by changing m (see Equation 6.2.3.8). However, any change in m may be neglected, since the range over which m varies is small [Butler 1985-b].

111

The data of Table 6.2 were used, and the oil mobility at steam temperature was varied to obtain an average production rate of 400 g/hr as a base case. Figure 6.13 shows the oil production rate as predicted by the present semi-analytical model, when oil mobility at steam temperature varied by multiples of 4.
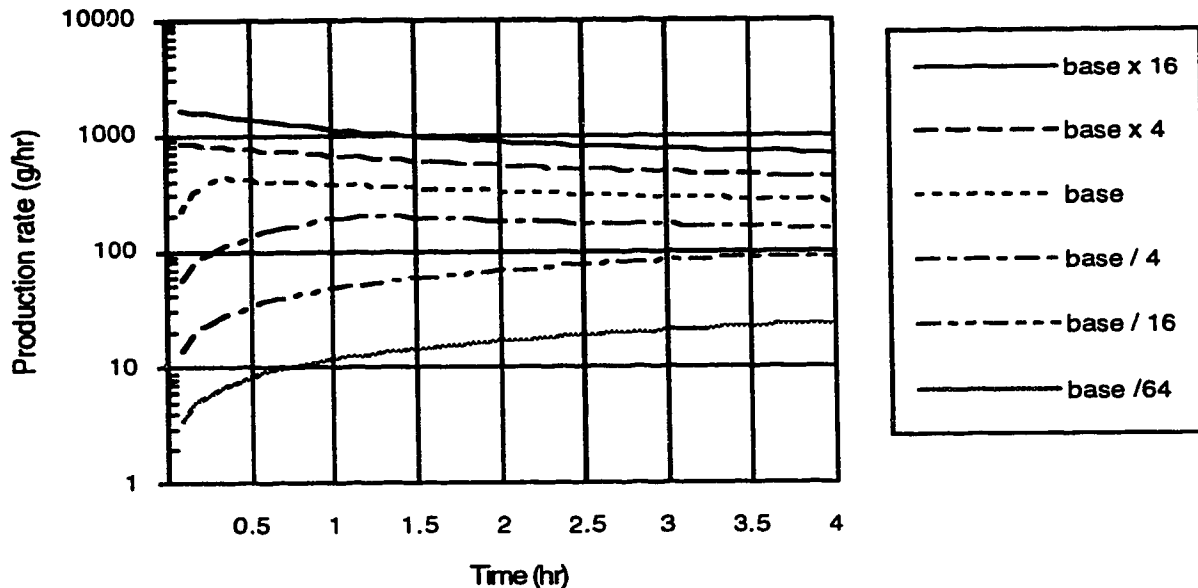
Figure 6.13. Effect of oil mobility at steam temperature on non-isothermal gravity drainage

Figure 6.13 indicates that if oil mobility at steam temperature is large, i.e., the Rayleigh No. is large, production rate is proportional to the square root of oil mobility. This behaviour was previously predicted by Butler *et al.* [1981]. However, Figure 6.13 indicates that for smaller values of the Rayleigh No., the production rate is approximately proportional to oil mobility itself. It seems that there has been no consensus on the effect of oil mobility on the production rate[10]. It is worth noting that the latter conclusion is in accordance with the analytical solution of non-isothermal gravity drainage from low permeability systems detailed in Chapter 5. For cases where the Rayleigh No. is similar to the base case, or smaller, Figure 6.13 indicates that oil production rate is proportional to oil mobility at steam temperature to a fractional power, and the exponent of the proportionality is between one and one half.

---

10   See the discussions of the fourth UNITAR conference, Edmonton, Alberta, 1988.

112

A similar study was performed to evaluate the effect of formation height. A relationship as simple as before was not observed. The effect of other parameters such as well-spacing and steam temperature were previously studied by previous researchers using similar semi-analytical models [Chung and Butler 1988-a, 1988-b, Butler 1985-b], and they will not be presented here.

6.3. A Semi-Analytical Model for the Radial SAGD Process

Thermal recovery processes are traditionally implemented with the application of vertical wells. Mathematical models were developed for the steam drive process which assumed a radially expanding steam zone with a steam interface perpendicular to the formation bedding [Yortsos and Gavalas 1981-a, 1981-b, 1982]. Later, Neuman [1985] assumed gravity forces to be important, and considered a steam zone that expanded radially as well as vertically. Farouq Ali [1982] presented a unified approach for modelling the steamflood process. He considered an areally expanding steam zone with a tilted interface before breakthrough. The behaviour of the steam interface during this stage was predicted by a combination of Mandl and Volek [1969] and van Lookeren's [1983] models. Upon breakthrough the process was considered to be dominated by a top down expansion of the steam zone, and steam production was assumed to be negligible. Numerous articles showed the accuracy and practicality of Farouq Ali's model [Farouq Ali 1982, Chen and Sylvester 1990, Harrigal and Wilcox 1992, Farouq Ali 1992].

Restricting steam production after an overlying steam zone has broken through the producer, as suggested by Farouq Ali [1982], is believed to increase the profitability of a steamflood project [Kimber et al. 1995]. Under the condition of negligible steam production, gravity drainage of the heated oil becomes the dominant producing mechanism [Vogel 1992, Closmann 1995]. Due to the restriction created by the radially converging path-lines, however, the productivity of vertical wells is much smaller than their horizontal counter-parts. Joshi and Threlkeld [1985] found that a SAGD process using a dually completed vertical well, i.e., concentric production and injection wells, did not perform as well as a horizontal wellpair. Nevertheless, many California type heavy oil reservoirs are believed to be operating under gravity drainage in radial coordinates [Vogel 1992]. The purpose of this section is to develop a mathematical model to study a thermal recovery project with a radially expanding steam interface, where the oil flows due to gravity forces. In contrast with the previous models [Reis 1992-b, Closmann 1995] the

113

shape of the interface is considered unknown *a priori* and is found as a part of the solution.

The physical problem is very similar to that shown in Figure 6.6 with x replaced by r. As the mathematical treatment is similar to that presented in Section 6.2, the development of the model is only discussed briefly, and the differences are emphasized. The assumptions in the radial SAGD model are very similar to those considered for the linear one. The temperature distribution, however, will be approximated by a vertically averaged solution of radial heat conduction ahead of the moving interface. This assumption is detailed later.

6.3.1. Heat Flow Problem

Heat is transferred ahead of the interface by conduction. For now, the 2-D problem is approximated by a 1-D heat equation,

$$\frac{\partial^2 T}{\partial r^2} + \frac{1}{r}\frac{\partial T}{\partial r} = \frac{1}{\alpha}\frac{\partial T}{\partial t} \qquad \dots\dots\dots\dots (6.3.1.1)$$

where α is the thermal diffusivity and T, and r are the temperature and space coordinate in the radial direction, respectively (For a discussion of the 1-D heat equation, see Section 6.2.1). Equation (6.3.1.1) holds ahead of an interface with a general equation of $\hat{r} = \hat{r}(z,t)$, where

$$\hat{r}(z,t) = \int_0^t U dv + r_w \qquad \dots\dots\dots\dots (6.3.1.2)$$

is the local steam zone radius, and U is the interface velocity in the radial direction.

By performing a transformation similar to that in Section 6.2 one obtains a convection-diffusion PDE as

$$\frac{\partial^2 \theta}{\partial \chi^2} + \left[\frac{1}{\chi + \hat{\chi}(\eta,\tau)} + N_{Pe}\right]\frac{\partial \theta}{\partial \chi} = \frac{\partial \theta}{\partial \tau} \qquad \dots\dots\dots\dots (6.3.1.3)$$

where the dimensionless variables are defined as

114

$$\theta = \frac{T - T_R}{T - T_s} \qquad \ldots\ldots\ldots\ldots (6.3.1.4)$$

$$\chi = \frac{r - \hat{r}(z,t)}{H} \qquad \ldots\ldots\ldots\ldots (6.3.1.5)$$

$$\tau = \frac{t\alpha}{H^2} \qquad \ldots\ldots\ldots\ldots (6.3.1.6)$$

$$N_{Pe} = \frac{UH}{\alpha} \qquad \ldots\ldots\ldots\ldots (6.3.1.7)$$

$$\hat{\chi}(\eta,\tau) = \int_0^\tau N_{Pe} dv + \frac{r_w}{H} \qquad \ldots\ldots\ldots\ldots (6.3.1.8)$$

where, $\hat{\chi}(\eta,\tau)$ is the dimensionless location of the steam-oil interface and χ is the dimensionless distance ahead of the interface. Equation (6.3.1.3), similar to Equation (6.2.2.2), is a nonlinear convective-diffusive PDE. The convective term has a component related to the radial geometry and a second one related to the moving interface. Note that convection due to penetration of hot fluids ahead of the front is neglected.

Having obtained the proper second order PDE (6.3.1.3), the Heat Integral Method (HIM) is used to transform Equation (6.3.1.3) to a first order ODE, which can be solved easily using several numerical methods, e.g., Runge-Kutta methods.

A polynomial is assumed to describe the unsteady-state temperature distribution ahead of the interface,

$$\theta = a_1(\tau) + a_2(\tau)\chi + a_3(\tau)\chi^2 + \ldots + a_{n+1}(\tau)\chi^n \qquad \ldots\ldots\ldots\ldots (6.3.1.9)$$

As in HIM, a heat penetration depth, $\delta(\tau)$, is considered beyond which there is no effect of heat transfer. Hence, θ and its derivatives with respect to η are zero there. Applying the latter boundary conditions to Equation (6.3.1.9) one obtains,

$$\theta = \left(1 - \frac{\chi}{\delta(\tau)}\right)^n \qquad 0 \le \chi \le \delta(\tau) \qquad \tau > 0 \qquad \ldots\ldots\ldots\ldots (6.3.1.10)$$

115

To find $\delta(\tau)$. Equation (6.3.1.5) is integrated between zero and $\delta(\tau)$, and θ is substituted for from Equation (6.3.1.10). By using the mentioned boundary conditions one obtains,

$$\frac{d(\delta^2)}{d\tau} = 2(n+1)\left[n - \left(\frac{1}{\hat{\chi}(\eta,\tau)} + N_{Pe}\right)\delta\right]$$

$$\ldots\ldots\ldots (6.3.1.11)$$

with the initial condition

$$\delta(\tau) = 0 \qquad\qquad \tau = 0 \quad\ldots\ldots\ldots (6.3.1.12)$$

Solution of ODE (6.3.1.11), with Equation (6.3.1.10) defines the temperature distribution ahead of the interface. Note that N_{Pe} is known only when the fluid flow part of the problem is solved and the velocity of the interface is known.

The validity of the 1-D HIM solution was checked by comparing it with the solution of PDE (6.3.1.3), assuming a varying front velocity. The comparison is shown in Figures 6.14 and 6.15 for an example discussed next. The HIM solution tends to underestimate the temperature distribution, especially when the steam zone radius is small. The discrepancy can be explained by the fact that HIM solutions are mostly suited for conductive problems. When steam zone radius is small, e.g., at the bottom of interface where steam interface is kept at the well perimeter, a large convective component is present. See the term in square bracket of Equation (6.3.1.3). This deficiency of the 1-D HIM model can be circumvented by vertically averaging the variables which determine the heat penetration depth in Equation (6.3.1.11).

Heat conduction ahead of the interface is a 2-D process. By neglecting the derivative of the interface location with respect to the vertical distance, the 2-D version of PDE (6.3.1.3) can be written as,

$$\frac{\partial^2 \theta}{\partial z^2} + \frac{\partial^2 \theta}{\partial \eta^2} + \left[\frac{1}{\eta + R^{\wedge}(z,\tau)} + N_{Pe}\right]\frac{\partial \theta}{\partial \eta} = \frac{\partial \theta}{\partial \tau}$$
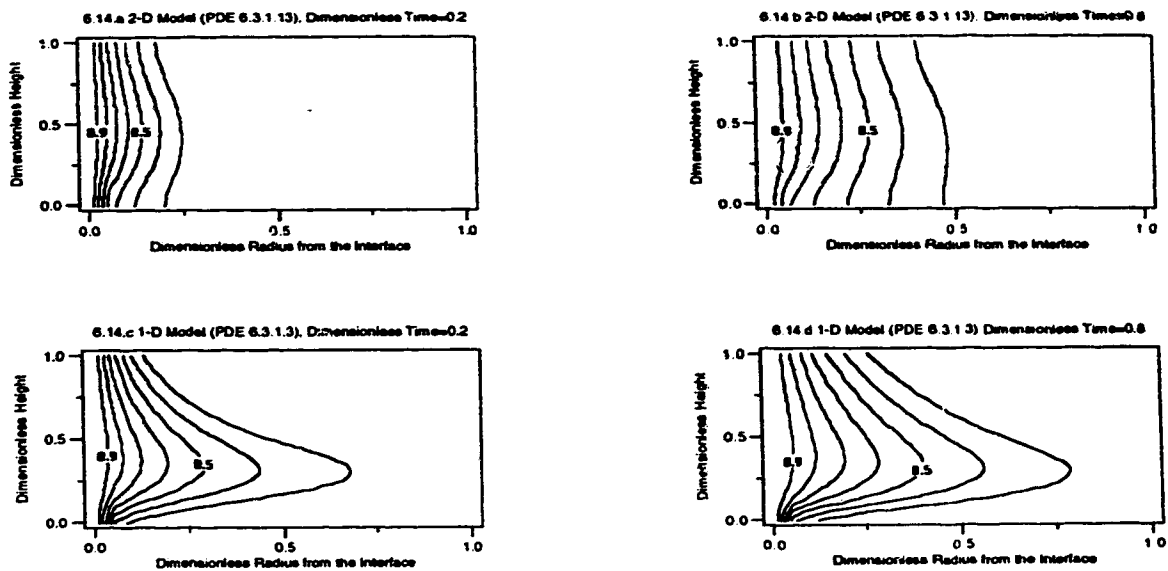
$$\ldots\ldots\ldots (6.3.1.13)$$

Figure 6.14. Dimensionless temperature distribution ahead of the moving interface of Equation (6.3.1.14) predicted by the 2-D PDE (6.3.1.13), and the 1-D PDE (6.3.1.3).
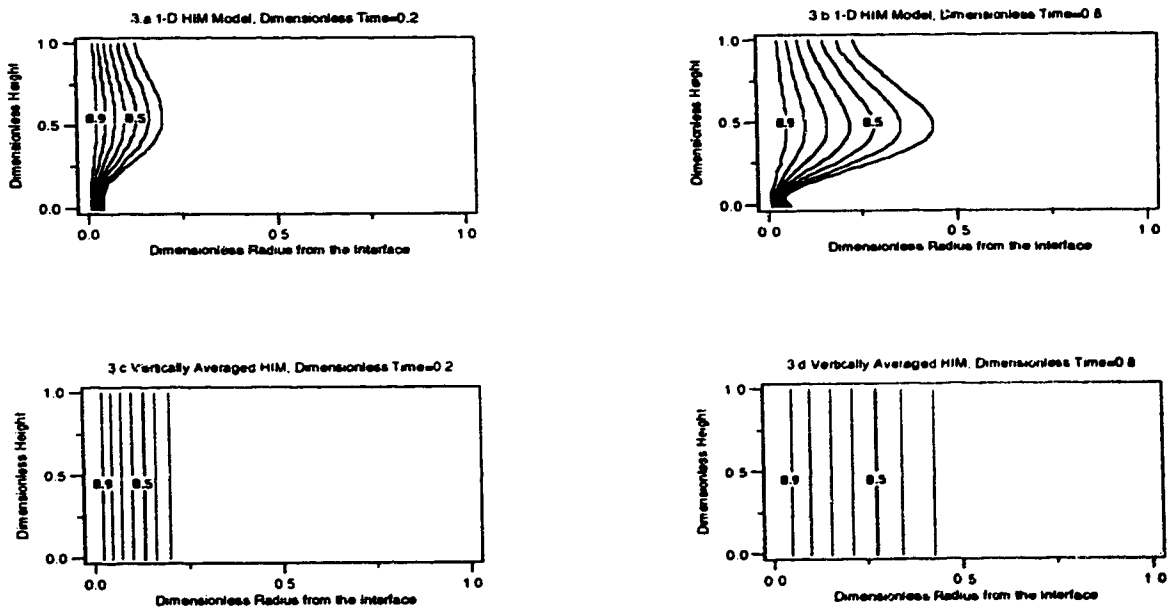
Figure 6.15. Dimensionless temperature distribution ahead of the moving interface of Equation (6.3.1.14) predicted by the 1-D HIM model, and the vertically averaged HIM model.

117
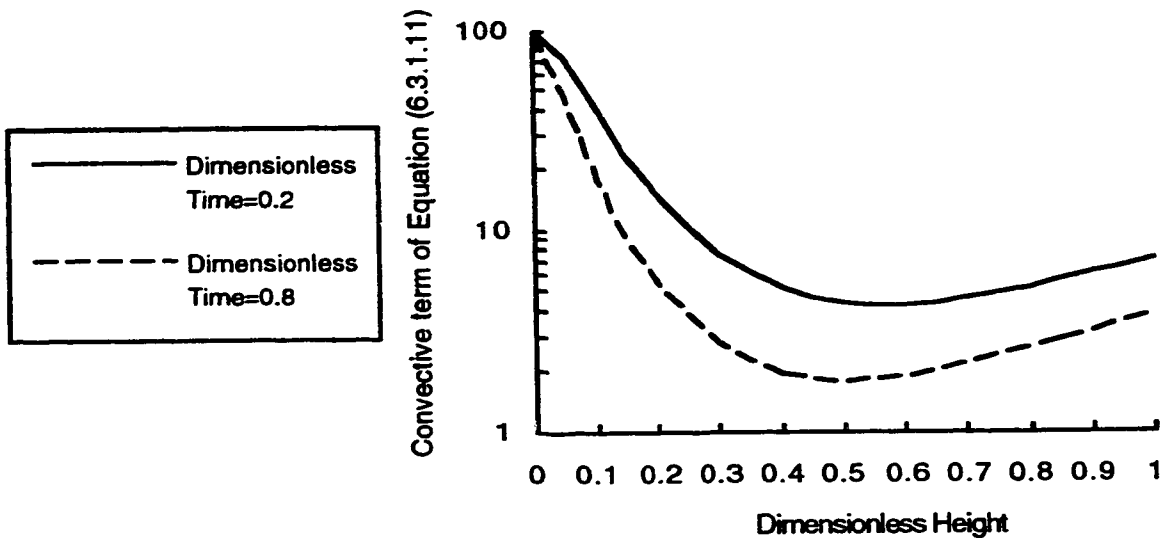
Figure 6.16. Peclet No. plus inverse steam
zone radius

It was found that the 1-D representation of the 2-D convective-diffusive PDE (6.3.1.13) results in poor accuracy for cases of variable interface velocity along the vertical axis, and small wellbore radius. To illustrate the limitations of the 1-D model, and justify the averaging process, consider an example where N_{Pe} is defined by,

$$N_{Pe} = \left(8\eta^2\right)\exp(-\tau) \qquad \dots\dots\dots\dots (6.3.1.14)$$

The above equation represents an interface which is stationary at the bottom of formation. At the top of the formation ($\eta = 1$), N_{Pe} has a maximum value of 8. $N_{Pe} = 8$ represents a front sweeping a formation of 10 m thickness with a well spacing of 100 m, i.e., a drainage area of 2 acres per well, within 2 years. Hence, Equation (6.3.1.14) covers the range from stationary boundary problem to a fast moving boundary problem. Also, the interface velocity, represented by Equation (6.3.1.14), decreases with time, as it happens in reality.

Figures 6.14 and 6.15 show the numerical solutions of the 2-D PDE (6.3.1.13) as well as those of the 1-D PDE (6.3.1.3) and the 1-D HIM solution, for a dimensionless well radius of 0.01 in an infinite medium for different times. A dimensionless time of one

118

corresponds to about 3 years for the above hypothetical example, assuming a thermal diffusivity of 10^{-6} m^2/s. Note that the horizontal axis, that is the distance from the moving interface, is stretched to magnify the differences. A comparison between Figures 6.14.a and 6.14.c (or 6.14.b and 6.14.d) indicates that the conductive component in vertical direction can not be neglected from Equation (6.3.1.13). To avoid complications of solving the 2-D PDE (6.3.1.13) at each time step, an average Peclet No., N_{Pe}, and average steam zone radius in Equation (6.3.1.11) are assumed to obtain a 2-D representation of the heat penetration depth. This approximation is used to account for the averaging behaviour of the diffusive component of PDE (6.3.1.13) in vertical direction, as well as circumventing the underestimation of the temperature distribution by 1-D HIM model. Figure 6.16 shows the magnitude of the term in the square brackets of Equation (6.3.1.11). Note that the above term is very large at the bottom of interface, and that the maximum peak of temperature profile in Figures 6.15.a and 6.15.b corresponds to the minimum of Figure 6.16. Figures 6.15.c and 6.15.d show the temperature distribution of Equation (6.3.1.14), predicted by Equations (6.3.1.10) to (6.3.1.12) and the averaging process explained above. Obviously, the computer effort for solving Equation (6.3.1.10) to (6.3.1.12) is much smaller than that for Equation (6.3.1.13).

Accurate modelling of oil flow requires accurate temperature distributions in the region very close to the interface. For example, the mobility of an oil particle on the 0.5 isotherm is only 12% of that on the interface, assuming a typical value of $m=3$ in Equation (6.3.2.2). A comparison between Figures 6.14.a and 6.15.c (or 6.14.b and 6.15.d) indicates that the proposed model is a good approximation of the 2-D process, especially in the region close to the interface.

Figures 6.14 and 6.15 indicate that heat transfer ahead of the interface is an unsteady-state problem for the example considered. The same behaviour is expected under most field conditions. Also Figures 6.14.a and 6.14.b show that iso-temperature lines are aligned almost parallel to the moving interface. This is in spite of the fact that the interface is stationary at the bottom of the formation and is moving with a N_{Pe} of 4 to 8 at the top.

Using the fact that the isotherms are approximately parallel to the moving interface, the approximation was introduced that oil particles move parallel to the interface; i.e., along the iso-viscosity lines.

119

6.3.2. Fluid Flow Problem

At some particular time, temperature and hence viscosity are functions of the distance from the oil-steam interface. At a distance r from the axis of the vertical well, the oil flow due to gravitational forces can be expressed using Darcy's law for an element of thickness dr as,

$$dq = \frac{k(\rho_o - \rho_s)g \sin \Theta}{\mu_o} 2\pi r dr \qquad \ldots \ldots \ldots \ldots (6.3.2.1)$$

where a piston-like displacement is assumed over the element of dr and capillary pressure is neglected. Using the viscosity-temperature relationship of (6.3.2.2) and the temperature distributions of Equation (6.3.1.10), Equation (6.3.2.1) can be integrated to obtain the flow rate,

$$\frac{v_{os}}{v} = \left(\frac{T - T_R}{T_s - T_R}\right)^m \qquad \ldots \ldots \ldots \ldots (6.3.2.2)$$

$$q(\tau) = \frac{2\pi H^2 gk \sin \Theta}{v_{os}\delta^{nm}} \int_0^\delta (\delta - \chi)^{nm}(\chi + \hat{\chi}(\eta, \tau)) d\chi \qquad \ldots \ldots \ldots \ldots (6.3.2.3)$$

or

$$q(\tau) = \frac{2\pi H^2 gk \sin \Theta}{v_{os}} \frac{\delta[\delta + (nm + 2)\hat{\chi}(\eta, \tau)]}{(nm + 2)(nm + 1)} \qquad \ldots \ldots \ldots \ldots (6.3.2.4)$$

where it has been assumed that $\rho_o - \rho_s = \rho_o$.

In Equation (6.3.2.3) the integration is performed within the heated zone, as oil flow in the cold region is assumed negligible.

Equation (6.3.2.4) determines the production rate as a function of some dynamic variables as well as constant rock and fluid properties. The dynamic variables include the dimensionless heat penetration depth, δ, the local angle of the interface with the horizon, and the dimensionless steam zone radius, $\hat{\chi}(\eta, \tau)$. The parameter δ is obtained from

120

Equation (6.3.1.11). The continuity equation (6.3.2.5) provides the required relation between $\hat{\chi}(\eta, \tau)$ and the drainage rate from each element,

$$\frac{\partial \dot{q}}{\partial z} = -2\pi \phi \Delta S_o \hat{r} U \qquad \dots\dots\dots\dots (6.3.2.5)$$

where $\hat{r}$, the steam zone radius, is defined in Equation (6.3.1.2). By knowing the interface velocity from Equation (6.3.2.5), the slope of the interface can be obtained using the geometric relation (6.3.2.6),

$$\tan \Theta = \frac{\partial z}{\partial r}\bigg|_{r=\hat{r}} \qquad \dots\dots\dots\dots (6.3.2.6)$$

To complete the formulation of the radial SAGD model, initial and boundary conditions similar to those explained in Section 6.2.4, and a numerical procedure similar to that in Section 6.2.5 will be used.

6.3.3. Results and Discussion of the 1-D Radial SAGD Model

Liebe and Butler [1991] reported the results of steam injection from a vertical injector in a cylindrical model to study improved gravity drainage due to steam injection. The physical properties of the rock and fluids are given in Table 6.3. The authors did not report the properties of the porous medium; however, they mentioned that they used 2 mm glass beads. In this study the data of Chung and Butler [1988-a], who used the same porous material, were used.

In Figures 6.17 and 6.18 a comparison is shown between the predictions of the above semi-analytical model and their experimental results. As shown, the model predicts oil production and steam interface movement accurately.

121
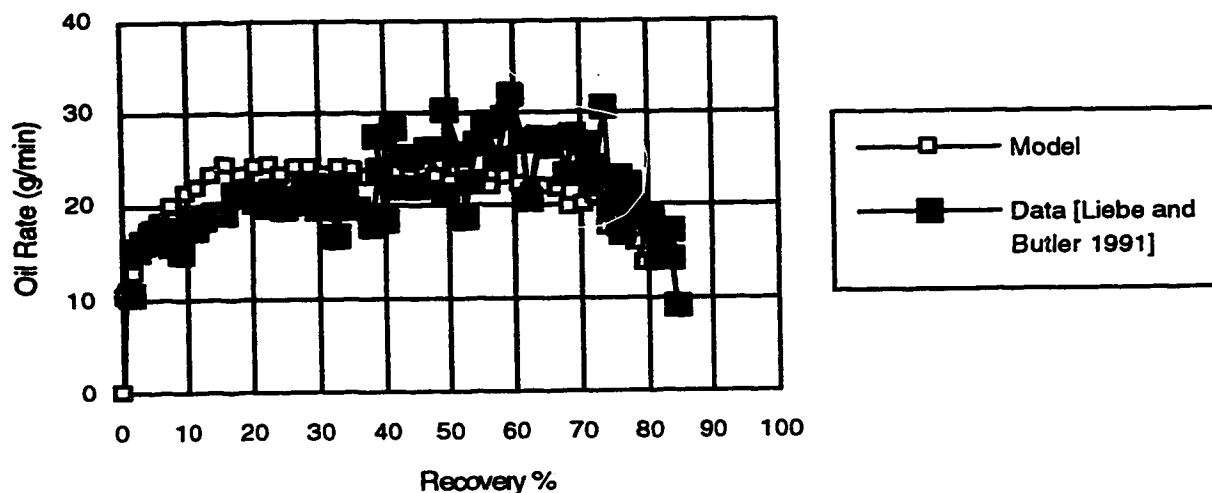
Figure 6.17. Oil rate - comparison between
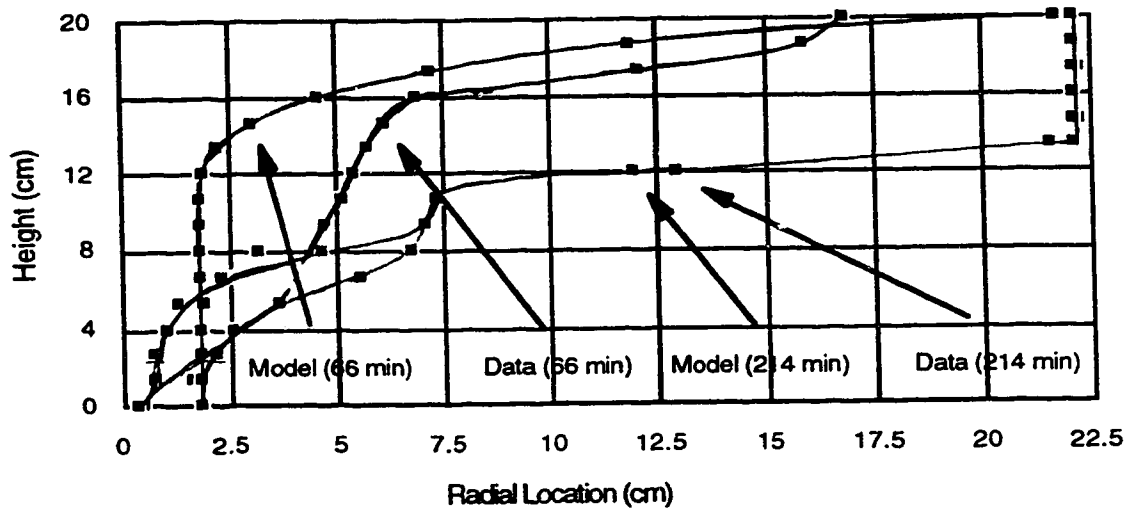model and data of Liebe and Butler [1991]

Figure 6.18. Interface location - comparison between model and data
of Liebe and Butler [1991]

Liebe and Butler [1991] performed their experiments at two different pressures. As they noted, the experimental pressure was the maximum pressure available for driving oil to the production well. The authors did not report the production pressure; however,

they avoided any steam production. This minimizes the effect of external pressure as a drive mechanism, since the injection and production sites were less than 0.05 m apart. Liebe and Butler [1991] noted that, at the higher injection pressure the oil steam interface was driven farther from the injection site. This provided more surface area for the draining oil behind the interface, as area increases proportional to the second power of radius in radial coordinates. To accommodate this effect a value of 0.018 m was used for well radius, about four times the actual value. A similar match was obtained for the experimental results reported at the second pressure.

As a second test the radial SAGD model is examined against the field data of two Californian heavy oil reservoirs. Their physical properties are given in Table 6.3. The same data as reported by Closmann [1995] were used. Figures 6.19 to 6.21 show the production rate and interface location for the Inglewood and Kern River 10-pattern fields, respectively, as obtained using the above gravity drainage model. For comparison the actual field data are also given [Closmann 1995]. In each case two well radii were used; one corresponding to the actual well radius, and the second one was chosen such that the production rate from the model matches with that using the field data. In reality the additional production from the reservoir is believed to be due to other mechanisms such as withdrawal of oil due to pressure forces at the production site, which provides more surface area for the flow of the heated oil.

The larger well radius is used to indicate the high potential of gravity drainage for producing Californian reservoirs, especially if the production surface is increased. Vertical wells restrict the fluid production due to congestion of the streamlines close to the wellbore, but horizontal producers provide a larger surface for oil flow, which can be highly beneficial in the case of such recovery mechanisms as gravity drainage, where the driving forces are low, and they act such that high sweep efficiencies can be obtained. The latter is shown in Figures 6.20, where the interface location is shown as a function of time. Gravity drainage under stable conditions achieves high sweep efficiencies [King et al. 1970, Vogel 1992].

123

Table 6.3
Rock and Fluid properties for the 1-D radial SAGD model

	Experimental study [Liebe and Butler 1991]	Inglewood Field [Closmann 1995]	Kern 10 pattern [Closmann 1995]
Height H	20 cm [0.20 m]	13.1 m	21.3 m
Permeability k	944 μm^2	5.8 μm^2	7.5 μm^2
Porosity $\times$ Saturation change $\phi \Delta S_o$	0.39 $\times$ 0.95	0.39 $\times$ 0.42	0.33 $\times$ 0.29
Kinematic oil viscosity at steam temperature v_{os}	36.7 $\times 10^{-6}$ m^2/s	4.35 $\times 10^{-6}$ m^2/s	7.19 $\times 10^{-6}$ m^2/s
Thermal diffusivity α	5.87 $\times 10^{-7}$ m^2/s	9.68 $\times 10^{-7}$ m^2/s	9.35 $\times 10^{-7}$ m^2/s
m	2.79	2.344	2.619
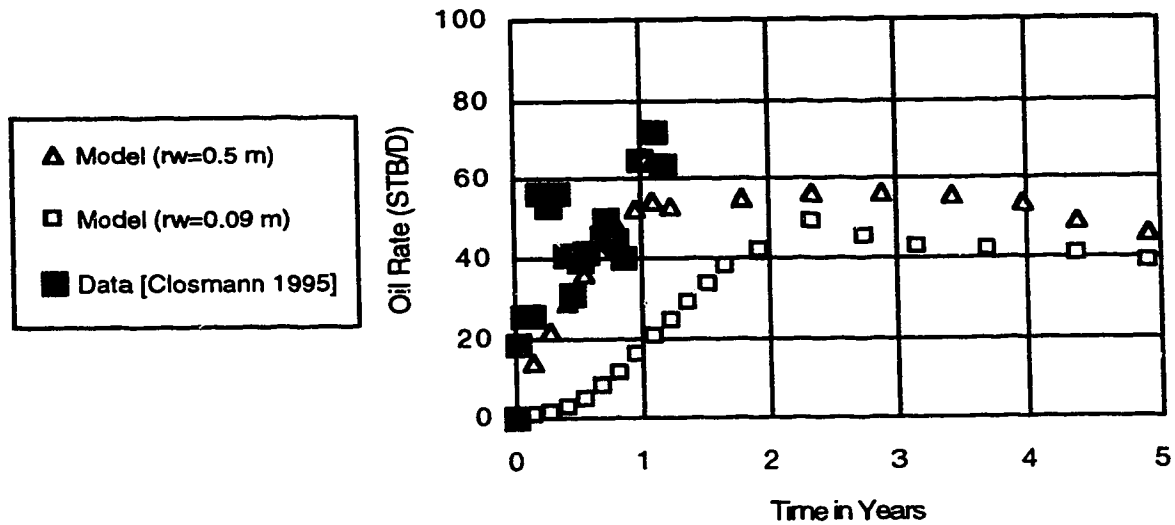
Figure 6.19. Oil rate from Inglewood field

124

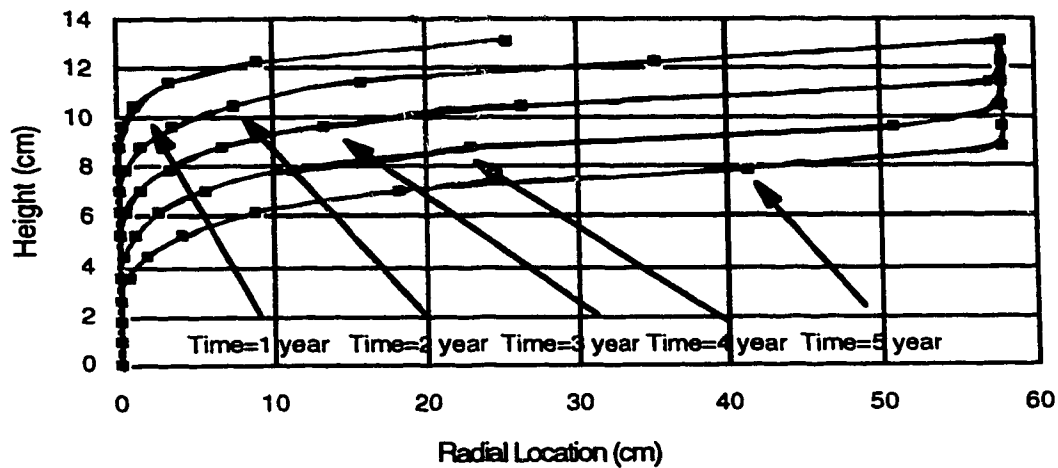Figure 6.20. Oil-Steam Interface location in Inglewood field
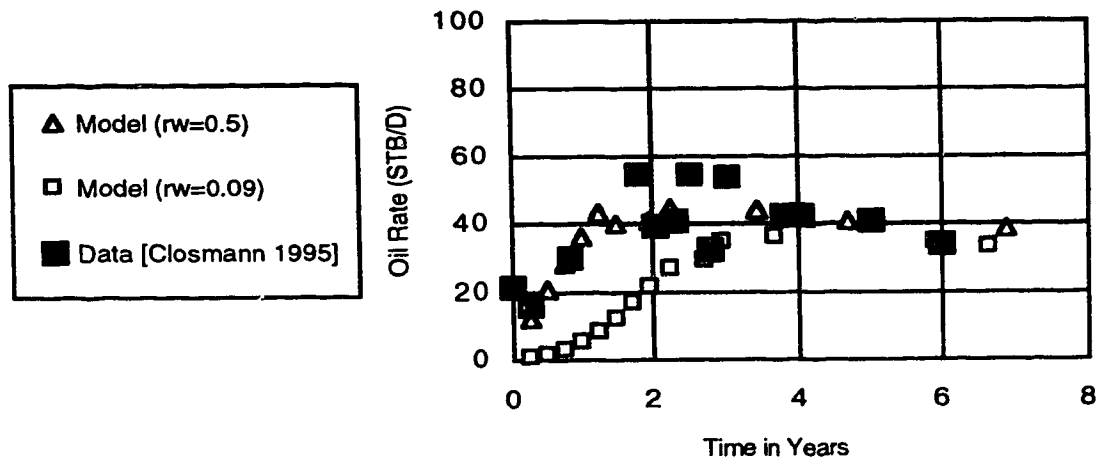(model predictions - rw=0.09 m)

Figure 6.21. Oil rate from Kern 10-pattern
field

For plotting Figures 6.20, a saturation change as reported by Closmann [1995] was used. If gravity drainage is implemented as the major recovery mechanism, higher recoveries might be obtained due to the low residual saturation obtained under gravity drainage.

125

7. DEVELOPMENT OF A 2-D NUMERICAL MODEL FOR THE SAGD PROCESS

The mathematical models commonly used for studying the SAGD process were reviewed in Chapter 2. It was indicated that the available analytical and semi-analytical models incorporated some assumptions that in many instances have not been yet justified. Nevertheless, they have been very useful in mechanistic studies of the SAGD process. Simple formulation and easy application of these models have made it possible to study the effect of the major parameters affecting the process.

On the other hand, rigorously developed thermal simulators are commonly used for field case studies. It seems that the capability of incorporating complex input data, and a lack of confidence in the assumptions underlying the simpler models have persuaded the industry to use the complex thermal simulators. Unfortunately, there is no thermal simulator that is specifically designed for the SAGD process. The availability of such a model is needed, because in commercially available thermal simulators accurate modelling of the heat and fluid flow processes in the vicinity of the steam interface is only possible if fine gridding is implemented for the global domain. This in turn, results in impractical computational time. The purpose of this chapter is to develop a conceptually simple numerical model, which permits high modelling accuracy ahead of the steam interface. Some of the assumptions involved in the previous simple models are relaxed, and incorporation of complex input data is permitted. The formulation is kept simple, such that mechanistic studies are possible. To develop such a model some of the assumptions that seem to be acceptable for the SAGD process are used. In Chapter 8 and through a comparison of the results with the experimental data, the applicability of the assumptions will be discussed.

7.1 General Features and Assumptions

Figure 7.1 shows a 2-D cross-section of the SAGD process perpendicular to the axis of the horizontal well. Focusing on the side-ways expansion phase of the process, 2-D heat conduction ahead of the interface accompanied with fluid flow due to gravity forces is modelled.

Similar to the previous 1-D semi-analytical models, a sharp interface is assumed to separate the steam and oil regions. Any potential gradients in the steam zone are

126

neglected due to the low viscosity of the steam as compared to the oil. This is believed to be one of the major assumptions of the present model, since the potential gradients required for steam flow through the capillary region may not be negligible. Some studies, however, have shown that capillary forces are insignificant at the steam oil interface, under field conditions [Palmgren *et al.* 1989].
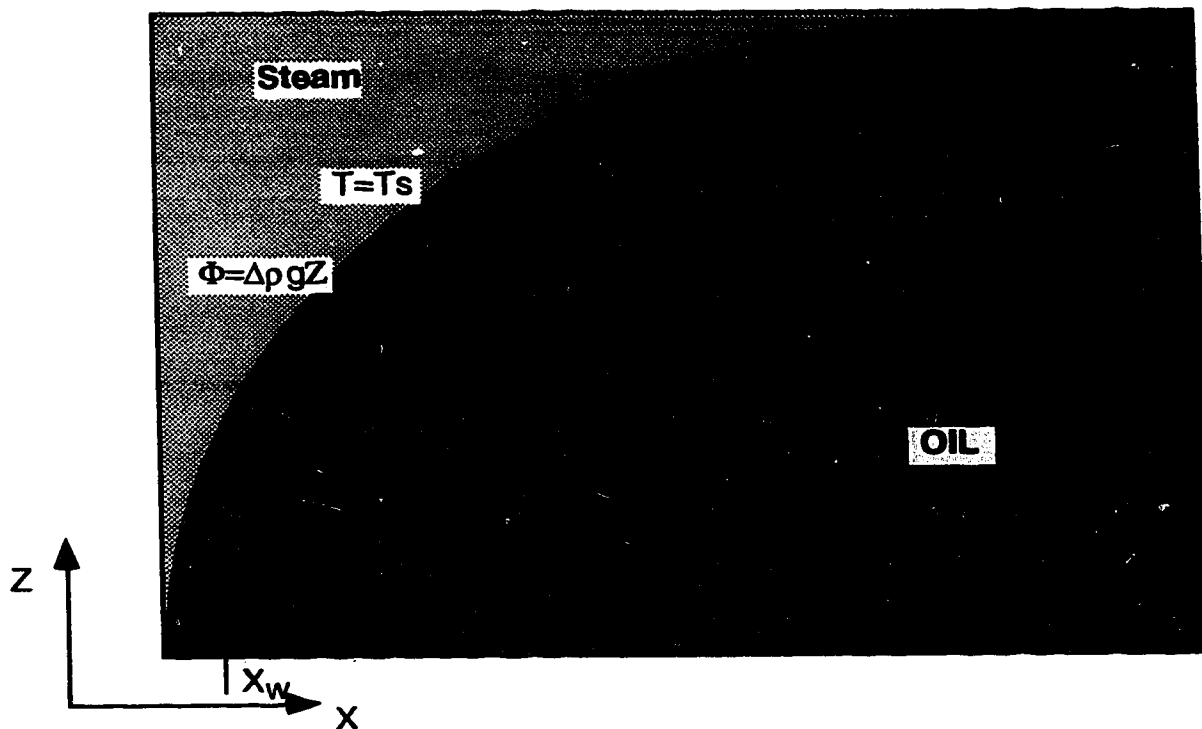
Figure 7.1   Schematic presentation of steam-oil interface under non-isothermal gravity drainage in the SAGD process

By considering a heat conduction problem, any convective effect due to penetration of the hot fluids ahead of the interface is neglected. Using typical thermal properties of a heavy oil reservoir it can be shown easily that temperature of the fluids produced from a unit volume of a reservoir drops by about 5 units in order to increase the temperature of the same volume of the formation ahead of the interface by one unit (the data reported by Chung and Butler [1988-b] were used). This happens if all the produced hot oil penetrates ahead of the interface. In the SAGD process, the hot fluids drain mostly downwards along the interface.

127

For a detailed discussion of the neglected mechanisms, please refer to Section 6.2.1.

7.2 Conservation Laws

In a 2-D system, where heat flows by conduction only, the conservation of energy can be expressed as

$$\frac{\partial}{\partial x}\left(\frac{\partial T}{\partial x}\right) + \frac{\partial}{\partial z}\left(\frac{\partial T}{\partial z}\right) = \frac{1}{\alpha}\frac{\partial T}{\partial t} \qquad x \geq \hat{x}(z,t) \qquad 0 \leq z \leq H \qquad t > 0 \quad \ldots\ldots\ldots (7.2.1)$$

where α, the thermal diffusivity of the formation is considered to be constant. The initial and boundary conditions of the heat flow problem can be written as Equation (7.2.2) to (7.2.6)

$$T = T_R \qquad x \geq 0 \qquad 0 \leq z \leq H \qquad t = 0 \quad \ldots\ldots\ldots (7.2.2)$$

$$\left.\frac{\partial T}{\partial z}\right|_{z=H^-} = \varepsilon\left.\frac{\partial T}{\partial z}\right|_{z=H^+} \qquad x \geq \hat{x}(z,t) \qquad z = H \qquad t > 0 \quad \ldots\ldots\ldots (7.2.3)$$

$$\left.\frac{\partial T}{\partial z}\right|_{z=0^+} = \varepsilon\left.\frac{\partial T}{\partial z}\right|_{z=0^-} \qquad x \geq \hat{x}(z,t) \qquad z = 0 \qquad t > 0 \quad \ldots\ldots\ldots (7.2.4)$$

$$T = T_s \qquad x = \hat{x}(z,t) \qquad 0 \leq z \leq H \qquad t > 0 \quad \ldots\ldots\ldots (7.2.5)$$

$$T = T_R \qquad x \to \infty \qquad 0 \leq z \leq H \qquad t > 0 \quad \ldots\ldots\ldots (7.2.6)$$

where ε is the ratio of the thermal conductivity of the surrounding rock to that of the formation, and $\hat{x}(z,t)$ is the location of the steam interface. Equations (7.2.3) and (7.2.4) express that heat is lost to the cap and base rock by a 1-D conduction process.

Liquid hydrocarbons are known to obey the behaviour of slightly compressible fluids. Equation (7.2.7) describes the behaviour of the density of a slightly compressible fluid with pressure.

$$c = \frac{1}{\rho}\frac{\partial \rho}{\partial P} \qquad\qquad \ldots\ldots\ldots (7.2.7)$$

128

where the compressibility of the fluid, c, is small and constant.

In a 2-D system, conservation of mass can be expressed as

$$-\frac{\partial}{\partial x}(\rho u_x) - \frac{\partial}{\partial z}(\rho u_z) = \phi \frac{\partial \rho}{\partial t} \qquad \dots\dots\dots(7.2.8)$$

where u_x and u_z are average fluid velocities in porous media. The fluid velocities can be found using Darcy's law, which has been shown to be an approximation for the steady-state Navier-Stokes equation of flow for viscous fluids when the inertial forces can be neglected [Hubbert 1956, Slattery 1969].

$$u_x = -\frac{k}{\mu_o}\frac{\partial P}{\partial x} \qquad \dots\dots\dots(7.2.9)$$

$$u_z = -\frac{k}{\mu_o}\left(\frac{\partial P}{\partial z} + \rho g\right) \qquad \dots\dots\dots(7.2.10)$$

where k the permeability of the formation is considered to be independent of flow direction. A discussion of the formulation of the problem in an anisotropic formation is given later.

Combining Equations (7.2.7) to (7.2.10) and neglecting the nonlinear terms, which are shown to be small for typical reservoirs [Odeh and Babu 1988], Equation (7.2.11) is obtained for pressure distribution in the formation,

$$\frac{\partial}{\partial x}\left[\frac{k}{\mu_o}\left(\frac{\partial P}{\partial x}\right)\right] + \frac{\partial}{\partial z}\left[\frac{k}{\mu_o}\left(\frac{\partial P}{\partial z} + \rho g\right)\right] = \phi c \frac{\partial P}{\partial t} \qquad \dots\dots\dots(7.2.11)$$

Using a potential function φ defined as Equation (7.2.12), Equation (7.2.11) can be simplified as Equation (7.2.13)

$$\varphi = P + \rho g z \qquad \dots\dots\dots(7.2.12)$$

$$\frac{\partial}{\partial x}\left[\frac{k}{\mu_o}\left(\frac{\partial \varphi}{\partial x}\right)\right] + \frac{\partial}{\partial z}\left[\frac{k}{\mu_o}\left(\frac{\partial \varphi}{\partial z}\right)\right] = \phi c \frac{\partial \varphi}{\partial t} \qquad x \ge \hat{x}(z,t) \qquad 0 \le z \le H \qquad t > 0$$

$$\dots\dots\dots(7.2.13)$$

129

The initial and boundary conditions of Equation (7.2.13) can be expressed as Equations (7.2.14) to (7.2.19).

$$\varphi = \varphi_R \qquad x \geq 0 \qquad 0 \leq z \leq H \qquad t = 0 \qquad \ldots\ldots(7.2.14)$$

$$\frac{\partial \varphi}{\partial z} = 0 \qquad x \geq \hat{x}(z,t) \qquad z = H \qquad t > 0 \qquad \ldots\ldots(7.2.15)$$

$$\frac{\partial \varphi}{\partial z} = 0 \qquad x \geq x_w \qquad z = 0 \qquad t > 0 \qquad \ldots\ldots(7.2.16)$$

$$\varphi = \varphi_R \qquad 0 \leq x \leq x_w \qquad z = 0 \qquad t > 0 \qquad \ldots\ldots(7.2.17)$$

$$\varphi = \varphi_R + \rho g z \qquad x = \hat{x}(z,t) \qquad 0 \leq z \leq H \qquad t > 0 \qquad \ldots\ldots(7.2.18)$$

$$\varphi = \varphi_R \qquad x \to \infty \qquad 0 \leq z \leq H \qquad t > 0 \qquad \ldots\ldots(7.2.19)$$

In Equation (7.2.18) the density of steam is neglected and a constant steam pressure at the interface is considered. Equation (7.2.17) specifies the well condition. Equations (7.2.17) and (7.2.18) indicate that there is no differential pressure between the interface and the well. This ensures no steam production. Additionally, it has been assumed that steam is injected into the reservoir at the initial reservoir pressure. Should the injection pressure be greater than the initial reservoir pressure, Equations (7.2.17) and (7.2.18) would have to be adjusted accordingly.

Equations (7.2.1) to (7.2.6) and (7.2.13) to (7.2.19) explain the heat and fluid flow processes, respectively. However, both of these processes occur ahead of an interface $\hat{x}(z,t)$. In the next section an equation is found for the interface, such that the formulation of the problem is complete. Before doing so, the above equations are written in terms of appropriate dimensionless variables defined as Equations (7.2.20) to (7.2.25).

$$X = \frac{x}{H} \qquad\qquad\qquad \ldots\ldots(7.2.20)$$

$$Z = \frac{z}{H} \qquad\qquad\qquad \ldots\ldots(7.2.21)$$

$$\tau = \frac{\alpha t}{H^2} \qquad\qquad \dots\dots.(7.2.22)$$

$$\Phi = \frac{\varphi - \varphi_R}{\rho g H} \qquad\qquad \dots\dots.(7.2.23)$$

$$\theta = \frac{T - T_R}{T_s - T_R} \qquad\qquad \dots\dots.(7.2.24)$$

$$\hat{X}(Z,\tau) = \frac{\hat{x}(z,t)}{H} \qquad\qquad \dots\dots.(7.2.25)$$

Using the above dimensionless variables the heat and fluid flow problem can be expressed as

$$\frac{\partial}{\partial X}\left(\frac{\partial \theta}{\partial X}\right) + \frac{\partial}{\partial Z}\left(\frac{\partial \theta}{\partial Z}\right) = \frac{\partial \theta}{\partial \tau} \qquad X \geq \hat{X}(Z,\tau) \qquad 0 \leq Z \leq 1 \qquad \tau > 0 \quad \dots\dots.(7.2.26)$$

$$\theta = 0 \qquad\qquad X \geq 0 \qquad 0 \leq Z \leq 1 \qquad \tau = 0 \quad \dots\dots.(7.2.27)$$

$$\left.\frac{\partial \theta}{\partial Z}\right|_{Z=1^-} = \varepsilon \left.\frac{\partial \theta}{\partial Z}\right|_{Z=1^+} \qquad X \geq \hat{X}(Z,\tau) \qquad Z = 1 \qquad \tau > 0 \quad \dots\dots.(7.2.28)$$

$$\left.\frac{\partial \theta}{\partial Z}\right|_{Z=0^-} = \varepsilon \left.\frac{\partial \theta}{\partial Z}\right|_{Z=0^+} \qquad X \geq \hat{X}(Z,\tau) \qquad Z = 0 \qquad \tau > 0 \quad \dots\dots.(7.2.29)$$

$$\theta = 1 \qquad\qquad X = \hat{X}(Z,\tau) \qquad 0 \leq Z \leq 1 \qquad \tau > 0 \quad \dots\dots.(7.2.30)$$

$$\theta = 0 \qquad\qquad X \to \infty \qquad 0 \leq Z \leq 1 \qquad \tau > 0 \quad \dots\dots.(7.2.31)$$

and

$$\frac{\partial}{\partial X}\left[\frac{\mu_{os}}{\mu_o}\left(\frac{\partial \Phi}{\partial X}\right)\right] + \frac{\partial}{\partial Z}\left[\frac{\mu_{os}}{\mu_o}\left(\frac{\partial \Phi}{\partial Z}\right)\right] = \beta \frac{\partial \Phi}{\partial \tau} \qquad X \geq \hat{X}(Z,\tau) \qquad 0 \leq Z \leq 1 \qquad \tau > 0$$

$$\dots\dots.(7.2.32)$$

$$\Phi = 0 \qquad\qquad X \geq 0 \qquad 0 \leq Z \leq 1 \qquad \tau = 0 \quad \dots\dots.(7.2.33)$$

$$\frac{\partial \Phi}{\partial Z} = 0 \qquad\qquad X \geq \hat{X}(Z,\tau) \qquad Z = 1 \qquad \tau > 0 \quad \dots\dots.(7.2.34)$$

131

$$\frac{\partial \Phi}{\partial Z} = 0 \qquad\qquad X \geq X_w, \qquad Z = 0 \qquad \tau > 0 \quad \ldots\ldots (7.2.35)$$

$$\Phi = 0 \qquad\qquad 0 \leq X \leq X_w, \qquad Z = 0 \qquad \tau > 0 \quad \ldots\ldots (7.2.36)$$

$$\Phi = Z \qquad\qquad X = \hat{X}(Z, \tau) \qquad 0 \leq Z \leq 1 \qquad \tau > 0 \quad \ldots\ldots (7.2.37)$$

$$\Phi = 0 \qquad\qquad X \to \infty \qquad 0 \leq Z \leq 1 \qquad \tau > 0 \quad \ldots\ldots (7.2.38)$$

where β is the ratio of thermal diffusivity to hydraulic diffusivity of the formation at steam temperature, and typically is a very small number. For incompressible systems β is zero, and the parabolic Equation (7.2.32) becomes elliptic.

$$\beta = \frac{\phi \mu_{os} c}{k} \times \alpha \qquad\qquad\qquad \ldots\ldots (7.2.39)$$

7.3 A New Interface Equation

To obtain an equation for the interface the property of the interface, namely the condition of constant pressure there is used. Hence, at the interface one can write

$$\frac{DP}{Dt} = \frac{\partial P}{\partial t} + \bar{U}.\nabla P = 0 \qquad\qquad x = \hat{x}(z,t) \qquad 0 \leq z \leq H \qquad \ldots\ldots (7.3.1)$$

where $\bar{U}$ is the velocity of the interface and is related to Darcy velocity, i.e., potential gradient by,

$$\bar{U} = \frac{1}{\phi \Delta S_o} \left(-\frac{k}{\mu_o} \frac{\partial \varphi}{\partial x}, -\frac{k}{\mu_o} \frac{\partial \varphi}{\partial z} \right) \qquad\qquad \ldots\ldots (7.3.2)$$

The pressure gradient in Equation (7.3.1) can be related to potential gradient using Equation (7.2.12)

$$\nabla P = \left(\frac{\partial \varphi}{\partial x}, \frac{\partial \varphi}{\partial z} - \rho g \right) \qquad\qquad \ldots\ldots (7.3.3)$$

132

Substituting from Equations (7.3.2) and (7.3.3) in Equation (7.3.1) and replacing for $\frac{\partial P}{\partial t} = \frac{\partial \varphi}{\partial t}$ an interface Equation (7.3.4) is obtained, similar to that derived by Bear [1972, P. 255].

$$\frac{\partial \varphi}{\partial t} = \frac{k}{\phi \Delta S_o \mu_{os}} \left[\left(\frac{\partial \varphi}{\partial x}\right)^2 + \left(\frac{\partial \varphi}{\partial z}\right)^2 - \rho g \frac{\partial \varphi}{\partial z} \right] \qquad x = \hat{x}(z,t) \qquad 0 \le z \le H \qquad \ldots \ldots \ldots (7.3.4)$$

Bear [1972] suggested an iterative procedure to find the location of the interface such that Equation (7.3.4) is valid there. Here, an explicit equation is derived for the location of the interface. The boundary condition (7.2.18) can be expressed as

$$\varphi\{\hat{x}(z,t), z, t\} = \varphi_R + \rho g z \qquad x = \hat{x}(z,t) \qquad 0 \le z \le H \qquad \ldots \ldots \ldots (7.3.5)$$

By differentiating Equation (7.3.5) with respect to t and z one obtains

$$\frac{\partial \varphi}{\partial x} \frac{\partial \hat{x}(z,t)}{\partial t} + \frac{\partial \varphi}{\partial t} = 0 \qquad x = \hat{x}(z,t) \qquad 0 \le z \le H \qquad \ldots \ldots \ldots (7.3.6)$$

$$\frac{\partial \varphi}{\partial x} \frac{\partial \hat{x}(z,t)}{\partial z} + \frac{\partial \varphi}{\partial z} = \rho g \qquad x = \hat{x}(z,t) \qquad 0 \le z \le H \qquad \ldots \ldots \ldots (7.3.7)$$

By substituting from Equation (7.3.6) and (7.3.7) into Equation (7.3.4) and simplifying one obtains

$$\frac{\partial \hat{x}(z,t)}{\partial t} = -\frac{k}{\phi \Delta S_o \mu_{os}} \left\{ \frac{\partial \varphi}{\partial x} \left[1 + \left(\frac{\partial \hat{x}(z,t)}{\partial z}\right)^2 \right] - \rho g \frac{\partial \hat{x}(z,t)}{\partial z} \right\} \qquad \ldots \ldots \ldots (7.3.8)$$

where it has been assumed that assumed $\frac{\partial \varphi}{\partial x} \ne 0$. For the interface to start moving in the formation from its initial location it is required that $\frac{\partial \varphi}{\partial x} \ne 0$. The well condition Equation (7.2.17) indicates that $\frac{\partial \varphi}{\partial x} = 0$ at $z = 0$. However, a boundary condition will be introduced there that will overrule Equation (7.3.8).

The interface equation (7.3.8) relates the movement of the interface to the shape of the interface and potential distribution in the formation. To the best of the author's knowledge, this is the first time that the interface Equation (7.3.8) has been introduced

133

into the literature. An analogous, but different, equation was previously derived for melt propagation due to conduction heating [Patel 1969].

Using the dimensionless variables defined by Equations (7.2.20) to (7.2.25), the interface Equation (7.3.8) can be expressed as

$$\frac{\partial \hat{X}(Z,\tau)}{\partial \tau} = -N_{Ra} \left\{ \frac{\partial \Phi}{\partial X} \left[1 + \left(\frac{\partial \hat{X}(Z,\tau)}{\partial Z} \right)^2 \right] - \frac{\partial \hat{X}(Z,\tau)}{\partial Z} \right\} \qquad \ldots\ldots (7.3.9)$$

where N_{Ra} is the Rayleigh No. which was previously found to be an important dimensionless group in thermal gravity drainage in porous media (see Section 5.2, 6.2.3, and 6.2.6.3)

$$N_{Ra} = \frac{kgH}{\phi \Delta S_o v_{os}} \times \frac{1}{\alpha} \qquad \ldots\ldots (7.3.10)$$

The initial condition of the interface Equation (7.3.9) is Equation (7.3.11), which states that the interface is initially located vertically at the origin.

$$\hat{X}(Z,\tau) = 0 \qquad\qquad \cdot \qquad\qquad 0 \le Z \le 1 \qquad \tau = 0 \qquad\qquad \ldots\ldots (7.3.11)$$

It was previously pointed out that in the SAGD process, the steam-oil interface is kept at the production site. This is achieved by adjusting the production pressure such that excessive steam production is avoided. To incorporate this in the mathematical model, condition (7.3.12) is introduced which holds the interface at the production well. It should be noted that the interface Equation ⟨7.3.9) is not valid at the bottom of the interface, because the condition $\frac{\partial \varphi}{\partial x} \ne 0$ is violated there. Hence, Equation (7.3.9) together with Equation (7.3.12) describes the behaviour of the interface.

$$\hat{X}(Z,\tau) = 0 \qquad\qquad Z = 0 \qquad \tau > 0 \qquad\qquad \ldots\ldots (7.3.12)$$

At the top of the formation where $\frac{\partial \Phi}{\partial Z} = 0$, the interface Equation (7.3.9) is expressed as

$$\frac{\partial \hat{X}(Z,\tau)}{\partial \tau} = -N_{Ra} \left(\frac{\partial \Phi}{\partial X} \right) \qquad \ldots\ldots (7.3.13)$$

134

7.4. Transformation

In Section 7.3 an equation was found to locate the oil-steam interface. This completes the formulation of the combined heat and fluid flow ahead of the moving interface, as discussed in Sections 7.2 and 7.3. Having a system of first and second order nonlinear partial differential equations makes it impossible to obtain analytical solutions. To develop an accurate numerical model, the physical domain is transformed onto a computational one such that the location of the moving interface is always known and constant. Immobilizing the interface by the transformation enables one to locate smaller grid blocks in the vicinity of the now stationary interface. It will be shown, however, that the transformation complicates the diffusion Equations (7.2.26) and (7.2.32).

A two dimensional diffusion Equation of (7.4.1) can be transformed from (X, Z, τ) to the moving coordinate (ξ, η, τ) defined by Equations (7.4.2) and (7.4.3)

$$\frac{\partial}{\partial X}\left(\Gamma \frac{\partial T}{\partial X}\right) + \frac{\partial}{\partial Z}\left(\Gamma \frac{\partial T}{\partial Z}\right) = \frac{\partial T}{\partial \tau} \qquad \dots \dots (7.4.1)$$

$$\xi = \xi(X, Z, \tau) \qquad \dots \dots (7.4.2)$$

$$\eta = \eta(X, Z, \tau) \qquad \dots \dots (7.4.3)$$

where T is the temperature or potential, and Γ is the diffusion coefficient. Kim and Kaviany [1992], among others, showed that Equation (7.4.1) translates to Equation (7.4.4) in the computational domain.

$$\frac{\partial}{\partial \xi}\left(\frac{\alpha_\xi}{h_\xi} \Gamma \frac{\partial T}{\partial \xi} + X_\tau T\right) + \frac{\partial}{\partial \eta}\left(\frac{\alpha_\eta}{h_\eta} \Gamma \frac{\partial T}{\partial \eta} + Z_\tau T\right) - \frac{\partial}{\partial \xi}\left(\frac{\beta_\xi}{h_\eta} \Gamma \frac{\partial T}{\partial \eta}\right) - \frac{\partial}{\partial \eta}\left(\frac{\beta_\eta}{h_\xi} \Gamma \frac{\partial T}{\partial \xi}\right) = \frac{\partial(JT)}{\partial \tau}$$

$$\dots \dots (7.4.4)$$

where

$$\alpha_\xi = \frac{h_\xi h_\eta^2}{J} \qquad \dots \dots (7.4.5)$$

135

$$\alpha_\eta = \frac{h_\eta h_\xi^2}{J} \qquad\qquad \ldots\ldots (7.4.6)$$

$$\beta_\xi = \frac{\lambda h_\eta}{J} \qquad\qquad \ldots\ldots (7.4.7)$$

$$\beta_\eta = \frac{\lambda h_\xi}{J} \qquad\qquad \ldots\ldots (7.4.8)$$

$$h_\xi = \sqrt{\left(X_\xi^2 + Z_\xi^2\right)} \qquad\qquad \ldots\ldots (7.4.9)$$

$$h_\eta = \sqrt{\left(X_\eta^2 + Z_\eta^2\right)} \qquad\qquad \ldots\ldots (7.4.10)$$

$$\lambda = X_\xi X_\eta + Z_\xi Z_\eta \qquad\qquad \ldots\ldots (7.4.11)$$

$$J = X_\xi Z_\eta - Z_\xi X_\eta \qquad\qquad \ldots\ldots (7.4.12)$$

and subscripts on the independent variables X and Z denote partial derivatives.

In this study the transformation Equations (7.4.13) and (7.4.14) are introduced to immobilize the moving interface .

$$\xi = X - \hat{X}(Z,\tau) \qquad\qquad \ldots\ldots (7.4.13)$$

$$\eta = Z \qquad\qquad \ldots\ldots (7.4.14)$$

Equation (7.4.13) ensures that the interface is always located at $\xi = 0$. Equation (7.4.13) permits one to use the so called "simultaneous node movement" technique [Hawken 1987]. In this technique the movement of the coordinate system is incorporated into the conservation equations. The alternative techniques are periodic and alternating node movement. In the latter techniques, the conservation equations are solved on stationary coordinates, and then the field variables are calculated at the new coordinate location using interpolation. For stiff problems, where the time scales of different flow processes differ by orders of magnitude, the latter technique may result in instabilities, unless the time steps are kept very small [Hawken 1987].

Using the Equation (7.4.13) and (7.4.14) and the relations (7.4.5) to (7.4.12) one can transform the 2-D diffusion Equations of (7.2.26) and (7.2.34), and their corresponding initial and boundary conditions. In doing so one obtains

$$\frac{\partial}{\partial \xi}\left\{\left[1+\left(\frac{\partial \hat{\xi}}{\partial \eta}\right)^2\right]\frac{\partial \theta}{\partial \xi}+\frac{\partial \hat{\xi}}{\partial \tau}\theta\right\}+\frac{\partial}{\partial \eta}\left(\frac{\partial \theta}{\partial \eta}\right)-\frac{\partial}{\partial \xi}\left(\frac{\partial \hat{\xi}}{\partial \eta}\frac{\partial \theta}{\partial \eta}\right)-\frac{\partial}{\partial \eta}\left(\frac{\partial \hat{\xi}}{\partial \eta}\frac{\partial \theta}{\partial \xi}\right)=\frac{\partial \theta}{\partial \tau} \qquad \ldots\ldots (7.4.15)$$

The cross-diffusion terms on the left hand side of Equation (7.4.15) are created because of the non-orthogonality of the computational domain, as was explained in Chapter 2. The convective term at the left hand side of Equation (7.4.15) represents the movement of the interface in the horizontal direction. If the transformations (7.4.13) and (7.4.14) are applied to Equation (7.2.26) through a chain rule or strong conservation law forms of Hawken [1987], Equation (7.4.15) is consistently obtained. Hence, using the transformations used in this study, the geometric errors that might be introduced due to inconsistent application of some transformations are not present. It is worth noting that by using the transformation (7.2.13) and (7.2.14) the interface Equation remains the same, that is,

$$\hat{\xi}(\eta,\tau)=\hat{X}(Z,\tau) \qquad \ldots\ldots (7.4.16)$$

The initial and boundary conditions of Equation (7.4.15) are

$\theta = 0$	$\xi \geq 0$	$0 \leq \eta \leq 1$	$\tau = 0$	$\ldots\ldots (7.4.17)$
$\left.\frac{\partial \theta}{\partial \eta}\right|_{\eta=1^-}=\varepsilon\left.\frac{\partial \theta}{\partial \eta}\right|_{\eta=1^+}$	$\xi \geq 0$	$\eta = 1$	$\tau > 0$	$\ldots\ldots (7.4.18)$
$\left.\frac{\partial \theta}{\partial \eta}\right|_{\eta=0^+}=\varepsilon\left.\frac{\partial \theta}{\partial \eta}\right|_{\eta=0^-}$	$\xi \geq 0$	$\eta = 0$	$\tau > 0$	$\ldots\ldots (7.4.19)$
$\theta = 1$	$\xi = 0$	$0 \leq \eta \leq 1$	$\tau > 0$	$\ldots\ldots (7.4.20)$
$\theta = 0$	$\xi \to \infty$	$0 \leq \eta \leq 1$	$\tau > 0$	$\ldots\ldots (7.4.21)$

The corresponding equations for the potential distribution is

137

$$\frac{\partial}{\partial \xi}\left\{\frac{\mu_{os}}{\mu_o}\left[1+\left(\frac{\partial \hat{\xi}}{\partial \eta}\right)^2\right]\left(\frac{\partial \Phi}{\partial \xi}\right)+\beta \frac{\partial \hat{\xi}}{\partial \tau}\Phi\right\}+\frac{\partial}{\partial \eta}\left[\frac{\mu_{os}}{\mu_o}\left(\frac{\partial \Phi}{\partial \eta}\right)\right]-\frac{\partial}{\partial \xi}\left[\frac{\mu_{os}}{\mu_o}\left(\frac{\partial \hat{\xi}}{\partial \eta}\frac{\partial \Phi}{\partial \eta}\right)\right]-\frac{\partial}{\partial \eta}\left[\frac{\mu_{os}}{\mu_o}\left(\frac{\partial \hat{\xi}}{\partial \eta}\frac{\partial \Phi}{\partial \xi}\right)\right]=\beta \frac{\partial \Phi}{\partial \tau}$$

$$\ldots \ldots (7.4.22)$$

with the following initial and boundary conditions

$\Phi = 0$	$\xi \geq 0$	$0 \leq \eta \leq 1$	$\tau = 0$	$\ldots \ldots (7.4.23)$
$\dfrac{\partial \Phi}{\partial \eta} = 0$	$\xi \geq 0$	$\eta = 1$	$\tau > 0$	$\ldots \ldots (7.4.24)$
$\dfrac{\partial \Phi}{\partial \eta} = 0$	$\xi \geq \xi_w$	$\eta = 0$	$\tau > 0$	$\ldots \ldots (7.4.25)$
$\Phi = 0$	$0 \leq \xi \leq \xi_w$	$\eta = 0$	$\tau > 0$	$\ldots \ldots (7.4.26)$
$\Phi = \eta$	$\xi = 0$	$0 \leq \eta \leq 1$	$\tau > 0$	$\ldots \ldots (7.4.27)$
$\Phi = 0$	$\xi \rightarrow \infty$	$0 \leq \eta \leq 1$	$\tau > 0$	$\ldots \ldots (7.4.28)$

Similarly, and by applying the chain rule to Equation (7.3.9), one can find the interface Equation in the computational domain,

$$\frac{\partial \hat{\xi}(\eta, \tau)}{\partial \tau}=-N_{Ra}\left\{\frac{\partial \Phi}{\partial \xi}\left[1+\left(\frac{\partial \hat{\xi}(\eta, \tau)}{\partial \eta}\right)^2\right]-\frac{\partial \hat{\xi}(\eta, \tau)}{\partial \eta}\right\} \qquad \ldots \ldots (7.4.29)$$

Correspondingly, Equations (7.3.11) and (7.3.12) can be written as,

$\hat{\xi}(\eta, \tau) = 0$	$0 \leq \eta \leq 1$	$\tau = 0$	$\ldots \ldots (7.4.30)$
$\hat{\xi}(\eta, \tau) = 0$	$\eta = 0$	$\tau > 0$	$\ldots \ldots (7.4.31)$

7.5 Solution Method

Equations (7.4.15), (7.4.22) and (7.4.29) form a system of coupled partial differential equations which, along with their initial and boundary conditions, describe

the behaviour of the 2-D linear SAGD process. The coefficients of the potential equation (7.4.22) are strongly dependent on the solution of the temperature Equation (7.4.15) due to the strong dependency of viscosity on temperature. Solution of potential Equation (7.4.22) in turn, affects the location of the interface in Equation (7.4.29). Due to the strong interaction between the above equations an implicit method will be used.

The interface is initially located vertically at the origin. By knowing the location and shape of the interface one can solve for the temperature distribution using Equations (7.4.15) to (7.5.21). The temperature solution is subsequently used to evaluate the coefficients of the potential Equation (7.4.22), which is then solved along with the initial and boundary conditions (7.4.23) to (7.4.28). The potential solution is then used to find the interface location by using Equation (7.4.29) to (7.4.31). By knowing the shape and velocity of the interface, the temperature and potential equations can be solved again. The calculation is repeated iteratively until a convergence criterion is met. Time is then incremented and the above cycle is repeated with the initial conditions of the equations replaced by the values obtained from the previous time step. Should the number of iterations before convergence be too high or low, the time step is adjusted accordingly.

The interface Equation (7.4.29) is an important part of the solution, especially in the case of fast moving boundary systems. The accuracy of its solution is increased by implementing a two-step procedure. At the end of each time step and after convergence is obtained, the location of the interface is obtained from Equation (7.4.29) for the following time step. An average of this location with the solution of Equation (7.4.29) at the next time step is considered as the location of the interface at any iteration. This is similar to the two-step Euler's method for solving first order differential equations. Figure 7.2 schematically shows the flow chart of the calculations as explained above.

It was briefly discussed in Section 7.2 that the effect of the unsteady-state term in the potential Equation is much smaller than that in the temperature Equation. This causes a large difference in the time scales of the two flow processes, being of the order of 10^6 for typical Canadian bituminous reservoirs. In order to obtain a stable solution and/or not to require impractically small time steps, each of the equations are solved implicitly. This is discussed in more detail later, when the system of algebraic equations are formed.
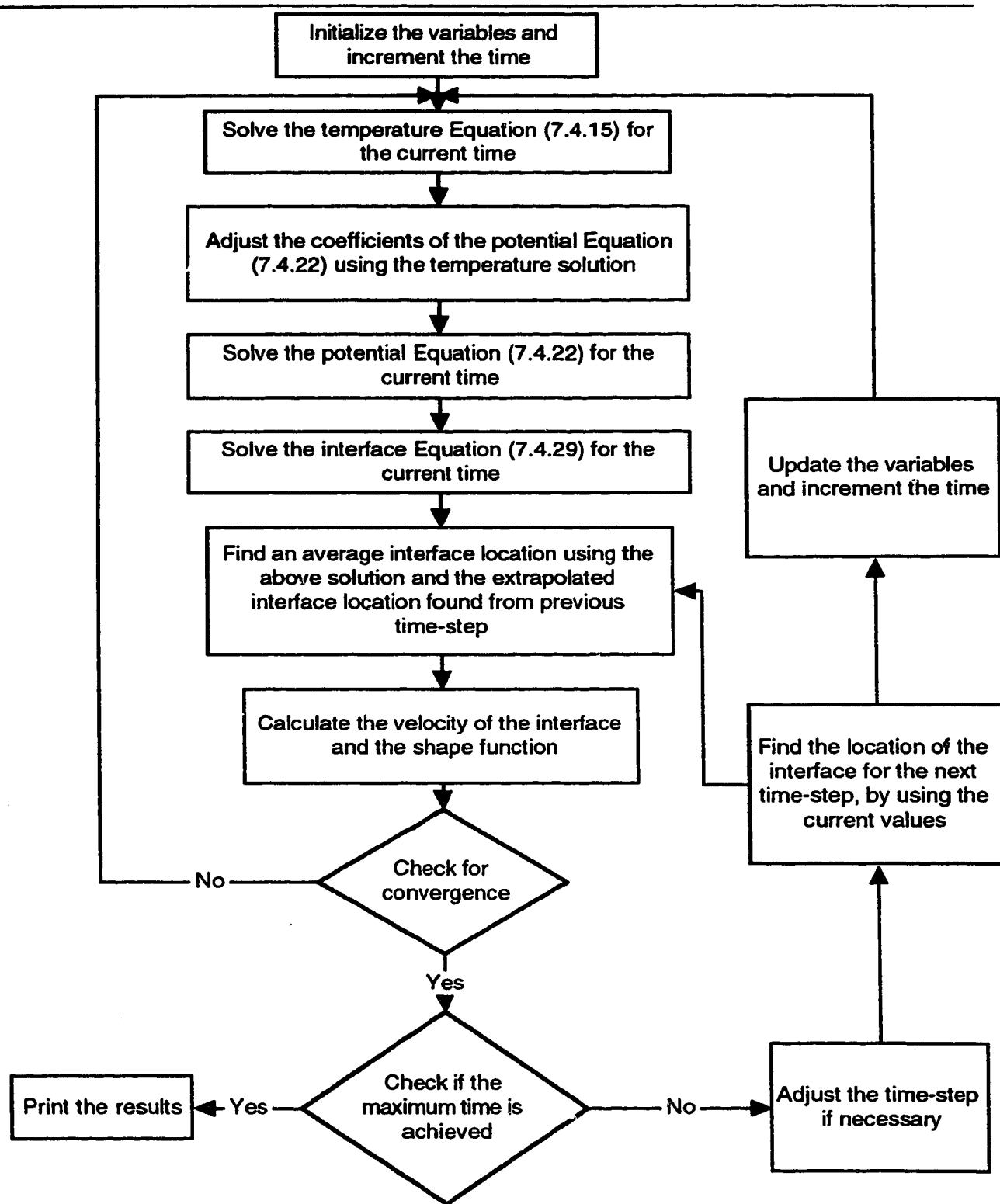
139

Figure 7.2   Calculation procedure

7.6 Discretization

Different methods of solving partial differential equations in general, and conservation equations in moving boundary problems in particular, were reviewed in Chapter 2. Among the three methods of finite element, finite difference and finite volume, the finite volume technique is used. It is shown in the literature that the latter approach is very successful in modelling conservation equations [Patankar 1980]. The advantage of a finite volume method lays in the fact that it achieves conservation, no matter how coarse the grid blocks.

In the finite volume method, each of the spatial derivative terms is integrated over a control volume (control surface for a 2-D problem). Then Green's theorem is implemented to write the expression as a boundary integral of the flux terms. The conservation property of the method is guaranteed because the flux terms are evaluated at the boundaries of the control volumes. In other words, what leaves a control volume enters the next one through the common control volume face. The integration of the unsteady-state term over a control volume is performed by assigning a constant value to the dependent variable over the corresponding control volume. The finer the control volumes the more accurate the approximation for the unsteady-state term.

Another advantage of the control volume approach is that it facilitates the understanding of the extra terms that are introduced due to the coordinate transformation. For example, the cross-derivative terms can be related easily to the non-orthogonality of the coordinate axes. Consider a control volume denoted by "P" in Figure 7.3. A flux entering the west boundary, for example, should be evaluated along the normal to the west boundary. The neighbouring nodes, however, are not aligned along the normal to the boundary. A proper representation of the normal flux requires using two other fluxes which are parallel to the non-orthogonal coordinate system, and which can be evaluated using the values obtained at the computational nodes [see for example Faghri, Sparrow, and Prata 1984, Halal and Lilley 1988].

In a numerical calculation, where unequal grid blocks are used, a question should be answered, whether the nodes are chosen at the center of the corresponding control volumes, or the two subsequent computational nodes are placed at equal distances from the common control volume face. The former approach provides more accuracy in

estimating the unsteady-state term, whereas, the latter approach more accurately represents the flux terms [Patankar 1980, Aziz 1993]. Nacul and Aziz [1991] showed that for the cases they studied, the solution accuracy was higher when priority was given to a higher accuracy for the flux terms rather than to the unsteady-state term. More accuracy in representing the flux terms is considered in this study. This offers simple expressions for approximating the cross derivative terms, as will be discussed later.
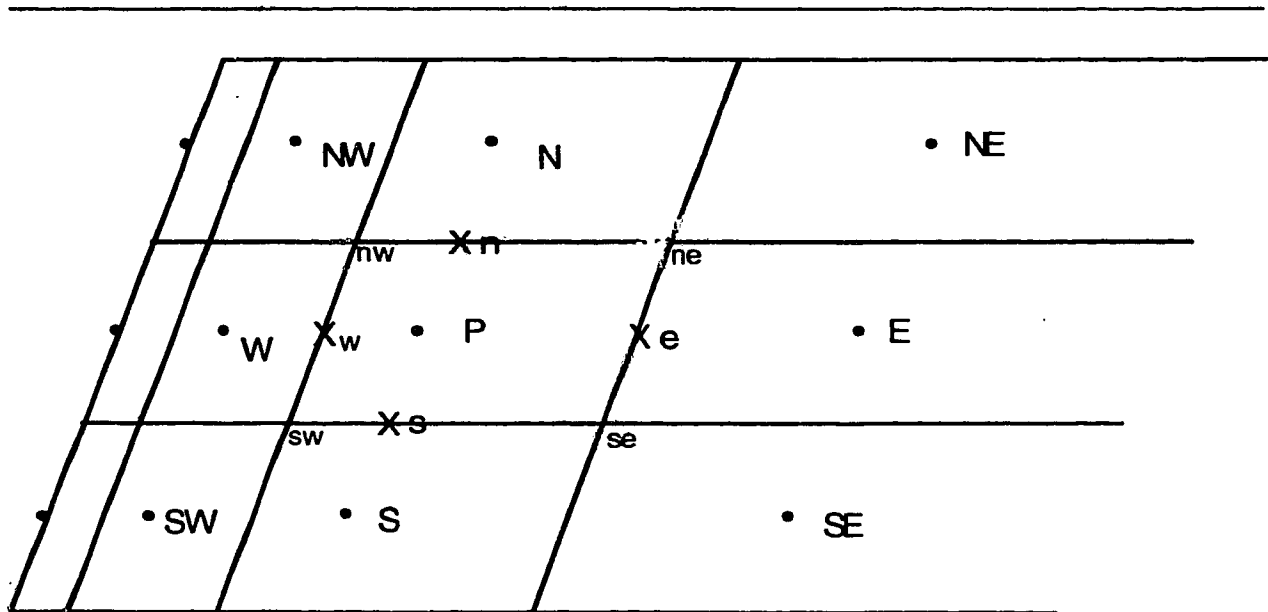

Figure 7.3 A schematic representation of the control volumes in the physical domain

The physical problem of interest suggests that temperature gradients are highest along the horizontal direction. Hence, unequal grid spacing along the horizontal axis is used to obtain high accuracy in the region close to the interface, and equal grid spacing is used along the vertical axis in the computational domain.

In the following a discretized system of equations for the potential Equation (7.4.22), given here again for convenience, is presented. The temperature Equation (7.4.15) can be similarly handled. Incorporation of the boundary conditions is explained later.

142

$$\frac{\partial}{\partial \eta}\left[\frac{\mu_{os}}{\mu_o}\left(\frac{\partial \Phi}{\partial \eta}\right)\right] + \frac{\partial}{\partial \xi}\left\{\frac{\mu_{os}}{\mu_o}\left[1+\left(\frac{\partial \hat{\xi}}{\partial \eta}\right)^2\right]\left(\frac{\partial \Phi}{\partial \xi}\right) + \beta\frac{\partial \hat{\xi}}{\partial \tau}\Phi\right\} - \frac{\partial}{\partial \xi}\left[\frac{\mu_{os}}{\mu_o}\left(\frac{\partial \hat{\xi}}{\partial \eta}\frac{\partial \Phi}{\partial \eta}\right)\right] - \frac{\partial}{\partial \eta}\left[\frac{\mu_{os}}{\mu_o}\left(\frac{\partial \hat{\xi}}{\partial \eta}\frac{\partial \Phi}{\partial \xi}\right)\right] = \beta\frac{\partial \Phi}{\partial \tau}$$

$$\ldots \ldots (7.6.1)$$

Starting with the left hand side, the first term of Equation (7.6.1) can be integrated over a control volume denoted by "P" in Figure 7.4, which shows the computational domain after performing the transformations denoted by Equations (7.3.13) and (7.3.14). Similar to that given by Patankar [1980] one can write

$$\int_w^e \int_s^n \frac{\partial}{\partial \eta}\left[\frac{\mu_{os}}{\mu_o}\left(\frac{\partial \Phi}{\partial \eta}\right)\right] d\eta d\xi = \left\{\left[\frac{\mu_{os}}{\mu_o}\left(\frac{\partial \Phi}{\partial \eta}\right)\right]_n - \left[\frac{\mu_{os}}{\mu_o}\left(\frac{\partial \Phi}{\partial \eta}\right)\right]_s\right\}\Delta\xi_P$$

$$\ldots (7.6.2)$$

$$= \left\{\left[\left(\frac{\mu_{os}}{\mu_o}\right)_n\left(\frac{\Phi_N-\Phi_P}{\Delta\eta}\right)\right] - \left[\left(\frac{\mu_{os}}{\mu_o}\right)_s\left(\frac{\Phi_P-\Phi_S}{\Delta\eta}\right)\right]\right\}\Delta\xi_P$$

Equation (7.6.2) can simplified as:

$$a_{N_1}\Phi_N + a_{S_1}\Phi_S + a_{P_1}\Phi_P \qquad \ldots \ldots (7.6.3)$$

where

$$a_{N_1} = \frac{\Delta\xi_P}{\Delta\eta}\left(\frac{\mu_{os}}{\mu_o}\right)_n \qquad \ldots \ldots (7.6.4)$$

$$a_{S_1} = \frac{\Delta\xi_P}{\Delta\eta}\left(\frac{\mu_{os}}{\mu_o}\right)_s \qquad \ldots \ldots (7.6.5)$$

$$a_{P_1} = -\left(a_{N_1} + a_{S_1}\right) \qquad \ldots \ldots (7.6.6)$$

Similarly integration of the second term at the left hand side of Equation (7.6.1) yields

143

$$\int_s^n \int_w^e \frac{\partial}{\partial \xi}\left\{\frac{\mu_{os}}{\mu_o}\left[1+\left(\frac{\partial \hat{\xi}}{\partial \eta}\right)^2\right]\left(\frac{\partial \Phi}{\partial \xi}\right)+\beta\frac{\partial \hat{\xi}}{\partial \tau}\Phi\right\}d\xi d\eta$$

$$=\left\{\left\{\frac{\mu_{os}}{\mu_o}\left[1+\left(\frac{\partial \hat{\xi}}{\partial \eta}\right)^2\right]\left(\frac{\partial \Phi}{\partial \xi}\right)+\beta\frac{\partial \hat{\xi}}{\partial \tau}\Phi\right\}_e -\left\{\frac{\mu_{os}}{\mu_o}\left[1+\left(\frac{\partial \hat{\xi}}{\partial \eta}\right)^2\right]\left(\frac{\partial \Phi}{\partial \xi}\right)+\beta\frac{\partial \hat{\xi}}{\partial \tau}\Phi\right\}_w\right\}\Delta\eta$$

$$\dots\dots (7.6.7)$$

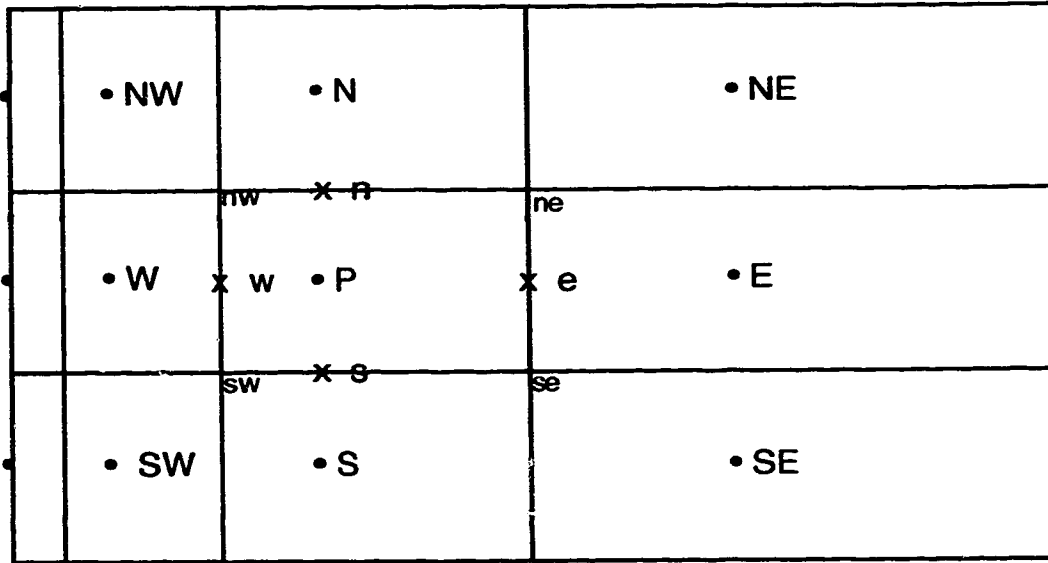|			
• NW	• N		• NE
	nw ✗ n	ne	
• W	✗ w • P	✗ e	• E
	sw ✗ s	se	
• SW	• S		• SE

Figure 7.4 A schematic representation of the control volumes in the computational domain

Patankar [1980] gave a detailed discussion, and suggested that the right hand side of Equation (7.6.7) is best approximated for a 1-D steady-state convection-diffusion problem if a power law scheme is used. The power law approximation simplifies to an upwind difference if the cell Peclet No. is greater or equal to 10, and degenerates to a central difference for a purely conductive problem. By using this approach, Equation (7.6.7) can be expressed as

$$a_{E_1}\Phi_E + a_{W_1}\Phi_W + a_{P_2}\Phi_P \qquad\dots\dots (7.6.8)$$

where

$$a_{E_1} = \left\{ \left(\frac{\mu_{os}}{\mu_o} \right)_e \left[1 + \left(\frac{\partial \hat{\xi}}{\partial \eta} \right)^2 \right] \frac{F(|P_e|)}{(\delta \xi)_e} + \left| \beta \frac{\partial \hat{\xi}}{\partial \tau}, 0 \right| \right\} \Delta \eta \qquad \dots \dots (7.6.9)$$

$$a_{W_1} = \left\{ \left(\frac{\mu_{os}}{\mu_o} \right)_w \left[1 + \left(\frac{\partial \hat{\xi}}{\partial \eta} \right)^2 \right] \frac{F(|P_w|)}{(\delta \xi)_w} + \left\| -\beta \frac{\partial \hat{\xi}}{\partial \tau}, 0 \right\| \right\} \Delta \eta \qquad \dots \dots (7.6.10)$$

$$a_{P_2} = -\left(a_{W_1} + a_{E_1} \right) \qquad \dots \dots (7.6.11)$$

where ‖ ‖ denotes the maximum value of its arguments, and the cell Peclet No., P, can be expressed as Equation (7.6.12) and the function F as Equation (7.6.13).

$$P = \frac{\beta \frac{\partial \hat{\xi}}{\partial \tau} (\delta \xi)}{\left(\frac{\mu_{os}}{\mu_o} \right) \left[1 + \left(\frac{\partial \hat{\xi}}{\partial \eta} \right)^2 \right]} \qquad \dots \dots (7.6.12)$$

$$F(P) = \left\| 0, (1 - 0.1|P|)^5 \right\| \qquad \dots \dots (7.6.13)$$

Integration of the cross-diffusion terms is performed as suggested by Karki and Patankar [1988].

$$\int_w^e \int_s^n -\frac{\partial}{\partial \eta} \left[\frac{\mu_{os}}{\mu_o} \left(\frac{\partial \hat{\xi}}{\partial \eta} \frac{\partial \Phi}{\partial \xi} \right) \right] d\eta d\xi = e_n - e_s \qquad \dots \dots (7.6.14)$$

where

$$e_n = -\left[\frac{\mu_{os}}{\mu_o} \left(\frac{\partial \hat{\xi}}{\partial \eta} \frac{\partial \Phi}{\partial \xi} \right) \right]_n \times \Delta \xi = -\left(\frac{\mu_{os}}{\mu_o} \frac{\partial \hat{\xi}}{\partial \eta} \right)_n (\Phi_{ne} - \Phi_{nw}) \qquad \dots \dots (7.6.15)$$

Similarly,

$$e_s = -\left[\frac{\mu_{os}}{\mu_o} \left(\frac{\partial \hat{\xi}}{\partial \eta} \frac{\partial \Phi}{\partial \xi} \right) \right]_s \times \Delta \xi = -\left(\frac{\mu_{os}}{\mu_o} \frac{\partial \hat{\xi}}{\partial \eta} \right)_s (\Phi_{se} - \Phi_{sw}) \qquad \dots \dots (7.6.16)$$

145

Using linear interpolation for finding the temperature at the corners of the control volume, and collecting terms, the integral (7.6.14) can be written as

$$a_{SW_1}\Phi_{SW} + a_{W_2}\Phi_W + a_{NW_1}\Phi_{NW} + a_{SE_1}\Phi_{SE} + a_{E_2}\Phi_E + a_{NE_1}\Phi_{NE} \qquad \ldots \ldots (7.6.17)$$

where

$$a_{SW_1} = -\frac{1}{4}\left(\frac{\mu_{os}}{\mu_o}\frac{\partial\hat{\xi}}{\partial\eta}\right)_s \qquad \ldots \ldots (7.6.18)$$

$$a_{W_2} = \frac{1}{4}\left(\frac{\mu_{os}}{\mu_o}\frac{\partial\hat{\xi}}{\partial\eta}\right)_n - \frac{1}{4}\left(\frac{\mu_{os}}{\mu_o}\frac{\partial\hat{\xi}}{\partial\eta}\right)_s \qquad \ldots \ldots (7.6.19)$$

$$a_{NW_1} = \frac{1}{4}\left(\frac{\mu_{os}}{\mu_o}\frac{\partial\hat{\xi}}{\partial\eta}\right)_n \qquad \ldots \ldots (7.6.20)$$

$$a_{SE_1} = \frac{1}{4}\left(\frac{\mu_{os}}{\mu_o}\frac{\partial\hat{\xi}}{\partial\eta}\right)_s \qquad \ldots \ldots (7.6.21)$$

$$a_{E_2} = \frac{1}{4}\left(\frac{\mu_{os}}{\mu_o}\frac{\partial\hat{\xi}}{\partial\eta}\right)_s - \frac{1}{4}\left(\frac{\mu_{os}}{\mu_o}\frac{\partial\hat{\xi}}{\partial\eta}\right)_n \qquad \ldots \ldots (7.6.22)$$

$$a_{NE_1} = -\frac{1}{4}\left(\frac{\mu_{os}}{\mu_o}\frac{\partial\hat{\xi}}{\partial\eta}\right)_n \qquad \ldots \ldots (7.6.23)$$

Similarly the integration of the other cross derivative term results in

$$\int_s^n\int_w^e -\frac{\partial}{\partial\xi}\left[\frac{\mu_{os}}{\mu_o}\left(\frac{\partial\hat{\xi}}{\partial\eta}\frac{\partial\Phi}{\partial\eta}\right)\right]d\xi d\eta = e_e - e_w \qquad \ldots \ldots (7.6.24)$$

where

$$e_e = -\left[\frac{\mu_{os}}{\mu_o}\left(\frac{\partial\hat{\xi}}{\partial\eta}\frac{\partial\Phi}{\partial\eta}\right)\right]_e \times \Delta\eta = -\left(\frac{\mu_{os}}{\mu_o}\frac{\partial\hat{\xi}}{\partial\eta}\right)_e (\Phi_{ne} - \Phi_{se}) \qquad \ldots \ldots (7.6.25)$$

146

...d

$$e_{w} = -\left[\frac{\mu_{os}}{\mu_o}\left(\frac{\partial\hat{\xi}}{\partial\eta}\frac{\partial\Phi}{\partial\eta}\right)\right]_{w} \times \Delta\eta = -\left(\frac{\mu_{os}}{\mu_o}\frac{\partial\hat{\xi}}{\partial\eta}\right)_{w}(\Phi_{nw} - \Phi_{sw})$$ .....(7.6.26)

Using linear interpolation as before one can express the integral (7.6.24) as

$$a_{SW_2}\Phi_{SW} + a_{NW_2}\Phi_{NW} + a_{S_2}\Phi_S + a_{N_2}\Phi_N + a_{SE_2}\Phi_{SE} + a_{NE_2}\Phi_{NE}$$ .....(7.6.27)

where

$$a_{SW_2} = -\frac{1}{4}\left(\frac{\mu_{os}}{\mu_o}\frac{\partial\hat{\xi}}{\partial\eta}\right)_{w}$$ .....(7.6.28)

$$a_{NW_2} = \frac{1}{4}\left(\frac{\mu_{os}}{\mu_o}\frac{\partial\hat{\xi}}{\partial\eta}\right)_{w}$$ .....(7.6.29)

$$a_{S_2} = \frac{1}{4}\left(\frac{\mu_{os}}{\mu_o}\frac{\partial\hat{\xi}}{\partial\eta}\right)_{e} - \frac{1}{4}\left(\frac{\mu_{os}}{\mu_o}\frac{\partial\hat{\xi}}{\partial\eta}\right)_{w}$$ .....(7.6.30)

$$a_{N_2} = \frac{1}{4}\left(\frac{\mu_{os}}{\mu_o}\frac{\partial\hat{\xi}}{\partial\eta}\right)_{w} - \frac{1}{4}\left(\frac{\mu_{os}}{\mu_o}\frac{\partial\hat{\xi}}{\partial\eta}\right)_{e}$$ .....(7.6.31)

$$a_{SE_2} = \frac{1}{4}\left(\frac{\mu_{os}}{\mu_o}\frac{\partial\hat{\xi}}{\partial\eta}\right)_{e}$$ .....(7.6.32)

$$a_{NE_2} = -\frac{1}{4}\left(\frac{\mu_{os}}{\mu_o}\frac{\partial\hat{\xi}}{\partial\eta}\right)_{e}$$ .....(7.6.33)

Integrating the right hand side of Equation (7.6.1), and assuming a constant value of potential over the control volume yields

$$\int_s^n\int_w^e \beta\frac{\partial\Phi}{\partial\tau}d\xi d\eta = \frac{\Delta\eta\Delta\xi_P}{\Delta\tau}\beta(\Phi_P - \Phi_P^0) = a_{P_3}\Phi_P + a_P^0\Phi_P^0$$ .....(7.6.34)

147

where

$$a_P^0 = -\frac{\Delta\eta\Delta\xi_P}{\Delta\tau}\beta \qquad\qquad \dots\dots(7.6.35)$$

$$a_{P_s} = -a_P^0 \qquad\qquad \dots\dots(7.6.36)$$

By collecting all the terms, the diffusion Equation (7.6.1) can be approximated by the algebraic expression (7.6.37)

$$a_{SW}\Phi_{SW} + a_W\Phi_W + a_{NW}\Phi_{NW} + a_S\Phi_S + a_P\Phi_P + a_N\Phi_N + a_{SE}\Phi_{SE} + a_E\Phi_E + a_{NE}\Phi_{NE} = a^0{}_P\Phi_P^0$$
$$\dots\dots(7.6.37)$$

where

$$a_{SW} = a_{SW_1} + a_{SW_2} = -\frac{1}{4}\left(\frac{\mu_{os}}{\mu_o}\frac{\partial\hat{\xi}}{\partial\eta}\right)_s - \frac{1}{4}\left(\frac{\mu_{os}}{\mu_o}\frac{\partial\hat{\xi}}{\partial\eta}\right)_w \qquad\qquad \dots\dots(7.6.38)$$

$$a_W = a_{W_1} + a_{W_2} = \left\{\left(\frac{\mu_{os}}{\mu_o}\right)_w\left[1+\left(\frac{\partial\hat{\xi}}{\partial\eta}\right)^2\right]\frac{F(|P_w|)}{(\delta\xi)_w} + \left|-\beta\frac{\partial\hat{\xi}}{\partial\tau},0\right|\right\}\Delta\eta + \frac{1}{4}\left(\frac{\mu_{os}}{\mu_o}\frac{\partial\hat{\xi}}{\partial\eta}\right)_n - \frac{1}{4}\left(\frac{\mu_{os}}{\mu_o}\frac{\partial\hat{\xi}}{\partial\eta}\right)_s$$
$$\dots\dots(7.6.39)$$

$$a_{NW} = a_{NW_1} + a_{NW_2} = \frac{1}{4}\left(\frac{\mu_{os}}{\mu_o}\frac{\partial\hat{\xi}}{\partial\eta}\right)_n + \frac{1}{4}\left(\frac{\mu_{os}}{\mu_o}\frac{\partial\hat{\xi}}{\partial\eta}\right)_w \qquad\qquad \dots\dots(7.6.40)$$

$$a_S = a_{S_1} + a_{S_2} = \frac{\Delta\xi_P}{\Delta\eta}\left(\frac{\mu_{os}}{\mu_o}\right)_s + \frac{1}{4}\left(\frac{\mu_{os}}{\mu_o}\frac{\partial\hat{\xi}}{\partial\eta}\right)_e - \frac{1}{4}\left(\frac{\mu_{os}}{\mu_o}\frac{\partial\hat{\xi}}{\partial\eta}\right)_w \qquad\qquad \dots\dots(7.6.41)$$

$$a_N = a_{N_1} + a_{N_2} = \frac{\Delta\xi_P}{\Delta\eta}\left(\frac{\mu_{os}}{\mu_o}\right)_n + \frac{1}{4}\left(\frac{\mu_{os}}{\mu_o}\frac{\partial\hat{\xi}}{\partial\eta}\right)_w - \frac{1}{4}\left(\frac{\mu_{os}}{\mu_o}\frac{\partial\hat{\xi}}{\partial\eta}\right)_e \qquad\qquad \dots\dots(7.6.42)$$

$$a_{SE} = a_{SE_1} + a_{SE_2} = \frac{1}{4}\left(\frac{\mu_{os}}{\mu_o}\frac{\partial\hat{\xi}}{\partial\eta}\right)_s + \frac{1}{4}\left(\frac{\mu_{os}}{\mu_o}\frac{\partial\hat{\xi}}{\partial\eta}\right)_e \qquad\qquad \dots\dots(7.6.43)$$

148

$$a_E = a_{E_1} + a_{E_2} = \left\{ \left(\frac{\mu_{os}}{\mu_o} \right)_e \left[1 + \left(\frac{\partial \hat{\xi}}{\partial \eta} \right)^2 \right] \frac{F(|P_e|)}{(\delta \xi)_e} + \left| \beta \frac{\partial \hat{\xi}}{\partial \tau}, 0 \right| \right\} \Delta \eta + \frac{1}{4} \left(\frac{\mu_{os}}{\mu_o} \frac{\partial \hat{\xi}}{\partial \eta} \right)_s - \frac{1}{4} \left(\frac{\mu_{os}}{\mu_o} \frac{\partial \hat{\xi}}{\partial \eta} \right)_n$$

$$\ldots \ldots (7.6.44)$$

$$a_{NE} = a_{NE_1} + a_{NE_2} = -\frac{1}{4} \left(\frac{\mu_{os}}{\mu_o} \frac{\partial \hat{\xi}}{\partial \eta} \right)_n - \frac{1}{4} \left(\frac{\mu_{os}}{\mu_o} \frac{\partial \hat{\xi}}{\partial \eta} \right)_e \qquad \ldots \ldots (7.6.45)$$

$$a_P = a_{P_1} + a_{P_2} + a_{P_3} = -\left(a_{W_1} + a_{S_1} + a_{N_1} + a_{E_1} - a_P^0 \right) \qquad \ldots \ldots (7.6.46)$$

The mid-point viscosity ratios are approximated by the harmonic average of the neighbouring values as shown by Equation (7.6.47)

$$\frac{1}{\left(\frac{\mu_{os}}{\mu_o} \right)_n} = \frac{1}{2} \left[\frac{1}{\left(\frac{\mu_{os}}{\mu_o} \right)_N} + \frac{1}{\left(\frac{\mu_{os}}{\mu_o} \right)_P} \right] \qquad \ldots \ldots (7.6.47)$$

To approximate the shape-factor, Equations similar to those expressed as Equation (7.6.48) and (7.6.49) are used.

$$\left(\frac{\partial \hat{\xi}(\eta, \tau)}{\partial \eta} \right)_w = \left(\frac{\partial \hat{\xi}(\eta, \tau)}{\partial \eta} \right)_e = \left(\frac{\partial \hat{\xi}(\eta, \tau)}{\partial \eta} \right)_P \qquad \ldots \ldots (7.6.48)$$

$$\left(\frac{\partial \hat{\xi}(\eta, \tau)}{\partial \eta} \right)_n = \frac{\hat{\xi}(\eta, \tau) \big|_N - \hat{\xi}(\eta, \tau) \big|_P}{\Delta \eta} \qquad \ldots \ldots (7.6.49)$$

Equation (7.6.37) is written such that all of the terms at the left hand side including the central node and its eight neighbouring nodes are solved for simultaneously. The term at the right hand side of Equation (7.6.37) is from the previous time step. An implicit solution of all nine nodes, as in Equation (7.6.37), is necessary since the potential solution has a very small time scale in the regions close to the interface, and approaches the steady-state solution in a very short time. The algebraic Equation (7.6.37) is solved implicitly for all the nodes in order to avoid very small time steps or unstability problems. It was noted in Chapter 2, that most of the numerical models on non-orthogonal grids

149

handle the corner points at the previous time step as a source term at the right-hand side of Equation (7.6.37).

7.7 Boundary Conditions

Boundary conditions for the temperature and potential Equations (7.4.15) and (7.4.22) indicate second and first type boundary conditions for the horizontal and vertical boundaries in the computational domain, respectively. Here, the effect of heat loss from the horizontal boundaries as indicated in Equations (7.4.18) and (7.4.19), is neglected and a numerical model is developed for insulated conditions. Including the heat loss effects can be performed similarly.

The computational nodes are chosen on the vertical boundaries, and the faces of the boundary control volumes on the horizontal boundaries, as shown in Figures 7.3 and 7.4. This configuration ensures that both types of boundary conditions can be satisfied exactly. To satisfy the Drichlet conditions all of the coefficients of Equation (7.6.37) are simply forced to be zero except a_P and a_P^0 which are set equal to one. To satisfy the no-flow boundary conditions the total flux entering from the horizontal boundaries is forced to be zero [Demirdzic and Peric 1990]. For example at the lower boundary, Equations (7.6.2) and (7.6.14) are replaced by Equations (7.7.1) and (7.7.2), respectively.

$$\int_w^e \int_s^n \frac{\partial}{\partial \eta}\left[\frac{\mu_{os}}{\mu_o}\left(\frac{\partial \Phi}{\partial \eta}\right)\right] d\eta d\xi = \left\{\left[\frac{\mu_{os}}{\mu_o}\left(\frac{\partial \Phi}{\partial \eta}\right)\right]_n\right\}\Delta\xi_P = \left\{\left[\left(\frac{\mu_{os}}{\mu_o}\right)_n\left(\frac{\Phi_N - \Phi_P}{\Delta\eta}\right)\right]\right\}\Delta\xi_P \quad \ldots \ldots (7.7.1)$$

$$\int_w^e \int_s^n -\frac{\partial}{\partial \eta}\left[\frac{\mu_{os}}{\mu_o}\left(\frac{\partial \hat{\xi}}{\partial \eta}\frac{\partial \Phi}{\partial \xi}\right)\right] d\eta d\xi = e_n \qquad \ldots \ldots (7.7.2)$$

The above Equations will be used to evaluate the corresponding coefficients. The derivative-type boundary conditions do not affect Equations (7.6.7) and (7.6.34); however, Equation (7.6.24) will be modified as follows.

After performing the integration of (7.6.24) for a control volume adjacent to the lower boundary, the values of Φ_{sw} and Φ_{se} in Equations (7.6.25) and (7.6.26) are evaluated such that the southern nodes are not incorporated. It can be shown easily that by the application of the Neuman boundary condition one can write

150

$$\Phi_{sw} = \frac{1}{2}\left[1 + \frac{\Delta\eta}{\Delta\xi}\frac{\partial\hat{\xi}}{\partial\eta}\right]\Phi_W + \frac{1}{2}\left[1 - \frac{\Delta\eta}{\Delta\xi}\frac{\partial\hat{\xi}}{\partial\eta}\right]\Phi_P \qquad \dots\dots(7.7.3)$$

$$\Phi_{se} = \frac{1}{2}\left[1 + \frac{\Delta\eta}{\Delta\xi}\frac{\partial\hat{\xi}}{\partial\eta}\right]\Phi_P + \frac{1}{2}\left[1 - \frac{\Delta\eta}{\Delta\xi}\frac{\partial\hat{\xi}}{\partial\eta}\right]\Phi_E \qquad \dots\dots(7.7.4)$$

For an orthogonal system, that is, $\frac{\partial\hat{\xi}}{\partial\eta} = 0$, and on a no-flow boundary, Equation (7.7.3) simplifies to $\Phi_{sw} = \frac{1}{2}(\Phi_W + \Phi_P)$. It should be noted that Equations (7.7.3) and (7.7.4) are not valid if the aspect ratio of the boundary control volumes $\frac{\Delta\xi}{\Delta\eta}$ is above two and the non-orthogonality is more than 45 degrees. However, such distorted control volumes will not be considered, because in such cases there will large errors involved in the estimation of the fluxes. As a general rule calculations are not recommended on highly non-orthogonal coordinates.

7.8. Calculation of the Flow Rate and Flow-Paths

The solution of the two diffusion-convection equations of (7.4.15) and (7.4.22) results in a 2-D temperature and potential distribution in the formation. These profiles can be analyzed to study the process. In a thermal recovery project, however, the important parameter is the rate of oil production. The low compressibility of the oil, and its high viscosity, does not allow appreciable compression or flow in the cold region. Hence, the interface location is used to calculate the production rate by assuming that the displaced oil is produced.

In order to obtain a qualitative feel for the flow patterns ahead of the interface, a stream function Ψ can be defined which is related to the potential gradient by

$$\frac{\partial\Psi}{\partial X} = \frac{\mu_{os}}{\mu_o}\frac{\partial\Phi}{\partial Z} \qquad \dots\dots(7.8.1)$$

Bear [1972] pointed out that in an unsteady-state process: "we can speak of instantaneous pictures of streamlines as the picture varies continuously." He used the term "path-lines" as the corresponding term for unsteady-state processes. Here, the time-

dependency of the flow field is ignored, and Equation (7.8.1) is used to obtain a qualitative measure of the stream-lines ahead of the interface.

7.9. Anisotropic Effects

It is well known that the mathematical formulation of fluid flow through an anisotropic formation involves cross-diffusion terms. Should one be interested in modelling the SAGD process in such a formation, the corresponding cross-diffusion terms can be added to the existing ones in Equations (7.4.15) and (7.4.22). It should be noted that in the current formulation the coordinate lines change direction in time; hence, the contribution of the cross-diffusion terms due to the anisotropy changes with time.

8. RESULTS AND DISCUSSION – NUMERICAL MODEL

Development of a 2-D unsteady-state numerical model for the linear SAGD process was detailed in Chapter 7. The transient conservation equations of mass, momentum and energy for the oil phase were coupled ahead of a moving interface. An additional equation was derived for the first time that explicitly revealed the location of the steam-oil interface with time. The solution of the final system of nonlinear differential equations was then discussed. In this chapter, the numerical model or its components will be validated against the available literature. Analytical solutions will be used for comparison. Then the numerical model will be used to study the behaviour of the linear SAGD process. Before doing so the features of the 2-D SAGD model will be reviewed and the choices in the development of the model will be discussed.

8.1 Features of the Numerical SAGD Model

The development of thermal simulators for heavy oil recovery processes is not a recent event. Almost without any exception however, a fixed grid approach was chosen, and a stationary computational grid was superimposed on the physical domain. The nonlinear equations of transport were then solved for the whole domain. Different strategies were later suggested to increase the accuracy of the solution where field variables varied most rapidly [for a review see Aziz 1993]. The fine-gridding techniques were mostly developed for fixed locations in the reservoir, e.g., around the wellbore. A society of petroleum engineers comparative solution project on gridding techniques [Quandalla 1993] studied the fine-gridding techniques implemented by five major institution on petroleum reservoir simulation to study an oil recovery project. In all the cases static fine gridding techniques were used. Initial attempts have been made to use dynamic fine-gridding techniques using Cartesian grids [Biterge and Ertekin 1992], for such attempts however, questions of accuracy and computer efficiency have yet to be resolved [Aziz 1993].

Most of the EOR methods are designed based on the development of an oil bank ahead of a displacing phase with sharp interfaces. In such cases, and in many other examples of multiphase flow through porous media, sharp interfaces occur; however, capillary forces tend to smear them out. It is believed that it is due to the effect of these forces, and to heterogeneity effects under field conditions, that researchers have chosen a stationary grid approach, and no additional equation for following the location of the

153

interface has been used. In contrast to the comprehensive reservoir simulators which use an Eulerian approach, numerous simpler models have been developed that emphasize the modelling of a front. Buckley and Leverett [1942] found that the problem of two-phase flow in porous media under pressure forces can be explained by a first order hyperbolic equation. This study suggested that the process of two phase flow exhibits a frontal behaviour if capillary forces are neglected. Bentsen [1978] studied the conditions under which capillary forces may be neglected, and showed that if capillary forces are included a second order parabolic equation is obtained. He showed that a frontal behaviour will be observed, if the capillary term is small. The Buckley-Leverett method was later extended to model three phase flow in porous media including temperature variations [Wingard and Orr 1994].

The Steam-Assisted Gravity Drainage process is one of those processes that might permit a sharp interface assumption. This is the case because firstly, the SAGD process is normally implemented in high permeability reservoirs where capillary forces are small, and secondly there are minimal pressure forces across the steam-oil interface to drive the steam condensate ahead of the interface and extend the two-phase region. Based on the above arguments, a transformed gridding method was chosen to take advantage of the special properties of this technique and study the SAGD process. To the best of the author's knowledge this is the first numerical model for predicting the behaviour of a thermal recovery project by satisfying the transient conservation laws ahead of an explicitly defined steam-oil interface. Steady-state models were previously reviewed [Butler at al. 1981, Palmgren et al. 1989, 1990].

In order to solve accurately the conservation laws ahead of the interface a simple algebraic transformation was used to immobilize the interface. An algebraic transformation was preferred over a numerically generated coordinate system, because solution of the partial differential equations to perform the latter transformation might become computationally too expensive to be performed at each time step. A recent article by Sharp and Anderson [1993] used the numerical approach to impose a nearly orthogonal computational grid over an irregularly shaped reservoir. In such cases where the computational domain needs to be generated only once, the numerical approach is generally preferred.

A simple transformation was chosen to avoid many difficulties that might occur with the application of more complicated transformation functions. Hindman [1982]

154

showed that for some complicated transformations the solutions became unstable, unless specific conditions were satisfied. By using a simple transformation a single equation in the transformed domain was obtained if either the chain rule or the strong conservation law forms of Hindman [1982] were applied. Additionally the Jacobian of the transformation is independent of time, and the geometric conservation law (GCL) is naturally satisfied [Thomas and Lombard 1979]. Demirdzic and Peric [1988] showed that if the transformed grids move along one coordinate line only, the GCL is satisfied always. Using the present transformation, the control volumes in the transformed domain do not change in shape, but travel along one of the coordinate lines only. Most importantly, the application of the transformation enables one to locate the interface position so that fine-gridding is possible in the vicinity of the interface where the temperature gradients are the highest, and high accuracy is required for estimation of potential gradient to model accurately the interface behaviour (see Equation 7.4.29). In order to keep the computational time to a minimum, the grid spacing is increased away from the interface where less accuracy is required.

A finite volume technique rather than a finite element one was selected, due to personal preference and to the lack of popularity of the latter in the petroleum literature. A discretization based on the finite volume approximation ensured global conservation and lack of error on the boundaries of the domain, as compared to a traditional finite difference approximation [Thomas and Lombard 1979]. The boundary nodes were selected on the boundaries where Drichlet conditions were specified. On the derivative type boundaries, however, the faces of the boundary control volumes formed the boundaries of the domain. These configurations were chosen so that both of the boundary conditions could be satisfied exactly on application of the control volume approach.

It was pointed out previously that the time scales of the fluid and heat flow processes differ by about 6 orders of magnitude. In order to avoid instabilities the simultaneous node movement technique was preferred over the periodic and alternate node movement methods. For the same reason, the system of linear equations obtained from discretization of the conservation equations are solved directly considering all the field values implicitly. A sequential method of solution was chosen to solve the three equations and an "outer iteration" was used to achieve convergence. Other methods such as simultaneous solution of the three nonlinear equations and a Newton-Raphson technique, which are computationally more intensive, were not found necessary.

155

8.2. Validation of the 2-D Numerical SAGD Model

In this section, the accuracy and validity of the numerical model developed in Chapter 7 will be examined. Simple tests will be performed first, and the complexity of the test problems will be increased step by step.

8.2.1. 1-D Heat Conduction Ahead of a Constant Velocity Moving Interface in a Semi-Infinite Medium

The energy conservation equation on the transformed domain was formulated as Equation (7.4.15). In a one-dimensional domain Equation (7.4.15) simplifies to the differential equation of heat conduction ahead of a moving interface, Equation (8.2.1.1)

$$\frac{\partial}{\partial \xi}\left(\frac{\partial \theta}{\partial \xi} + N_{P_e}\theta\right) = \frac{\partial \theta}{\partial \tau} \qquad \ldots\ldots (8.2.1.1)$$

The analytical solution of Equation (8.2.1.1) for a constant frontal velocity and initial and boundary conditions expressed as Equation (7.4.17), (7.4.20) and (7.4.21) can be written as [Carslaw and Jaeger 1959]

$$\theta = \frac{1}{2}\left[\mathrm{erfc}\left(\frac{\xi + N_{P_e}\tau}{2\sqrt{\tau}}\right) + e^{-N_{r_e}\xi} \times \mathrm{erfc}\left(\frac{\xi - N_{P_e}\tau}{2\sqrt{\tau}}\right)\right] \qquad \ldots\ldots (8.2.1.2)$$

Figure 8.1 shows the accuracy of the numerical solution as compared with the analytical solution, obtained from Equation (8.2.1.2). To examine the incorporation of the boundary condition a 2-D test was performed on an orthogonal grid with Equations (7.4.15) and (7.4.17) to (7.4.21). The top and bottom boundary conditions of Equations (7.4.18) and (7.4.19) were replaced by insulated conditions such that a 1-D case is represented. A Peclet No. of 1 was chosen. In a semi-infinite medium any arbitrary length can be chosen to introduce the dimensionless quantities. However, if the height of formation is chosen as before a dimensionless time of one in Figure 8.1 corresponds to about 12 years for a 20 m thick formation.
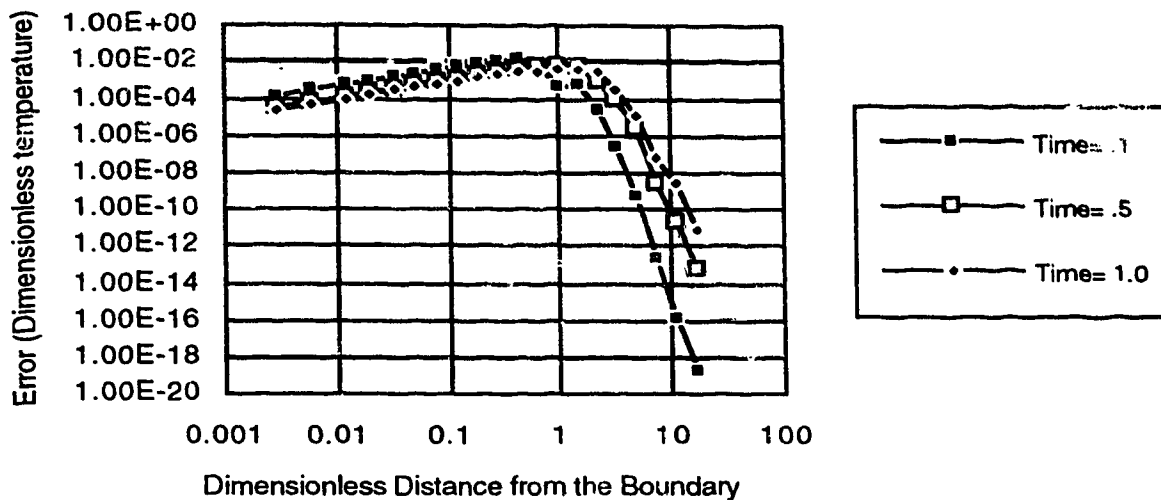
156

Figure 8.1 Error estimation (1-D moving boundary semi-infinite case)

Figure 8.1 indicates that The error is about 0.01% in the vicinity of the interface, and it increases to about 1% at a dimensionless distance of about 1, and then rapidly decreases farther from the interface. In the above example the grid size increased by multiples of 1.5, starting from an initial value of 0.005. Twenty grid blocks were selected and a time step equal to 0.005 was used. The fact that the error is increasing farther from the interface indicates that the rate by which the grid blocks sizes are increasing is greater than the accuracy requirement of the equation. This is especially true at earlier time when the gradients are larger. It was not attempted to improve upon this as the same method is used in the SAGD numerical model, and the accuracy adjacent to the interface is high. For modelling a semi-infinite case a finite medium was considered; however, it was chosen large enough such that the effect of the far boundary on the solution is negligible.

8.2.2. 2-D heat Conduction in a Square

After examining the accuracy of the numerical model for a 1-D problem, a similar study for a 2-D geometry is performed. Again a problem with an analytical solution is chosen.

157

Consider a square initially at zero temperature, which is exposed to a boundary condition in the form of a step function from all four sides. Considering an element of symmetry, the problem can be formulated using dimensionless variables as Equations (8.2.2.1) to (8.2.2.6).

$$\frac{\partial}{\partial \xi}\left(\frac{\partial \theta}{\partial \xi}\right) + \frac{\partial}{\partial \eta}\left(\frac{\partial \theta}{\partial \eta}\right) = \frac{\partial \theta}{\partial \tau} \qquad \dots \dots (8.2.2.1)$$

$\theta = 0$	$0 \le \xi \le 1$	$0 \le \eta \le 1$	$\tau = 0 \quad \dots\dots (8.2.2.2)$
$\theta = 1$	$\xi = 0$	$0 \le \eta \le 1$	$\tau > 0 \quad \dots\dots (8.2.2.3)$
$\frac{\partial \theta}{\partial \xi} = 0$	$\xi = 1$	$0 \le \eta \le 1$	$\tau > 0 \quad \dots\dots (8.2.2.4)$
$\theta = 1$	$0 \le \xi \le 1$	$\eta = 0$	$\tau > 0 \quad \dots\dots (8.2.2.5)$
$\frac{\partial \theta}{\partial \eta} = 0$	$0 \le \xi \le 1$	$\eta = 1$	$\tau > 0 \quad \dots\dots (8.2.2.6)$

The analytical solution for the above problem can be found by separation of variables, or by multiplying two 1-D solutions similar to that found in Appendix A.

$$\theta = 1 - \frac{16}{\pi^2} \sum_{m=1}^{\infty} \sum_{n=1}^{\infty} \frac{\sin\left(\frac{(2n-1)\pi}{2}\xi\right)}{2n-1} \frac{\sin\left(\frac{(2m-1)\pi}{2}\eta\right)}{2m-1} \exp\left\{-\left[\left(\frac{2n-1}{2}\right)^2 + \left(\frac{2m-1}{2}\right)^2\right]\pi^2\tau\right\}$$

$$\dots\dots (8.2.2.7)$$

The above problem was solved using a numerical code similar to what is used for solving the conservation laws in the 2-D numerical SAGD model. Figure 8.2 shows the error of the numerical model at $\xi = 0.5$ and $\eta = 0.5$.

A base case was run using 10 grid blocks in each direction and a dimensionless time step of 0.005 was chosen. Figure 8.2 indicates that a maximum error of about 2% occurs at early times, which then decreases as the system approaches the steady-state conditions. A limited sensitivity study indicated that the error could be significantly reduced using smaller time steps. Increasing the number of grid blocks did not improve the accuracy, suggesting that the time truncation error was dominant. Nevertheless,

158

Figure 8.2 indicates very good accuracy after early times for all the cases studied. In all of the calculations a constant block size was chosen.
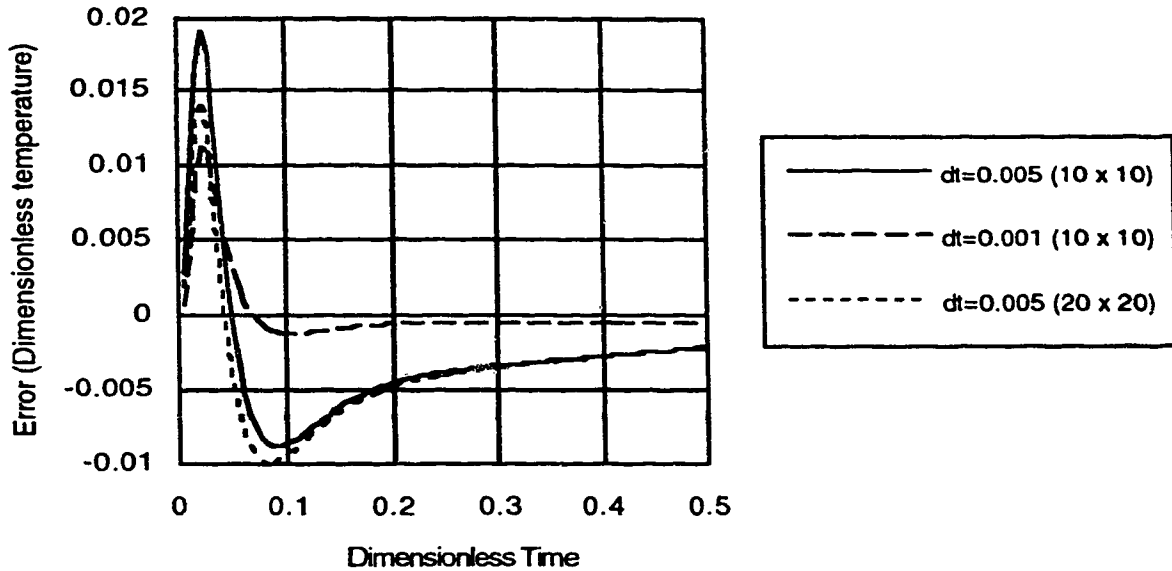

Figure 8.2 Error estimation at x=0.5,
z=0.5 (2-D conduction)

8.2.3. 2-D Heat Conduction in a Parallelepiped

Some of the articles discussing the incorporation of the cross-diffusion terms that are the result of non-orthogonality of a computational coordinate system were reviewed in Chapter 2. In this section it is intended to examine the accuracy of the numerical code in predicting diffusive flow using non-orthogonal grids.

Figure 8.3 shows a parallelepiped cut into a rectangle. Solution of the heat conduction problem in a rectangle can be obtained using an analytical solution similar to that of Section 8.2.2. All four boundaries of the rectangle are kept at $\theta = 1$. The analytical solution is used to obtain the temperature on AB and CD in Figure 8.3. This will serve as the time-dependent boundary condition for the heat conduction problem in the parallelepiped ABCD. The solutions as obtained from the numerical code on EF is compared with the analytical values obtained at the same location.
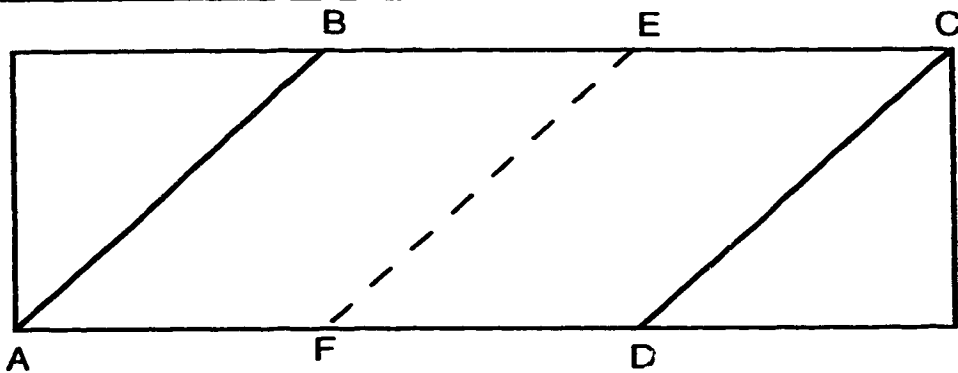
159

Figure 8.3 A parallelepiped in a rectangle

Figure 8.4 shows the error of the calculations using 20 grid blocks along the horizontal axis and 10 along the vertical one. A dimensionless time step of 0.005 was chosen for the calculations in Figure 8.4.
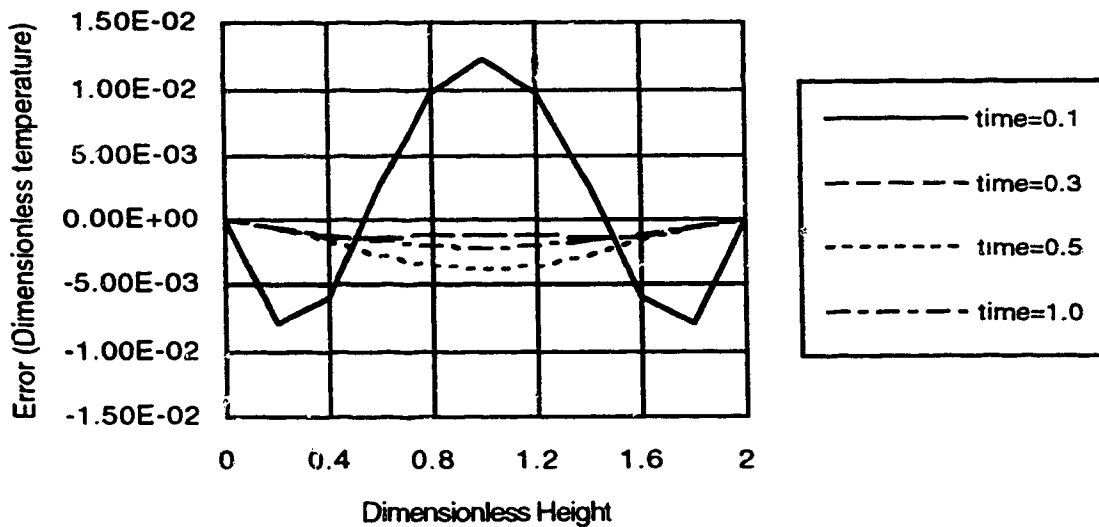

Figure 8.4 Error estimation on EF of
Figure 8.3 (20 x 10, dt=0.005)

Figure 8.4 indicates a maximum error of about 1% of the boundary temperature at early times. Figure 8.5 shows the same comparison increasing the number of grid blocks by a factor of two. It seems that the error at early times has decreased by a factor of two. In other words reducing the size of the grid blocks by half reduced the error by half when the gradients are steeper. However, the late-time error has not changed significantly. This might suggest that the dominant error is that related to time truncation error. To examine this the time step size was decreased by a factor of five.
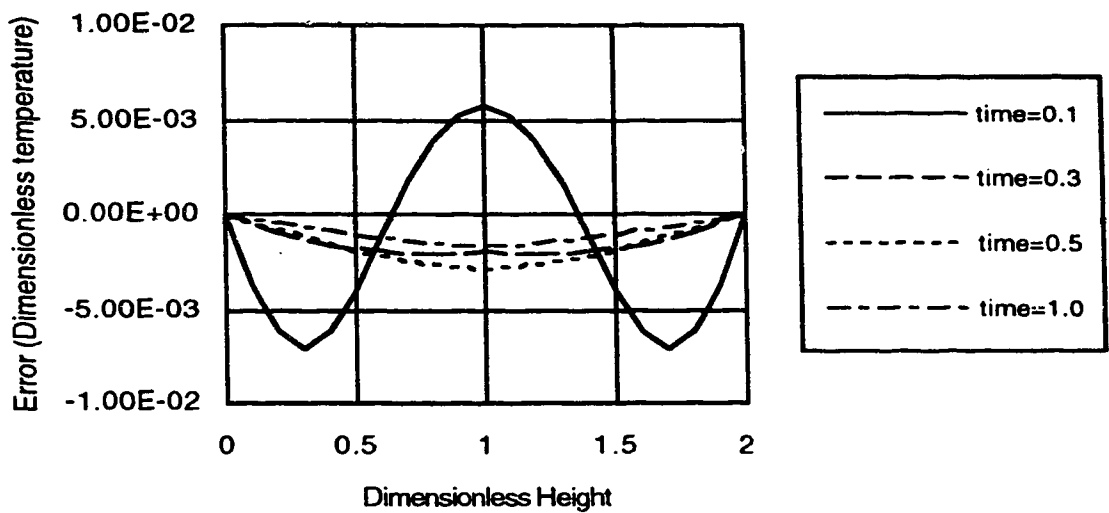

Figure 8.5 Error estimation on EF of
Figure 8.3 (40 x 20, dt=0.005)

Figure 8.6 shows the error for a dimensionless time step of 0.001. A close look at the results indicated that the average error decreased by a factor of 3, 8, 4, and 4, for dimensionless time equal to 0.1, 0.3, 0.5, and 1.0, respectively. In other words decreasing the time step size by a factor of five decreased the error by the same order. This is in agreement with the time truncation error in the present formulation which is of the order of one.
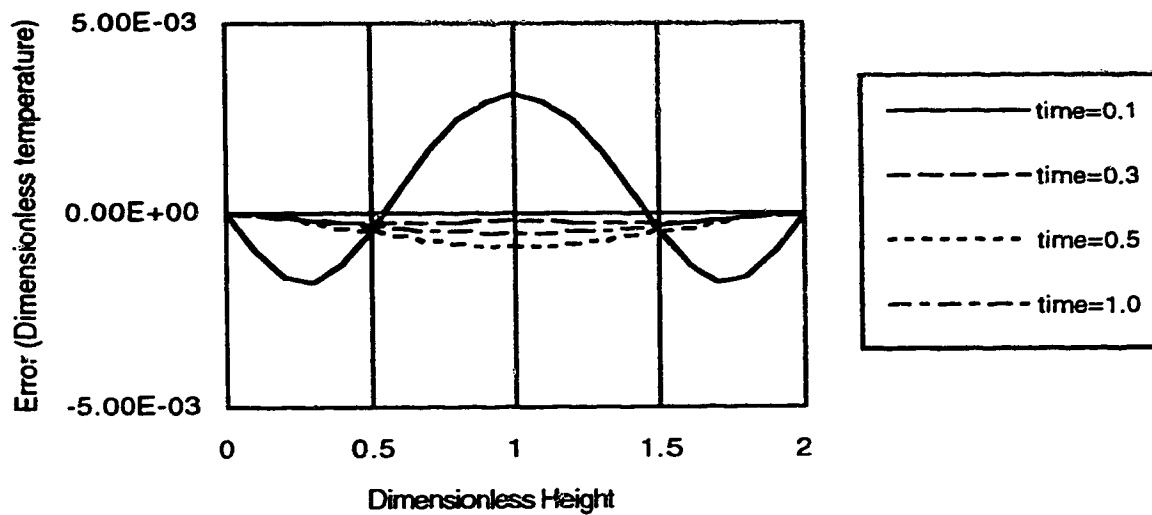
Figure 8.6 Error estimation on EF of Figure 8.3
(40 x 20, dt=0.001)

8.2.4 Fluid Flow Ahead of a Moving Boundary

In Sections 8.2.1 to 8.2.3 solutions of the conservation laws were tested on different geometries. In all of the cases examined the flow occurred on a domain with stationary boundaries, and the equations were linear. In this section an analytical solution is developed for a nonlinear 1-D moving boundary problem in a semi-infinite domain. The accuracy of the numerical model will then be studied using the analytical results.

8.2.4.1 An Analytical Solution for Gas Injection in a Semi-Infinite Medium

Consider a semi-infinite linear porous medium saturated with oil. An inviscid gas is injected at a constant pressure into the porous medium which drives the oil down stream. A sharp interface is considered between the oil and gas regions. The pressure at the front is equal to the injection pressure, since the viscosity of the gas is neglected. The pressure distribution in the oil phase can be expressed by a diffusivity equation similar to Equation (7.2.11)

$$\frac{\partial}{\partial x}\left(\frac{\partial P}{\partial x}\right) = \frac{\phi \mu_o c}{k}\frac{\partial P}{\partial t} \qquad x \geq \hat{x}(t) \qquad \ldots (8.2.4.1.1)$$

162

The initial and boundary conditions of the problem can be expressed as

$$P = P_R \qquad\qquad x \geq 0 \qquad t = 0 \quad \ldots (8.2.4.1.2)$$

$$P = P_F \qquad\qquad x = \hat{x}(t) \qquad t > 0 \quad \ldots (8.2.4.1.3)$$

$$P = P_R \qquad\qquad x \to \infty \qquad t > 0 \quad \ldots (8.2.4.1.4)$$

where $x = \hat{x}(t)$ is the gas-oil interface location, and P_F is the gas pressure at the front which is equal to the injection pressure. The statement of constant pressure at the interface, Equation (8.2.4.1.3), is used in order to obtain an equation for the interface location,

$$\frac{DP}{Dt} = \frac{\partial P}{\partial t} + \bar{U}.\nabla P = 0 \qquad\qquad x = \hat{x}(t) \qquad\qquad \ldots (8.2.4.1.5)$$

where $\bar{U}$ the interface velocity is related to Darcy's law, that is, potential gradient by Equation (8.2.4.1.6)

$$\bar{U} = -\frac{1}{\phi \Delta S_o}\frac{k}{\mu_o}\nabla P \qquad\qquad \ldots (8.2.4.1.6)$$

By substituting Equation (8.2.4.1.6) into Equation (8.2.4.1.5) one can obtain

$$\frac{\partial P}{\partial t} = \frac{k}{\phi \mu_o \Delta S_o}\left(\frac{\partial P}{\partial x}\right)^2 \qquad\qquad \ldots (8.2.4.1.7)$$

By differentiating Equation (8.2.4.1.3) with respect to time one can obtain

$$\frac{\partial P}{\partial t} + \frac{\partial P}{\partial x}\frac{\partial \hat{x}}{\partial t} = 0 \qquad\qquad x = \hat{x}(t) \qquad\qquad \ldots (8.2.4.1.8)$$

Substituting from Equation (8.2.4.1.8) into Equation (8.2.4.1.7) and noting that $\frac{\partial P}{\partial x} \neq 0$ one obtains

$$\frac{\partial \hat{x}}{\partial t} = -\frac{k}{\phi \mu_o \Delta S_o}\frac{\partial P}{\partial x} \qquad\qquad \ldots (8.2.4.1.9)$$

163

Equation (8.2.4.1.9) is the one-dimensional version of the interface Equation (7.3.8), and its initial condition can be expressed as

$$\hat{x}(t) = 0 \qquad\qquad t = 0 \qquad ...(8.2.4.1.10)$$

Equations (8.2.4.1.1) to (8.2.4.1.4) with the interface Equation (8.2.4.1.9) and its initial condition (8.2.4.1.10) constitute the 1-D problem of interest. To solve the above problem the similarity solution method in diffusion problems is used. Before doing so, the following dimensionless variables and parameters are defined.

$$\Pi = \frac{P - P_R}{P_F - P_R} \qquad\qquad ...(8.2.4.1.11)$$

$$\tau = \frac{kt}{\phi\mu_o c(1)^2} \qquad\qquad ...(8.2.4.1.12)$$

$$X = \frac{x}{1} \qquad\qquad ...(8.2.4.1.13)$$

$$\gamma = \frac{c(P_F - P_R)}{\phi s} \qquad\qquad ...(8.2.4.1.14)$$

Using the above dimensionless quantities the 1-D problem can be expressed as Equations (8.2.4.1.16) to (8.2.4.1.20)

$$\frac{\partial}{\partial X}\left(\frac{\partial \Pi}{\partial X}\right) = \frac{\partial \Pi}{\partial \tau} \qquad\qquad X \geq \hat{X}(\tau) \qquad\qquad ...(8.2.4.1.15)$$

$$\Pi = 0 \qquad\qquad X \geq 0 \qquad\qquad \tau = 0 \qquad ...(8.2.4.1.16)$$

$$\Pi = 1 \qquad\qquad X = \hat{X}(\tau) \qquad\qquad \tau > 0 \qquad ...(8.2.4.1.17)$$

$$\Pi = 0 \qquad\qquad X \to \infty \qquad\qquad \tau > 0 \qquad ...(8.2.4.1.18)$$

$$\frac{\partial \hat{X}}{\partial \tau} = -\gamma \frac{\partial \Pi}{\partial X} \qquad\qquad ...(8.2.4.1.19)$$

$$\hat{X}(\tau) = 0 \qquad\qquad \tau = 0 \qquad ...(8.2.4.1.20)$$

164

A solution to Equations (8.2.4.1.15) and (8.2.4.1.18) can be expressed as

$$\Pi = A\mathrm{erfc}\left(\frac{X}{2\sqrt{\tau}}\right)$$ ...(8.2.4.1.21)

By applying Equation (8.2.4.1.21) to Equation (8.2.4.1.17) one can obtain

$$1 = A\mathrm{erfc}\left(\frac{\hat{X}}{2\sqrt{\tau}}\right)$$ ...(8.2.4.1.22)

Equation (8.2.4.1.22) can be an identity only if the argument of the complementary error function is a constant, that is,

$$\hat{X}(\tau) = 2\lambda\sqrt{\tau}$$ ...(8.2.4.1.23)

where λ is a constant, and the multiplier 2 is introduced for later convenience. The initial condition (8.2.4.1.20) is satisfied by the interface Equation (8.2.4.1.23). Solving from Equations (8.2.4.1.22) and (8.2.4.1.23) for A and substituting in Equation (8.2.4.1.21), one obtains

$$\Pi = \frac{\mathrm{erfc}\left(\frac{X}{2\sqrt{\tau}}\right)}{\mathrm{erfc}(\lambda)}$$ ...(8.2.4.1.24)

By differentiating Equations (8.2.4.1.23) and (8.2.4.1.24) and substituting in the interface Equation (8.2.4.1.19) one obtains

$$\frac{\gamma}{\sqrt{\pi}} = \lambda\; \cdots \; 1)\exp\left(\lambda^2\right)$$ ...(8.2.4.1.25)

The constant λ can be obtained by solving Equation (8.2.4.1.25) for any specific value of γ, and then can be substituted in Equations (8.2.4.1.23) and (8.2.4.1.24) to obtain the interface location and pressure distribution in the oil phase, respectively.

The 1-D moving boundary problem as formulated above is analogous to the ablation problem, where a constant temperature melting front propagates through a semi-

165

infinite solid which was initially at a temperature below the melting temperature. In the ablation problem the melt is removed immediately after formation. To the best of the author's knowledge this concept is used here for the first time to model a single phase moving boundary flow problem through porous media.

Development of the above 1-D model mostly is of academic interest only. This is because, in the above problem, oil is not produced from the porous medium, but is compressed in the semi-finite formation. The analytical solution, however, can be used to examine the accuracy of the numerical models developed for some moving boundary problems. This is done in the following section.

8.2.4.2. Accuracy of the Numerical Model vs. the Analytical Solution (1-D Moving Boundary Problem)

The 1-D moving boundary problem discussed above, i.e., Equations (8.2.4.1.15) to (8.2.4.1.20), describes the one-dimensional version of the problem investigated in Chapter 7, neglecting the temperature effects. Hence, it can serve as an ideal model to examine the nonlinear coupling of the potential distribution in the formation with the interface velocity. Figure 8.7 shows the interface location for a typical value of $\gamma = 0.001$[11] as obtained by the analytical and numerical models.

Figure 8.7 indicates a very close match between the two models. Using the interface location as obtained from the numerical model, the value of λ is back calculated from Equation (4.2.4.1.23). The numerical results started from $\lambda = 56.8 \times 10^{-5}$ and leveled off very quickly at a value of $\lambda = 57.0 \times 10^{-5}$. The value of λ using the analytical solution, i.e., Equation (8.2.4.1.25), was $\lambda = 56.45 \times 10^{-5}$, which indicates less than 1% error in the numerical results.

For the numerical calculations 40 grid points were used, which were distributed similar to the previous semi-infinite case in Section 8.2.1, and a dimensionless time step of 0.1 was used.

---

[11]   A compressibility of about 10^{-6} vol./vol./kPa, and a differential pressure of about 10^3 kPa were considered.
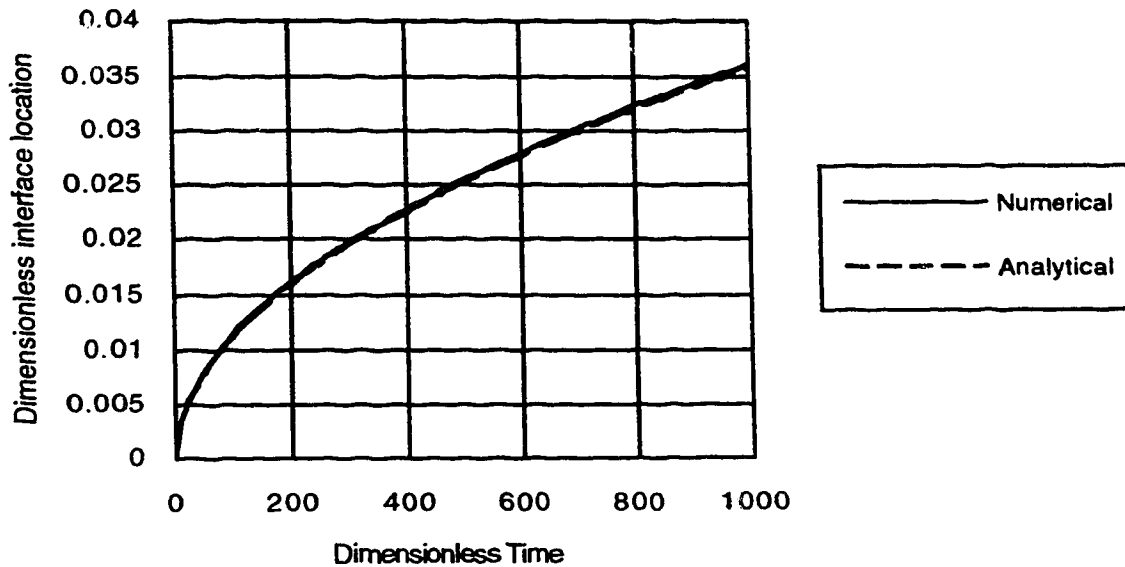
Figure 8.7 Interface location – analytical vs.
numerical results (1-D moving boundary)

8.3. Mechanistic and Case Studies

The accuracy of the 2-D SAGD numerical model was examined in Section 8.2 by predicting the behaviour of different phenomena involved in the SAGD process. It was shown that the conservation laws were accurately modelled in the 1-D and 2-D geometries. Application of the orthogonal and non-orthogonal grids was tested. A 1-D nonlinear problem was also studied, where the conservation law was satisfied ahead of a moving boundary. The velocity of the moving boundary was found as a part of the solution. Comparison with analytical solutions indicated that in all the cases studied, the magnitude of the error was about 1% or less. Having obtained confidence in the accuracy of the numerical model, in this section it is intended to study the SAGD process.

8.3.1. A Case Study

The experimental studies of the SAGD process [Chung and Butler 1988-a, 1988-b] were modelled in Section 6.2 using the 1-D SAGD model. Here, the same experimental data are used in the 2-D numerical model. The production well is explicitly

167

incorporated by assigning a constant potential to the boundary nodes representing the well. Three nodes were needed to represent the well radius.

Figure 8.8 shows the production rate and Figure 8.9 presents the interface location at one hour intervals, as obtained from the numerical model. Twenty grid blocks were used in the vertical direction, and 40 in the horizontal one. The latter were variably spaced to represent the semi-infinite medium, and also to obtain high accuracy close to the interface. A total length of above 50,000 dimensionless units was covered by using 40 control volumes in the horizontal direction. Two features are notable from Figures 8.8 and 8.9. The small oscillations in Figure 8.8 are believed to be due to numerical effects.
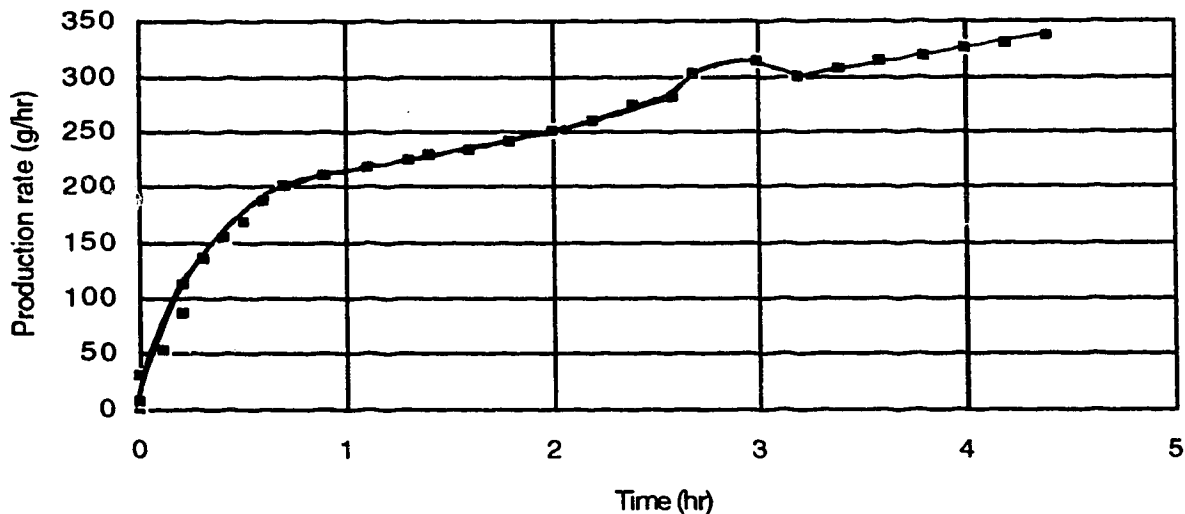

Figure 8.8. Production rate obtained from the 2-D numerical SAGD model

The production rate as predicted by the 2-D numerical model is somewhat higher than that obtained from the 1-D semi-analytical model (see Figure 6.8)[12]. A study of Figure 8.9 indicates that the steam-oil interface separates almost completely from the vertical axis, regardless of the fact that the lowest node is kept at the origin. This causes a large non-orthogonality for the boundary control volumes which in turn reduces the accuracy of the calculation. The large error can accelerate the separation of the interface even further. It was thought that if the accuracy of the calculation of the non-

---

12   The predictions of the 1-D semi-analytical model were in good agreement with those obtained from the experiments of Chung and Butler [1988-b].

168

orthogonality coefficient, the derivative of the interface location, is increased better results may be obtained. An exponential spline was used to fit the interface location using the discrete data at every time step. The exponential spline was preferred over the cubic one, because the latter can exhibit extraneous inflection points, wiggles [Rentrop 1980, McCartin 1983]. Application of the exponential spline, however, did not change the results. An attempt was made to decrease the effect of the discretized boundary condition on the results, by increasing the number of the grid blocks in the vertical direction. Forty and then fifty grid blocks were used, but the same behaviour was observed as before.
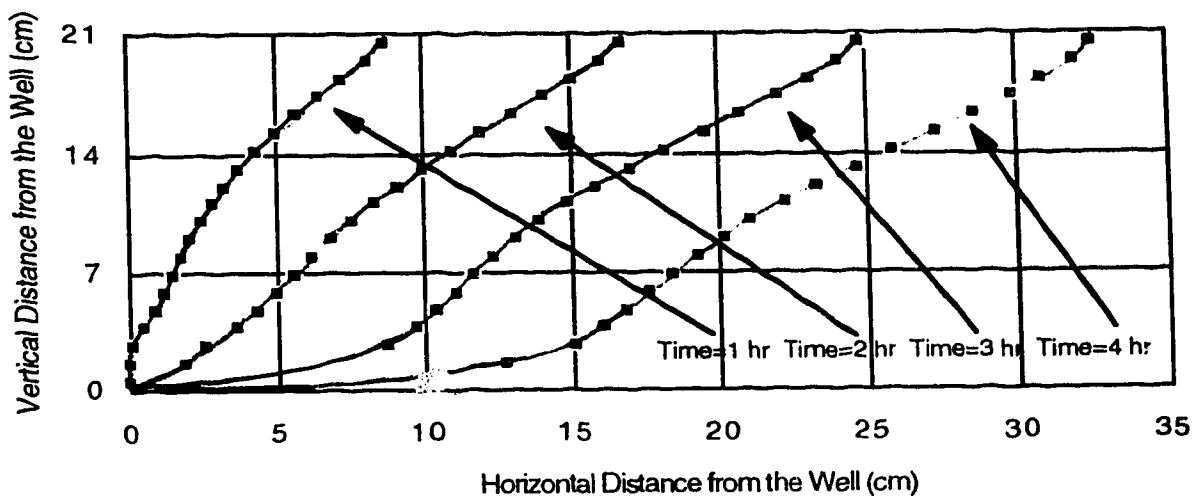

Figure 8.9. Interface location obtained from the 2-D numerical SAGD model

.evere separation of the interface at the lower part of the interface creates a very hig .... orthogonality, resulting in low calculation accuracy, as explained before. Figure 8.10 and 8.11 show the 2-D temperature and potential distribution ahead of the interface at one and three hours, respectively. It can be observed that at early time the iso-temperature and iso-potential lines are perpendicular to the upper and lower boundaries indicating accurate representation of the no-flow boundaries. Figure 8.11, however, indicates that at a later time when the coordinate lines at the lower boundary are highly non-orthogonal a large error in calculation has occurred. Figures 8.10 and 8.11 show also the streamlines. Their significance will be discussed later.

Temperature Distribution (1 hr)
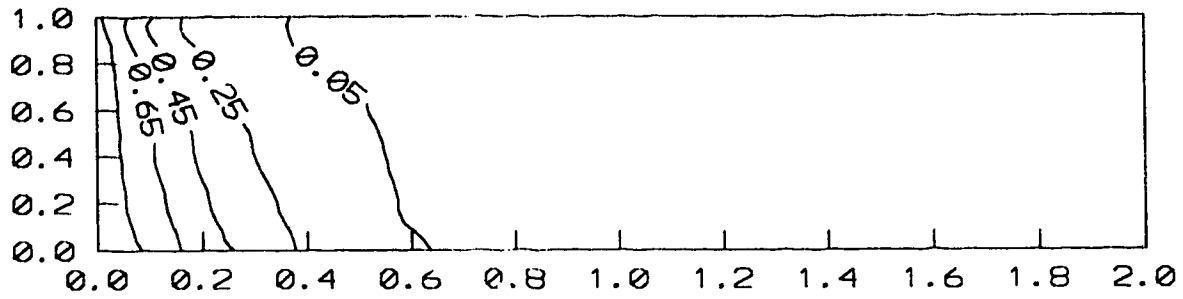
Potential Distribution (1 hr)
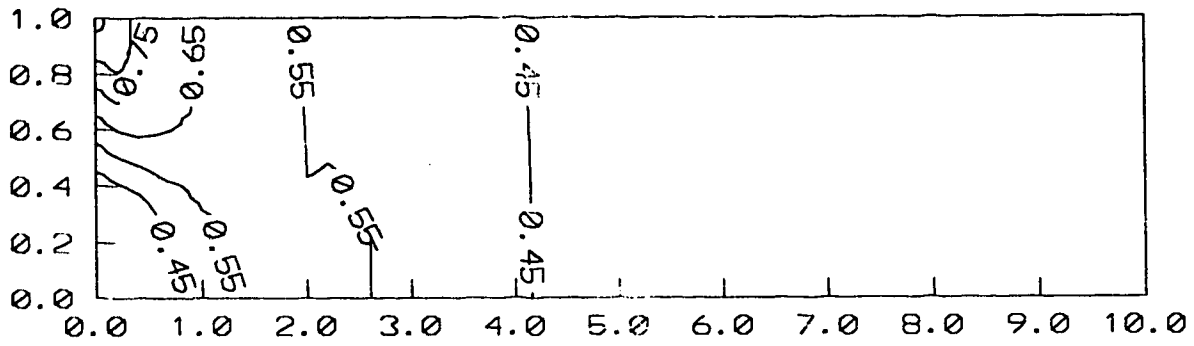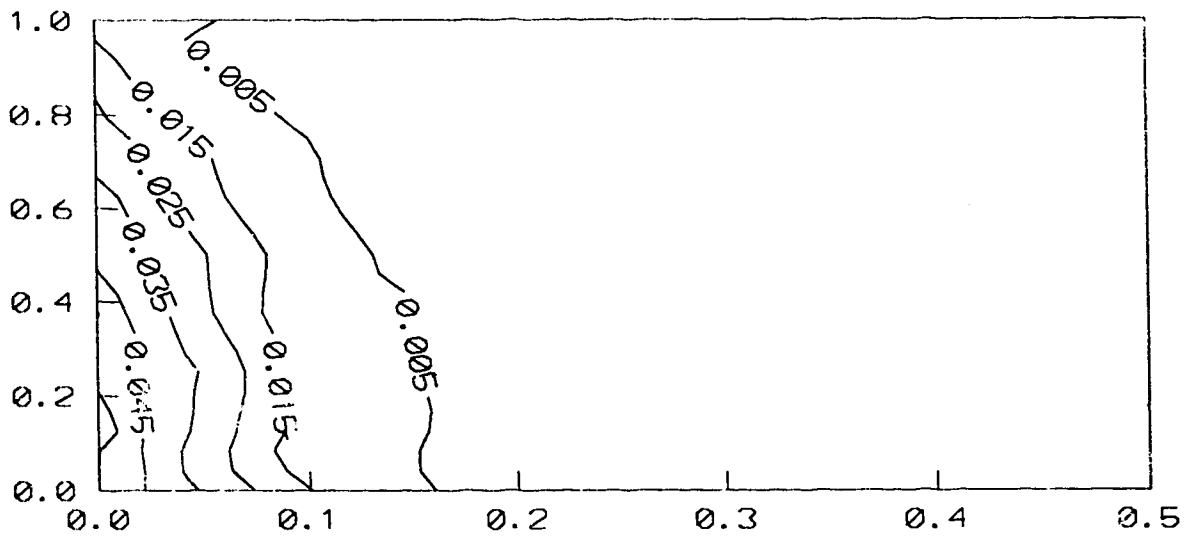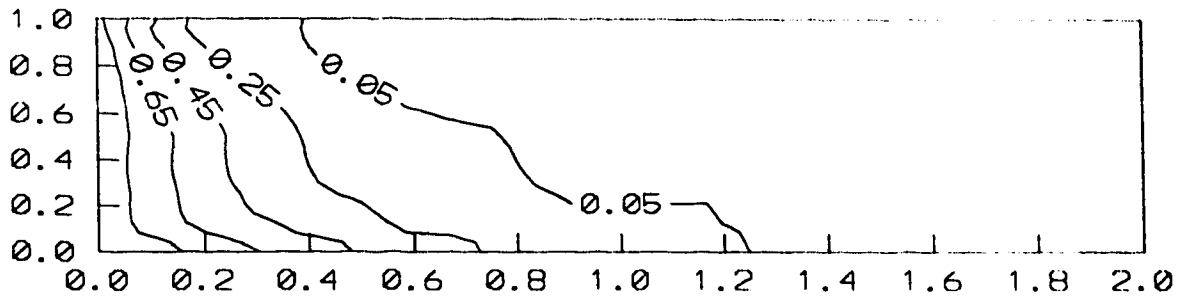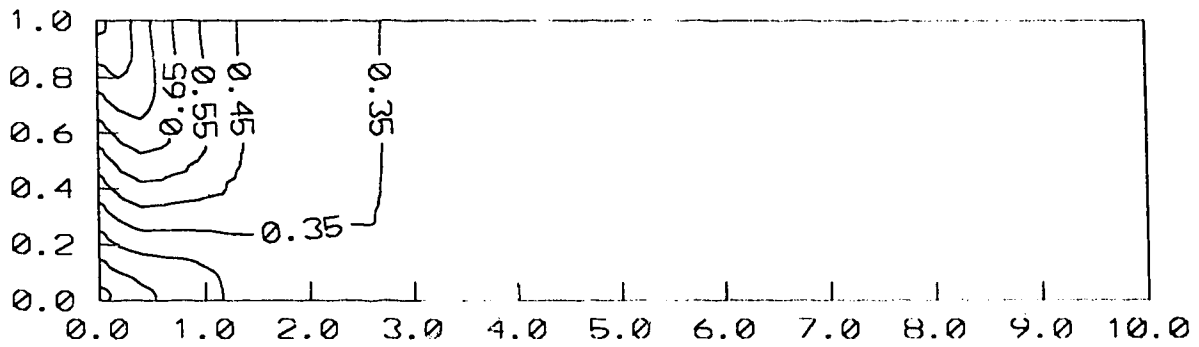
Streamlines (1 hr)

Figure 8.1C   Temperature and potential distribution and streamlines ahead of the interface
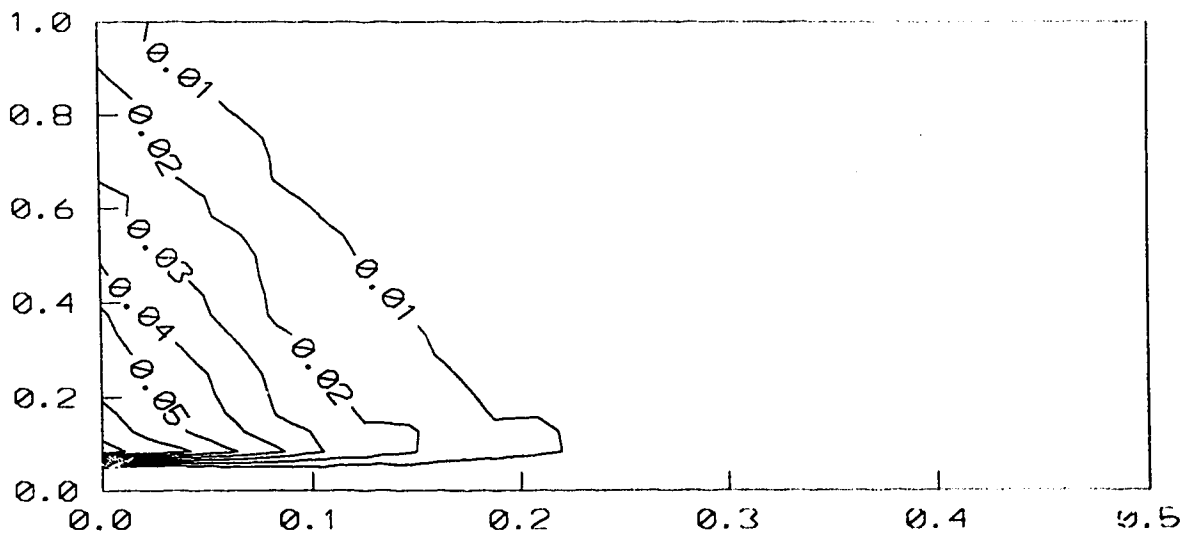(1 hr)

170

Figure 8.11   Temperature and potential distribution and streamlines ahead of the interface
(3 hrs)

The sharp edges and wiggles observed in the 2-D profiles shown in the previous and following pages are believed to be due to interpolation used by the contouring program used. In examining the 2-D profiles, one should note that the horizontal scale of temperature, potential, and streamline distributions are 10, 2, and 0.5 dimensionless units, respectively.

It was noted previously that in the present formulation the multiphase flow phenomena and the capillary forces were neglected. It is interesting to note that capillary forces play a stronger role at the lower part of the steam-oil interface where the threshold height is approached. To alleviate the limitations observed in the application of the numerical model, a transformation which ensures a low degree of non-orthogonality is suggested. This is not, however, included in the present work.

8.3.2. A Time Scale Study

The SAGD process, as formulated in Chapter 7, exhibits three different time scales. The characteristic time for heat conduction, $\frac{H^2}{\alpha}$, can be thought of as the operational time of a thermal recovery process. For a typical bituminous reservoir of Alberta with the physical properties of Table 8.1, a dimensionless time of one corresponds to about 12 years. The characteristic time for heat conduction was selected as the basis since it corresponds to a reasonable project time.

Table 8.1
Rock and Fluid properties of typical bituminous reservoir or Alberta

Permeability k	1×10^{-12} m^2
Formation height H	20 m
Porosity × Saturation change $\phi \Delta S_o$	0.35×0.37
Density difference $\Delta \rho$	1000 kg/m^3
Thermal diffusivity α	1×10^{-6} m^2/s
Formation compressibility c	1×10^{-9} 1/Pa
Oil viscosity at steam temperature μ_{os}	10×10^{-3} Pa s

172

The potential distribution for a low viscosity, slightly compressible fluid exhibits a very small characteristic time. The ratio of the characteristic time of the potential distribution to that of heat conduction was previously defined by Equation (7.2.39), $\beta = \frac{\phi\mu_{os}C}{k} \times \alpha$. The value of β for the data of Table 8.1 is about 4×10^{-6}. Another characteristic time in the SAGD process is that of drainage of the heated oil due to gravity forces. Its ratio to the characteristic time of heat conduction is the inverse of the Rayleigh No., $N_{Ra} = \frac{kgH\Delta\rho}{\phi\Delta S_o\mu_{os}} \times \frac{1}{\alpha}$. The Rayleigh No. is about 150 for the data of Table 8.1, and its inverse is of the order of 1×10^{-2}. Hence, for the above data, the drainage of the heated oil acts about 150 times faster than heat conduction, and the potential distribution acts about 1000 times faster than the drainage.

The experience of Section 8.3.1. indicated that large errors are incurred if the 2-D numerical model is used for a SAGD process in which the drainage rate acts 100 times faster than heat conduction[13]. For the purpose of some mechanistic studies a base case is chosen where the process is governed by an inverse Rayleigh No. of 10^{-1}, and a β of 10^{-6}. Other information used for the base case are listed in Table 8.2

Table 8.2
Physical properties used for the mechanistic studies (base case)

$N_{Ra} = \frac{kgH\Delta\rho}{\phi\Delta S_o\mu_{os}} \times \frac{1}{\alpha}$	10
$\beta = \frac{\phi\mu_{os}C}{k} \times \alpha$	1×10^{-6}
Oil viscosity at steam temperature μ_{os}	10×10^{-3} Pa s
Initial reservoir temperature T_R	10 °C
Steam temperature T_s	190 C
Dimensionless wellbore radius	0.0025
Number of control volumes used	40×20
Porosity $\times$ Saturation change $\phi\Delta S_o$	1

Figure 8.12 shows the production rate and Figure 8.13 presents the interface location at intervals of a dimensionless time equal to 0.1.

---

[13] For the experimental data of Chung and Butler [1988-b]. N_{Ra} was about 90, and β was of the order of 1×10^{-8}.
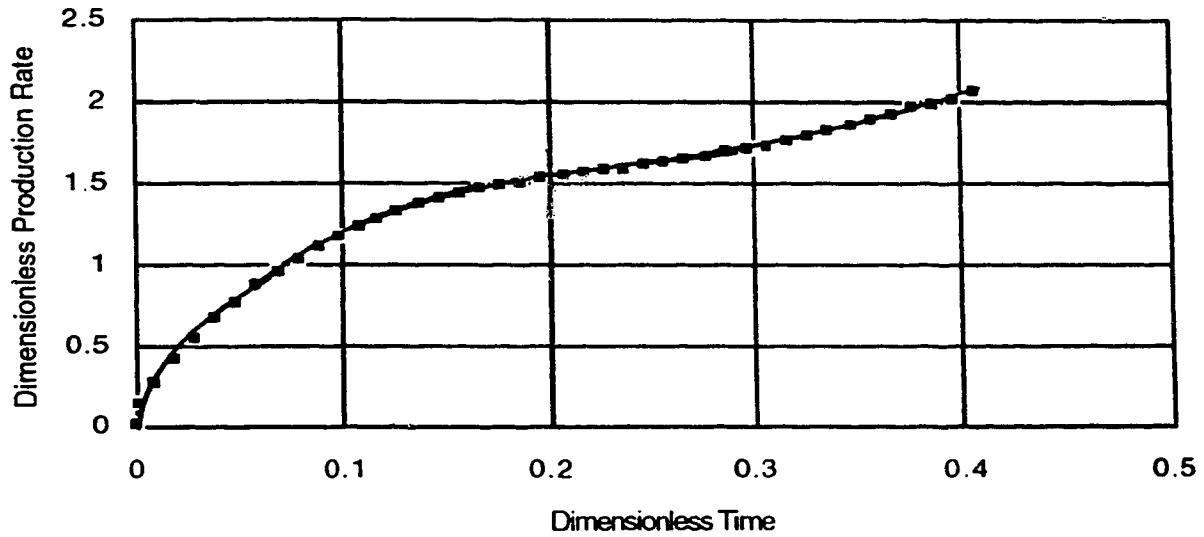
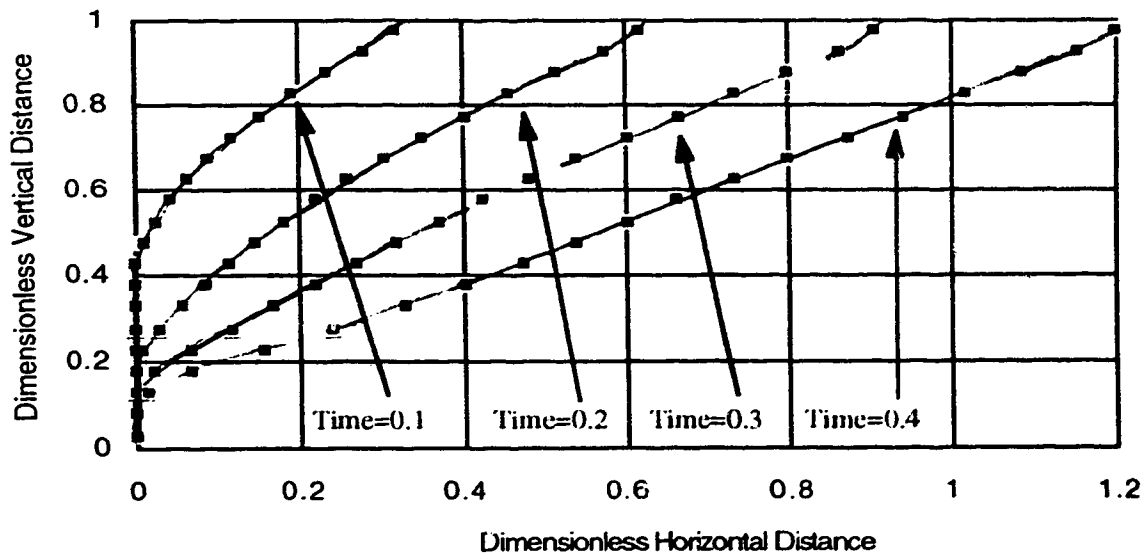Figure 8.12. Production rate obtained from the 2-D numerical SAGD model

Figure 8.13. Interface location obtained from the 2-D numerical SAGD model

174

Figure 8.13 indicates that about half of a dimensionless area of one is recovered by a dimensionless time of 0.4. Figure 8.14 shows the temperature and potential distribution and the streamline pattern ahead of the interface at a dimensionless time of 0.3. The iso-temperature and iso-potential lines indicate that the boundary conditions are modelled accurately. In Figure 8.14 isotherms are closely located at the top of the formation. This is of course due to the large convective effect caused by the movement of the interface. This cannot be observed in the potential solution, since the movement of the interface is negligible with respect to the very small time scale of potential distribution in the formation. An interesting point to be observed from Figure 8.14 is that the streamlines are neither horizontal, nor parallel to the interface. It was reviewed previously that some studies assumed flow parallel to the steam-oil interface [Butler *et al.* 1981, Butler 1985-b, Reis 1992-b] and some others invoked the Dupuit assumption and considered the streamlines to be horizontal [Towson and Boberg 1967, van Lookeren 1983, Palmgren *et al.* 1989, Bruining *et al.* 1990, Kimber *et al.* 1995].

A careful study of the 2-D potential distribution close to the interface of Figure 8.10 (or Figures 8.14 and 8.15) indicates clearly that there is a component of the potential gradient which is normal to the interface. This creates a component of oil velocity which is normal to the interface, as the oil viscosity is finite, and in fact small at the interface. The normal component of oil flow was neglected in the previous semi-analytical models of the SAGD process, such as that reported by Butler [1985-b], and those developed in Chapter 6. It is important to notice, that most of the oil flows parallel to the interface, however; streamlines of Figures 8.10 and 8.14 indicate that, appreciable error can occur if the flow normal to the interface is neglected. Similar behaviour of the streamlines can be observed in the unsteady-state free surface gravity flow of water as illustrated in Figure 7.1.3 of Bear [1972]. For a corresponding steady-state process, however, Figure 7.1.2 of Bear [1972] shows that the free boundary is a streamline.

It is worth noting that Equation (7.3.2), which relates the interface velocity to the Darcy velocity, suggests that, application of a no-flow boundary condition along the vertical direction, at the contact line between the formation and the cap-rock, results in a single component of the interface velocity, that, is along the horizontal line. In other words, the direction of the interface velocity below the cap-rock is horizontal.
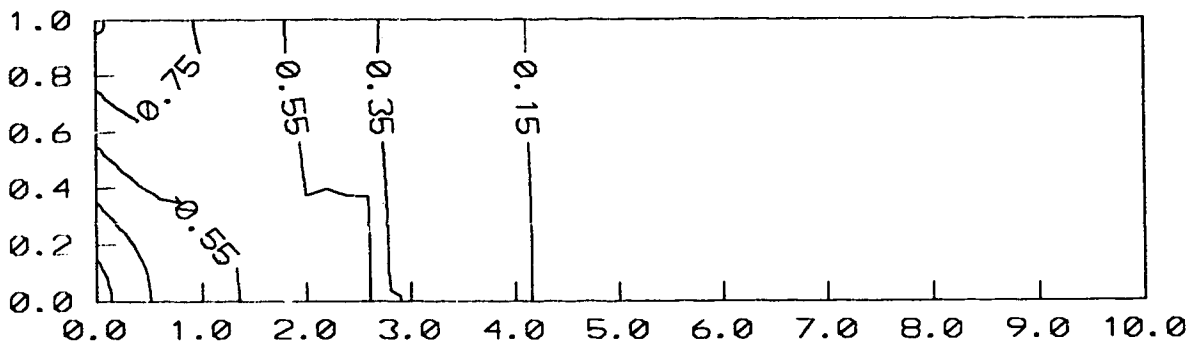
8.3.2.1. Potential Distribution

One of the assumptions often used in the modelling of thermal recovery processes is to neglect the compressibility of the fluids ahead of the steam-oil interface. In Chapter 6 the above assumption was invoked and it was assumed that the potential gradients was due to gravity forces on an inclined surface under steady-state conditions. Here two runs similar to the base case are performed, and the value of β is varied by four orders of magnitude. Figure 8.15 shows the potential distribution in the formation for the above two cases and the base case at a dimensionless time of 0.4. It can clearly be noted that potential disturbances diffuse much faster if the hydraulic diffusivity of the formation is higher, i.e., β is lower. Interestingly, however, there is no difference in production rate for the above three cases. A careful study of Figure 8.15 indicates that the potential distribution is almost identical in the vicinity of the interface. The low viscosity of the oil adjacent to the interface allows diffusion of potential disturbances to be so fast that changing the corresponding diffusion coefficient, that is, the hydraulic diffusivity by four orders of magnitude does not alter the final state. This can be observed clearly in Figure 8.16, where streamlines are plotted. Figure 8.16 indicates that the streamlines disappear rapidly away from the heated zone, and that the streamlines exhibit a very similar pattern for the three cases studied. It should be noted that the horizontal scale of Figures 8.15 and 8.16 are different.

Using the above observation one can conclude that, for the purpose of flow rate calculations adjacent to the interface the potential distribution can be assumed at steady-state conditions. This is of course only true for a slightly compressible fluid, with very low oil mobility in the cold region.

176

Temperature Distribution (Time=0.3)
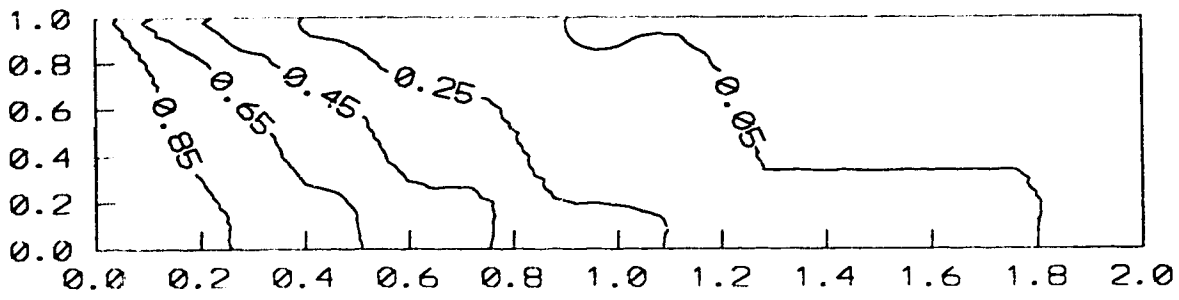
Potential Distribution (Time=0.3)

Streamlines (Time=0.3)
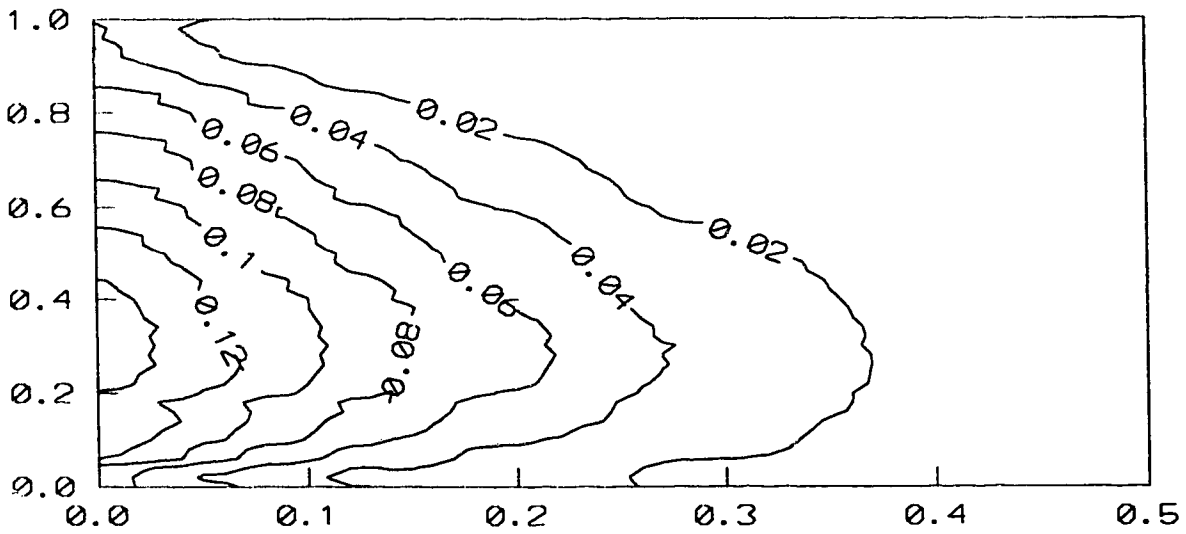
Figure 8.14   Temperature and potential distribution and streamlines ahead of the interface at a dimensionless time of 0.3 (Base case)

177

Potentiol Distribution (beta=1E-8)

Potentiol Distribution (beta=1E-6)
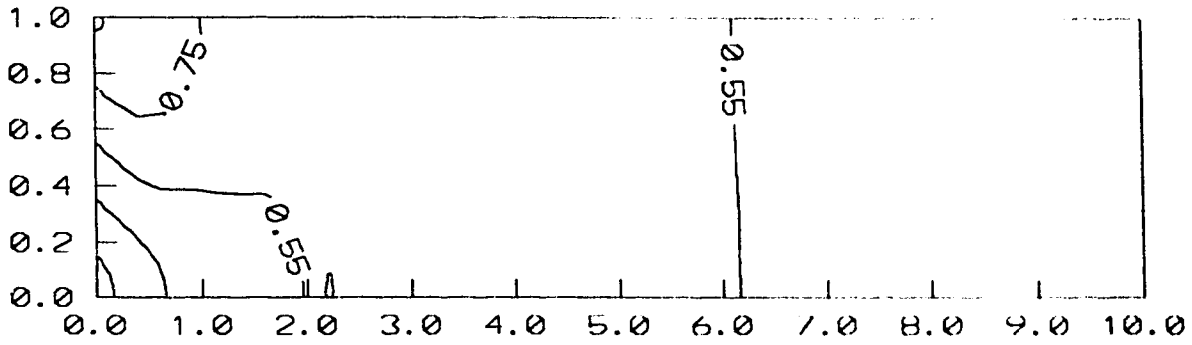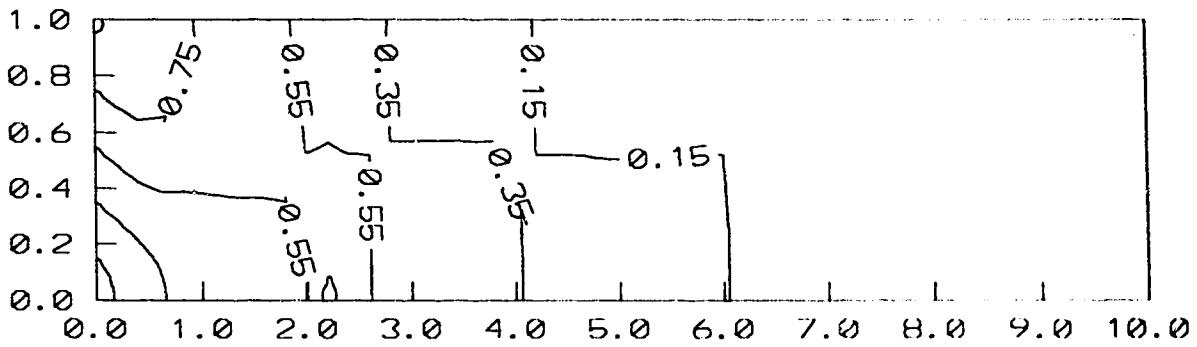
Potentiol Distribution (beta=1E-4)

Figure 8.15   Potential distribution ahead of the interface at a dimensionless time of 0.4
(Evaluation of the steady-state assumption for potential distribution)

Streamlines (beta=1E-8)

Streamlines (beta=1E-6)

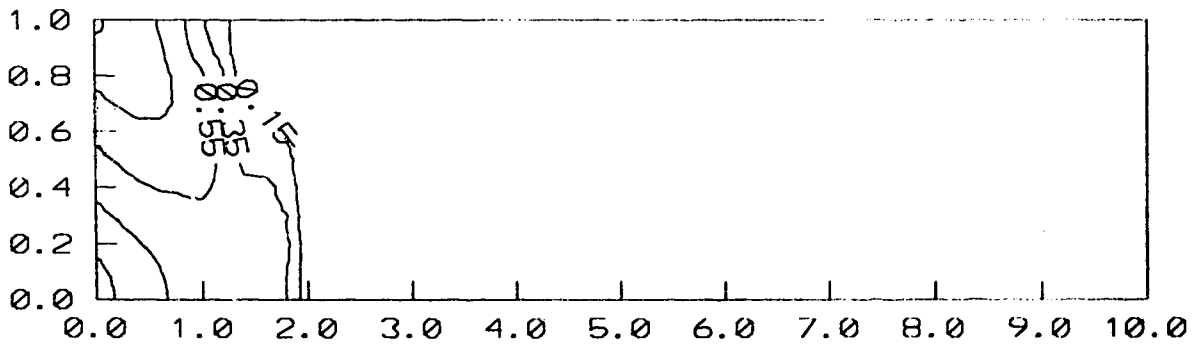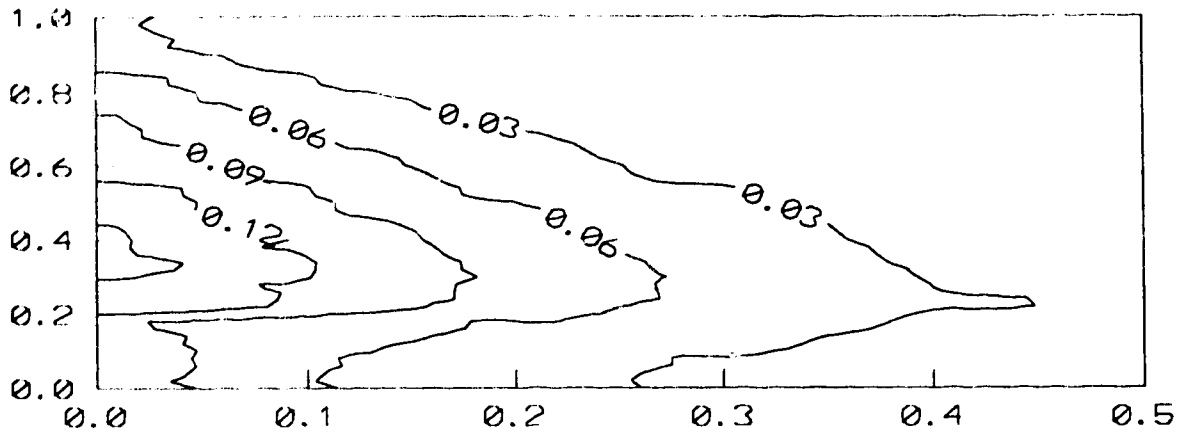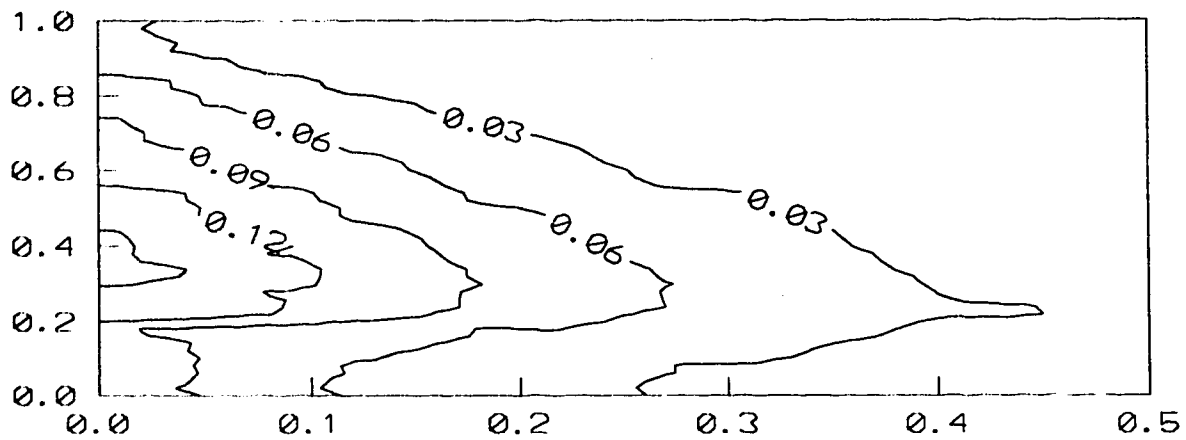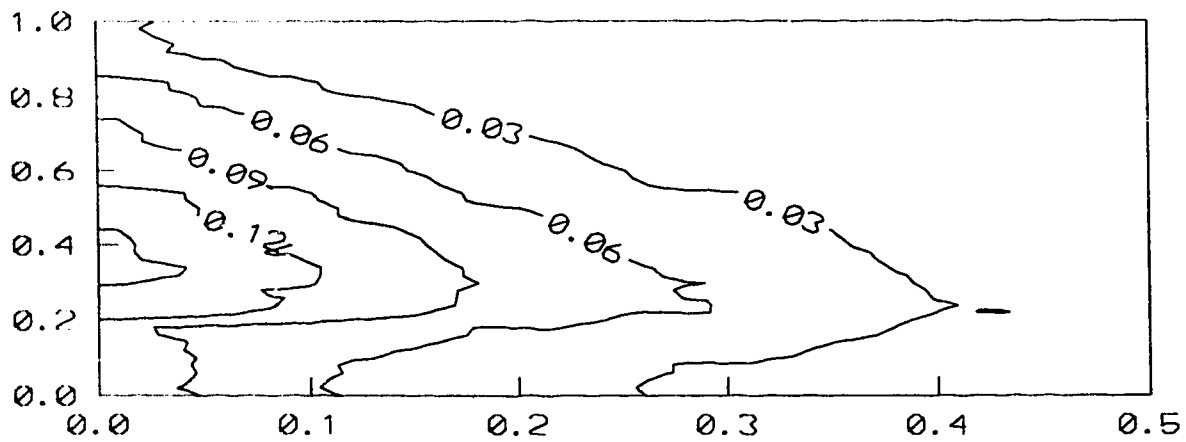Streamlines (beta=1E-4)

Figure 8.16   Streamline distribution ahead of the interface at a dimensionless time of 0.4
(Evaluation of the steady-state assumption for potential distribution)

179

8.3.2.2. Heat Conduction

Figures 8.15 and 8.16 indicated that the potential distribution approaches that of steady-state conditions in the heated region. As the heat diffuses in the formation the extent of the formation contributing to flow expands. This can be observed through a comparison of the streamlines shown in Figure 8.14, and those in Figure 8.16, for dimensionless times of 0.3, and 0.4, respectively.

The expansion of the heated zone ahead of the interface is shown in Figure 8.17. The unsteady-state behaviour of heat flow in the formation and its major effect in the development of the streamlines suggests that large errors are incurred if the heat flow process is considered steady-state. In fact, for the lower part of the formation, where the interface velocity is zero, a steady-state assumption is meaningless.

8.3.2.3. Drainage Rate

It was shown previously that the ratio of the characteristic times of drainage of the heated oil to that of heat conduction is represented as the inverse of the Rayleigh No. Figure 8.18 shows the drainage rate for the base case and for those with smaller values of N_{Ra}. A Rayleigh No. of 0.04 corresponds to the typical fractured reservoir considered in Table 4.1.

Figure 8.18 indicates that production rate decreases linearly with the Rayleigh No., when N_{Ra} is small. One can equally say that the thermal gravity drainage rate is proportional to the oil mobility at steam temperature for the range of Figure 8.18. The hydraulic diffusivity of a formation is proportional to its permeability, and formations with different permeability exhibit different potential diffusion rates. It was previously found however, that variation of hydraulic diffusivity over the practical range does not affect the process. Hence, extending the conclusions of Figure 8.18 to oil mobility at steam temperature is independent of the potential solution.

180

Temperature Distribution (Time=0.1)
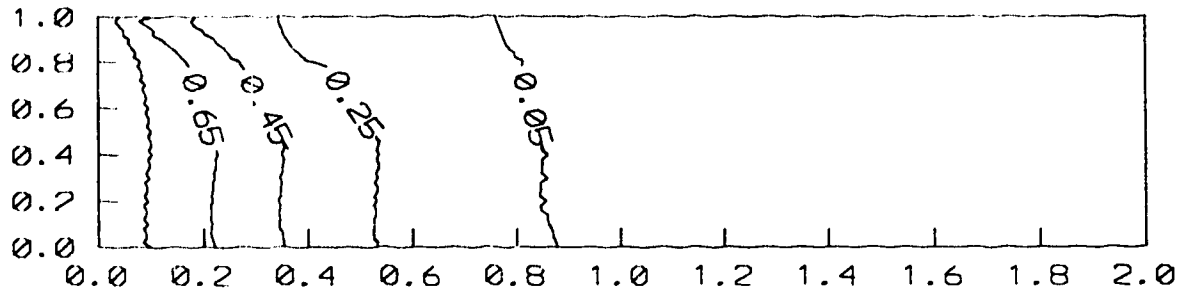
Temperature Distribution (Time=0.2)
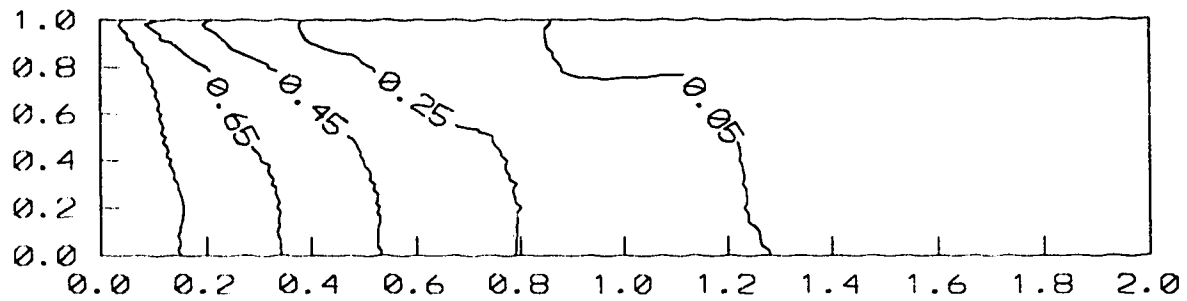
Temperature Distribution (Time=0.3)
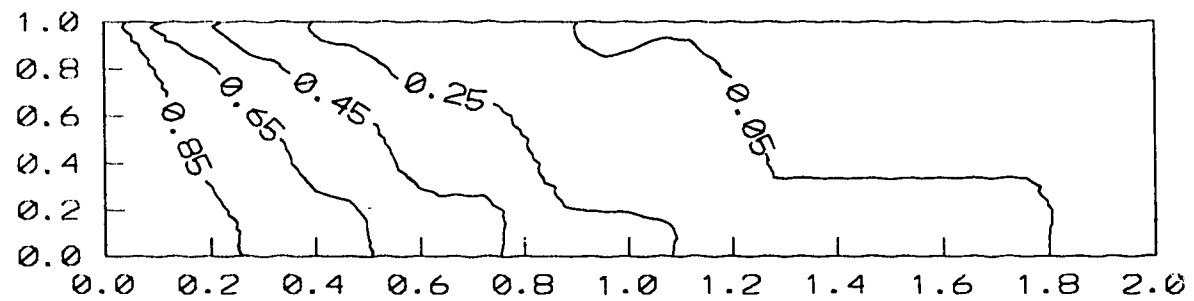
Figure 8.17   Temperature distribution ahead of the interface at different times

181
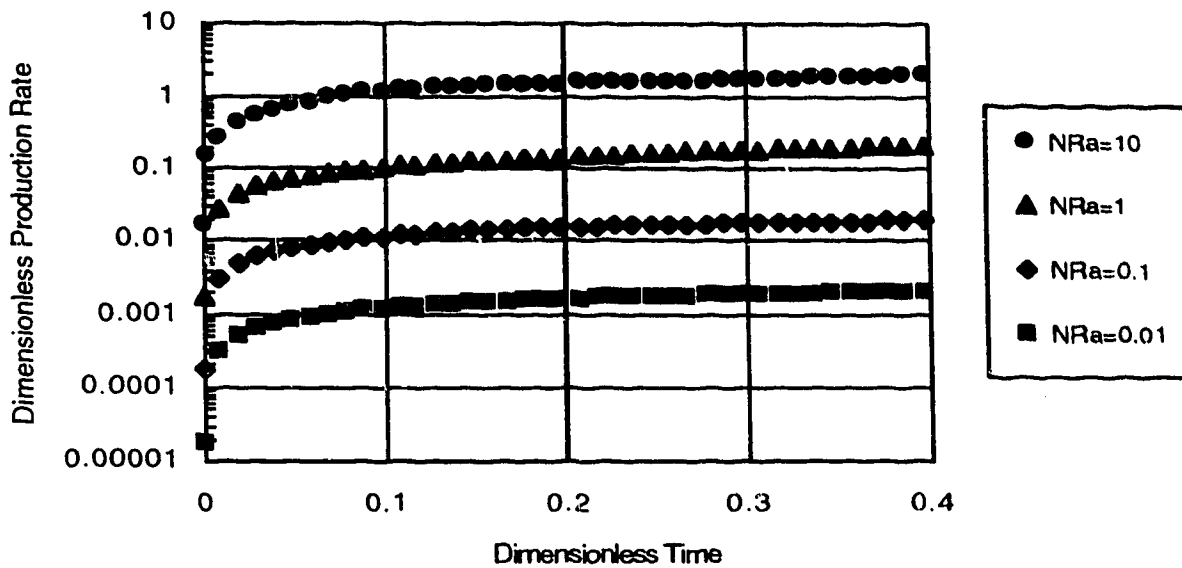
Figure 8.18. Effect of Rayleigh No. on production rate

8.3.3. Effect of Wellbore Radius

Figure 8.19 shows the drainage rate of a SAGD process with physical properties of Table 8.2. Two wellbore radii are chosen. The smaller one corresponds to a wellbore radius of 2 in. in a formation with 20 m thickness. No difference in production rate can be observed. This suggests that even the smaller wellbore radius could freely receive the heated draining oil. It should be noted that the diameter of the production well should be designed such that it not only receives the drained oil freely, but also does not cause large pressure drops due to flow in the wellbore.

In Section 6.3 it was found that the radius of a vertical well affected the production rate in a SAGD process. Application of horizontal wells facilitates the oil production rate by avoiding strongly converging streamlines, as happens in the case of vertical wells. The other major advantage gained by the application of horizontal wells is related to the length of the horizontal well at the base of the steam zone. In the case of a vertical well, the heating area around the expanding conical steam zone is determined solely by drainage and production of oil. In the case of a horizontal well, the heating area

182

is directly proportional to the length of the horizontal well, should uniform injection and production be achieved. In other words, a horizontal well acts as a line sink at the base of a steam zone, whereas a vertical well acts as a point sink.
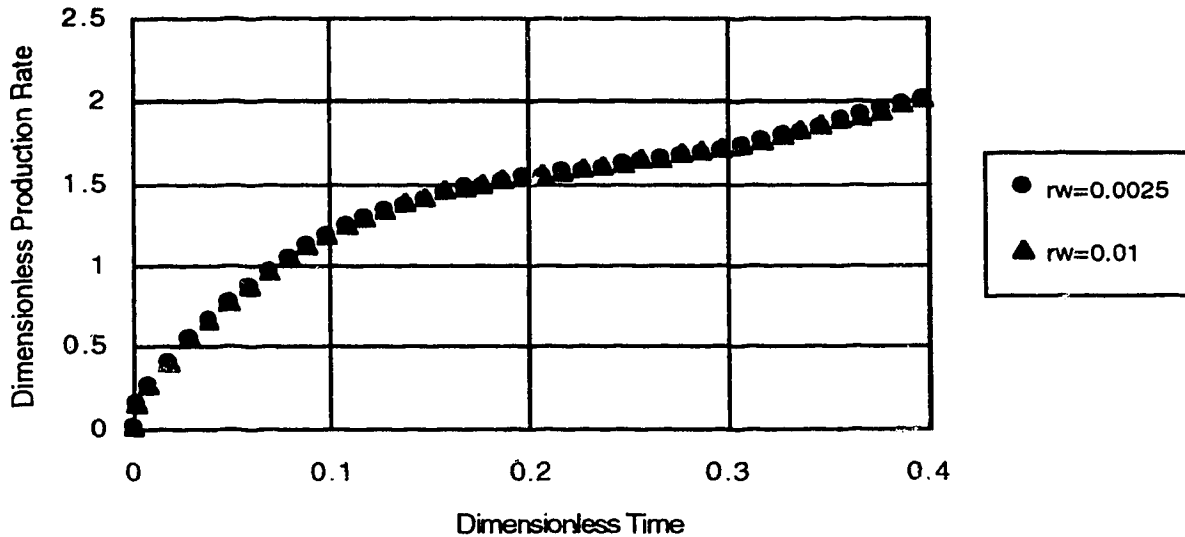
Figure 8.19. Effect of Wellbore radius on production rate

In a single phase flow process, the potential distribution around a vertical well corresponds to that of a line sink penetrating the formation. Their application in a SAGD process, however, represents a point sink only. On the other hand, the total length of a horizontal well participates in flow in both the cases of single phase flow and in thermal projects. Hence, application of horizontal wells as producers in thermal recovery processes based on gravity drainage offers more advantage than their application in primary oil recovery projects.

8.3.4. Effect of Number of Vertical Elements

It was noted previously that the interface location as obtained by the 1-D SAGD models was sensitive to the number of grid blocks used in the vertical direction. Figure 8.20 shows the interface location for the data of Table 8.2, using 40 control volumes along the vertical direction for dimensionless times of 0.1 and 0.2. A similar sensitivity is apparent. Possible reasons of this sensitivity were discussed before.
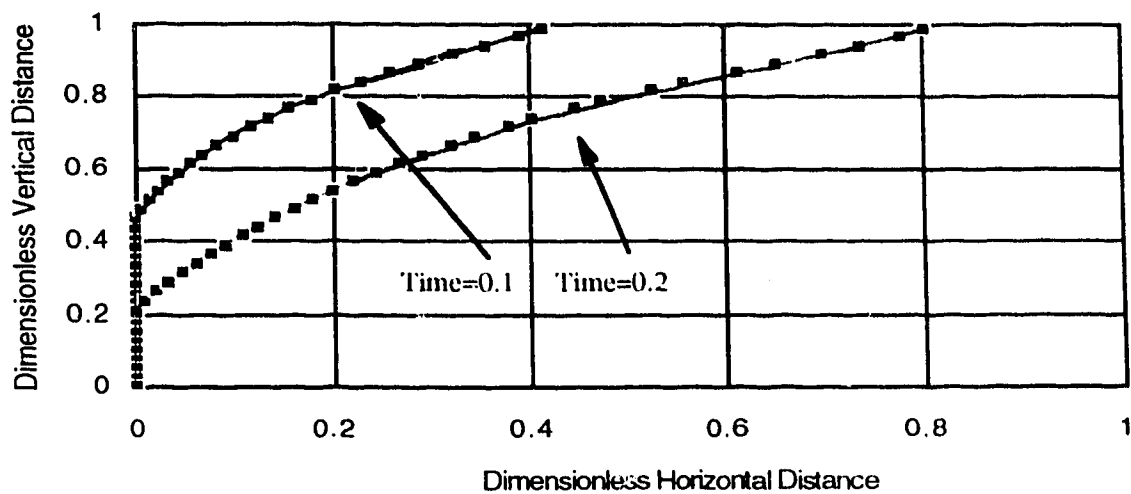
Figure 8.20. Interface location obtained from the 2-D numerical SAGD model (40 vertical control volumes)

9. CONCLUSIONS AND RECOMMENDATIONS

In this work, the problem of non-isothermal gravity drainage of heavy oil in fractured and non-fractured porous media was studied by means of analytical and numerical techniques. The study leads to the following conclusions.

1) The nonlinear fracture-matrix heat transfer can be modelled analytically, neglecting convective heat flow. The magnitude of the error introduced by this approximation depends on the oil mobility at steam temperature, and was found to be of the order of 1% for typical fractured reservoirs.

2) A time scale analysis indicated that the large effect of the convective heat flow observed in some experimental studies was an artifact of the physical properties of the experiments, that is, the high matrix permeability. Application of this technique revealed that in order to perform scaled experimental studies of thermal gravity drainage, the Rayleigh No. should be the same for the model and the prototype.

3) The developed analytical solutions of thermal gravity drainage from a single block indicated that oil rate is linearly proportional to oil mobility at steam temperature. The secondary parameters are block size and thermal diffusivity. Oil viscosity at average temperature can be used in the thermal gravity drainage calculations with minor error.

4) The Heat Integral Method (HIM) can be used effectively to obtain simple solutions for thermal recovery processes dominated by diffusion phenomena. The developed models included an analytical solution for thermal gravity drainage from a single block, a closed-form solution for the steam-drag process, and semi-analytical models for linear and radial Steam-Assisted Gravity Drainage (SAGD). It was found that

> a) Semi-analytical models of the SAGD process can be used to match the experimental data in the literature.

> b) Production rate varies linearly with the first power of the Rayleigh No. when the latter is small, and with the half power of the Rayleigh No. when it is large.

5) Dynamic gridding techniques can be used to calculate more accurately flow processes in the SAGD process. The study indicated that the potential distribution can be

185

considered steady-state; however, transient effects of heat conduction should be accounted for. It was found that streamlines in the oil zone and ahead of the a steam interface are neither horizontal nor parallel to the interface. The applicability of the Dupuit assumption for such systems should be reexamined.

Recommendations

1) The experience gained through this research indicated that the adaptive gridding techniques offer compelling attractions for accurate and efficient numerical modelling of flow processes in porous media. It is suggested that application of such methods for reservoir simulation be investigated further.

2) The study showed that the application of the 2-D numerical SAGD model was limited to the cases where the interface did not completely separate from the origin. To alleviate this limitation, application of a transformation which ensures a higher degree of orthogonality of the coordinate system is recommended.

3) Development of a similar numerical model as that in this study, however in terms of a stream function rather than a potential function is recommended. This can be used to examine the Dupuit assumption and the possibility of 1-D modelling of the oil flow ahead of the steam interface.

10. REFERENCES

Abdassah, D. and Ershaghi, I., 1986: "Triple Porosity Systems for Representing Naturally Fractured Reservoirs," *SPEFE* (April 1986), 113-27.

Adegbesan, K.O., Leaute, R.P., and Courtnage, D.E., 1991: "Performance of a Thermal Horizontal Well Pilot," paper SPE 22892 presented at the 1991 Annual Technical Conference and Exhibition of SPE, Dallas, Texas, Oct 6-9.

Antoniadi, D.G., Budnikov, V.F., and Garushev, A.R., 1988: "High Viscosity Oil Recovery from Carbonate Reservoirs by Thermal Methods," paper No. 223 presented at the 1988 UNITAR/UNDP Conference on Heavy Crude and Tar Sands, Edmonton, Alberta.

Aziz, K., 1993: "Reservoir Simulation Grids: Opportunities and Problems," paper SPE 25233 presented at the 1993 Symposium on Reservoir Simulation, New Orleans, LA. Feb. 28 - March 3.

Baibakov, N.K. and Garushev, A.R., 1989: *Thermal Methods of Petroleum Production*, Elsevier Science Pub. Co., New York, N.Y. (1989).

Bear, J., 1972: *Dynamics of Fluids in Porous Media*, Dover Pub. Co., New York, N.Y. (1972).

Beckermann, C. and Viskanta, R., 1988: "Natural Convection Solid/Liquid Phase Change in Porous Media," *Int. J. Heat Mass Transfer* (1988) **31**, 35-46.

Bell, G.E., 1978: "A Refinement of the Heat Balance Integral Method Applied to a Melting Problem," *Int. J. Heat Mass Transfer* (1978) **21**, 1357-62.

Bentsen, R.G., 1978: "Conditions Under Which the Capillary Term Can Be Neglected," *J. Cdn. Pet. Tech.* (1978) **17**, No. 4, 25-30.

Biterge, M.B. and Ertekin, T., 1992: "Development and Testing of Static/Dynamic Local Grid-Refinement Technique," *JPT* (April 1992) 487-495.

Blevins, T.R., 1990: "Steamflooding in the U.S.: A Status Report." *JPT* (May 1990) 548-554.

Briggs, P.J., Baron, R.P., Fulleylove, R.J., and Wright, M.S., 1988: "Development of Heavy Oil Reservoirs." *JPT* (Feb. 1988) 206-214.

Briggs, P.J., 1989: "A Simulator for the Recovery of Heavy Oil from Naturally Fractured Reservoirs Using Cyclic Steam Injection." paper SP. 17954 presented at the 1989 SPE Middle East Oil Technical Conference and Exhibition. Manama, Bahrain, March, 11-14.

Briggs, P.J., Beck, D.L., Black, C.J.J., and Bissell, R., 1992: "Heavy Oil from Fractured Carbonate Reservoirs." *SPERE* (May 1992) 173-79.

Britton, M.W., Martin, W.L., Leibrecht, R.J., and Harman, R.A., 1983: "The Street Ranch Pilot Test for Fracture-Assisted Steamflood Technology." *JPT* (March 1983) 511-22.

Bruining, J., Duijn, C.J. van, and Palmgren C.T.S., 1990: "Sharp Interface Modelling for Steam drive Recovery of Oil." Delft University of Technology Report (May 1990).

Buckley, S.E. and Leverett, M.C., 1942: "Mechanism of Displacement in Sands." *Trans.*, AIME (1942) **146**, 107.

Butler, R. M., 1985-a: "New Interpretation of the Meaning of the Exponent "m" in the Gravity Drainage Theory for Continuously Steamed Wells." *AOSTRA Journal of Research* (1985) **2**, No. 1, 67-71.

Butler, R.M., 1985-b: "A new Approach to the Modelling of Steam-Assisted Gravity Drainage." *J. Cdn. Pet. Tech.* (1985) **24**, No. 3, 42-51.

Butler, R.M., 1986: "The Expansion of Tar Sands During Thermal Recovery." *J. Cdn. Pet. Tech.* (1986) **25**, No. 6, 51-56.

Butler, R.M., 1987: "Rise of Interfering Steam Chambers." *J. Cdn. Pet. Tech.* (1987) **26**, No. 3, 70-75.

188

Butler, R.M., 1991: *Thermal Recovery of Oil and Bitumen*, Prentice Hall Pub. Co., New Jersey (1991).

Butler, R.M., 1994: *Horizontal Wells for the Recovery of Oil, Gas, and Bitumen*, Petroleum Society of CIM, Monograph No. 2, (1994).

Butler, R.M., McNab, G.S., and Lo, H.Y., 1981: "Theoretical Studies on the Gravity Drainage of Heavy Oil During In-Situ Steam Heating," *Can. J. Chem. Eng.* (1981) 455-60.

Butler, R.M. and Stephens, D.J., 1981: "The Gravity Drainage of Steam-Heated Heavy Oil to Parallel Horizontal Wells," *J. Cdn. Pet. Tech.* (1981) 20, No.2, 90-96.

Cardwell, W.T. and Parsons, R.L., 1948: "Gravity Drainage Theory," *Trans.*, AIME (1948) 174, 199-215.

Carslaw, H.S. and Jaeger, J.C., 1959: *Conduction of Heat in Solids*, 2nd ed., Oxford University Press, London (1959).

Chen, H.L. and Sylvester, N.D., 1990: "Appraisal of Analytical Steamflood Models," paper SPE 20023 presented at the 1990 California Regional Meeting, Ventura, CA. April 4-6.

Chen, W.H., Wasserman, M.L., and Fitzmorris, R.E., 1987: "A Thermal Simulator for Naturally Fractured Reservoirs," paper SPE 16008 presented at the 1987 Symposium on Reservoir Simulation, San Antonio, TX, Feb. 1-4.

Chung, K.H. and Butler, R.M., 1988-a: "Geometrical Effect of Steam Injection on the Formation of Emulsions in the Steam-Assisted Gravity Drainage Process," *J. Cdn. Pet. Tech.* (1988) 27, No. 1, 36-42.

Chung, K.H. and Butler, R.M., 1988-b: "A Theoretical and Experimental Study of Steam-Assisted Gravity Drainage Process," paper No. 89 presented at the 1988 UNITAR/UNDP Conference on Heavy Crude and Tar Sands, Edmonton, Alberta.

189

Closmann, P.J., 1995: "A Simplified Gravity Drainage Oil Production Model for Mature Steam drives," *SPERE* (May 1995) 143-148.

Closmann, P.J. and Smith, R.A., 1983: "Temperature Observations and Steam-Zone Rise in the Vicinity of a Steam-Heated Fracture," *JPT* (Aug. 1983) 575-86.

Cordell, G.M., 1982: "Reservoir Simulation of a Grosmont Carbonate Pilot," paper presented at the 1982 AOSTRA Annual Conference on Advances in Petroleum Recovery and Upgrading Technology, Calgary, Alberta, June 10-12.

Couderc, B., Monfrin, D., Quettier, L., and Sahuquet, B., 1989: "Emeraude Vapeur – An Offshore Steam Pilot," *J. Pet. Science Engineering* (1989) 2, 179-91.

Crank, J., 1988: *Free and Moving Boundary Problems*, Oxford Science Pub. Co., New York, N.Y. (1988).

de Haan, H.J. and van Lookeren, L. 1969: "Early Results of the First Large-scale Steam-Soak Project in the Tia Juana Field, Western Venezuela," *JPT* (Jan. 1969) 101-110.

Demirdzic, I. and Peric, M., 1988: "Space Conservation Law in Finite Volume Calculations of Fluid Flow," *Int. J. Numerical Methods Fluids* (1988) 8, 1037-1050.

Demirdzic, I. and Peric, M., 1990: "Finite Volume Method for Prediction of Fluid Flow in Laminarly Shaped Domains with Moving Boundaries," *Int. J. Numerical Methods Fluids* (1990) 10, 771-790.

Denbina, E.S., Boberg, T.C., and Rotter, M.B., 1991: "Evaluation of Key Reservoir Drive Mechanisms in the Early Cycles of Steam Stimulation at Cold Lake," *SPERE* (May 1991) 207-11.

Dietz, D.N., 1953: "A Theoretical Approach to the Problem of Encroaching and By-Passing Edge Water," *Proc.* Akad. van Wetenschappen, Amsterdam (1953) 56-B, 83-92.

Dindoruk, B. and Firoozabadi, A., 1994: "Computational of Gas Liquid Drainage in Fractured Porous Media Recognizing Fracture Liquid Flow," paper 94-23 presented at the 1995 CIM Annual Technical Meeting, Calgary, Alberta.

Donnelly, J.K. and Chmilar, M.J., 1995: "The Commercial Potential of Steam-Assisted Gravity Drainage," paper SPE 30278 presented at the 1995 Intl. Heavy Oil Symposium, Calgary, AB, June 19-21.

Dreher, K.D., Kenyon, D.E., and Iwere, F.O., 1986: "Heat Flow During Steam Injection Into a Fractured Carbonate Reservoir," paper SPE 14902 presented at the 1986 SPE/DOE Symposium on EOR, Tulsa, April 20-23.

Duda, J.L., Malone, M.F., and Notter, R.H., 1975: "Analysis of Two-Dimensional Diffusion Controlled Moving Boundary Problems," *Int. J. Heat Mass Transfer* (1975) 18, 901-910.

Dutra, T.V. and Aziz, K., 1992: "A New Double-Porosity Reservoir Model for Oil/Water Flow Problems," *SPERE* (Nov. 1992) 419-425.

Dykstra, H., 1978: "The Prediction of Oil Recovery by Gravity Drainage," *JPT* (May 1978) 818-830.

Edmunds, N.R., 1984: "A Model of the Steam Drag Effect in Oil Sands," *J. Cdn. Pet. Tech.* (1984) 23, No. 5, 34-39.

Edmunds, N.R., 1987: "UTF Gravity Drainage Process Development," presented at the Advances in Petroleum Recovery and Upgrading Technology, Edmonton, 1987.

Edmunds, N.R., Haston, J.A., and Best, D.A., 1988: "Analysis and Implementation of Steam-Assisted Gravity Drainage at the AOSTRA UTF," paper No. 125 presented at the 1988 UNITAR/UNDP Conference on Heavy Crude and Tar Sands, Edmonton, Alberta.

Edmunds, N.R., Kovalsky, J.A., Gittins, S.D., and Pennacchioli, E.D., 1994: "Review of Phase A Steam Assisted Gravity Drainage Test," *SPERE* (May 1994) 119-124.

Edmunds, N.R. and Suggett, J.C., 1995: "Design of a Commercial SAGD Heavy Oil Project," paper SPE 30277 presented at the 1995 Intl. Heavy Oil Symposium, Calgary, AB, June 19-21.

Escovedo, B.M., 1995: "Conceptual Steamflood Design Using Horizontal Wells to Maximize Project Profitability," paper SPE 30279 presented at the 1995 Intl. Heavy Oil Symposium, Calgary, AB, June 19-21.

Faghri, M., Sparrow, E.M., and Prata, A.T., 1984: "Finite-Difference Solutions of Convection-Diffusion Problems in Irregular Domains Using a Nonorthogonal Coordinate Transformation," *Numerical Heat Transfer* (1984) 7, 183-209.

Farouq Ali, S.M., 1982: "Steam Injection Theories – A Unified Approach," paper SPE 10746 presented at the 1982 SPE California Regional Meeting, San Francisco, CA, March 24-26.

Farouq Ali, S.M., 1992: *Odyssey of a Steamflood Model*, University of Alberta, Edmonton, (Oct. 1992).

Farouq Ali, S.M., 1994: "CSS – Canada's Superstrategy for Oil Sands," *J. Cdn. Pet. Tech.* (1994) 33, No. 9, 16-19.

Farouq Ali, S.M. and Redford, D.A., 1977: "Physical Modelling of Recovery Methods for Oil Sands," paper presented at the 1977 Canada-Venezuela Oil Sands Symposium, Edmonton, Canada, CIM Special Volume No. 17, 319-26.

Farouq Ali, S.M., Redford, D.A., and Islam, M.R., 1987: "Scaling Laws for Enhanced Oil Recovery Experiments," paper No.9 presented at the 1987 China-Canada Heavy Oil Tech. Symp., Zhuo Zhuo City, China.

Firoozabadi, A. and Hauge, J., 1990: "Capillary Pressure in Fractured Porous Media," *JPT* (June 1990) 784-91.

Gebhart, B., 1971: *Heat Transfer*, 2nd ed., McGraw-Hill Pub. Co., New York, N.Y. (1971), 235.

Gilman, J.R., 1986: "An Efficient Finite-Difference Method for Simulating Phase Segregation in Matrix Blocks in Dual-Porosity reservoirs," *SPERE* (July 1986) 403-13.

Goodman, T.R., 1958: "The Heat-Balance Integral and Its Application to Problems Involving Change of Phase," *Trans.*, ASME (1958) **80**, 335-42.

Goodman, T.R., 1959: "The Heating of Slabs with Arbitrary Heat Inputs," *J. Aero/space Sci.* (1959) **26**, 187-88.

Goodman, T.R., 1961: "The Heat-Balance Integral–Future Considerations and Refinements," *Trans.*, ASME *J. Heat Transfer* (1961) **83**, 83-86.

Griffin, P.J. and Trofimenkoff, P.N., 1985: "Laboratory Studies of the Steam-Assisted Gravity Drainage process," *AOSTRA J. Research* (1985) **2**, No. 4, 197-203.

Hagoort, J., 1980: "Oil Recovery by Gravity Drainage," *SPEJ* (June 1980) 139-50.

Halal, A.S. and Lilley, D.G., 1988: "A Simple Nonorthogonal Grid Technique for Handling Irregular Boundaries on Heat and Fluid Flow Predictions," in *Computers in Engineering* (1988) 479-84.

Hamm, R.A. and Ong, T.S., 1995: "Enhanced Steam-Assisted Gravity Drainage: A New Horizontal Well Recovery Process for Peace River, Canada," *J. Cdn. Pet. Tech.* (1995) **34**, No. 4, 33-40.

Harrigal, R.L. and Wicox, G.G., 1992: "An Improved Steamflood Analytical Modelling Tool: Updating Old Methodologies with New Approaches to Increase Engineering Productivity," paper SPE 24434 presented at the 1992 Petroleum Computer Conference, Houston, TX. July 19-22.

Hawken, D.F., 1987: "Review of Adaptive Grid Techniques for Solution of Partial Differential Equations," *Prog. Aerospace Sci.* (1987) **24**, 29-49.

Higgins, R.V., 1953: "Factors That Influence Gravity Drainage," *The Petroleum Engineer* (May 1953) B-83 - B-92.

Hindman, R.G., 1982: "Generalized Coordinate Forms of Governing Fluid Equations and Associated Geometrically Induced Errors," *AIAA J.* (1982) **20**, 1359-1367.

193

Horie, T., Firoozabadi A., and Ishimoto, K., 1990: "Laboratory Studies of Capillary Interaction in Fracture/Matrix System," *SPERE* (Aug. 1990) 353-360.

Hsu, C.F., Sparrow, E.M., and Patankar, S.V., 1981: "Numerical Solution of Moving Boundary Problems by Boundary Immobilization and a Control-Volume-Based Finite-Difference Scheme," *Int. J. Heat Mass Transfer* (1981) **24**, 1335-43.

Hubbert, M.K., 1956: "Darcy's Law and the Field Equation of the Flow of Underground Fluids," *Trans.*, AIME (1956) **207**, 222-239.

Jensen, T.B. and Sharma, M.P., 1991: "Mechanisms of Oil Displacement by Steam and Hot Water in Fractured Porous Media: Experimental and Numerical Modelling Studies," *Multiphase Transport in Porous Media*, ASME 1991, FED **122**/HTD **168**, 83-91.

Joshi, S.D. and Threlkeld, C.B., 1985: "Laboratory Studiues of Thermally Aided Gravity Drainage Using Horizontal Wells," *AOSTRA J. Research* (1985) **2**, No. 1, 11-19.

Karki, K.C. and Patankar, S.V., 1988: "Calculation Procedure for Viscous Incompressible Flows in Complex Geometries," *Numerical Heat Transfer* (1988) **14**, 295-307.

Kececioglu, I., 1993: "An Adaptive Variational Finite Element Method for Computation Coupled Porous Media Problems with Moving Fronts," *SPE Advanced Technology Series* (1993) **1**, No. 1, 42-51.

Kharrat, R., Jamialahmadi, M., Pooladi-Darvish, M., and Vossoughi, S., 1993: "Moving Boundary Heat Conduction in Porous Media Accompanied with Fluid Flow," in *Transport Phenomena in Thermal Engineering*, ed. Lee, J.S., Chung, S.H., and Kim, K.H., Begell House Inc.Pub. Co., 721-724 (1993).

Kim, C.J. and Kaviany, M., 1990: "A Numerical Method for Phase-Change Problems," *Int. J. Heat Mass Transfer* (1990) **33**, 2721-34.

Kim, C.J. and Kaviany, M., 1992: "A Numerical Method for Phase-Change Problems with Convection and Diffusion," *Int. J. Heat Mass Transfer* (1992) **35**, 457-67.

194

Kimber, K.D., Deemer, A.R., Luce, T.H., and Sharpe, N.H., 1995: "A New Analytical Model for Assessing the Role of Steam Production in Mature Steamfloods," paper SPE 29657 presented at the 1995 Western Regional Meeting, Bakersfield, CA. March 8-10.

King, R.L., Stiles, J.H.Jr., and Waggone, J.M., 1970: "A Reservoir Study of the Hawkins Woodbine Field," paper SPE 2972 presented at the 1970 SPE Annual Fall Meeting, Houston, Oct. 4-7.

Kisman, K.E. and Yeung, K.C., 1995: "Numerical Study of the SAGD Process in the Brunt Lake Oil Sand Lease," paper SPE 30276 presented at the 1995 Intl. Heavy Oil Symposium, Calgary, AB, June 19-21.

Kumar, D., Patel, H.N., and Denbina, E.S., 1986: "Use of a Gravity Override Model of Steamflooding at Cold Lake," in *Canadian Heavy Oil Association Reservoir Handbook* (1986) 139-47.

Labastie, A., 1990: "Capillary Continuity Between Blocks of a Fractured Reservoir," paper SPE 20515, presented at the 1990 Annual Technical Conference and Exhibition, New Orleans, LA, Sept. 23-26.

Lacroix, M., 1989: "Computation of Heat Transfer During Melting of a Pure Substance from an Isothermal Wall," *Numerical Heat Transfer, Part B* (1989) **15**, 191-210.

Lacroix, M. and Garon, A., 1992: "Numerical Simulation of Phase Change Problems: An Eulerian-Lagrangian Approach," *Numerical Heat Transfer, Part B* (1992) **19**, 57-78.

Lacroix, M. and Voller, V.R., 1990: "Finite Difference Solutions of Solidification Phase Change Problems: Transformed Versus Fixed Grids," *Numerical Heat Transfer, Part B* (1990) **17**, 25-41.

Landau, H.G., 1950: "Heat Conduction in a Melting Solid," *Quartely of Applied Mathematics* (1950) **8**, 81-94.

Lardner, T.J. and Pohle, F.V., 1961: "Application of Heat Balance Integral to Problems of Cylinderical Geometry," *Trans.*, ASME (1961) **83**, 310-312.

Lee B.Y.Q and Tan T.B.S., 1987: "Application of a Multiple Porosity/Permeability Simulator in Fractured Reservoir Simulation," paper SPE 16009 presented at the 1987 SPE Symposium on Reservoir Simulation. San Antonio, TX, Feb.1-4.

Liebe, R.H. and Butler, R.M., 1991: "A Study of the Use of Vertical Steam Injectors in the Steam-Assisted Gravity Drainage Process," paper CIM 91-32 presented at the 1991 CIM Annual Technical Meeting, Banff, Alberta, April 21-24.

Lock, G.D., 1986: "Normalization," *Int. J. Mech. Eng. Ed.* (1986), **14**, 193-204.

Macaulay, R.C., Krafft, J.M., Hartemink, M., and Escovedo, B., 1995: "Design of a Steam Pilot in a Fractured Carbonate Reservoir – Qarn Alam Field, Oman", paper SPE 30300 presented at the 1995 SPE International Heavy Oil Symposium, Calgary, AB, Canada, June 19-21.

Mandl, G. and Volek, C.W., 1969: "Heat and Mass Transport in Steam Drive Process," *SPEJ* (March 1969) 57-79.

Marx, J. and Langenheim, R.N., 1959: "Reservoir Heating by Hot Fluid Injection," *Trans.*, AIME (1959) **216**, 312-15.

McCartin, B.J., 1983: "Application of Exponential Splines in Computational Fluid Dynamics," *AIAA J.* (1983) **21**, 1059-65.

McDonald, A.E., Beckner, B.L., Chan, H.M., Jones, T.A., and Wooten, S.O., 1991: "Some Important Considerations in the Simulation of Naturally Fractured Reservoirs," paper SPE 21814 presented at the 1991 Rocky Mountain Regional Meeting and Low-Permeability Reservoirs Symposium, Denver, Colorado, April 15-17.

Miller, M.A. and Leung, W.K., 1985: "A Simple Gravity Override Model of Steam Drive," paper SPE 14241 presented at the 1985 Annual Technical Conference and Exhibition, Las Vegas, NV, Sept. 22-25.

Moritis, G., 1994: "EOR Dips in U.S. but Remains a Significant Factor," *Oil & Gas J.* (Sept. 26, 1994) 51-79.

Moshtaghian, A., Malekzadeh, R., and Azarpanah, A., 1988: "Heavy Oil Discovery in Islamic Republic of Iran," Paper No. 99 presented at the 1988 UNITAR/UNDP Conference on Heavy Crude and Tar Sands, Edmonton, Alberta.

Murty, C.R.K., Al-Saleh, N., and Dakessian, B.A., 1987: "Forty Seven Years' Gas Injection in a Preferentially Oil-Wet, Low Dip Reservoir," *JPT* (March 1987) 363-368.

Nacul, E.C. and Aziz, K., 1991: "Use of Irregular Grid in Reservoir Simulation," paper SPE 22886 presented at the 1991 Annual Technical Conference and Exhibition, Dallas, TX. Oct. 6-9.

Neuman, C.H., 1985: "A Gravity Override Model for Steam Drive," *JPT* (Jan 198:).

Nolan, J.B., Ehrlich, R., and Crookston, R.B., 1980: "Applicability of Steamflooding for Carbonate Reservoirs," SPE 8821presented at the 1980 SPE/DOE Symposium on EOR, Tulsa, April 20-23.

Oballa, V., Coombe, D.A., and Buchanan, W.L., 1993: "Factors Affecting Thermal Response of Naturally Fractured Reservoirs," *J. Cdn. Pet. Tech.* (1993) **32**, No.8, 31-42.

Odeh, A.S. and Babu, D.K., 1988: "Comparison of Solutions of the Nonlinear and Linearized Diffusion Equation," *SPERE* (Nov. 1988) 1202-1206.

Ozisik, M.N., 1980: *Heat Conduction*, John Wiley & Sons Pub. Co. (1980).

Palatnik, B.M., Shandrygin, A.N., and Segin, T.N., 1992: "A New Approach for Small-Scale Simulation of Multiphase Flow in Naturally Fractured Reservoirs," paper SPE 24263 presented at the 1992 European Petroleum Computer Conference, Stavanger, Norway, May 25-27.

Palmgren, C.T.S., Bruining, J., and de Haan, H.J., 1989: "The Effect of Viscous, Gravity, and Capillary Forces on the Dynamic Behaviour of the Steam Condensation Front," *Proc.* of the 1989 European Symposium on Improved Oil Recovery, Budapest, April 25-27, 561-573.

Palmgren, C.T.S., Bruining, J., de Haan, H.J., Guemrah, F., and Biezen, E.N., 1991; "Water of Condensation and the Steam Condensation Front During Steamdrive," *Proc.* of the 1991 European Symposium on Improved Oil Recovery, Stavanger, Norway, May 21-23, 863-872.

Palmgren, C.T.S. and Bruining, J., 1992: "An Interface Model To predict Vertical Sweep During Steamdrive," paper SPE 24077 presented at the 1992 Western Regional Meeting, Bakersfield, CA, March 30- April 1.

Patankar, S.V., 1980: *Numerical Heat Transfer and Fluid Flow*, Hemisphere Pub. Co., Washington D.C. (1980).

Patel, P.D., 1969: "Interface Condition in Heat Conduction Problems with Change of Phase," *AIAA J.* (1969) **6**, 2454.

Peric, M., 1987: "Efficient Semi-Implicit Solving Algorithm for Nine-Diagonal Coefficient Matrix," *Numerical Heat Transfer* (1987) **11**, 251-279.

Pohlhausen, K., 1921: "Zur naeherungsweisen Integration der Differentialgleichung der laminaren Grenzschicht," *Zeitschrift fuer angewandte Mathematik und Mechanik* (1921), **1**, 252-268.

Pooladi-Darvish, M., 1992: "Improved Gravity Drainage by Steam Injection in Fractured Reservoirs," M.Sc. Thesis, University of Petroleum Industry, Iran (April 1992).

Prats, M., 1982: *Thermal Recovery*, Monograph Series, Richardson, (1982) **7**.

Pruess, K. and Narasimhan, T.N., 1985: "A Practical Method for Modelling Fluid and Heat Flow in Fractured Porous Media," *SPEJ* (Feb. 1985) 14-26.

Pruess, K. and Wu, Y.-S., 1993: "A New Semianalytical Method for Numerical Simulation of Fluid and Heat Flow in Fractured Reservoirs," *SPE Advanced Technology Series* (1993) **1**, No. 2, 63-72.

Pujol, L. and Boberg, T.C., 1972: "Scaling Accuracy of Laboratory Steamflooding Models," paper SPE 4191 presented at the 1972 Annual California Regional Meeting of SPE, Bakersfield.

Quandalle, P. 1991: "Eighth SPE Comparative Solution Project: Gridding Techniques in Reservoir Simulation," paper SPE 25263 presented at the 1991 Symposium on Reservoir Simulation, New Orleans, LA, Feb. 28 - March 3.

Ramanathan, S. and Ranganathan, K., 1988: "Comparison of Boundary-Fitted Coordinates with Finite Element Approach for Solution of Conduction Problems," *Numerical Heat Transfer* (1988) **14**, 187-211.

Reis, J.C., 1992-a: "An Analysis of Oil Expulsion Mechanisms from Matrix Blocks during Steam Injection in Naturally Fractured Reservoirs," *In Situ* (1992), **16**, No. 1, 43-73.

Reis, J.C., 1992-b: "A Steam-Assisted Gravity Drainage Model for Tar Sands: Linear Geometry," *J. Cdn. Pet. Tech.* (1992) **31**, No. 10, 14-20.

Reis, J.C., 1993: "A Steam Assisted Gravity Drainage Model for Tar Sands: Radial Geometry," *J. Cdn. Pet. Tech.* (1993) **32**, No. 8, 43-48.

Rentrop, P., 1980: "An Algorithm for the Computation of the Exponential Splines," *Numer. Math.* (1980) **35**, 81-93.

Sahuquet, B.C. and Ferrier, J.J., 1982: "Steam-Drive Pilot in a Fractured Reservoir: Lacq Supérieur Field," *JPT* (April 1982) 873-880.

Saidi, A.M., 1975: "Mathematical Simulation Model Describing Iranian Fractured Reservoirs and Its Application to Haft Kel Field," *Proc.* Ninth World Petroleum Congress, Tokyo (1975) 209-19.

Saidi, A.M., 1983: "Simulation of Naturally Fractured Reservoirs," paper SPE 12270 presented at the 1983 SPE symposium on Reservoir Simulation, San Francisco, CA, Nov. 15-18.

199

Saidi, A.M., 1987: *Reservoir Engineering Aspects of Fractured Reservoirs – Theoretical and Practical Aspects*, Total Press, Paris (1987).

Saidi, A.M., 1991: "Gas Injection will Hike Oil Recovery from High Permeability Reservoirs Produced under Gravity Drainage," paper presented at the 1991 Iranian Oil & Gas Symposium, Isfahan, Sept. 1991.

Saidi, A.M., Tehrani D.H., and Wit, K., 1979: "Mathematical Simulation of Fractured Reservoir Performance Based on Physical Model Experiments," paper PD 10 *Proc.* Tenth World Pet. Cong., Bucharest (1979) 3, 225-33.

Satman, A., 1988: "Solution of Heat- and Fluid-Flow Problems in Naturally Fractured Reservoirs: Part 1-Heat Flow Problems," *SPEPE* (Nov. 1988) 463-66.

Schlichting, H., 1955: *Boundary Layer Theory*, Mc Graw-Hill Pub. Co., Inc. New York, N.Y. (1955), Chapter 12.

Schreiber, W.C., 1990: "The Numerical Simulation of Heat Conduction in Irregularly-Shaped Materials of Thermally-Dependent Properties," *Int. J. Numerical Methods Engineering* (1990) 30, 679-696.

Sharp, H.N. and Anderson, D.A., 1993: "Orthogonal Adaptive Grid Generation with Fixed Internal Boundaries for Oil Reservoir Simulation," *SPE Advanced Technology Series* (1993) 1, No. 2, 53-62.

Shen, C. and Ruth, D.W., 1994: "Impact of Inlet Boundary Condition on the Numerical Simulation of One-Dimensional Coreflooding," paper CIM 94-75 presented at the 1994 CIM Annual Technical Meeting, Calgary, Alberta, June 12-15.

Slattery, J.C., 1969: "Single-phase Flow Through Porous Media," *AIChE J.* (1969) 15, 866-872.

Soni, Y. and Harman, R.A., 1986: "Simulation of Saner Ranch Fracture-Assisted Steamflood Technology," *J. Cdn. Pet. Tech.* (1986) 25, No. 1, 57-70.

Sparrow, E.M., Patankar, S.V., and Ramadhyani, S., 1977: "Analysis of Melting in the Presence of Natural Convection in the Melt Region," *Trans.*, ASME (1977) **99**, 520-526.

Stang, H.R. and Soni, Y., 1987: "Saner Ranch Pilot Test of Fracture-Assisted Steamflood Technology," *JPT* (1987) 684-96.

Sumnu, M.D., Aziz, K., Brigham, W.E., and Castanier, L.M., 1994: "Use of Simulators in the Design of an Experiment for Steam Injection into a Fractured System," paper SPE 27742 presented at the 1994 SPE/DOE symposium on Improved Oil Recovery, Tulsa, OK, April 17-20.

Svrcek, W.Y. and Mehrotra, A.K., 1988: "One Parameter Correlation for Bitumen Viscosity," *Chem. Eng. Res. Des.* (1988) **16**, 323-27.

Thomas, P.D. and Lombard, C.K., 1979: "Geometric Conservation Law and Its Application to Flow Computations on Moving Boundaries," *AIAA J.* (1979) **17**, 1030-1037.

Thompson, J.F. and Warsi, Z.U.A., 1982: "Boundary-Fitted Coordinate Systems for Numerical Solution of Partial Differential Equations – A Review," *J. Comput. Physics* (1982) **47**, 1-108.

Thompson, J.F., Warsi, Z.U.A., and Mastin, C.W., 1985: *Numerical Grid Generation –*

van Wunnik, J.N.M. and Wit, K., 1992: "Improvement of Gravity Drainage by Steam Injection into a Fractured Reservoir: An Analytic Evaluation," *SPERE* (Feb. 1992) 59-66.

Vinsome P.K.W. and Westerveld, J., 1980: "A Simple Method for Predicting Cap and Base Rock Heat Losses in Thermal Reservoir Simulators," *J. Cdn. Pet. Tech.* (1980) 19, No. 3, 87-90.

Viswanath, R. and Jaluria, Y., 1993: "A Comparison of Different Solution Methodologies for Melting and Solidification Problems in Enclosures," *Numerical Heat Transfer, Part B* (1993) 24, 77-105.

Vogel, J.V., 1992: "Gravity Drainage Vital factor for Understanding Steam Floods," *Oil & Gas J.* (Nov.30 1992) 42-47.

Voller, V.R., Swaminathan, C.R., and Thomas, B.G., 1990: "Fixed Grid Techniques for Phase Change Problems: A Review," *Int. J. Numerical Methods Engineering* (1990) 30, 875-898.

Warren, J.E. and Root, P.J., 1963: "The Behaviour of Naturally Fractured Reservoirs," *SPEJ* (March 1963) 245-55.

Weaver, J.A. and Viskanata, R., 1986: "Melting of Frozen Porous Media Contained in a Horizontal or Vertical Cylindrical Capsule," *Int. J. Heat Mass Transfer* (1986) 29, 1943-1951.

Wingard, J.S. and Orr, F.M. Jr., 1994: "An Analytical Solution for Steam/Oil/Water Displacements," *SPE Advanced Technology Series* (1994) 2, No. 2, 167-176.

Yortsos, Y.C., 1991: "A Theoretical Analysis of Vertical Flow Equilibrium," paper SPE 22612 presented at the 1991 Annual Technical Conference and Exhibition, Dallas, TX, Oct. 6-9.

Yortsos, Y.C. and Gavalas, G.R., 1981-a: "Analytical Modelling of Oil Recovery by Steam Injection: Part I: Upper Bounds," *SPEJ* (April, 1981) 162-178.

202

Yortsos, Y.C. and Gavalas, G.R., 1981-b: "Analytical Modelling of Oil Recovery by Steam Injection: Part II: Asymptotic and Approximate Solutions," *SPEJ* (April, 1981) 179-190.

Yortsos, Y.C. and Gavalas, G.R., 1982: "Heat Transfer Ahead of Condensation Fronts in Thermal Oil Recovery Processes," *Int. J. Heat Mass Transfer* (1982) **25**, 305-316.

Zauderer, E., 1989: *Partial Differential Equations of Applied Mathematics*, 2nd ed. Wiley Pub. Co., New York, N.Y. (1989).

Zhou, G., Zhang, R., Shen, D., and Pu, H., 1995: "Horizontal Well Application in High Viscous Oil Reservoir," paper SPE 30281 presented at the 1995 Intl. Heavy Oil Symposium, Calgary, AB, June 19-21.

APPENDIX A

A.1. Temperature Distribution in a Slab Using HIM

It was shown in the main text that matrix heating in a typical fractured reservoir can be explained by conduction. Equations (A.1.1) to (A.1.4) describe 1-D heating of a slab:

$$\frac{\partial^2 \theta}{\partial \xi^2} = \frac{\partial \theta}{\partial \tau} \qquad\qquad 0 \le \xi \le 1 \qquad \tau \ge 0 \qquad \ldots\ldots (A.1.1)$$

$$\theta = 0 \qquad\qquad 0 \le \xi \le 1 \qquad \tau = 0 \qquad \ldots\ldots (A.1.2)$$

$$\theta = 1 \qquad\qquad \xi = 0 \qquad \tau > 0 \qquad \ldots\ldots (A.1.3)$$

$$\frac{\partial \theta}{\partial \xi} = 0 \qquad\qquad \xi = 1 \qquad \tau > 0 \qquad \ldots\ldots (A.1.4)$$

where the dimensionless variables are defined in the main text (see Equation (4.2.1.1) to (4.2.1.3).

An analytical solution for the above problem can be obtained by using the method of separation of variables:

$$\theta = 1 - \frac{4}{\pi} \sum_{n=1}^{\infty} \frac{\sin\left(\frac{(2n-1)\pi}{2}\xi\right)}{2n-1} \exp\left[-\left(\frac{2n-1}{2}\right)^2 \pi^2 \tau\right] \qquad \ldots\ldots (A.1.5)$$

Analytical coupling of the temperature distribution Equation (A.1.5) with Darcy's law and an EOS is not possible. Hence, the Heat Integral Method will be used to obtain a good approximation for the above solution that permits analytical solutions. In order to approximate the exact equation a third order polynomial is considered in terms of dimensionless distance from the boundary.

$$\theta = a(\tau) + b(\tau)\xi + c(\tau)\xi^2 + d(\tau)\xi^3 \qquad \ldots\ldots (A.1.6)$$

For an unsteady-state problem, the coefficients a, b, c and d are functions of dimensionless time, and can be obtained using the actual boundary condition of the problem, Equation (A.1.3), and the auxiliary boundary condition (A.1.7) to (A.1.9)

$$\theta = 0 \qquad\qquad \xi = \delta \qquad\qquad \dots\dots (A.1.7)$$

$$\frac{\partial \theta}{\partial \xi} = 0 \qquad\qquad \xi = \delta \qquad\qquad \dots\dots (A.1.8)$$

$$\frac{\partial^2 \theta}{\partial \xi^2} = 0 \qquad\qquad \xi = \delta \qquad\qquad \dots\dots (A.1.9)$$

The auxiliary boundary conditions state that there is no effect of heat flow beyond the penetration depth. Equation (A.1.9) is referred to as a smoothing condition because it tends to make the temperature profile go smoothly in the initial temperature. The smoothing condition has been used before [Goodman 1959], where a third order polynomial was chosen.

In HIM different auxiliary boundary conditions can be chosen. Goodman [1961] states that "In selecting a derived constraint at one end of the interval in order to determine an additional constant in the profile, the accuracy will be improved only if preference is given to one which involves the lower order derivative. If the highest order derivative involved in both possibilities is the same, then the choice is arbitrary." For a problem of constant temperature at the boundary, however. Goodman [1961] explains that it is impossible to follow the above rule.

Using Equations (A.1.3) and (A.1.7) to (A.1.9) one can obtain the temperature distribution as:

$$\left(1 - \frac{\xi}{\delta}\right)^3 \qquad\qquad \dots\dots (A.1.10)$$

The integrated form of heat conduction equation over the heat penetration depth can be written as

$$\left.\frac{\partial \theta}{\partial \xi}\right|_\delta - \left.\frac{\partial \theta}{\partial \xi}\right|_0 = \frac{d}{d\tau}\int_0^\delta \theta \, d\xi \qquad\qquad \dots\dots (A.1.11)$$

205

Upon substitution of the temperature profile (A.1.10) into Equation (A.1.11) and by using the auxiliary boundary conditions, an ordinary differential equation is obtained for the heat penetration depth

$$\frac{d\delta(\tau)}{d\tau} = \frac{12}{\delta(\tau)} \qquad\qquad \dots\dots \text{(A.1.12)}$$

Equation (A.1.12) along with the initial condition (A.1.13) can be solved to obtain the heat penetration depth as Equation (A.1.14)

$$\delta = 0 \qquad\qquad\qquad\qquad \tau = 0 \qquad\qquad \dots\dots \text{(A.1.13)}$$

$$\delta = \sqrt{24\tau} \qquad\qquad\qquad\qquad\qquad\qquad \dots\dots \text{(A.1.14)}$$

and the temperature distribution Equation (A.1.10) can be written as

$$\left(1 - \frac{\xi}{\sqrt{24\tau}}\right)^3 \qquad\qquad \tau \le \frac{1}{24} \qquad\qquad \dots\dots \text{(A.1.15)}$$

Equation (A.1.15) is the unsteady-state temperature distribution for the slab before the heat penetration depth equals half of the block thickness. However, Equation (A.1.15) is not valid after $\tau = \frac{1}{24}$, when temperature at the center rises. This is because Equations (A.1.7) and (A.1.9) can not be used any more. In fact there is no meaning for penetration depth afterwards. As it was indicated in the text two temperature profiles have to be considered to obtain an accurate solution.

$$\theta_1 = a(\tau) + b(\tau)\xi + c(\tau)\xi^2 \qquad 0 \le \xi \le \frac{1}{2} \qquad \tau \ge \frac{1}{24} \quad \dots\dots \text{(A.1.16)}$$

$$\theta_2 = e(\tau) + f(\tau)\xi + g(\tau)\xi^2 \qquad \frac{1}{2} \le \xi \le 1 \qquad \tau \ge \frac{1}{24} \quad \dots\dots \text{(A.1.17)}$$

Four of the coefficients can be found using appropriate boundary conditions (A.1.18) to (A.1.21),

$$\theta_1 = 1 \qquad\qquad\qquad\qquad \xi = 0 \qquad\qquad \dots\dots \text{(A.1.18)}$$

206

$$\frac{\partial \theta_2}{\partial \xi} = 0 \qquad \xi = 1 \qquad \dots \dots (A.1.19)$$

$$\theta_1 = \theta_2 \qquad \xi = \frac{1}{2} \qquad \dots \dots (A.1.20)$$

$$\frac{\partial \theta_2}{\partial \xi} = \frac{\partial \theta_1}{\partial \xi} \qquad \xi = \frac{1}{2} \qquad \dots \dots (A.1.21)$$

Equations (A.1.16) and (A.1.17) can be simplified using the above boundary conditions,

$$\theta_1 = 1 + b(\tau)\xi + c(\tau)\xi^2 \qquad 0 \le \xi \le \frac{1}{2} \qquad \tau \ge \frac{1}{24} \quad \dots \dots (A.1.22)$$

$$\theta_2 = 1 + b(\tau)(-\frac{1}{4} + 2\xi - \xi^2) + c(\tau)(-\frac{1}{2} + 2\xi - \xi^2) \qquad \frac{1}{2} \le \xi \le 1 \qquad \tau \ge \frac{1}{24} \quad \dots \dots (A.1.23)$$

Now, Equations (A.1.22) and (A.1.23) are forced to satisfy the integrated form of the heat equation over their corresponding half intervals. Hence,

$$\frac{\partial \theta_1}{\partial \xi}\bigg|_{\frac{1}{2}} - \frac{\partial \theta_1}{\partial \xi}\bigg|_0 = \frac{d}{d\tau}\int_0^{\frac{1}{2}} \theta_1 d\xi \qquad \dots \dots (A.1.24)$$

$$\frac{\partial \theta_2}{\partial \xi}\bigg|_1 - \frac{\partial \theta_2}{\partial \xi}\bigg|_{\frac{1}{2}} = \frac{d}{d\tau}\int_{\frac{1}{2}}^1 \theta_2 d\xi \qquad \dots \dots (A.1.25)$$

After performing the required algebra, two ODEs for $b(\tau)$ and $c(\tau)$ are obtained.

$$c(\tau) = \frac{1}{8}\frac{db(\tau)}{d\tau} + \frac{1}{24}\frac{dc(\tau)}{d\tau} \qquad \dots \dots (A.1.26)$$

$$b(\tau) + c(\tau) = -\frac{1}{3}\frac{db(\tau)}{d\tau} - \frac{5}{24}\frac{dc(\tau)}{d\tau} \qquad \dots \dots (A.1.27)$$

Simultaneous solution of Equations (A.1.26) and (A.1.27) yields the relation of $b(\tau)$ and $c(\tau)$ with dimensionless time,

$$b(\tau) = -0.58579A_1 \exp(m_1\tau) - 3.41421A_2 \exp(m_2\tau) \qquad \dots\dots (A.1.28)$$

$$c(\tau) = A_1 \exp(m_1\tau) + A_2 \exp(m_2\tau) \qquad \dots\dots (A.1.29)$$

where $m_1 = -31.689$
$\qquad m_2 = -2.5967$

There are two more conditions that should be used to find the coefficients A_1 and A_2. These conditions correspond to continuity of temperature and heat flux, when the second set of temperature profiles (A.1.22) and (A.1.23) are replaced for the first Equation (A.1.15),

$$\theta_2 = 0 \qquad\qquad \xi = 1 \qquad\qquad \dots\dots (A.1.30)$$

$$\frac{\partial\theta_1}{\partial\xi} = \frac{\partial\theta_2}{\partial\xi} \qquad\qquad \xi = 0 \qquad\qquad \dots\dots (A.1.31)$$

Using equations (A.1.30), (A.1.31), which are valid at $\tau = \frac{1}{24}$ the coefficients A_1 and A_2 are obtained

$$A_1 = 7.32903$$
$$A_2 = 0.60492$$

Figure 4.6 compares the exact solution, Equation (A.1.5) with the approximate ones obtained by using HIM, that is, Equations (A.1.15), (A.1.22) and (A.1.23).

A.2. Analytical Solutions for Thermal Gravity Drainage in a Slab

To obtain the gravity driven oil flow rate from a single block Darcy's law, which is written for an element of thickness dx of constant temperature as Equation (A.2.1), is combined with EOS (A.2.2):

$$dq = \frac{k}{\mu_o(T)} \Delta\rho g(2Ldx) \qquad \dots\dots\dots\dots\dots\dots (A.2.1)$$

208

where a piston-like displacement was assumed over the element, and capillary pressure was neglected.

$$\frac{v_{os}}{v_o} = \left(\frac{T - T_R}{T_s - T_R}\right)^m \qquad \text{.................... (A.2.2)}$$

In order to obtain non-isothermal gravity drainage the above equations are combined,

$$q = \frac{1}{L}\frac{kg}{v_{os}} \int_0^L \theta^m dx \qquad \text{..... (A.2.3)}$$

where it has been assumed $\Delta\rho = \rho_o$. The variable q is the production rate per unit area of the block.

In order to perform analytically the above integration and to obtain a closed-form solution for non-isothermal gravity drainage, the approximate temperature distributions in polynomial form that were found in Section A.1 are used. Hence,

$$q_D(\tau) = \frac{\sqrt{24\tau}}{3m + 1} \qquad\qquad \tau \leq \frac{1}{24} \qquad \text{..... (A.2.4)}$$

In Equation (A.2.4) q_D is normalized with respect to the maximum drainage rate at steam temperature:

$$q_D(\tau) = \frac{q(\tau)}{q_s} \qquad \text{...................... (A.2.5)}$$

where,

$$q_s = \frac{4kgL^2}{v_{os}} \qquad \text{...................... (A.2.6)}$$

Thus, $q_D(\tau) = 1$ corresponds to isothermal gravity drainage at steam temperature. Equations (A.2.5) and (A.2.6) indicate that non-isothermal gravity drainage from a single block, similar to the corresponding isothermal one, is linearly proportional to the oil viscosity at steam temperature and matrix permeability.

209

Equation (A.2.4) is valid for $\tau \le \frac{1}{24}$; however, for $\tau \ge \frac{1}{24}$ Equations (A.1.26) and (A.1.27) are used and the analytical integration is performed for a value of $m=4$, as obtained in Appendix B for the Grosmont bitumen of Alberta. The solution is plotted in Figure 4.8, which shows that the drainage rate approaches that at steam temperature after $\tau = 2$. For comparison the thermal gravity drainage with the exact temperature distribution, Equation (A.1.5), is plotted also. Obviously, the latter is obtained using numerical estimation of the infinite series and numerical integration of the final flow integral. Also, the solution from a free equation of state, Equation (B.3) from Appendix B, is shown. Similar to the solutions for the cylindrical block, the close similarity of the solutions indicates that the approximations involved in using the temperature distribution from HIM and also in evaluating the exponent m in Appendix B are all justified.

A.3. Average Temperature Assumption

In the previous section the temperature distribution was analytically incorporated in the integral of the flow rate from a single block. Here, it is intended to examine the average temperature assumption as performed for the cylindrical block. Under the average temperature assumption thermal gravity drainage from a single block can be evaluated as

$$\bar{q} = \frac{kg}{v(T_{av.})} = q_s \frac{v_{os}}{v_o(T_{av.}(\tau))} \qquad \dots\dots\dots\dots\dots\dots\dots \text{(A.3.1)}$$

or,

$$\bar{q}_D(\tau) = \frac{v_{os}}{v_o(\theta_{av.}(\tau))} \qquad \dots\dots\dots\dots\dots\dots\dots \text{(A.3.2)}$$

where the bar indicates the production rate at the average temperature.

As mentioned in the text, Equation (A.3.2) is valid for both the cylinder and the slab cases. If one uses equation of state (A.2.2), Equation (A.3.2) can be written as

$$\bar{q}_D(\tau) = [\theta_{av.}(\tau)]^m \qquad \dots\dots\dots\dots\dots\dots\dots\dots \text{(A.3.3)}$$

Using temperature distributions from HIM, as found in Section A.1, one obtains

210

$$\bar{q}_D(\tau) = (1.5\tau)^{\frac{m}{2}} \qquad\qquad \tau \le \frac{1}{24} \qquad \dots\dots\dots\dots\dots \text{(A.3.4)}$$

$$\bar{q}_D(\tau) = \left[1 + \frac{11}{24}b(\tau) + \frac{1}{4}c(\tau)\right]^{m} \qquad \tau \ge \frac{1}{24} \qquad \dots\dots\dots\dots\dots \text{(A.3.5)}$$

where $b(\tau)$ and $c(\tau)$ are expressed as Equations (A.1.28) and (A.1.29).

The drainage rate under average temperature, Equations (A.3.4) and (A.3.5), is compared in Figure 4.10 with the drainage rate using the exact temperature distribution, Equation (A.1.5) and EOS (B.3). Figure 4.10 indicates that the drainage rate is under-predicted at early time using the average temperature when the flow rate is small.

APPENDIX B:
CALCULATION OF THE EXPONENT m FOR THE GROSMONT CRUDE

To calculate the exponent m for a particular heavy oil, Butler [1985-a] suggested Equation (B.1)

$$m = \left[v_{os} \int_{T_R}^{T_s} \left(\frac{\frac{1}{v_o} - \frac{1}{v_{oR}}}{T - T_R} \right) dT \right]^{-1} \qquad \dots\dots\dots\dots\text{(B.1)}$$

This equation was obtained for assumptions which do not apply to the single block problem. However, Equation (B.1) will be used here to calculate m, and later the error introduced in flow rate calculations will be evaluated.

The Grosmont formation contains a 7 °API bituminous heavy oil of viscosity 1.6×10^6 (mPa s) at a reservoir temperature of 11 °C [Cordell 1982]. Svrcek and Mehrotra [1988] presented a single parameter correlation for bitumen viscosity in Alberta

$$\log[\log(\mu_o + 0.7)] = b_1 - 3.63029 \log(T) \qquad \dots\dots\dots\dots\text{(B.2)}$$

where the viscosity is in (mPa s) and the temperature is in (K). It has been reported that the corresponding correlation in terms of kinematic viscosity is [Butler 1991]

$$\log[\log(v_o + 0.7)] = b_2 - 3.5556 \log(T) \qquad \dots\dots\dots\dots\text{(B.3)}$$

Using the single viscosity data of the Grosmont bitumen and Equation (B.3), the exponent m is evaluated by numerically integrating Equation (B.1). A trapezoidal method was used and the number of intervals was increased until a convergence of the order of 10^{-5} was obtained. At a steam temperature of 195 °C, corresponding to saturated steam at an initial reservoir pressure of 1400 kPa [Cordell 1982], the exponent m was found to be 4.00, which is used in this study.

Recently, Butler [1994] presented another calculation method for finding m. The latter method was developed for the 1-D steady-state SAGD process. Similar results were obtained provided that the lower limit of integration was set close to the initial reservoir temperature.

212